POROUS ANODIC ALUMINA MEMBRANES FOR LARGE BIOMOLECULE SEPARATIONS

A THESIS SUBMITTED TO

UNIVERSITY COLLEGE LONDON

FOR THE DEGREE OF

DOCTOR OF PHILOSOPHY

BY

ANSHUL SHARMA

DEPARTMENT OF BIOCHEMICAL ENGINEERING

UNIVERSITY COLLEGE LONDON

BERNARD KATZ BUILDING

LONDON WC1E 6BT

2018

DECLARATION

"I, Anshul Sharma, confirm that the work presented in this thesis is my own. Where information has been derived from other sources, I confirm that this has been indicated in the thesis."

Signed ……..

Date……..

ABSTRACT

Manufacturing of large biomolecules such as viral vectors used in emerging gene therapies suffers from low product yields due to limitations of traditional resin-based chromatography in downstream processing. Ultrafiltration based purification techniques are being considered for purification of such viral vectors by separating these viral vectors from impurities such as host cell proteins. Improvements in yields of viral vectors have so far concentrated on the design of new chromatography stationary phases such as monoliths, membrane adsorbers, nanofibers and gigaporous resins. Improvement in the architecture of ultrafiltration membranes has not been studied for application in viral vector purifications. Porous anodic alumina (PAA) membranes, exhibit narrow pore size distribution and straight through pore channels compared to traditional polymeric membranes which have broad pore size distributions and tortuous channels. The present work evaluated porous anodic alumina membranes for potential applications in virus ultrafiltration using model protein solutes.

Protein nanoparticles of 80-90nm diameter and thyroglobulin of 20 nm diameter were used as the physical mimics for two of the most commonly used viral vectors, Adenovirus and Adeno-associated viruses respectively and a small protein of 8 nm, bovine serum albumin was used as the model impurity. A reproducible and high yielding protocol was developed for the synthesis of protein nanoparticles from bovine serum albumin using a de-solvation process. Based on comparable hydraulic permeability, dextran sieving curve and mean pore size 20 nm rated PAA membrane and 300 kDa rated polymeric ultrafiltration membranes were compared for filterability of the model solutes. PAA membranes were found to have superior fouling resistance (1.5-2.5 times higher values of recoverable membrane permeability) and up to 4 times higher transmission than the polymeric membranes for large model solutes. These findings were attributed to the differences in the membrane architecture resulting in different sieving behaviour. PAA membranes were found to be susceptible to leaky transmissions of large solutes due to the presence of surface defects.

Separation performance of binary mixtures of model solutes was studied using a diafiltration process. Electrostatic interactions and transmembrane pressure were identified as crucial process parameters to improve separation performance of the alumina membranes. Lot-to-lot variations in the alumina membranes were also characterised using electron microscopy and were found to influence the separation performance. PAA membranes were found to be compatible for virus processing as similar infectivity recovery of 60-70% was observed for both PAA and the polymeric membranes along with 60 % removal of the impurities.

IMPACT STATEMENT

The work presented in this thesis is related to the design of new materials for challenging bioseparations. For the membrane manufacturing industry, the work lays out recommendations to improve the quality of commercial porous anodic alumina membranes and suggests a new application of the membranes. This work identifies manufacturing issues such as defects and variations among lots which are hindering the application of these membranes in bioseparations. The study demonstrated superior fouling resistance and flux performances by PAA membranes compared to traditional polymeric membranes. This outcome is appealing to the bioprocessing industry for potential applications of such membranes in continuous bioprocessing by avoiding long cleaning cycles and reducing overall processing times. However, membrane manufacturer needs further developmental work to market these membranes as high retention and low fouling membranes for high-value products such as viral vectors. Such development work includes reducing membrane defects, lot variations and design of scalable membrane modules compatible with the fragile ceramic membranes.

Academic interest in the present work relates to understanding the mechanistic differences in particle retention between alumina and polymeric membranes especially with respect to drastic differences in their pore morphology. A possible step would be to utilise these differences to bring greater tuning of protein fractionations especially for purification of larger biomolecules such as viral vectors. Tuneability can be established by altering the chemical composition of the membranes to achieve separations through multiple mechanisms along with size exclusion. The present work also suggests an investigation into block copolymer membranes, membranes resembling porous anodic alumina membrane in architecture but without some of the challenges associated with the brittle nature of the alumina membranes.

An ideal situation for further development in this field would be a collaborative work with commercial membrane manufacturers, academia and end users such as biopharmaceutical manufacturers. Most of the manufacturers of porous alumina membranes are recently founded start-ups who can utilise the findings and challenges elaborated in the present work for the design of their products. A collaborative approach will be helpful to develop cheaper and commercially viable membrane products tailored for viral vector separations at large scales with minimum wastage of resources. Development of highly retentive and selective membranes with minimal cleaning requirements could contribute to lowering the manufacturing costs of viral vectors thus bringing affordability to gene therapy.

ACKNOWLEDGEMENTS

I am very grateful to my supervisor**,** Professor Daniel Bracewell for his consistent support and encouragement and sound advice throughout my research. He has given me the freedom to shape my research work and have always encouraged me to think independently. I would also like to thank UCL and the department for the award of the Overseas Research Scholarship and funding for the research work.

I want to thank Jordon Turnbull for assistance with virus production and infectivity assay, David Ward for helping me set up the refractive index detector for dextran sieving experiments and Mrs Ludmila Ruban for training me with mammalian cell culture. I would also like to thank all the members of the Bioseparation laboratory, who have been very cordial throughout my stay. Special thanks to Nehal Patel, Sushobhan Bandyopadhyay and Dr Scott Kimmins for the discussions on various experiments which helped me in planning and designing my experiments.

I would also like to thank lab manager for bioseparation laboratory, Stanislaus Dhushy and all the members of professional services of the department for their support in maintaining the research facilities and hassle-free administrative work including procurement of various materials used in this work. I would also like to acknowledge the support I received from my friends, Archit Sharma and Arpita Vats, who have made my stay comfortable in the UK. Last but not least, I am grateful to my parents and family for their support throughout my studies.

,

TABLE OF CONTENTS

LIST OF FIGURES

LIST OF TABLES

ABBREVIATIONS USED

AAV	Adeno-associated virus
AdV	Adenovirus
ATPS	Aqueous two-phase system
BSA	Bovine serum albumin
DEAE	Diethylaminoethyl
DLS	Dynamic light scattering
DV	Dia-volume
IEX	Ion exchange chromatography
HCP	Host cell proteins
HPLC	High-pressure liquid chromatography
LMH	Litre per meter square area per hour
MWCO	Molecular weight cut off
NFF	Normal flow filtration
NP	Nanoparticles
NTA	Nanoparticles tracking analysis
PAA	Porous anodic alumina
PDI	Polydispersity index
PES	Polyethersulfone
PBS	Phosphate buffer saline
RPM	Rotations per minute
SD	Standard deviation
SEC	Size exclusion chromatography
SEM	Scanning electron microscopy
SSR	Sum of squares of residuals
TEM	Transmission electron microscopy
TFF	Tangential flow filtration
TG	Thyroglobulin
TMP	Transmembrane pressure
UF/DF	Ultrafiltration/Diafiltration
VLP	Virus-like particle

CHAPTER 1 INTRODUCTION, AIM AND OBJECTIVES OF THE THESIS

1.1 Overview of the thesis

The thesis examines highly ordered porous anodic alumina (PAA) membranes for use in the separation of large biomolecules such as viral vectors used in gene therapy. The PAA membranes were evaluated by comparison with traditionally used polymeric membranes.

Chapter 1 provides an introduction to the emerging therapies based on viral vectors and the associated manufacturing challenges, motivation and objectives for the present work.

Chapter 2 discusses viral vectors and their purification challenges in depth. The chapter focuses on chromatography and membranes based processes. The chapter also reviews the literature for porous anodic alumina membranes and protein nanoparticles.

Chapter 3 covers experimental work directed at the synthesis of protein nanoparticles and subsequent characterisation studies prior to use as a model system for virus particles.

Chapter 4 describes the characterisation of porous anodic alumina membranes, filtration performance of porous anodic alumina membranes using model nanoparticle solutes, including analysis of fouling mechanisms.

Chapter 5 presents an analysis of new experimental data on the separation performance of the porous anodic alumina membranes focused on methods to improve performance and retention of Adenovirus during processing of a biological feedstock.

Chapter 6 offers the conclusion for the present work and future studies.

1.2 Emerging therapies in the biopharmaceutical industry

The 35-year-old bio-pharmaceutical industry began with small therapeutic proteins such as insulin, growth factors etc. in the early 1980s, progressed to monoclonal antibodies in the late 1990s onwards and gene and cell therapies from the early 2010s. This shift is the result of advances made in the field of genomics, which has helped identify the genetic elements responsible for many disorders. These advances have helped the industry design new therapies to cure such disorders which were otherwise considered untreatable. So far, traditional therapies had focussed on management of such disorders by supplementation of a missing functional protein. Emerging therapies such as gene therapy, however, aim to cure the disorder by supplementation of the genetic element. These emerging therapies are expected to reduce the dependence on a burdensome lifetime treatment regime for patients using traditional therapies.

The number of clinical trials for various gene and cell therapies has grown from 2 in 1990 to 132 in 2017 with a total of 2600 clinical trials undertaken or ongoing so far worldwide (Ginn *et al.*, 2018). These clinical trials have targetted a variety of indications with the majority in cancer and monogenic diseases and supplemented genes for a variety of proteins such as antigens, cell receptors, cytokines and deficient enzymes. These therapies involve the transfer of genes to cells in cell therapies or directly to the patient. Viruses, known to infect human beings, are used as the vector to transfer the genes. Cell therapies involve the use of these vectors outside the human body to transfer genes to cells harvested from patients and gene therapies, generally, involve direct injection of the viruses carrying the gene of interest into patients. These vectors are usually engineered to remove the virulence-related viral genes and inserted with a desired human gene (which is identified to be missing or dysfunctional in a disorder). In the past five years, western regulatory agencies have approved two viral vector gene therapies, Glybera (UniQure, NL) and Luxturna (Spark Therapeutics, USA) for treatment of a genetic lipase deficiency and inherited eye blindness respectively. Three more cell-based therapies, Kymriah (Novartis, CH), Strimvelis (GlaxoSmithKline, UK) and Yescarta (Gilead Sciences, USA) have been approved in the past two years.

Another healthcare area where new therapies are emerging is vaccines where antigen presentation is crucial and the antigen presenting surface can have an impact on potency as well as the efficacy of the vaccine. Traditional vaccines are often attenuated strains of the pathogen itself. Engineered recombinant viruses and virus-like particles (VLPs) are being investigated as vaccine candidates. Protein engineering of VLPs to display multiple antigens is also being considered to create a single multivalent vaccine that can be used for a number of infections or to protect from multiple strains of pathogens. These approaches can have a long-term impact on strategies for accessibility and ease of manufacturing of the much-needed vaccines, especially in pandemic situations.

1.3 Viral vectors for gene therapy and vaccines

The shift from traditional therapies to cell and gene therapies have also changed the nature and complexity of the therapeutic agent. The most apparent change is the size of the therapeutic agent used. Traditional therapies are small protein molecules such as insulin and monoclonal antibodies, but emerging therapies use supramolecular assemblies such as cells and viruses as therapeutic agents. Viral vectors can be a magnitude larger than the traditional biologics. Monoclonal antibodies which are approximately 150 kilodaltons in molecular weight have dimensions of 10 nm in diameter (Nobbmann *et al.*, 2007). Viral vectors, on the other hand, can range from 20 nm to 400 nm in diameter and megadaltons in their molecular weights. Parvoviruses, the smallest known viruses, are approximately 22 nm in diameter.

Both VLPs and recombinant viruses can be designated in a single class as viral vectors due to the similarity in the structural complexity. A distinction between virus-like particles and recombinant viruses is that the former does not carry any genetic material thus do not have infectivity associated with them. A typical viral vector is formed of a capsid, a highly ordered structure formed from the association of usually multiple proteins and may also have an additional lipid or lipoprotein envelope around it. The complexity of size and composition of the viral vectors in comparison to the traditional protein biologics is illustrated in **Figure 1-1**. Notice the different colour on capsids of the virus and VLPs signifying different viral proteins.

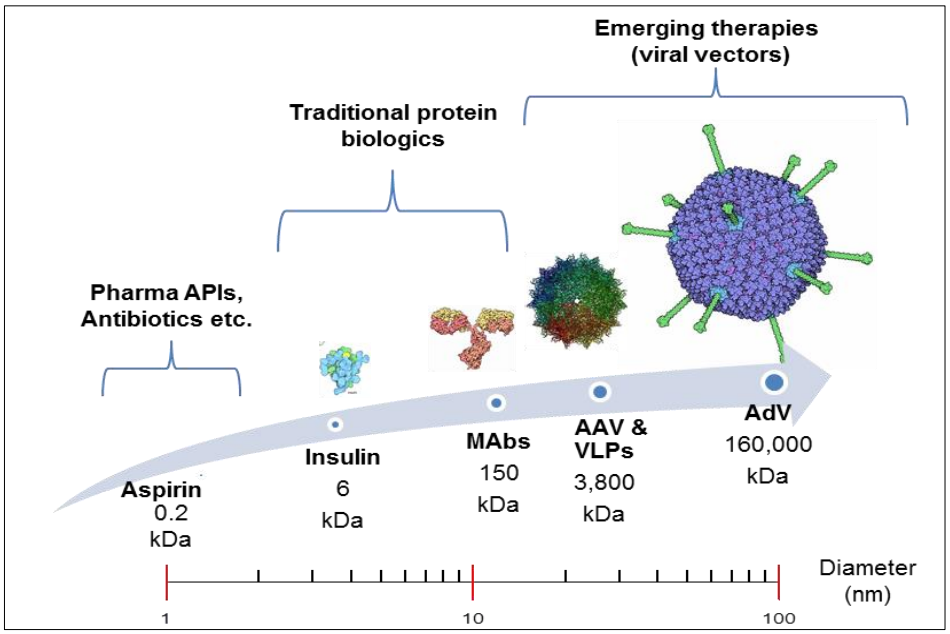

Figure 1-1 Illustration of the range of the biopharmaceutical products used in various therapies including gene therapies showing increasing size and structural complexity for viral vectors.

Cartoon structures for various molecules were obtained from protein database (PDB; http://www.rcsb.org/). MAb, AAV, VLP and AdV stands for monoclonal antibody, adeno-associated virus, virus-like particles and adenovirus respectively.

1.4 Impact of viral vectors on biomanufacturing

Production of smaller biologics especially monoclonal antibodies has dominated the biomanufacturing activities of the industry as well as academia. The size of the product has a significant impact on some of the unit operations in downstream processing of biologics, especially filtration and chromatography based processes. These processes use meso (pores dimensions of 2-50 nm) or macroporous material (pore dimensions above 50 nm) as solid matrices. These processes discriminate between product molecules and the impurities through a variety of properties such as size, charge or hydrophobicity and affinity. Accessibility of various molecules to the porous architecture of solid matrices often defines the recovery of the valuable product as both convection and diffusion drive the mass transfer. Diffusive mass transfer limitations are often observed in chromatography and filtrations.

Chromatography processes, which are typically operated in a bind and elute mode, are expected to preferentially bind the protein of the interest to maximum amount with a minimum amount of the solid matrix and reject the impurities. Filtration processes are also expected to either retain or pass through the maximum amount of product with the minimum amount of the matrix used. The capacity of these chromatography or filtration matrices is thus defined by the amount of protein purified and recovered. For surface active processes such as chromatography, size and number of pores will determine the specific surface area (area per unit volume or amount) of such porous material. Diffusive mass transfer of any particular molecule is dependent on the size of the molecule with respect to the size of pores. A solute might not be able to penetrate deeper into the porous matrix if it encounters steric hinderances from pore walls thus only utilising a fraction of the maximum capacity of the matrix. In the case of viruses, binding capacities have been reported to be an order of magnitude lower than those for the smaller proteins (Trilisky and Lenhoff, 2007). Such a scenario may result in the adequate purity of the product but significant loss of the product or low recovery.

Recovery of the product can be crucial especially for high value and low volume products which is usually the case for most of the biologics. The high cost of the materials used for these processes is also an essential factor when the selection of a chromatography or membrane material is required. A material with low capacity can result in significant losses of the product during processing or may result in significant investment for the increased amount of the often expensive porous matrices. Most of the porous materials have been developed and characterised concerning smaller biologics such as monoclonal antibodies and not for the viral vectors. It has been observed that the capacity of these processes which are optimised for monoclonal antibodies are very low for large biomolecules such as viral vectors.

1.5 Motivation and aim of the present thesis

Only five gene and cell therapies have been approved so far, and at present, these therapies are expensive with a range of USD 0.2 to 1 million (Mullin, 2017). Cost is on the upper end of this range for the viral vector-based approved therapies which were mentioned in the section 1.2. Such a high cost can affect the affordability of these therapies. High manufacturing cost and low dose frequency are reported to be a major contributing factor towards the high cost of these vector-based therapies (Waehler *et al.*, 2007, Rader, 2018). Downstream challenges such as those described in the previous section (1.4) hinder the development of robust processes for viral vector purifications. Alternative materials such as monoliths and nanofibres are being looked into to debottleneck chromatography unit operation. These materials are of radically different design compared to conventional resins and aim to increase binding capacities for large biomolecules such as viral vectors thus reducing the loss of the valuable product (Trilisky *et al.*, 2009, Ruscic *et al.*, 2017).

While new materials are being actively investigated for potential use as chromatography adsorbers, tradition membrane-based processes have received little attention. A possible reason for this could be that membrane-based processes are traditionally used for depth filtration, concentration and buffer exchange applications and not for high-resolution separation as in chromatography. Development of new membranes for biopharmaceutical processing is mostly confined to the refinement of polymeric membranes for fouling resistance or cleaning resistance. Nonetheless, development of novel membranes have been actively carried out in other fields such as water purification, gas purification with different membrane materials and different porous architectures have been fabricated and tested.

A very common reason often cited for poor separation performance of membranes even as adsorbers is non-uniformities in the membrane architecture such as the presence of wide pore distribution (Orr *et al.*, 2013). Thus, studying a membrane material with narrow pore size distribution is interesting for bioprocess applications and especially for viral vectors where the difference in size among viral vectors and smaller protein impurities could be utilised for effective separation using membranes. This thesis aims to characterise such membranes made of porous anodised alumina for viral vector separations and to compare them with traditionally used polymeric ultrafiltration membranes. To overcome the challenges of producing and studying actual viral vectors, protein nanoparticles have been used as physical mimics to the viral particles. Fouling mechanisms and separation performance of these membranes have been studied and compared with those of conventional polymeric ultrafiltration membranes.

1.6 Objectives defined for the thesis

Objective 1: Preparation and characterisation of BSA protein nanoparticles as a mimic of virus particles

The first objective of the present work will be to synthesise monodisperse preparations of BSA protein nanoparticles in the range of 70-100 nm particle diameter similar to the size of common viral vectors such as Adenovirus and lentivirus. A protocol will be developed to achieve high yield, high repeatability and shorter preparation time. Nanoparticle preparations will be characterised by the shape of nanoparticles, light scattering characteristics, surface charge characteristics and stability during storage. Finally, nanoparticle preparations will be tested against viral feed to ensure the validity of the protein nanoparticles as mimic to viral particles in membrane separation processes. This study is explained in Chapter 3.

Objective 2: Characterisation of porous anodic alumina (PAA) membranes for filterability of protein solutions of single model solutes

The second objective of the thesis is to investigate the filtration performance of the PAA membranes using the protein model solutes of different hydrodynamic size representing smaller host cell protein impurities (bovine serum albumin), smaller viruses (thyroglobulin) and larger viral vectors (BSA nanoparticles). Parallel comparison of the PAA membranes and conventional polymeric ultrafiltration membranes for filterability of these protein model solutes will be carried out. Such a comparison has never been reported in the literature. Membranes will be compared for flux decline, fouling mechanism, fouling resistance and solute transmission. A systematic experimental approach will be used to select appropriate membrane ratings from both classes of the membranes so that the filtration performance of the membranes could be correlated to the difference in their morphology. Chapter 4 discusses the outcome for this objective in detail including the materials and methods used.

Objective 3: Separation performance of porous anodic alumina (PAA) membranes for binary mixtures of the model solutes

PAA membranes will be evaluated for fractionation of the mixture of the model solutes for viruses (protein nanoparticles and thyroglobulin) and model impurity (bovine serum albumin). Impact of process parameters such as operating conditions, transmembrane pressure and diafiltration mode will be studied. The utilisation of the electrostatic interactions of solutes and ceramic membranes will be studied for enhancing the fractionation. PAA membranes will also be investigated for compatibility with viral feeds by studying infectivity losses and comparing them with those observed for conventional ultrafiltration membranes. Chapter 5 discusses the outcomes of these experiments including the materials and methods used.

CHAPTER 2 REVIEW OF THE LITERATURE

2.1 Overview of the chapter

The chapter is arranged in six major sections (2.2 to 2.7) describing the manufacturing challenges for large biomolecules such as viral vector production especially for downstream processing (Section 2.2 and 2.3), a review of membrane-based processes for biologics purification including fundamentals of filtration processes (Section 2.4) inclduing studies reported for virus ultrafiltration, a review of the fabrication and applications of porous anodic alumina membranes (Section 2.5), a brief review of the challenges in working with viruses and the need for appropriate model systems (Section 2.6) and finally the literature on synthesis and applications of protein nanoparticles (Section 2.7).

2.2 Common viral vectors

Commonly used viral vectors in gene therapy clinical trials are illustrated in the bar chart below.

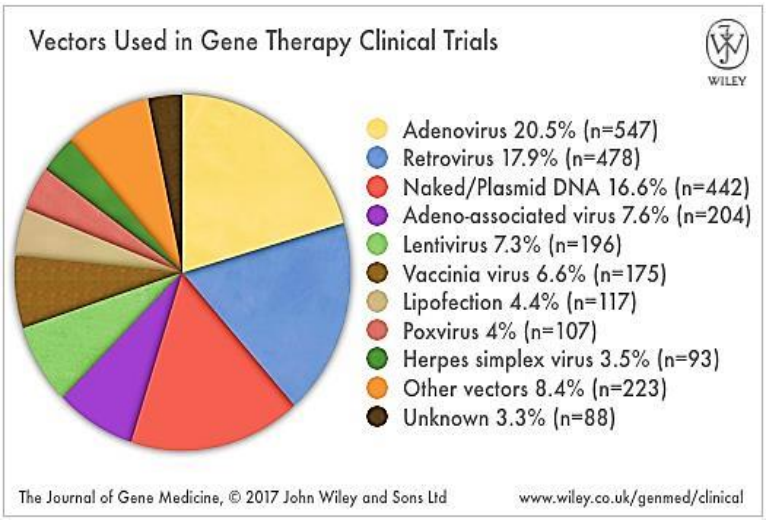

Figure 2-1 Distribution of various vectors used in 2600 clinical trials up to 2017 for gene therapy clinical trials worldwide. Source: Ginn *et al.*,(2018).

As shown in **Figure 2-1**, Adenovirus (AdV) and retrovirus form the most commonly used vectors for gene therapy. Non-viral vectors such as naked DNA and lipofection form a minority share in the clinical trials. However, very few gene therapy products approved so far are based on Adenovirus or adeno-associated virus (AAV). So most of the discussion in this chapter will be focused on the literature for these viruses. Non-gene therapy viral vectors such as virus-like particles will also be discussed to a limited extent.

Vector	Genome size (kilobases)	Capsid envelope	Size (nm)	Pathogenic
Adenovirus (AdV)	40	Absent	90-110	Yes
Adeno associated virus (AAV)	5	Absent	~25	No
Retrovirus	9	Present	120	Yes
Hepes Simplex Viruse	12	Present	180	Yes
Vaccinia virus	280	Present	350	Yes

Table 2-1 Common viral vectors used in gene therapy and their characteristics Information sourced from Ponder *et al.*,(2002).

Choice of the vector as a gene therapy candidate is influenced by many factors including the size of the genetic material to be transferred and the ability of the virus to accommodate that genetic material. From **Table 2-1**, it can be seen that the vaccinia virus has a large genome size and particle size. Enveloped viruses such as Vaccinia and Retrovirus have another layer of lipids or proteins around the proteinaceous capsid of the virus which plays a role in the infectivity of the virus. Generally, enveloped viruses are considered difficult to process due to the fragility of the envelope layer. Size of the virus vector used in the gene therapies can vary from 25 nm for AAVs to 350 nm for vaccinia virus. Tissue or organ specificity of various viruses and their serotypes can also influence the choice of the vector for a particular gene therapy application.

2.3 Manufacturing challenges for viral vectors

At present, there are no production processes specifically designed for mass production of virus-based therapeutics. Though production titres are improving, purification processes are still not optimised for these vectors. Implications are enormous on downstream processing as it contributes around 70% of total manufacturing cost (Morenweiser, 2005) and overall process yields for viral vectors are about 30% at the moment (Vijayaragavan *et al.*, 2014). Following sections discuss the reported studies on purification of viral vectors and factors identified for such low yields.

2.3.1 Downstream processing of viral vectors

Viral vectors are relatively new to manufacturing floors and optimisation of processes and establishing a purification platform is still underway. Viral vectors have additional challenges to their purification due to their composition and structural differences from traditional protein biologics. These molecules are relatively large and supramolecular assembly called capsid made up of one or more protein subunits. Another complexity is the presence of nucleic acid inside this supramolecular assembly. Different components of a typical feed for virus purification as illustrated in **Figure 2-2** Illustration showing the complexity of a typical cell lysate feed containing viral vector product along with various product and process related impurities. In gene therapy application, the most critical quality attribute of a viral vector is the infective titre in the dose being given to a patient. Preserving the intactness of the fragile capsid is crucial to maintaining the infectivity of the particles.

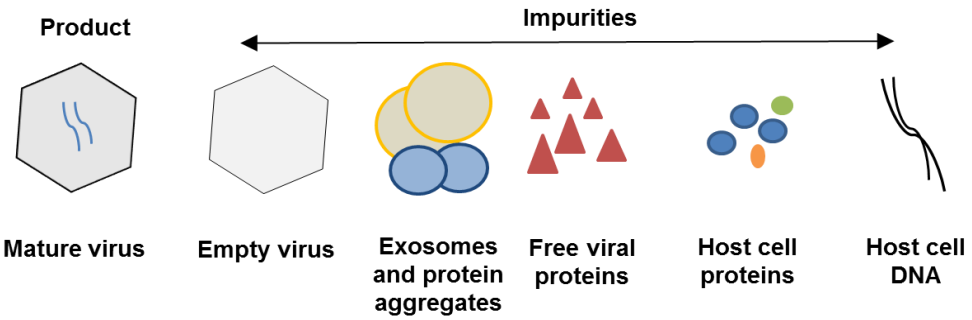

Figure 2-2 Illustration showing the complexity of a typical cell lysate feed containing viral vector product along with various product and process related impurities.

Mature and empty viruses have very limited structural differences except presence of DNA. Exosomes and protein aggregates can be of similar in dimensions as of virus particles. Host cell DNA can interact with virus particles and alter their interaction with chromatography resin. Free viral protein or unassembled capsids have similar chemical composition as of fully formed virus particles. Another complexity can arise from presence of lipoprotein envelope around virus particles or aggregated particles.

Loss of infectivity can result from harsher treatment to viral capsid often encountered in various stages of processing. A typical purification train as shown in **Figure 2-3** for viral vectors involves many unit operations exposing capsids to high shear. Even if intactness of capsids is preserved, a significant fraction of the capsids can be empty (without DNA) which do not have any therapeutic value for gene therapy. Titre of the empty particles can be 20-30 times than that of mature active virus particles increasing effective dose size (Lock *et al.*, 2010). These particles can induce an adverse immune response in patients thus reducing the overall efficacy of gene therapy (Mingozzi and High, 2013). Therefore high-resolution particle separation techniques such as ultracentrifugation are required for viral vector purifications.

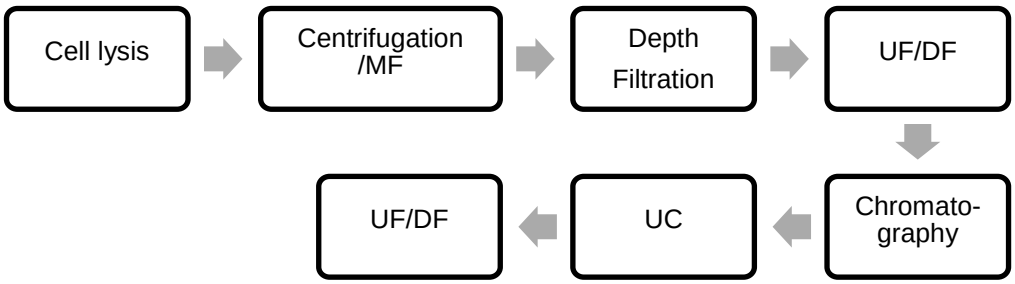

Figure 2-3 A typical downstream processing train for viral vector purifications.

A variety of particle separation techniques such as centrifugation, microfiltration (MF), ultrafiltration (UF) and ultracentrifugation (UC) are used for downstream processing of viral vectors.

Ultrafiltration, chromatography and ultracentrifugation are the key unit operations driving high-resolution separation, so only their impact on virus processing is discussed further.

2.3.2 Key unit operations for viral vector purifications

2.3.2.1 Ultracentrifugation

Ultracentrifugation uses very high centrifugal forces to separate molecules of different molecular weight in different layers typically through the density gradient fluid matrix. The technique has been primarily used as an analytical method. Ultracentrifugation is not a commonly used technique for process development or large-scale biomanufacturing for traditional biologics. However, for viral vector purifications, this technique is frequently employed due to its ability to resolve between empty and mature virus particles based on the difference in the mass due to the nucleic acid.

However, issues of the scalability and co-sedimentation of high molecular weight impurities are often reported. The technique also exposes virus particles to the high shear environment due to high g-forces (above 50,000x g) used in centrifuges for long processing times with 2 to 3 cycles. CsCl used to establish density gradient is known to be highly cytotoxic, so extensive dialysis step is required to remove the salt after extracting the band containing virus particles. Extraction of the band itself is a difficult task. Loss of infectivity of the mature particle as high as 85 % has been reported with exposure to CsCl up to 72 hours (Auricchio *et al.*, 2001). Use of idioxinal instead of CsCl has been suggested to significantly reduce the process time from 3 days to 1 day but with compromise in the fractionation of the empty particles (Strobel *et al.*, 2015).

2.3.2.2 Chromatography

Chromatography is considered as the workhouse of biopharmaceutical manufacturing. Chromatography utilises differential interaction of various components or solutes with a solid matrix to separate these components. Solid matrix or resin, usually porous beads of sub 100 um size, are used in chromatography. These beads can have inert surfaces or functionalised with ligands. Inert resins are solely used for size exclusion chromatography where particles are retained or excluded based on their ability to enter and extent of entry into the porous structure of the beads. Most commonly used chromatography for large-scale manufacturing, however, utilises functionalised porous beads. Theoretically, the chromatography techniques used for protein purification can also be used to purify viral vectors due to the proteinaceous makeup of the capsid. However, notable deviations from traditional protein purification have been observed when conventional chromatography resins were applied for virus purifications.

Such deviations are :

- Reduced pore accessibility for virus particles has been reported as a prime reason for low capacity of resins for viruses. Yu *et al.*, (2014) have compared gigaporous media with large channels (120 and 280 nm) and traditional agarose-based resins with 20 and 35 nm pore channels for a 20 nm VLP and found higher loading capacities and recoveries for gigaporous media.
- Reduced pore accessibility has also been reported for larger VLPs (100 nm) even in the gigaporous resins which have outer large (800-900 nm) pores and smaller (50-100 nm) internal diffusive pores (Wu *et al.*, 2013). These observations were supported using confocal microscopy of gigaporous resin for binding of fluorescent IgG and VLPs (**see Figure 2-5).** It signifies that even gigaporous resins would not have good capacities for large viral vectors such as Adenovirus and lentivirus.
- Significant losses of infectivity or activity have been reported with traditional resins even for smaller viral particles such as VLPs. The losses have been attributed to irreversible disassembly (**see Figure 2-4**) of the virus particles during the adsorption-desorption process in the narrow channels of resins. Gigaporous media have been demonstrated to reduce such disassembly (Yu *et al.*, 2014).
- Lack of a platform affinity chromatography resin for viral vectors, unlike Protein A chromatography used for a wide range of monoclonal antibodies is also a hindrance to process development. Few affinity ligands have been developed by utilising the specificity of the virus-host cell interactions. Development of such a platform affinity resins is restricted by the variety of viral vectors and serotypes of each vector used in clinical trials which have significantly different host cell receptors.

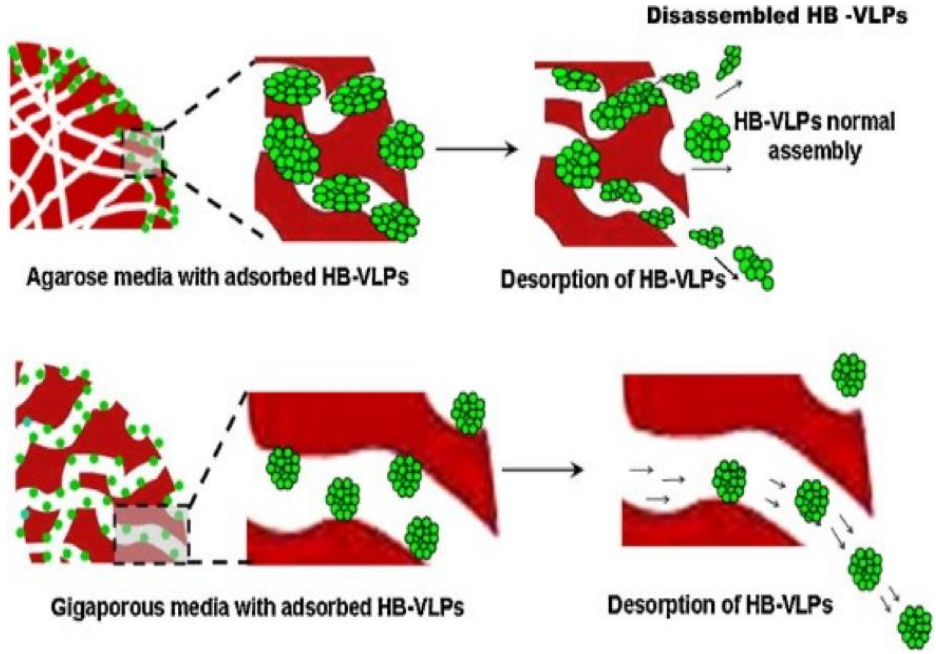

Figure 2-4 Disassembly of the Hepatitis B VLP capsid illustrated for traditional agarose media and giga-porous media. (Source: Yu *et al*., 2014)

Image reproduced with permission from Yu et al., (2014).

1. Adsorption of 2 mg/mL IgG in flow cell at 1000 cm/hr

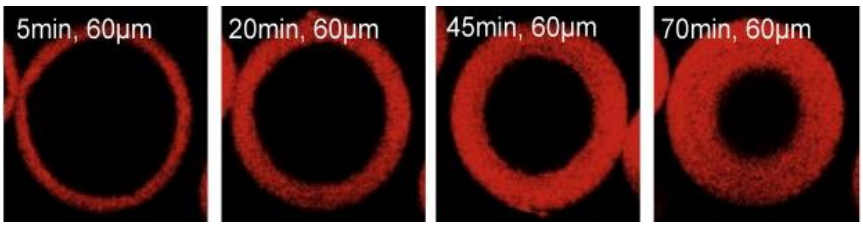

2. Adsorption of 0.2 mg/mL VLP in flow cell at 1000 cm/hr

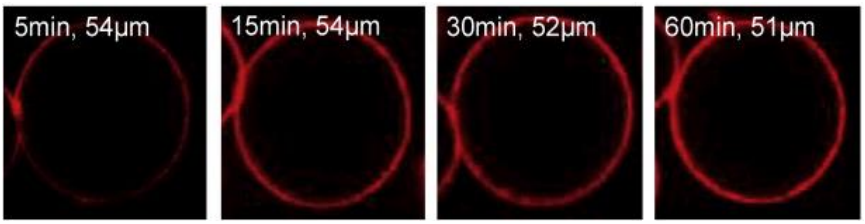

Figure 2-5 Effect of the solute size on utilisation of the resin capacity of a perfusive resin under dynamic conditions, demonstrated using confocal laser scanning microscopy of the resin beads. (Source: Wu *et al*., 2013).

Resin was loaded with smaller protein, IgG and larger 100 nm solute, VLP. For intermediate sized (20 nm) solute, Thyroglobulin, perfusion resin was found to be fully saturated. Images were reproduced and modified with permission from Wu et al., (2013).

Ion exchange chromatography has been the most commonly used technique for the purification of various viral vectors. Significant differences have been observed for purification of different serotypes of the same virus using similar ion exchange methods (Potter *et al.*, 2014). Methods have also found utility in the separation of empty and mature virus capsids by exploiting the small difference in the isoelectric points of these two capsids (Qu *et al.*, 2007). No such separation has been reported for Adenovirus. Use of perfusive resin such as POROS has been widely reported for IEX purification of AAV vectors. Qu *et al.* (2015) have summarised various purification techniques used for AAV purification including ion exchange chromatography. Mixed mode resin such as ceramic hydroxyapatite has been found efficient for virus purifications (Zhou *et al.*, 2011). Ion exchange chromatography has also been extensively used for Adenovirus purification. Most of the studies focus on the use of monoliths and membrane adsorbers for Adenovirus purification. One study reported only marginal improvement with 34% process recovery using Q derivatised monolith compared to 28% with Q sepharose (Lucero *et al.*, 2017). Tentacled ion exchange resins such as Fractogel have been reported to improve the binding capacity for Adenovirus (Bo *et al.*, 2015).

Hydrophobic interaction chromatography has been used more commonly for VLPs. For viruses, it has been suggested that high salt concentration used in HIC can cause aggregation and negatively affect the infectivity of the virus particles (Qu *et al.*, 2015). Chahal *et al.*, (2007) have reported a step yield of 72% for HIC based polishing of AAV. Some reports have suggested high recoveries for gene therapy vectors as well such as 88% for canine Adenovirus (Segura *et al.*, 2012).

Methods describing the affinity-based purification of AAVs have been published as employing ligands such as heparin (Auricchio *et al.*, 2001), mucin (Wilson *et al.*, 2003) and VHH domain antibody fragments (Smith *et al.*, 2009). No affinity-based method has been reported so far for purifications of Adenovirus and retrovirus. The high cost of the affinity-based resins and difficulty in cleaning in place are a significant factor in limiting their application at large scale. The cost of AVB sepharose resin with VHH domain ligand is approximately 50 times higher than a typical ion exchange resin such as SP-sepharose (Potter *et al.*, 2014). Size exclusion chromatography has been less extensively used due to limited loading capacity and pressure tolerance though the technique is gentler than other chromatography modes. However, Nestola *et al.*, (2014b) have advocated size exclusion chromatography in a two-column simulated moving bed mode to overcome these limitations and reported improvement of recovery from 56% in a batch process to 86% in simulated moving bed mode.

.

2.3.2.3 Newer chromatography materials for virus purifications

Challenges observed in the purification of large viral vectors with traditional resins are mainly due to the design of the architecture of the resins primarily developed for smaller proteins especially monoclonal antibodies. Thus, the focus of the resin manufacturers, as well as the research community studying viral purifications, has shifted to designing novel materials with improved pore accessibility for larger particles. These efforts have culminated in extensive studies on the use of highly convective materials such as membranes, monoliths and nanofibres as adsorbers.

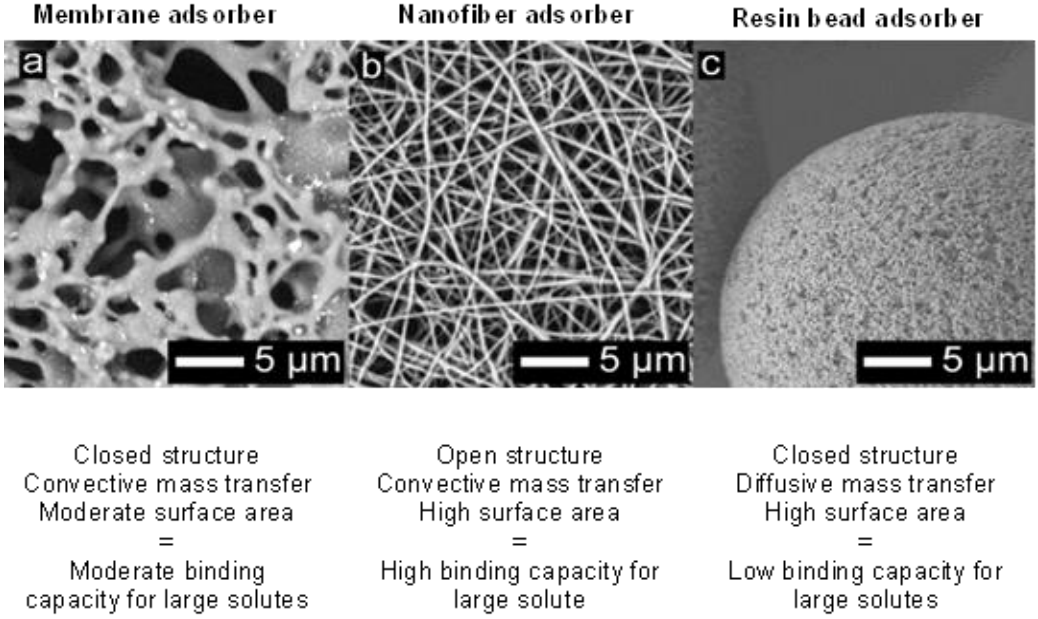

Figure 2-6 Porous architectures of membranes and nanofiber based adsorbent compared to bead based adsorbents. Images were reused with permission from Dods *et al.*, (2015).

2.3.2.3.1 Membrane Adsorbers

Membrane adsorbers have been tested extensively for viral purifications. Peixoto *et al.*,(2008) have reported a 62% step recovery for AdV purification using sartobind ion exchange membranes. It has been suggested that optimal ligand density for efficient binding of the viral vectors is much lower than the ligand density on the commercial membrane adsorbers and use of lower ligand density can increase recovery by 20 % (Nestola *et al.*, 2014c). Irregularity in the pore size distribution of membranes has been reported to affect membrane performance such as sharpness of breakthrough curve, elution peak volume and binding capacity for large solutes (Wickramasinghe *et al.*, 2006).

2.3.2.3.2 Monoliths

Monoliths resemble membranes in the porous architecture but can tolerate higher flow rates without affecting the binding capacities. Monoliths have a higher thickness (few mm to few cms) of the continuous stationary bed. Microscopically, monoliths are micro-granular structures unlike membranes with mesh-like structure, but both have interconnected channels of 0.5 to 1 um width. For membrane chromatography modules, multiple membranes are usually stacked which can result in inefficient flow distribution. Monoliths are continuous materials (no stacking) and are reported to have sharper breakthrough curves and higher binding capacities than membrane adsorbers.

Monoliths have been used for purification of VLPs (Burden *et al.*, 2012). Recovery as low as 6% (Wu *et al.*, 2016) and15-18 % (Zaveckas *et al.*, 2015) for some VLPs have been reported when purified using monoliths. Wu *et al.*,(2016) have speculated entrapment of the VLPs in the initial denser layer of the material in a monolithic bed resulting in significant loss of particles when compared with a gigaporous resin. Segura *et al.,* (2012) reported a 58-69% step recovery of canine Adenovirus in monolith based cation exchange chromatography. Almost 100 % particle recovery was reported for Adenovirus purification using bio-based monoliths (Fernandes *et al.*, 2015) but it was not clear if it was because of different material of monoliths or the structure of the monolith. Recently, application of monoliths for purification of vaccinia viruses has been reported (Vincent *et al.*, 2017).

2.3.2.3.3 Nanofibres

Application of nanofibres has been more recent compared to membranes and monoliths. Nanofibers are non-woven fibres of nanometre diameters formed into a random mesh using electrospinning fabrication technique. Nanofibers not only have the robustness of monoliths by offering high flow rates due to large inter-fibre open spaces but also higher specific surface area compared to both monoliths and membranes (Dods *et al.*, 2015). Hardick *et al.*, (2013) described a method for synthesis of DEAE functionalised cellulose nanofibers and reported significantly higher productivity for nanofiber compared to the commercial resin (8 times) and membrane adsorber (2 times) with the similar functional group. Use of the functionalised chitosan nanofibers for high log removals of waterborne viruses from water has been published (Mi and Heldt, 2014). So far no application of nanofiber-based adsorbents for gene therapy viral vectors has been formally reported in the published literature, but active research is underway on such applications (Ruscic *et al.*, 2017). Highly open structure of the nanofibers can potentially reduce polarisation and physical fouling effects observed with membranes and monolith based absorbers.

Broadly all of these materials could be classified as membranes. Additional benefits of these materials are the ease of scalability (often linear unlike column chromatography), robust performance at high flow rates (low-pressure drop), and minimal pre-use preparations such as packing and validation as required for the resins. Such benefits offer advantages in process design and overall productivity.

2.3.2.4 Non-chromatography processes

Purification of viral particles from protein and nucleic acid impurities has been studied for newer techniques like partitioning in aqueous two-phase systems (ATPS). ATPS separate molecules into two different immiscible aqueous phases in contact by differential partitioning of the molecules. Loss of particles as high as 60-72% for Adenovirus (Braas *et al.*, 2000), 33-45% (Luechau *et al.*, 2011) and around 35 % for parvoviruses, similar to AAV, (Vijayaragavan *et al.*, 2014, Ladd Effio *et al.*, 2015) have been published. Such high losses of viral particles in ATPS are attributed to the localisation of the particles at the interface of the two aqueous phases, which is often difficult to recover. Other processes such as ultrafiltration have been widely used for viral vector purifications often with high recoveries. However, at large scales, ultrafiltration has primarily been used for concentration and buffer exchange steps, not for high-resolution separation. A detailed review of these processes is given in the next section of this chapter.

General findings from this literature review are summarised as below:

Ultracentrifugation	**Chromatography**	**Non-chromatography**
• Can separate empty and mature particles (very high resolution) • Shear damage to the virus particles • Long and labourius procedure (>12 hours) • Difficult to scale up	• High resolution separation and scalable • Low particle binding capacities(diffusional limitations with resins due to narrow pores) • Virus and serotype specific methods (lack of platform affinity chromatography) • Monoliths, membranes and nanofibers are the emerging adsorber materials.	• **Ultrafiltration** • High recoveries • Low resolution • Shear exposure • Traditional polymeric membranes used. • **Aqueous two phase systems** • Poor recoveries due to the losses at the interface between two phases

Figure 2-7 A summary of the literature findings on key purification tools used for purification of viral vectors and associated challenges.

2.4 Membrane-based processes

A membrane can be defined as a thin and porous barrier between two fluids which allow selective transport of one or more components across the barrier while retaining other components behind the barrier. Most common mode of selective transport is exclusion or inclusion of solutes by the size of the solute with respect to the size of the pores.

Membranes are used for a variety of unit operations in the biopharmaceutical industry. Various applications of membranes in a typical bioprocess train includes:

- Clarification of homogenised harvested feed **(Depth filtration)**
- Separation of cells and supernatant **(Microfiltration)**
- The concentration of clarified feed/output of the previous operation for subsequent unit operation such as chromatography **(Ultrafiltration)**
- Buffer exchange of a feed or load to pre-condition before subsequent unit operation **(Ultrafiltration)**
- Removal of impurities from the feed **(Ultrafiltration)**
- Removal of contaminant viruses from the product **(Virus filtration/ Nanofiltration)**
- Removal of any contaminant microbes before fill and finish of final drug product **(Sterile filtration)**

All of the above applications of membranes can be summarised as filtration processes. A typical downstream processing train for biologics includes most of these filtration processes if not all. Membrane chromatography uses ligand-functionalised membranes called membrane adsorber used to bind proteins or impurities. Membrane adsorbers have been discussed in a previous section (2.3.2.3.1) of this chapter and are typically not included as filtration processes.

The focus of subsequent sections will be on the classification of the filtration processes, type of membranes and membrane structure, mechanisms of filtrations including factors affecting the performance of filtration processes, phenomenon observed during filtration processes such as fouling, concentration polarisation, separation etc. and finally on the reported literature on the applications in viral vector separations. For detailed information on membrane technology used in bioprocessing, a detailed review published by vanReis and Zydney (2007) can be referred.

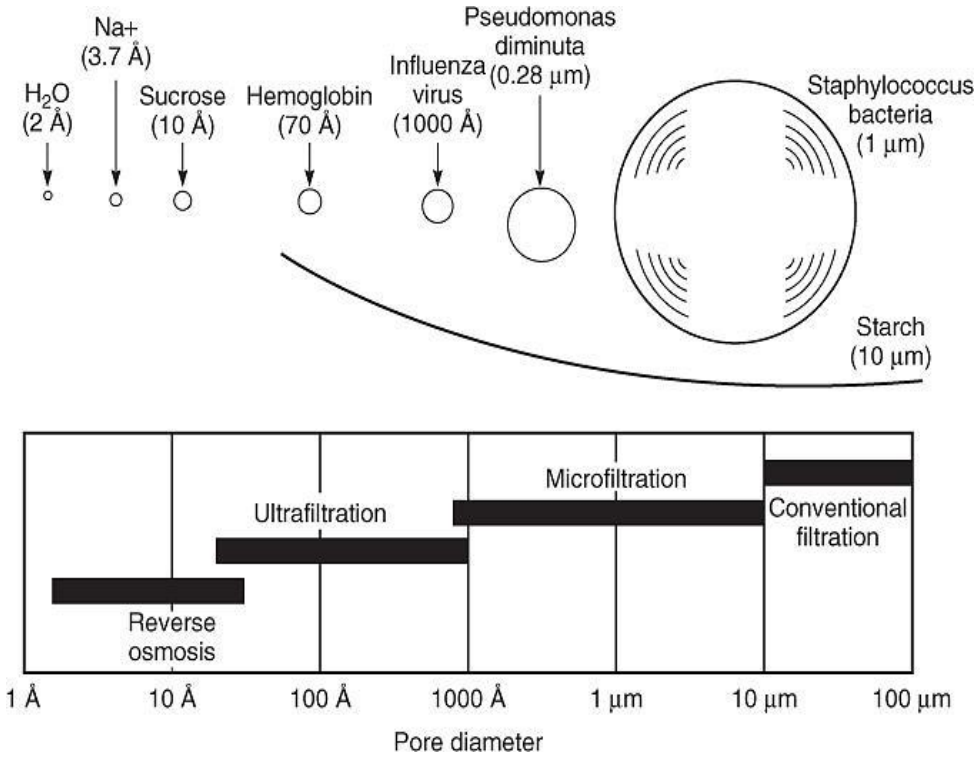

Figure 2-8 Variety of solutes and the range of membrane pore sizes used in corresponding membrane processes. Image reproduced with permission from Baker (2012).

Figure 2-8 shows the classification of various filtration processes with respect to the particle size and average pore size of the membranes used. The filtration processes can be categorised broadly into two categories by the size of retained species. The first category includes microfiltration, depth filtration and sterile filtration which are intended to separate large particles (above 0.2 μm) such as cells and cell debris which as complex assemblies of thousands of molecules. Depending upon membrane pore structure and mode of operation, the membranes or filters used these processes can retain these particles inside the porous structure or above the porous structure. The retention mechanism is size-based as well as adsorptive, especially in the depth filtration.

The second category includes those filtration processes where solutes to be retained or removed are molecules or less complex molecular assemblies than cells. These molecules can be water, proteins, salts, nucleic acids and viruses. Ultrafiltration, nano-filtration, virus filtration processes and reverse osmosis are processes where separations are at the molecular level. Typically separation in ultrafiltration membrane occurs at membrane surface or in the active layer of the membranes. However, with virus filtration membranes, retention of the viruses occurs inside membrane bed similar to that observed in the depth filtration. Microfiltration and ultrafiltration membranes usually retain solutes at the surface and can be termed as screen filters (Cheryan, 1998).

2.4.1 Fundamentals of the filtration process

All filtration processes are driven by an external driving force acting upon fluid being pushed or pulled through a static membrane. In general, filtration processes are carried out either at constant transmembrane pressure or constant filtrate flux. Solvent transport across the membrane is given by the filtrate flux across, described by a simplified equation of Darcy's law as below:

$$J_v = \frac{\Delta P}{R_t \mu}$$

where J_v refers to the filtrate flux across the membrane and can be calculated by dividing the volume of the filtrate by product of the membrane area and the time taken for filtration, ΔP is the transmembrane pressure (TMP) or applied pressure across the membrane, *A* is the active filtration area, R_t is total resistance incurred by the fluid and μ is the viscosity of the fluid. Total resistance is the sum of the hydraulic resistance of the membrane material and additional resistances encountered in filtration processes.

2.4.1.1 Goal and performance of a filtration process

Filtration processes are used to separate different components of a feed, merely concentrate a feed or to replace the buffer in the feed. Separation in ultrafiltration processes is often termed as fractionation. Performance of filtration processes is described as filterability of the feed and separation performance of the membrane. Filterability is studied to evaluate the impact of phenomena such as fouling, concentration polarisation and osmotic pressure on the membrane. These phenomena can also impact the ability of the membrane to separate two components. Properties of feed influence both filterability and separation performance of a filtration process, membrane and the way filtration are carried out. Significant parameters of feed, membrane and filtration operation are outlined in **Figure 2-9**. The figure also outlines the parameters monitored to measure the performance of the filtration

Parameters such as capacity, processing time and hydraulic permeability are universally measured for all filtration processes. The capacity of the membrane defined as the volume of feed filtered per unit area of membrane is often established at a minimum transmission or flux decline through the membrane. Impact of fouling on the membrane is assessed by measurement of the loss of the hydraulic permeability of the membrane after filtration. Cleaning efficiency of a cleaning method is established by its ability to reverse the loss of hydraulic permeability. Factors such concentration and viscosity of the feed and hydraulic permeability of the membrane will have a direct impact on filtrate flow rate through the membrane and hence the processing times. Processing conditions such as transmembrane pressure, feed flow rate, cross flow rate and choice of modules can alter the fouling thus affecting filtrate flow,

permeability loss of membrane and cleaning requirement. Throughout the filtration run, flux through the membrane is calculated by measuring the volume of filtrate collected. Mechanism of flux decline is deduced from the shape of the flux decline curve. Transmission of different solutes into filtrate solution is measured in terms of sieving coefficients. Sieving coefficients are obtained by normalising the solute concentration in filtrate to that in the initial feed solution. These parameters are studied during process design and monitored for consistent processing of a designed process.

Yield and purity of the product to be retained or passed through the membrane are essential parameters for separation performance. Separation factor or selectivity of the membrane is obtained as the ratio of sieving coefficients of smaller solute to large solute. For fractionations, purification factor (ratio of the yield of product to that of impurity) and final purity of solution is used. Ideal membrane for fractionation should completely retain one component and pass through another one. Membrane morphology and pore size distribution are critical for such fractionation. Hence the selection of a suitable membrane is crucial. Some of these factors are discussed in detail in the next sections.

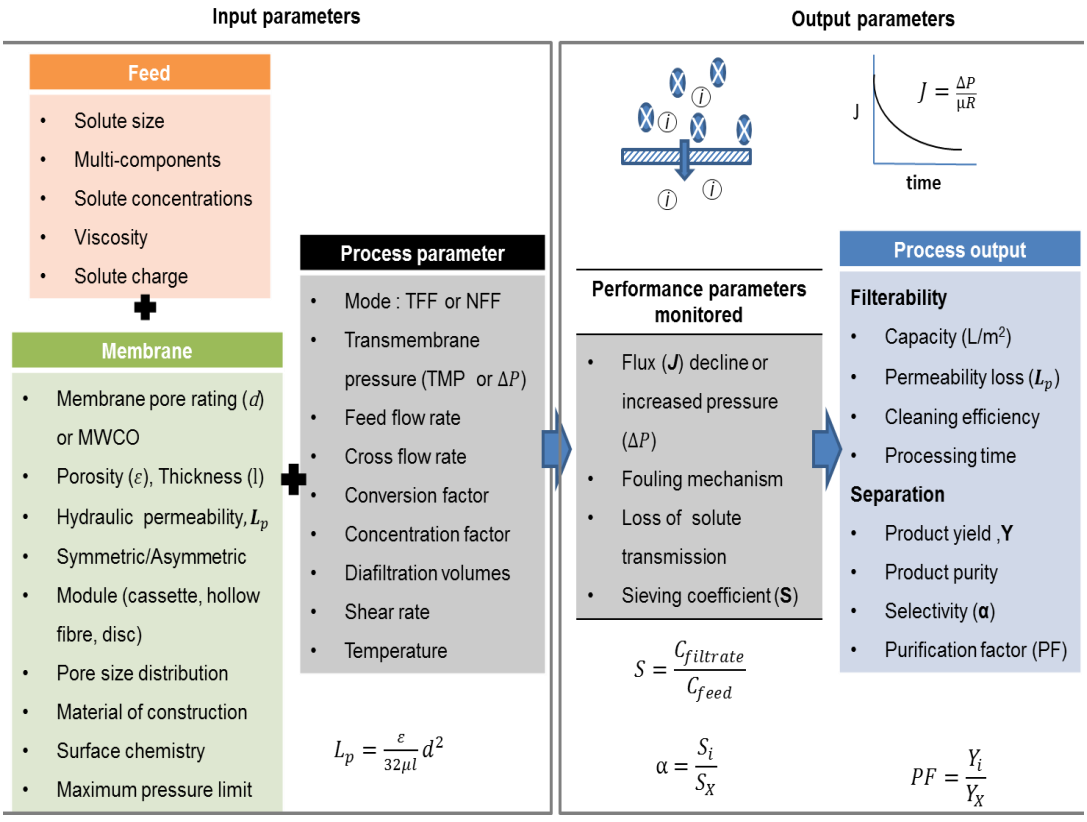

Figure 2-9 Parameters related to membranes, feed solution and processing conditions which impact performance of an ultrafiltration process.

Performance of the ultrafiltration process depends upon properties of feed, membrane and operating conditions of the process. Equation for sieving coefficient, selectivity and purification factor is explained with respect to separation of two solutes (X and i).

2.4.2 Phenomena affecting the performance of the filtration processes

2.4.2.1. Membrane fouling

Membrane fouling is the result of deposition or interaction of the solutes or suspended solids in the feed being processed in a filtration operation with membrane material. Fouling can either add additional resistance to the convective flow or reduce the number of open pores or effective pore diameter available for the solvent flow. For constant transmembrane pressure operation, fouling manifests in the form of a decline in the filtrate flux. For constant flux operations, fouling results in increased transmembrane pressure required to maintain the flux.

Fouling can alter the separation performance of the membrane and results in loss of the hydraulic permeability of the membrane. Regeneration of the permeability requires harsher cleaning regime depending upon the nature or foulant and compatibility of the membrane material with the cleaning agent. Protein fouled membranes are often cleaned using highly alkaline solutions, sodium hypochlorite or protein degrading enzyme solutions. Such cleaning regime has been known to result in ageing of the membrane thus limiting the number of reuse. Control of fouling is thus necessary for consistent and repeated membrane operation, and remedial action often depends upon the mechanism of the fouling identified.

2.4.2.1.1 Mechanism of fouling

Generally, four fundamental mechanisms of the fouling have been proposed. Mathematical models and expression have been well defined. A majority of these mechanisms have been proposed for microfiltration or sterile filtration membranes (Boyd and Zydney, 1998, Ho and Zydney, 2001, Kelly and Zydney, 1997, Velasco *et al.*, 2003, Zydney and Ho, 2003). Standard blocking model is based on the reduction of the internal pore diameter due to deposition of the fouling solute on pore walls and occurs when particles are much smaller than the pore diameter. Complete blocking model assumes that every particle arriving at membrane surface plugs the pore entrance thus reducing the number of open pores over time. Blocked pores do not participate in the fluid flow. The intermediate blocking model assumes that only a portion of particles approaching the membrane surface will directly plug the pores and other particles only participate in partial blockage. Both complete blocking and intermediate blocking models attempt to calculate the area of membrane available for flow. In cake filtration, a resistant layer of the particle is deposited on the membrane surface and thickness of the layer increases over time without a direct plugging of pores. **Figure 2-10** gives a graphical representation of these mechanisms.

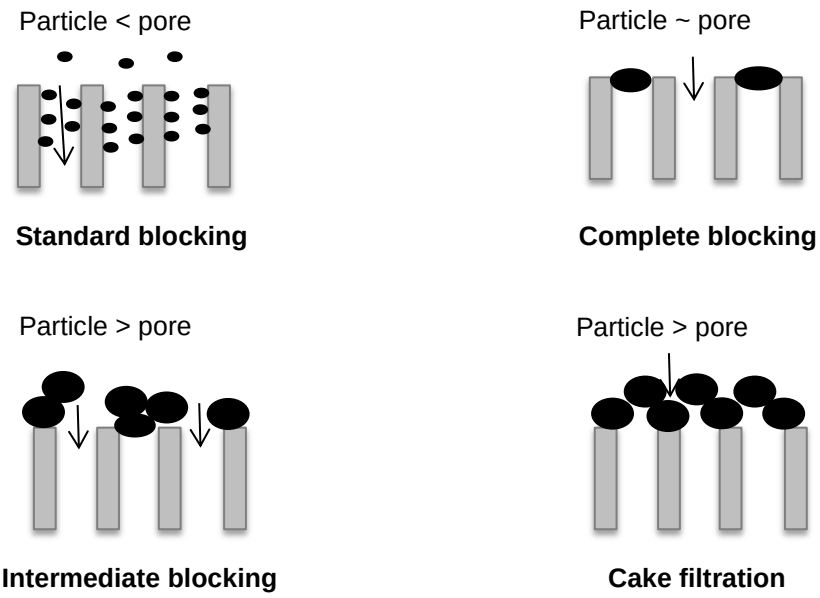

Figure 2-10 Illustration of the fundamental mechanisms of fouling in membranes

Mechanism	Mathematical expression for filtrate volume (V)
Standard blocking (SB)	$V = \left(\frac{1}{J_O t} + \frac{K_s}{2}\right)^{-1}$
Complete blocking (CB)	$V = \frac{J_O}{K_b}\left(1 - exp(-K_b t)\right)$
Intermediate blocking (IB)	$V = \frac{1}{K_i} ln(1 + K_i J_o t)$
Cake filtration (CF)	$V = \frac{1}{K_c J_o}\left(\sqrt{(1 + 2K_c J_O^2 t)} - 1\right)$

Table 2-2 Mathematical expression of fundamental mechanisms of membrane fouling.

A mechanism is identified to be dominant mechanism by fitting these expressions to experimental data (volume filtered, V (m^3/m^2); time, t (s) and initial flux, $J_{o,}$ (m/s)). K_x represents fouling constants for respective models. Expressions were described by Bolton et al., (2006) for constant pressure filtrations. Volume filtered is normalised to the membrane area.

These models as semi-empirical and assume that only a single mechanism is responsible for the fouling. Simplified mathematical expression, as shown in **Table 2-2** for different mechanisms of fouling relating volume of the filtration or pressure across the membrane with time and initial membrane permeability has been established. Complex mathematical expressions combining various fundamental mechanisms in sequence or concurrently have also been published (Bolton *et al.*, 2006, Ho and Zydney, 2000, Palacio *et al.*, 2002). Models accommodating protein adsorption along with classical pore plugging have also been elaborated assuming zero order kinetics of adsorption on pore walls. A drawback of these mechanisms is that they depend on the statistical fitting of the data to the mathematical expressions. Theoretically, initial flux through the membrane can also be predicted by these expressions but can result in overfitting of the data, resulting in unrealistic values for initial flux which otherwise can be measured experimentally. Bolton *et al.*, (2006) have developed simplified expressions for these models with single parameters by providing experimentally measured initial flux. These expressions are also numerically simpler to implement than those developed previously (Ho and Zydney, 1999, Ho and Zydney, 2000) where details of feed concentration, pore density, pore diameter, membrane thickness etc. were required.

2.4.2.2 Osmotic pressure

Another contributing factor for reduced flux through a membrane is osmotic pressure across the membrane system. Separation of the solute above the membrane surface and a low solute concentration solution across the membrane can create the osmotic pressure. Osmotic pressure will tend to force the solvent in reverse direction. Thus osmotic pressure exerts itself in the direction opposite to the applied transmembrane pressure **(see Figure 2-11**). This results in a reduced effective transmembrane pressure across the membrane and consequently reduced flux. For monoclonal antibodies, significant osmotic pressures are observed at concentrations above 20 g/L in the feed solutions. Osmotic pressure depends upon intermolecular interactions among proteins, and solvent molecules thus can change with temperature, ionic environment (salt concentration and pH), concentration and nature of the protein (Binabaji *et al.*, 2014) dramatically.

2.4.2.3 Concentration polarisation

Concentration polarisation is the reversible build-up of entirely or partially retained solute near the membrane surface due to the balance of convective transport of the solute to the membrane surface and back-transport of the solute from membrane surface to the bulk solution (**see Figure 2-11**). A weaker back transport of solute results in high polarisation near the membrane surface and is controlled by the diffusivity of the solute and mass transfer capabilities of the module. The build-up results in additional resistance to convective flow thus decreasing the flux through the membrane. Additionally, the polarised layer can be less permeable to the smaller impurities thus reducing their transmission or removal from the feed. An unintended consequence of the concentration polarisation is leakage of the polarising solute across the membrane thus resulting in loss of the solute in the filtrate (Narsaiah and Agarwal, 2007). So in a fractionation application, concentration polarisation can result in low yields of retained product and loss of separation performance as the transmission of impurities will also decrease.

Concentration polarisation is a pressure dependent and reversible phenomenon and exists as long as the driving force, i.e. the transmembrane pressure is applied. A fundamental difference, thus, between fouling driven flux decline and that due to concentration polarisation is that membrane permeability can be recovered as soon as the driving force is removed (Porter, 1972). Flux decline observed with concentration polarisation especially for a completely or significantly retained solute is not result of membrane fouling unless the concentration of solute near membrane results in solute-solute or solute-membrane interactions leading to another mode of fouling such as cake formation due to precipitation of the solute with low solubility.

Mathematical models have been developed for concentration polarisation by assuming a stagnant film of solute above membranes surface alone (Zydney, 1997, Johnston *et al.*, 2001) or in combination with osmotic pressure model (Tandon *et al.*, 1994). It has been suggested to run ultrafiltration at constant wall concentrations by a feedback control on transmembrane pressure or the filtrate flux designed using the mathematical models developed for concentration polarisation (van Reis *et al.*, 1997). Such an approach can ensure greater predictability in the performance of the ultrafiltration operation.

Concentration polarisation can be limited by changing the processing conditions. High membrane permeability, high flux or transmembrane pressure can increase the polarisation as the driving force pushing solute molecules towards the membrane will be high. Back transport of the solute from the polarised region to the bulk solution is diffusive. Thus concentration polarisation is challenging for large macromolecular solutes which have low diffusivity. Membrane module and cross flow over the membrane surface can aid in the back transport of the solute to alleviate the concentration polarisation to some extent.

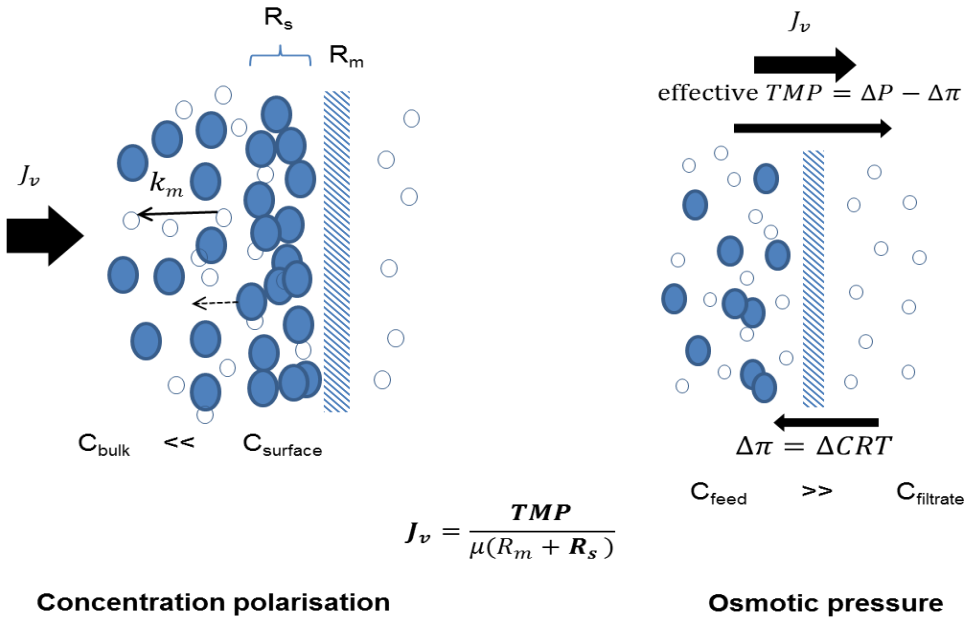

Figure 2-11 Illustration showing concentration polarisation and osmotic pressure and how it affects filtrate flux (J_v) and effective trans-membrane pressure (TMP).

R_m and R_s represent resistance to the convection offered by membrane itself and fouling or concentration polarisation respectively. The concentrations of solute at various locations are represented by $C_{subscript}$. Applied trans-membrane pressure and osmotic pressure are represented by ΔP and ΔΠ respectively.

Fouling, concentration polarisation and osmotic pressure poses significant challenges to ultrafiltration processes by affecting the filterability of a feed, capacity of the membrane and selectivity of the membrane. So these phenomena must be studied in detail, and appropriate remediation strategies should be devised for any particular feed. This involves identifying the dominant mechanism of flux decline, its impact and optimisation of the processing conditions such as transmembrane pressure, cross-flow rate and cleaning strategy to reduce their impact. Following section will emphasise upon impact of properties of membranes, feed and operating conditions on these phenomena.

2.4.3 Impact of membrane and feed properties on process performance

2.4.3.1 Membrane architecture

Membranes can be categorised as symmetric or asymmetric membranes based on the uniformity of the porous morphology across the membrane thickness. Symmetric membranes have a uniform porous network (with respect to pore size, porosity and interconnectivity) across the membrane thickness. Asymmetric membranes usually have a thin and tighter layer of smaller pores called the active layer, or skin side and an underlying layer of larger pores called the support layer. Support layer itself can have a gradient of pore structures from open, highly porous layer to a tighter porous structure at the junction of the skin layer. **Figure 2-12** illustrates two categories of membranes.

The implication of the porous structure of the membranes can be significant depending upon the application of the membrane. Usually, asymmetrical membranes are used more commonly in the bioprocesses. Sterile filtration, microfiltration and ultrafiltration membranes are operated with feed facing skin side. Virus filtration and depth filtrations are usually carried out with skin side down, i.e. more open side of the asymmetric membrane facing the input feed. Transmission (or sieving) of the solutes can be significantly altered depending on which side of the membrane faces the feed solution (Bakhshayeshi *et al.*, 2011a, Syedain *et al.*, 2006).

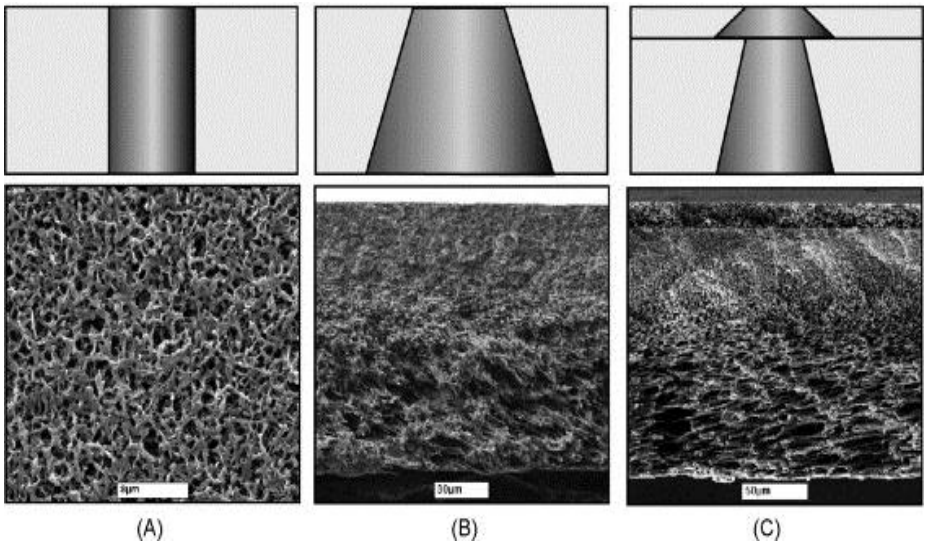

Figure 2-12 Symmetric (A) and asymmetric membranes (B and C): morphology of the porous structure of two membrane types as observed with electron microscopy (Source: van Reis and Zydney, 2007).

2.4.3.2 Membrane ratings

Membranes are rated for their ability to screen or exclude a particle of a specific size to a specified extent. Such ratings are called nominal ratings. Usually, microfiltration and sterile filtration membranes are rated by a bacterial challenge test. These membranes are rated in terms of physical size (in μm) of the particles retained by the membranes to a specified extent. Ultrafiltration membranes are often rated in terms of molecular weight cut off (MWCO) limits, which are the molecular weight of the solute that would be retained by the membrane more than 90 or 99%. Such ratings are assigned by performing a dextran sieving test with a mixture of dextran of varying molecular weights filtered through the membrane at almost no polarisation. These ratings are however merely indicative for membrane selection and do not predict membrane performance for any actual feed. Further, the standard operating procedure for such ratings can vary between manufacturers (Mulherkar and van Reis, 2004). Mehta and Zydney (2005) have put forward a selectivity permeability trade-off plot with a model protein solute as an alternative method to assess and compare performances of different membranes.

2.4.3.3 Membrane material

A majority of membranes used in bioprocess applications are polymeric especially made of low protein binding materials such as polyethersulfone (PES) and regenerated cellulose. Non-specific binding to the membrane surface can result in fouling as well as yield loss of the product. The implication of the selection of appropriate material is highly significant for feeds with very low protein concentrations. Apart from size exclusion, electrostatic exclusion of solutes has also been observed in charged membranes. Altering the ionic environment around the solutes such as salt concentrations or pH of the feed can affect the fouling (Martinez *et al.*, 2000, Miao *et al.*, 2017) and separation performance (Millesime *et al.*, 1996, Shukla *et al.*, 2000, Sorci *et al.*, 2013). Such processes have been classified as high-performance tangential flow filtrations (HPTFF) which are capable of separating close sized molecules such as product variants and can achieve higher selectivity than conventional ultrafiltration.

2.4.3.4 Membrane module

Commercial membranes are available in a variety of formats such as circular discs, cassettes, spiral and hollow fibre modules with cassettes being used more commonly. Module designs such as cassette include turbulence promoting screen below and above the membrane surface. Selection of appropriate screen can help reduce concentration polarisation and improve filterability of a feed (Lutz *et al.*, 2017).

2.4.4 Impact of operating conditions on process performance

2.4.4.1 Mode of operation

Filtration processes can be operated in two modes, Normal flow filtration (NFF) and Tangential flow filtration (TFF). Feed is applied perpendicularly or normal to the membrane surface in NFF. In TFF, the feed is applied parallel to the membrane surface along with the transmembrane pressure pushing the feed towards the membrane (see **Figure 2-13**). Thus, the feed hits the membrane at an angle. TFF mode of operation aids in the back-transport of the solutes and prevents plugging of pores. Thus TFF mode helps to reduce polarisation and can increase the capacity of the filtration process. Membrane capsules and stirred cells are used to perform NFF. NFF operations are typically batch operation. Sterile filtration, virus filtration and depth filtration are usually carried out in NFF mode. Cassettes and hollow fibre modules are commonly used for TFF. Ultrafiltration and microfiltration applications are typically carried out in TFF mode.

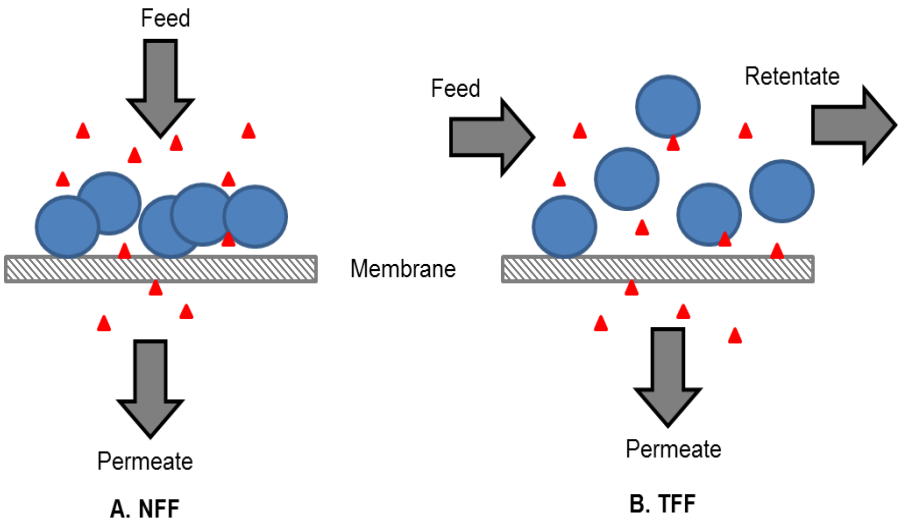

Figure 2-13 Two modes of filtrations: Normal flow filtration (NFF) and Tangential flow filtrations (TFF).

Cross flow helps to clean membrane surface by sweeping off the large solutes from depositing on the membranes.

2.4.4.2 Selection of the operating conditions

Transmembrane pressure can affect fouling and concentration polarisation. In TFF mode, the feed flow rate and cross-flow velocity are optimised for a particular feed. Cross-flow velocity can impact concentration polarisation, as well as thickness and mass of fouling layer (Choi *et al.*, 2005), and in conjunction with TMP can change retention of solutes (Pradanos *et al.*, 1994). For the stirred cell, cross-flow is controlled by stirring speed though is difficult to be quantified in terms of fluid velocity. With feeds containing large solutes, concentration polarisation can lead

to a pressure-independent flux after a certain transmembrane pressure. Operating at fluxes below the critical flux is thus crucial.

2.4.4.3 Impact of filtration modules

Cassettes and hollow fibre modules are used in cross-flow filtration systems and are the preferred systems for large-scale operations due to ease of the scale up. Disc membranes can only be used in stirred cell modules. Mass transfer properties of cross-flow filtration modules are superior compared to that of the stirred cells which result in higher polarisation in the later. Becht *et al.* (2008) have demonstrated significantly higher protein rejection and filtrate fluxes for filtration of serum albumin through a 50 kDa membrane when stirred cell and cross flow setups were compared. However, stirred cells are used more commonly for characterisation studies or comparison of membranes as they have uniform mass transfer characteristics across the membrane surface. Hollow fibre and cassette modules can have a significant pressure drop across the length of the membrane and axial variation of the transmembrane pressure resulting in a module with zones of different membrane performance (Bakhshayeshi *et al.*, 2011b). Such variations need to be accounted for when studying overall separation performance and scale up an ultrafiltration process. Module shear can also impact the activity of the shear-sensitive protein.

2.4.4.4 Constant flux and constant pressure operation

Constant transmembrane pressure ensures that a constant force is applied to the fluid being pushed or pulled across the membrane. However, as the filtration proceeds, resistance to the fluid increases due to various reasons and hence flow rate across the membrane decreases. Here, the filtration process is limited by output flow rate at a particular transmembrane pressure. Constant filtrate flux mode, on the other hand, maintains the same output flow rate through the membrane and does not control the transmembrane pressure. Resistance to the fluid flow increases due to similar reasons but filtration system responds to increased resistance by increasing the transmembrane pressure to maintain the same output flow rate. Such a process is limited by maximum pressure that will be tolerable to the membrane without damaging the membrane.

2.4.4.5 Concentration and diafiltration

UF processes for concentration are optimised for fold concentration to be achieved without causing aggregation of the product. Diafiltration processes are optimised for the number of diavolumes (buffer volume normalised to retentate volume) for maximal removal of smaller solutes (buffer components or impurities) as well as shear damage to the product.

2.4.5 Application of ultrafiltration in viral vector processing

Using membranes with pore sizes similar to virus particles will result in sharper loss of permeate flux and possible entrapment of virus particles in the pores (Grzenia *et al.*, 2008, Czermak *et al.*, 2008, Grzenia *et al.*, 2006). Impact of the cell growth media component can also influence the flux performance of the membranes. It was demonstrated that virus feed with serum-free media has a lower flux compared to the virus feed with serum-rich media (Grzenia *et al.*, 2006). This effect was attributed to an increase in total host cell proteins secreted in cultures with serum-free media as opposed to serum containing media.

High-performance tangential flow filtration (HPTFF) was reported to result in lower but stable permeate flux compared to regular tangential flow filtration for small sized viruses, densonucleosisvirus (AeDNV) as a model system of adeno-associated viruses (Grzenia *et al.*, 2006, Grzenia *et al.*, 2008). One study compared 30, 50, 100 and 300 kDa membranes in TFF setup for 10 fold concentration of AeDNV (26 nm diameter) and reported loss of virus particles in permeate for 300 kDa and lower relative flux (normalized to water flux) for 300 kDa membrane compared to 100 kDa membrane (Czermak *et al.*, 2008). HPTFF has also been demonstrated to increase recoveries of Adenovirus from 40-60 % to 80 % in hollow fibre based module of 0.05 µm pore ratings (Weggeman, 2013). TMP in HPTFF mode was around 0.17 bar, and hence low filtrate fluxes of 10-15 LMH were obtained during this ultrafiltration. The author also reported higher purity in HPTFF mode.

A comprehensive study comparing different membranes (materials and format) for Adenovirus concentration and diafiltration application has demonstrated 50-90 % host cell protein removal while retaining more than 75% infective titre with most of the membranes (Nestola *et al.*, 2014a). Fluxes for all the membranes, however, remained below 100 LMH for processing of approximately 20 L/m^2 of Adenovirus feed. Authors reported a regenerate cellulose based membrane of ~500 kDa MWCO to result in complete recovery of infectious particles. Authors showed that PES membranes had lower particle recoveries (23-58%) as opposed to RC based membranes where particle recoveries ranged from 69 to 93 % after 10-fold concentration and five diavolumes of diafiltration. Losses were attributed to higher MWCO for PES membranes (around 1000 kDa).

Flux values of less than 40 LMH were also reported for Adenovirus concentration for at least five-fold using membranes of 0.05 µm, 300 and 400 kDa ratings in hollow fibre modules (Subramanian *et al.*, 2005). Constant TMP pressure of 0.5 ± 0.17 bar was used for this study,

and more than 80 % infectious virus particles were reported to be recovered. Average flux for 0.05 µm (50 LMH) was better than 300 and 400 kDa (20 LMH) membranes. Ultrafiltration processes for other viruses have also been published. Limited studies have been published for ultrafiltration of enveloped viruses. One of the studies compared 100 and 300 kDa rated membranes for ultrafiltration of human influenza virus and reported that 300 kDa membrane results in 80 % host cell DNA removal along with 90% removal for HCPs. (Wickramasinghe *et al.*, 2005) Authors also implied that 300 kDa membrane could remove virus fragments. Fluxes for this membrane were reported to be between 40-50 LMH. Peixoto *et al.*,(2008) have reported a loss of Adenovirus yield from 96 % to 42% as membrane rating was increased from 300 to 750 kDa but at the expense of increased process time.

Reduced retention of the virus particles at high TMPs have been reported in a number of published literature and has been in general attributed to the presence of larger pores in the membranes. One study, however, has rejected this explanation and argued that enlargement of pores at higher TMPs to be responsible for the leakage of the viruses in permeate (Arkhangelsky and Gitis, 2008). However, authors did not give any direct evidence of any pore enlargement occurring with TMP increase, though reported an increase in mean pore size of the same membrane with an increase in pressure using polymer probe based evaluation and a method based on hydraulic permeability of the membranes. Authors also argue that the lack of any virus leakage in permeate in a diffusion-driven membrane indirectly supports the hypothesis of enlargement of pores with pressure. One study has reported an increase in recovery of retrovirus particles with an increase in TMP in an ultrafiltration step using 500 kDa membrane (Rodrigues *et al.*, 2007). Authored attributed this observation to the reduced absorbance of virus particles to membranes at higher TMP as other proteins will form a thicker layer preventing adsorption of virus particles as protein removal decreased with increasing TMP.

A detailed summary of the above-discussed literature and their key findings are tabulated in **Table 2-3**. Most of these studies have not studied the mechanisms of fouling associated with observed losses in the flux. These studies have only used conventional polymeric membranes and except a few, were targeted for concentration and buffer exchange application and not for the fractionation. Thus studying membrane-based processes for high-resolution separation is relatively unexplored especially with respect to membrane morphology.

Literature	Virus	Virus Size (nm)	Mode	Module used	Membranes used	Area (m^2)	Scale (L)	Conc. Factor	TMP (bar)	Flux reported (LMH)	Remarks
Wichramasinghe et al, 2005	Human Inf. virus	100	TFF	Cassettes	PES; 100, 300 kDa , 0.1µm	0.02	0.5- 0.6 L	~4	0.4 bar	40-50 (300 kDa)	Membrane with 80 % DNA and 90% HCP removal; reported fractionation of damaged viruses
Negrete et al, 2014	HIV-gag-VLPs	100-300	TFF	Hollow fibres	PES; 500kDa	0.005	0.2 L	~6	1.25 bar	20-30	Various shear conditions and TMPs were screened.
Czermak et al, 2008	AeDNV	26	TFF	Cassettes	PES; 30,50. 100 and 300kDa	0.02	0.45 L	~10	NR	NR	Higher log retention of virus for 100 kDa (~7) compared to 300 kDa (~2). Entrapment of AdV particles in 300 kDa membrane.
Grzneia et al, 2008	AeDNV	26	TFF[1] and HPTFF[2]	Cassettes	PES; 30,50. 100 and 300kDa	0.02	0.45 L	~10	0.18-0.23[1] 0.09-0.2[2] bar	20-30 (300 kDa); 5 (100 kDa) [2]	HPTFF results in transmission of viral fragment through 100 kDa membrane. HPTFF results in more stable flux for 300 kDa.
Nestola et al, 2014	AdV	90-100	TFF	Cassettes, Hollow fibres	Different polymers; 300-1000 kDa	0.02	0.4 L	~10	1.2 bar	20-100	100 % particle recovery using 500 kDa RC membrane with HCP and HC-DNA removal of 71 and 57 % respectively.
Subramanian et al, 2005	AdV	80	TFF	Hollow fibres	300, 400 kDa and 0.05 µm	5.6	240 L	~12-20	0.5 ± 0.17 bar	20-100	Shear induced release of virus from cells during TFF with 80 % recovery.
Weggeman, 2005	AdV	100	HPTFF	Hollow fibres	0.05 µm			5	0.17 bar	10-20	Increased purity and recovery of Adenovirus particles in HPTFF process
Rodrigues et al, 2005	RV		TFF	Hollow fibres	500 kDs	0.003	0.2 L	~11-16	NR	NR	Increase in TMP resulted in improved recovery of virus particles.

Table 2-3 Summary of the reported literature on application of membrane based processes for separations of viral vectors. NR represents not reported. TFF stands for tangential flow filtration.

2.5 Porous anodic alumina (PAA) membranes

Porous anodic alumina (PAA) membranes are a unique category of porous material which has highly ordered porous morphology characterised by self-organised hexagonal cells with cylindrical pores and surrounding aluminium oxide material. PAA membranes exhibit narrow pore size distribution and straight channels compared to the array of pore sizes and tortuous channels in membranes traditionally used in various membrane processes. These traditional membranes included ceramic alumina membranes, polymeric ultrafiltration and microfiltration membranes. It is worth noting that membranes with narrow and uniform pore size have also been produced in the polymeric materials such as polyester and polycarbonates called track-etched membranes. **Figure 2-14** shows the different morphology of top surfaces and pore channels of typical polymeric, track-etched and PAA membranes.

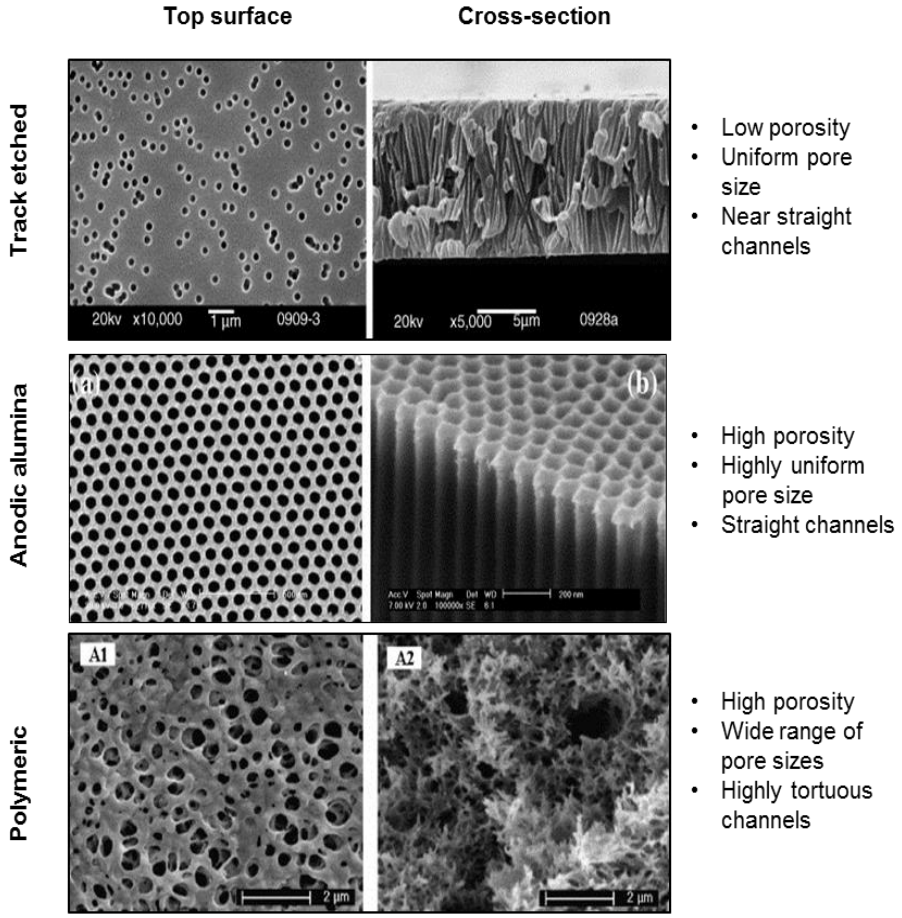

Figure 2-14 Differences in the porous morphology of a typical track-etched[1], conventional polymeric[2] membranes and porous anodic alumina[3] membranes visualised using electron microscopy.

Images were reused with permission from [1]Xie et al., (2005), [2]Mu and Zhao, (2009) and [3]Lei et al., (2007). Notice the highly ordered structure of the anodic alumina membranes with seemingly uniform pore diameter for all pores. Track etched membrane have near uniform pore sizes but larger pores with two pores merged can also be seen.

Porous ordered porous materials with well-arranged pores of uniform size are attractive materials to design new tools and techniques for various applications as they offer greater control of the transport and optical properties. The ability to control molecular transport at nano-scale is a characteristic of highly selective systems such as highly ordered natural membranes in living systems. Ordered porous materials, thus present an opportunity to design membranes with very high selectivity. Conventional polymeric membranes suffer from low selectivity due to broad pore size distribution (Urase *et al.*, 1994, Urase *et al.*, 1996). Track-etched membranes which have narrow pore size distributions and straight channels have been used for such investigations but suffer from low porosity (Ho and Zydney, 1999) and smaller membrane thickness (Stroeve and Ileri, 2011). PAA membranes offer higher porosity and improved ordered isoporous structure compared to the track-etched membranes (Stroeve and Ileri, 2011). Apart from the ordered porous morphology, PAA membranes, upon high-temperature treatment can exhibit superior thermal stability and acid/base resistance (pH 2-10) hence are suitable for high-temperature sterilisation as required in bioprocessing (Lee *et al.*, 2000). Unlike polymeric membranes, inorganic PAA membranes are low extractable materials as they are fabricated without using any monomers, adhesives or plasticisers (GE Healthcare Life Sciences, 2018). All these properties make PAA membranes an interesting material to study for bioseparations.

2.5.1 Fabrication of PAA membranes

Highly ordered porous anodic alumina is fabricated by electrochemical oxidation of high purity aluminium sheets under specific conditions. Electrochemical oxidation of aluminium is also known as anodisation as the aluminium metal acts as an anode in the process. Anodisation has been known to develop a corrosion resistant oxide layer caller barrier layer under normal environmental conditions. This barrier layer is, however, a non-porous layer (Sulka, 2008). Under acidic conditions using mild acids as an electrolyte, anodisation of the aluminium metal results in a porous oxide layer exhibiting self-assembly behaviour to form a regular array of cylindrical pores organised in a honeycomb-like structure. Optimisation of various fabrication parameters such as quality of aluminium sheet, the magnitude of the anodising voltage, choice of electrolyte and choice of etching method has been extensively studied for fine tuning the porous morphology. A typical fabrication process for PAA membranes comprises of three major processing steps starting with pre-treatment of aluminium sheet used as substrate followed by anodisation of the pre-treated sheet to form porous anodic alumina layer and finally detachment of the porous layer from residual sheet to form a free-standing membrane. All three stages are thoroughly discussed in following sub-sections:

2.5.1.1 Pre-treatment of the aluminium substrate

Surface roughness, crystalline structure and the purity of aluminium sheet can also impact the fabrication process (Sulka, 2008). Aluminium sheets of high purity, usually above 99.90% are used for fabrication. Pre-treatment of the aluminium sheet is carried out before the anodisation process, which can include various steps such as annealing, ultra-sonicating and polishing of the sheet. Annealing is carried out by subjecting the metal sheet to high temperature (usually one-third of the melting point of the metal) followed by gradual cooling. Ultra-sonication in organic solvents such as acetone and ethanol is carried out to remove the organic contaminants. Polishing, primarily by electrochemical methods, is carried out to reduce the surface roughness and cavities formed during the mechanical and thermal processing of the metal sheets. Electropolishing by application of 30-50 V voltages on the metal sheet for short duration (5-30 sec) in a solution of perchloric acid and ethanol has been demonstrated to result in remarkably refiner porous structure compared to the non-electropolished samples (Wu *et al.*, 2002).

2.5.1.2 Anodisation of the pre-treated substrate

Anodisation of the aluminium can result in two types of the oxide layers: non-porous barrier-type layer and porous layer depending upon the nature of electrolyte used. Porous oxide layers are formed if acidic electrolytes such as phosphoric, sulfuric, oxalic, chromic, malic, tartaric and citric acids are used. Non-porous layers are formed in neutral electrolytes (pH 5-7). A two-step anodisation process is commonly used for the fabrication of porous anodic alumina membranes (Masuda and Fukuda, 1995, Yuan *et al.*, 2004, Choudhary and Szalai, 2016). **Figure 2-15** A illustrates the two anodisation steps (Lee and Park, 2014) followed by a post-anodisation processing. In the first anodised step, irregular pores are formed (step (i)) on the side of metal sheet exposed to the electrolyte solution with gradual reordering of the pores into a self-ordered array as the oxidation occurs deeper in the sheet thickness. The disordered layer of the porous oxide is then selectively removed by chemical etching (step (ii)) resulting in an aluminium sheet with a textured surface in the form of an array of hemispherical pits. A second anodisation (step (iii)) is then carried out on this textured aluminium sheet using the same conditions as used for the first anodisation step. Pre-texturing creates an array of highly ordered pore nucleation centres which grow perpendicularly during the second anodisation step resulting in straight pore channels. Each anodisation step can take up to 24 hours if anodisation is carried out at lower current density, also known as mild anodisation. Mild anodisation uses lower current densities compared to hard anodisation and can result in more ordered porous structure and higher pore density but as a cost of lower film growth rate of 2 μm/h compared to 50-60 μm/h for hard anodisation (Lee, 2013).

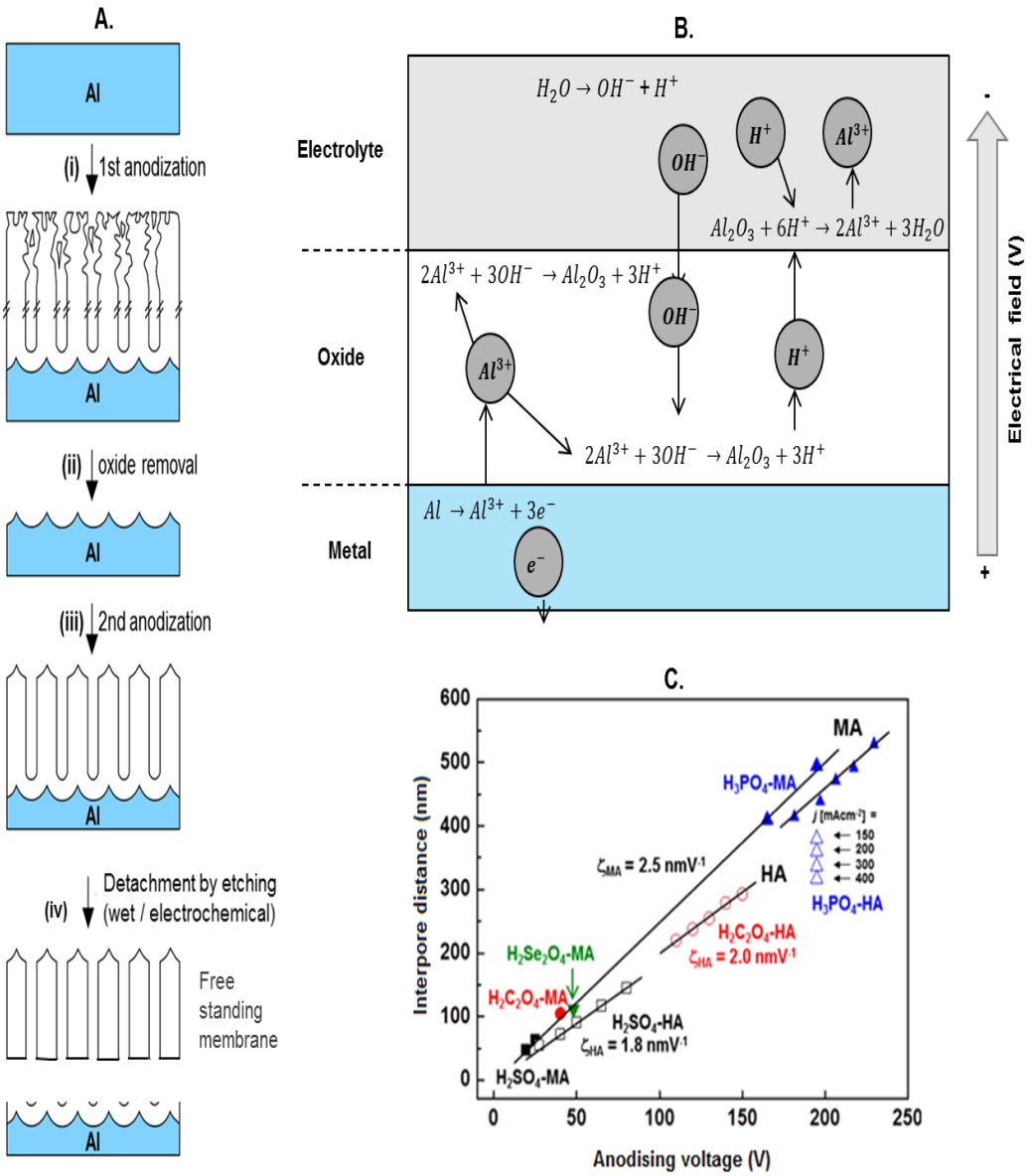

Figure 2-15 Diagrams showing the fabrication of porous anodic alumina membranes using a two-step anodisation method (A), chemical reactions and ion migration during the anodisation process resulting in the formation and dissolution of the oxide layer at different interfaces (B) and the relationship of the anodising voltage and the porous morphology formed using different electrolytes during anodisation.

A. Fabrication process of porous anodic alumina membrane using two-step anodisation method (Lee and Park, 2014) followed by an etching step to remove residual non-anodised metal and barrier oxide layer B. Chemical reactions occurring during anodisation of the aluminium sheet at both interfaces (metal/oxide and oxide/electrolyte) resulting in growth and simultaneous dissolution of alumina (Thamida and Chang, 2002) C. the graph showing a linear relationship between the anodising voltage and the interpore distance for different acidic electrolytes using mild (MA) and hard anodising (HA) condition represented respectively by filled and empty symbols. The slope of the plot is displayed as the proportionality constant (ζ). Symbol shape: square- sulfuric acid, circles- chromic acid, triangle-phosphoric acid and inverted triangles- selenic acid. Images A and C were reprinted and adapted with permission from Lee and Park, 2014. Copyright (2014) American Chemical Society.

The mechanism of the pore formation and growth in the anodisation process is less well understood. It has been suggested that a dynamic equilibrium occurs between the formation and dissolution of the oxide resulting in a porous oxide layer. Migration of the Al^{3+}, OH^- and H^+ ions under the electrical field across the oxide layer is reported to result in different chemical reactions at different interfaces (Thamida and Chang, 2002). **Fig. 2-15 B** shows an illustration of various chemical reactions occurring at metal/oxide and oxide/electrolyte interfaces. Even in acidic electrolytes, initially, a barrier- type layer is formed followed by initiation of pores. Pre-existing ridges on the metal surface and high tensile stress on the initial barrier layer is thought to result in the formation of cracks and pits which are accessible to the electrolyte (Shimizu *et al.*, 1992). As a result, the oxide layer is thinner on the pit surface. Uneven oxide layer thickness results in a local increase in the electrical field on pit surface forming scallop shaped metal/oxide interface. Most widely cited model, the field assisted dissolution model advocates the enhanced dissolution of the oxide layer at the pore base by increased strength of the local electrical field as a result of the concave curvature of pits and high electric field aiding in the breakage of Al-O bonds (O'Sullivan and Wood, 1970). The field-assisted dissolution model asserts that the rate of formation of the oxide at the electrolyte/metal interface in such pits is much lower than the dissolution rate of the oxide resulting in thinning of the oxide layer which is compensated by the oxide formation at the metal/oxide interface leading to the pore growth as a consequence of maintaining a constant thickness of the initial barrier layer. The alternative model, such as flow model proposed by Sheldon *et al.*(2006) argues that the field-assisted dissolution occurs primarily in the initial pore formation stage and the further pore growth is mainly driven by the viscous flow of the oxide material from the base of the pores to the pore walls due to large compressive stress and to maintain a constant initial barrier layer thickness. This model can account for the experimental observations not explained by the field-assisted dissolution model such as the presence of electrolyte anions in porous oxide film by predicting the mobility of anions in the oxide layer and the volume expansion of the porous anodic oxide compared to the oxidised metal.

The strength and duration of the electrical field, generated by the application of external voltage called anodising voltage, is adjusted according to the electrolyte used and the desired pore size, pore interval (also referred as interpore distance) and thickness of the film. **Figure 2-15 C** shows the range of anodising voltages used and measured interpore distances in the porous anodic alumina fabricated using different acidic electrolytes. The choice of the electrolyte can influence the chemical composition of the PAA membranes as the acid anions are known to get incorporated into the oxide during the fabrication process (Pedimonte *et al.*, 2014a, O'Sullivan and Wood, 1970). Incorporated anions can potentially change the reactivity and surface charge

characteristics of the membranes which can be relevant depending upon the intended use of the membranes.

2.5.1.3 Detachment of the porous film from the residual substrate

Following the pore formation in the anodisation process, the alumina oxide is still covered by a barrier oxide layer on the residual aluminium sheet and needs to be detached in order to form a free-standing membrane (see step (iv) of **Figure 2-15 A**). The removal of residual aluminium is achieved by electrochemical etching in strong acids such as hydrochloric or perchloric acid under an operating voltage in the range of 1-5 V. Electrochemical etching will expose the U-shaped pore bottoms formed by the barrier oxide layer. A wet chemical method is then used to open the pores. The method employs exposure of the bottom side of the anodised sheet in solutions of acids such as phosphoric acid, chromic acid and sulfuric acid (Sulka, 2008). The time required for opening of the pores can vary with the thickness of the barrier layer which depends upon the anodisation conditions (Zaraska *et al.*, 2011). Usually, phosphoric, sulfuric and oxalic acids are preferred over malic, citric and tartaric acids as they form thinner barrier layers (Lee and Park, 2014).

Lee and Park (2014) have given a comprehensive review of the anodisation process to synthesise porous anodic alumina templates including the chemical processes involved, kinetics and mechanisms of the pore formation and the fabrication of various pore geometries. It should be noted that the above-described process for the fabrication of the PAA membranes differs significantly from the fabrication process used to prepare the polymeric membranes which involves polymerisation of the residue followed by a phase separation to form porous networks.

2.5.2 Biotechnological applications of PAA membranes

2.5.2.1 Biosensors

A significant share of the reported literature on the applications of porous anodic alumina membranes is in the field of biosensors. Uniform pore size distribution and cylindrical geometry of the nanopores of PAA membranes enables accurate quantification of the transport of solutes and their interactions in pores. Label-free detection of viruses such as Ebola, Hepatitis B and Dengue virus using specific virus DNA (Tsang *et al.*, 2016, Deng and Toh, 2013, Chen *et al.*, 2016) and detection of viruses of different sizes through change in electric impedances across the pores (Chaturvedi *et al.*, 2016) have been published. Capability to study drug-protein interactions by optical reflective spectroscopy (Nemati *et al.*, 2016) and detection of biomarker enzymes on modified nanopores using the similar reflective technique (Nemati *et al.*, 2015) have also been demonstrated.

These studies have stressed on PAA membranes as a template material for low-cost sensors to enable faster discovery of drugs by label-free studying drug-protein interactions and to develop faster and cheaper point-of-care systems for diagnosis of infections. The goal is to develop assays using simple detection methods such as measuring changes in electrical conductivity of the pores or optical rather than expensive and sophisticated methods such as ELISA or PCR based techniques which need labelling molecules such as antibodies and dyes.

2.5.2.2 Bio-separations

Limited applications of PAA membranes have been reported for use as a chromatography medium for bind and elute mode of separations. Functionalised PAA membranes have been demonstrated to be functionalised and used as affinity membranes for removal of bilirubin and haemoglobin from the blood (Shi *et al.*, 2008, Shi *et al.*, 2010). Highly ordered structure of the membrane is cited as a reason for the investigation of PAA membranes for affinity chromatography to achieve sharper breakthrough curves but these studies do not compare other critical performance parameters such as binding capacities with affinity membranes of different architecture. Yamashita *et al.*, (2009) have demonstrated the use of unmodified PAA membranes for separation of nucleosides and nucleotides by the phosphate group of analytes interacting with the membrane material. Such interaction of the phosphate group with anodic alumina material has also been utilised to enrich phospho-peptides for mass spectrometry analysis (Wang *et al.*, 2007).

A majority of studies dealing with the application of PAA membranes in bioprocessing have dealt with filtration based processes. PAA membranes have been evaluated for haemodialysis application and were reported to have 2-3 times larger mass transport of small metabolites like urea compared to polymeric membranes and without loss of albumin protein (Attaluri *et al.*, 2009). Lee and Mattia (2013) had fabricated tubular PAA membranes of sub-20 nm pore diameters with asymmetric and symmetric pore geometry and characterised these membranes for BSA filtration. These tubular membranes were found to be highly retentive to BSA molecules, especially asymmetric membranes.

Similarly, commercial PAA membranes with pore diameter rating of 20 nm (Anopore, Anotec) have been characterised for separations for proteins of different molecular weight (Pradanos *et al.*, 1994, Pradanos *et al.*, 1996). These experiments were however conducted at a very low transmembrane pressure of 0.05 bar and with cross flow present above the membrane surface. Protein with a molecular weight of 270 kDa was reported to be fully retained by the membranes, and cake filtration was found to be the mechanism of fouling by this protein. These experiments, however, did not explore the separation performance of the membrane, i.e. fractionation of the mixture of proteins.

Ultrathin anodic alumina membrane with 20 nm pore diameter has also been reported to be capable of high-resolution separation (selectivity of ~41) of similarly sized proteins, hemoglobulin and serum albumin through charge based mechanism (Osmanbeyoglu *et al.*, 2009). The experiment was however conducted with custom-made membranes and in the diffusion cell. Commercial membrane-based processes, however, are convection based instead of purely diffusive.

Few studies have focused on PAA membranes for virus separations (Moon *et al.*, 2009, Jeon *et al.*, 2014). Moon *et al.*, (2009) have reported higher transmission of bacteriophage empty capsids compared to mature capsids through a PAA membrane with pore sizes smaller than bacteriophage particles under centrifugal filtration setup. Observations were explained by the fragility of the empty capsids enabling them to squeeze through smaller nanopores. Authors, however, did not study the fouling and capacity of the membranes for such viral feed which will be highly relevant for process scale operations. Jeon *et al.*, (2014) have used fabricated hierarchical PAA membranes with large support layer pores and smaller pores in the thin active layer for the enrichment of Hepatitis C virus (HCV) from cell culture and reported higher enrichment of infectious virus particles when compared to ultracentrifugation. Again, this study was also not comprehensive enough to investigate the filtration performance of PAA membranes.

There are no reports published so far on the application of PAA membranes for the purification of viral vectors. It is clear that these membranes offer significant advantages because of their unique morphology. However, a majority of the reported applications of PAA membranes in literature did not use the experimental conditions similar to those present in membrane-based bioprocessing of protein biologics.

2.6 Challenges in studying viral vectors and the need for model systems

Studying viral vectors for process development can be difficult due to a variety of factors

- Stringent containment requirements (biosafety level 2 or above) to ensure appropriate personnel protection from genetically modified and infectious viral vectors
- Longer production time (10-15 days) for mammalian cell cultures used to produce viruses and requirement of the aseptic environment throughout processing
- Variable production titres in cell cultures for viruses and subsequent purification requirement
- Costly raw materials such as serum used for cell culturing
- Complex analytical requirements (Infectivity assay, TEM, NTA, PCR, ELISA etc.)

These factors can be prohibitive for studying processes extensively as they tend to take a long time and consume a significant amount of the resources. Due to this, only a limited number of studies can be conducted in a defined time and space. Further, studies may require purified virus material to study the impact of viral particles without risk of the influence of other non-viral components originating from complex cell cultures. A model system for viral vector can be helpful for some of the studies. An ideal model system shares elemental composition and structural complexity of viral vectors, is easy to prepare in short period, Virus-like particles usually produced in genetically modified yeast-based expression systems can be used as model systems to bypass the requirement of stringent containment as they are not infectious. However, VLPs will need to be produced and purified from yeast cell cultures. Similarity, bacteriophages produced using bacterial cells also have similar limitations.

Synthetic polymer nanobeads coated with proteins have also been used as model systems. An example of efficient use of protein conjugated latex nanobeads as viral mimic was published to assess the impact of protein particle size in binding capacity of monolith based chromatography support targetted for virus purification (Kalashnikova *et al.*, 2007). Similar particles but with fluorescence tags have been used to study virus retention mechanism of virus removal filters used in biopharmaceutical manufacturing (Fallahianbijan *et al.*, 2017). Gold nanoparticles have been used as virus mimic to study retention mechanism and pore structure of virus removal filters (Kosiol *et al.*, 2017). Brass *et al.*,(2000) have used inclusion bodies obtained from *E.coli* as surrogate particles for Adenovirus to explore the utility of aqueous two-phase partitioning in viral purifications. These studies show the utility of model particles in studying virus separations in various unit operations where particle size has a significant impact on the design and outcome of the process. In this study, the use of protein nanoparticles formed from the aggregation of protein is proposed as a mimic for virus particles. Further discussion on protein nanoparticles is done in the following section.

2.7 Protein nanoparticles

Entities with dimensions in the range of 10 to 1000 nm, usually a complex assembly of molecules are classified as nanoparticles. Protein nanoparticles are biodegradable complexes synthesised from self-assembly of protein subunits of either single or a combination of multiple proteins. Synthesis of such protein nanoparticles involves the creation of conditions conducive to the self-assembly process followed by chemical modification to the assembled unit to achieve a stable and irreversible unit.

2.7.1 Applications of protein nanoparticles

Majority of the reported application of protein nanoparticles are as drug delivery vehicles because of their high drug loading capacity due to the high surface area, controlled drug release and improved circulation time in the body. Nanoparticles synthesised from human proteins such as serum albumin are preferred as drug carriers over conventional non-protein micro-particles made from synthetic polymer due to human proteins having low toxicity, low immunogenicity and high biodegradability. In fact, a commercial product based on albumin nanoparticles is already in the market (See **Table 2-4** for more information).

Other less extensively studied applications of protein nanoparticles are in the field of novel vaccines, as gene therapy vectors and for functional food. Some of the reported studies are displayed in the table. For vaccines, protein nanoparticles have been used as antigen presenting surfaces to design multi-antigen vaccines. Such vaccines carrying multiple antigens offer protection against multiple diseases or multiple strains of a disease-causing pathogen thus providing comprehensive protection with a single product. Nanoparticles based vaccines also offer an alternative method of vaccine production which is less extensive and laborious than a traditional bioprocessing route involving the production of antigens through fermentation and subsequent purification.

Protein nanoparticles have also been used as non-viral vectors for gene therapy but limited by lack of specificity and low transfection rates. Surface modification of DNA loaded protein nanoparticles has been tried to solve these issues. (Look *et al.*, 2015, Steinhauser *et al.*, 2008) Protein nanoparticles have also been used to create functional foods by using them as carrier systems for bioactive molecules such as vitamins and other metabolites for nutraceutical applications. Specific examples of these applications are outlined in the table.

Application area	Remarks and examples
Drug delivery vehicles	➢ Non-toxic, low immunogenic, biodegradable carriers for small drug molecules (especially hydrophobic drugs) ➢ Drugs such as paclitaxel (Celgene, 2015), doxorubicin (Dreis *et al.*, 2007, Thao le *et al.*, 2016), cyclophosphamide (Gulfam *et al.*, 2012), cis-platin (Zhen *et al.*, 2013) used for cancer treatment have been loaded on protein nanoparticles. ➢ Specific organ targeting of drug conjugated nanoparticles by conjugating cell-penetrating peptides to cross the blood-brain barrier (Lin *et al.*, 2016) or other cell-specific proteins (Thao le *et al.*, 2016) ➢ Marketed chemotherapy product ABRAXANE ®, paclitaxel-loaded 130 nm albumin nanoparticle (Celgene, 2015)
Vaccines	➢ Nanoparticles as highly immunogenic particles due to high antigen density ➢ Improved antigen response to nanoparticles formed with Thiolated protein (Pfs25M) antigen crosslinked to Maleimide modified protein (EPA) compared to antigen alone (Jones *et al.*, 2016) ➢ **Multi-antigen vaccine** (matrix proteins and H1 HA2, H3 HA2 domains) for comprehensive protection from Influenza virus (Deng *et al.*, 2017)
Gene therapy vectors	➢ Albumin nanoparticles with an antisense oligonucleotide against herpes simplex virus conjugated with trastuzumab to target breast cancer cells (Steinhauser *et al.*, 2008)
Functional foods/Nutraceuticals	➢ Encapsulate hydrophobic metabolites and vitamins to increase their bioavailability through foods ➢ Protein nanoparticles loaded with metabolites such as curcumin (Zou *et al.*, 2016) and cholesterol reducing phytosterols (Cao *et al.*, 2016)

Table 2-4 Examples of various applications of protein nanoparticles reported in the literature

2.7.2 Synthesis of protein nanoparticles

Albumin has been the most common protein used in a number of studies studying the synthesis of protein nanoparticles (Galisteo-Gonzalez and Molina-Bolivar, 2014, Langer *et al.*, 2008, Lin *et al.*, 2016, Weber *et al.*, 2000, Anhorn *et al.*, 2008). Other proteins such as lactoglobulin (Arroyo-Maya *et al.*, 2014), casein (Zhen *et al.*, 2013) and zein (Zou *et al.*, 2016) have also been used.

Most of the literature has used either of two major thermodynamic processes to synthesise the protein nanoparticles. These are emulsification and coacervation. Other methods such as chemical cross-linking of proteins have also been attempted especially for vaccine applications.

1. Emulsification process

Emulsification uses the addition of protein solution to the solution of oil and surfactant to form protein nanoparticles at the water-oil interface (Zhang and Zhong, 2009, Muller *et al.*, 1996). A significant drawback of this method is the necessity to remove oil and surfactant from the final preparation using additional organic compounds.

2. Coacervation process

Coacervation employs controlled precipitation of the proteins in a defined aqueous solution by addition of a de-solvating agent which is usually a polar organic compound such as acetone and alcohol. Coacervation is a more commonly used method and unlike emulsification does not require the further addition of organic compounds to remove de-solvating agent.

A possible mechanism of formation of the nanoparticles is explained on the basis of removal of hydration layer around protein upon addition of a de-solvating agent resulting in exposure of hydrophobic patches. Hydrophobic interaction among protein molecules in a crowded solution results in the formation of aggregates which act as nuclei for further growth. Coalescing of aggregated proteins to form large nanoparticle is favoured thermodynamically to reduce the high potential energy of the dehydrated protein and aggregates.

This mechanism suggests a role of macromolecular crowding and the rate of transport of proteins to nuclei. Possibly this is the reason that most of the reported protocols have used high concentrations of protein in excess of 20 g/L and up to 100 g/L and a minimum of 25 g/L suggested by one report (Galisteo-Gonzalez and Molina-Bolivar, 2014). It is unclear if the presence of nuclei such protein aggregates in the initial solution has any effect of initiation of the process or not. The same report also suggests that nucleation and subsequent growth of the nuclei is a delicate balance between various factors. Nucleation rate will increase with an increase in supersaturation of the solution but decrease with increased collision rate. High

concentration protein solutions have increased viscosity and reduced diffusion which will act to reduce collision, but crowded protein solutes due to such a supersaturated solution will have increased probability to collide. The growth of nuclei is favoured by increased collision rate thus resulting in larger particles. Increasing the temperature from 15 to 35 °C increased the particle size which was attributed to increased particle collision due to reduced viscosity and reduced supersaturation resulting in growth of nuclei.

Controlling the rate of addition of de-solvating agent has been emphasised as effective control of particle size distribution in final preparations by allowing sufficient time for mixing thus preventing high local concentrations of a de-solvating agent, which can result in uncontrolled aggregation (Paik *et al.*, 2013). Mixing of de-solvating agent would also be crucial to control local concentrations. Effect of stirring rate has been reported insignificant above a minimum stirring rate which is essential to decrease local concentration of de-solvating agent and possibly fragment large aggregates into smaller nanoparticles (Storp *et al.*, 2012).

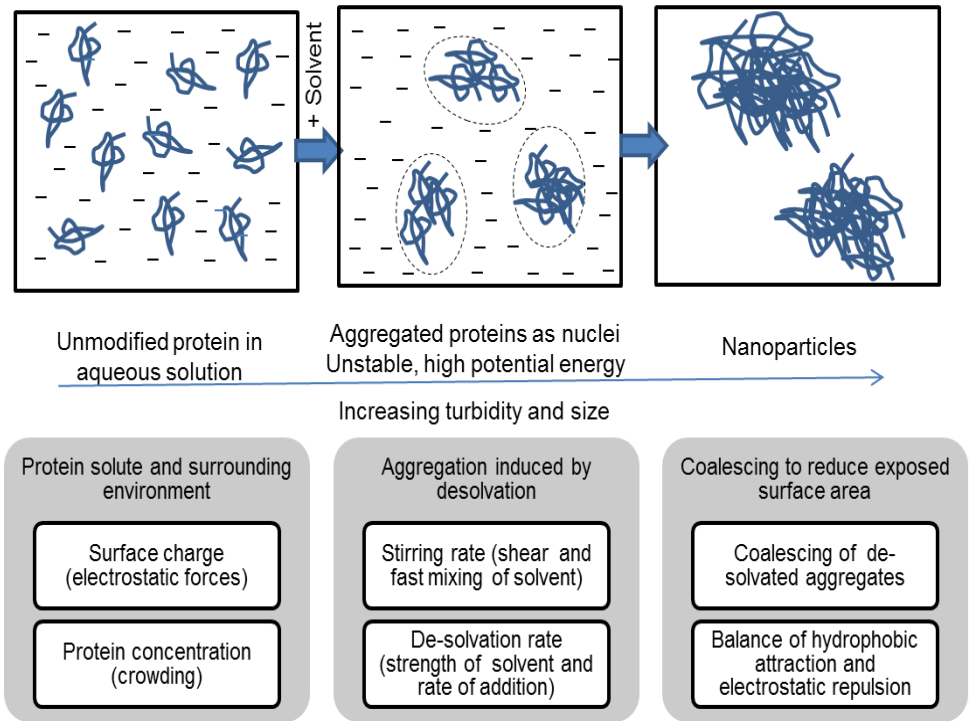

Figure 2-16 Pictorial representation of the possible mechanism of formation of nanoparticles of proteins using de-solvation method and factor influencing the mechanism listed in the boxes below.

Proteins being charged molecules are affected by the ionic environment around them. The magnitude of the charge on protein solute affects their molecular motion and interactions due to electrostatic repulsion. Increasing salt concentration and using pH near protein isoelectric points

have been consistently reported to increase aggregation and result in the larger size of nanoparticles (Galisteo-Gonzalez and Molina-Bolivar, 2014). Buffer solutions are usually avoided due to interferences of buffer components in the cross-linking process and formation of large aggregates (Langer *et al.*, 2003).

The choice of the de-solvating agent and their composition such as a mixture of acetone and ethanol or methanol has been reported to affect the particle size distributions significantly. A correlation between the dielectric constant of the de-solvating agent, and final particle size has been reported (Storp *et al.*, 2012). Authors advocated the use of de-solvating agents with high dielectric constant such as methanol to achieve monodisperse preparations with small nanoparticles and attributed it to more controlled and slower dehydration. Nanoparticles formed after de-solvation are often cross-linked to form irreversible particles using crosslinker molecules such as glutaraldehyde. Crosslinker amount is determined by calculation of the number of the binding group present on the total amount of protein used.

2.7.3 Stability of protein nanoparticles

Stability of protein nanoparticles would influence their utility in a variety of applications. Protein nanoparticles because of their high charge density and large surface area are less prone to aggregation and sedimentation due to large repulsive forces and thus are reported to form stable protein solutions. Albumin nanoparticles have been reported to be stable after two months of storage at 4°C (Galisteo-Gonzalez and Molina-Bolivar, 2014) and could also be easily re-suspended to a dispersed solution with original particle size distribution from settled solution over an extended period of storage (Jun *et al.*, 2011). Use of appropriate storage buffer solution should be studied for storage of protein nanoparticles since the surface charge can change with the solution pH and ionic strength.

CHAPTER 3 PREPARATION AND CHARACTERISATION OF BSA PROTEIN NANOPARTICLES AS A MIMIC OF VIRUS PARTICLES

3.1 Objective of the chapter

Purpose of this chapter is to screen various protocols available in the literature for the preparation of protein nanoparticles by desolvation method. The rationale of the work is the necessity to establish a repeatable protocol for nanoparticle preparations for various studies for objective 2 and 3. A variety of protocols are reported in the literature with different particle size and distributions and different proteins used. Since there is no clear understanding or modelling of the processes involved in the synthesis of nanoparticles, it is imperative that available protocols must be trial tested and appropriately adjusted for a targeted specification of nanoparticle solution. Filtrations studies proposed for objective 2 and 3 intend to compare different membranes for the separation of viruses like Adenovirus and adeno-associated virus, which are sub 100 nm particles. So the target size for the nanoparticle preparation is 100 nm or below. Protein nanoparticles preparations also need to be thoroughly characterised for any potential differences from the constituent protein which might affect their stability and utility in future experiments.

3.2 Introduction

Virus processing studies require the viral material which is laborious to generate due to the requirement of aseptic conditions for mammalian cell culture and subsequent purification activity, not to mention a burden of analytical tools (such as electron microscopy, infectivity assays, real-time PCR etc.) needed to estimate the amount of virus. Long production times in mammalian cell cultures (typically 1-2 weeks) along with variability of final titres present additional challenges to process development studies. Testing a new product for virus processing, such as new chromatography resins or ultrafiltration membranes, would require a significant amount of virus feed to characterise various variants of products as well as a variety of the processing conditions. Such testing is carried out to find the best-operating conditions for the product and also to draw specifications, guidelines and application notes for end users.

On the other hand, in a process development program for virus-based therapy, there may be a necessity to choose the best suitable commercial product from a range of products available. In such scenarios, usually, the goal is to screen a variety of materials (such as resins or membranes) and a variety of process conditions (such as flow rate, flux, transmembrane pressure etc.). In such scenario, a material which is a mimic to viral particles in fundamental physical and chemical properties could help to achieve these goals in the shortest time frame possible and using simplest analytical tools compared to generating and using the viral material. This means an ideal mimic would be a nanoparticle with protein surface and nucleic acid core

but which can be synthesised in a reasonably good amount, preferably in excess of 10^{12} particles per mL and in a much smaller time frame than that for virus production.

Protein nanoparticles are nano-particulate materials in size range of 10 to 1000 nm dimensions, synthesised by inducing and controlling the self-assembly phenomenon in proteins molecules. Through careful manipulation of the operating conditions nanoparticles as small as 40 nm can be synthesised in monodisperse preparations. Viruses range from 20 nm to microns in size; however, viruses used gene therapy applications are usually in the range of 20 nm to 400 nm depending on the class of virus such as Adeno-associated virus (~ 22 nm), Adenovirus (~90 nm) and Vaccinia virus (~300 nm). Protein-nanoparticle preparations in these size ranges could be used as a mimic for the virus capsids as both structures are proteinaceous in composition besides having similar size. Such nanoparticles have been used for various applications primarily for drug delivery for hydrophobic drugs (Lin *et al.*, 2016, Thao le *et al.*, 2016), functional foods (Zou *et al.*, 2016) and gene therapy vehicles to carry nucleic acids (Steinhauser *et al.*, 2008).

Most commonly these protein nanoparticles have been synthesised using albumin and by controlled precipitation of albumin through the addition of a de-solvating agent which dehydrates the protein resulting in interactions among protein molecules. Controlling the process conditions during the procedure of preparation is very crucial to achieve targeted size characteristics of the final preparation. Usually, concentrated protein solutions in water with well-defined pH and salt concentration are used as starting material. Choice of the desolvating agent is also crucial for desired output. Formed nanoparticles are then cross-linked into irreversible nanoparticles, usually using glutaraldehyde. Protein nanoparticles synthesis is a short procedure generally lasting no more than a day, and minimum processing is required afterwards as the starting material is a purified protein.

3.2.1 Methodology used

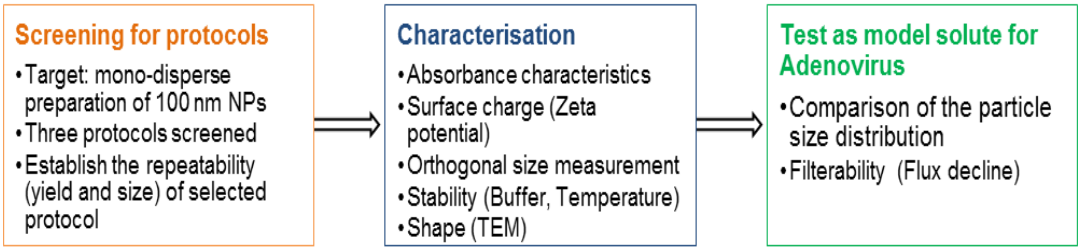

Figure 3-1 Methodology followed for the preparation of BSA nanoparticles for subsequent use as a model solute for adenovirus particles (70-100 nm).

Protocols reported in literature were screened for reproducibility. The best reproducible protocol was studied further for repeatability of the method. Obtained nanoparticle preparations were then characterised for size, charge, absorbance, shape and stability. Filtration curves obtained for filtration of 80 nm protein nanoparticles solution and adenovirus feed, both containing similar number of particles were compared to assess suitability of protein nanoparticles as model system.

3.3 Materials and Methods

3.3.1 Materials used

Bovine serum albumin manufactured as the heat shock fraction at pH 7 with >98% purity (Product no. A706, Sigma-Aldrich, USA) was used for the synthesis of protein nanoparticles. HPLC grade ethanol, acetone and methanol (Fisher, UK) were used as de-solvating agents. Glutaraldehyde (P/N 340885; Sigma-Aldrich, USA) was used for cross-linking reaction. Phosphate buffer saline tablets (Gibco® P/N 18912-014; ThermoFisher Scientific, UK) were used to prepare the buffer for protein solutions. A magnetic stirrer (Starlab, UK) was used for stirring during nanoparticle synthesis. A syringe pump (Aladin, World Precision Instruments, USA) was used for the controlled addition of de-solvating agents. A stirred cell filtration unit of 25 mm diameter and 10mL capacity, Amicon 8010 (Millipore EMD, USA) was used for filtration studies with 25 mm diameter commercial PAA membrane discs of 0.1 μm rating, Anodisc^{TM} (GE Healthcare, UK). For virus related experiments, T75 (75 cm^2 tissue culture flasks with sterile filter caps), HYPERFlask M (1720 cm^2 tissue culture flasks) and 96 well tissue culture plates (Nunc) were obtained from Corning Inc., USA. Fetal bovine serum and Dulbecco's PBS (without Ca and Mg) were obtained from Sigma Aldrich, USA. Dulbecco's Modified Eagle's Medium (DMEM with Pyruvate and without glutamine), L-glutamine and antibiotics Pen-Strep were purchased from Gibco, Thermo-Scientific, UK.

3.3.2 Methods for preparation of protein nanoparticles

Three protocols were selected from three different literatures describing the preparation of serum albumin nanoparticles. Conditions described for a target diameter of 100 nm or below were used from respective literature. Details of the three protocols (also summarised in **Table** 3-1 are as follows:

- **Method A (**adapted from Jun *et al.*, (2011))

BSA solution of 1 % w/v (10 g/L) was prepared in distilled water and pH of the solution was adjusted to 9.0 using 1 M NaOH. The solution was stirred overnight at 500 rpm to allow complete hydration and was subsequently filtered through a 0.22 µm PES filter. The pure acetone solution was added continuously using a syringe pump to 50 mL of the BSA solution under stirring speed of 500 rpm until the solution started turning turbid. The flow rate of acetone addition was maintained at 1 mL/min. Upon observing the turbidity, 100 µL of 4% (v/v) glutaraldehyde solution was added to the protein solution and solution was left under stirring conditions for another 3 hours. Preparations were diluted in water and size distribution was measured.

- **Method B** (adapted from Paik *et al.,* (2013))

BSA solution of 1 % w/v (10 g/L) was prepared in distilled water and was allowed to hydrate entirely by stirring at 700 rpm for 1hour. The solution was then filtered using 0.22 µm PES filter after adjusting the pH to 9.0 using 1M NaOH. For de-solvating, ethanol (98%) solution was added intermittently at 1 mL/min flow rate to 50 mL of BSA solution under stirring conditions (500 rpm). Each 1 mL addition of ethanol was followed by 5 minutes of stirring without any ethanol addition. The intermittent addition was repeated until protein solution became turbid. The turbidity of the protein solution was tracked by measuring absorbance at 545 nm, after the end of each 1 mL addition of ethanol to be able to correlate the outcomes with what was reported in the original method. At the appearance of turbidity 200 µL of 4 % (v/v) glutaraldehyde solution was added to the solution and solution was stirred for another 2 hours.

- **Method C** (adapted from Storp *et al.* (2012))

BSA solution of 10 % w/v (100 g/L) was prepared in 10 mM NaCl solution, and pH of the solution was adjusted to 8.0. The solution was then filtered through a 0.22 µm PES filter. Precipitation was carried out by addition of a mixture of methanol and ethanol (70:30 in %v/v) at 1 mL/min flow rate to 1 mL of concentrated protein solution. The solution was stirred at 500 rpm through the procedure. Glass beaker of defined dimension (diameter 25 mm; height 60 mm) was used along with a magnetic stirrer bar (diameter of 6 mm; length 20 mm) as similar

dimensions were described in the referenced literature. After observing turbidity, 60 µL of 8 % (v/v) glutaraldehyde solution was added to the solution and solution was stirred for a minimum of 2 hours or overnight. Targeted size in this protocol was 60 nm as per the referenced literature. Since method A and B used BSA solutions without any NaCl in them, method C was further modified and repeated without NaCl in the protein solution.

	Method A	**Method B**	**Method C**
Initial BSA concentration. (g/L)	10		100
Volume of protein solution (mL)	Unspecified (50 mL)		1 mL
Solvent	Deionized water, pH 9.0		10mM NaCl, pH 8.0
De-solvating agent	Acetone	Ethanol	Methanol + Ethanol
Rate of addition	1 mL/min		
Mode of addition	Continuous	Intermittent	Continuous
Stirring speed	500 rpm	700 rpm	500 rpm
Temperature	Room temperature		
Vessel	250 mL beaker	250 mL beaker	50 mL beaker

Table 3-1 Process conditions for various methods screened for albumin nanoparticles preparation. Method A, B and C were adopted from Jun *et al.*, (2011), Paik *et al.*, (2013) and Storp *et al.,* (2012) respectively.

3.3.3 Particle size characterisation using Dynamic light scattering (DLS) and Nanoparticle tracking analysis (NTA)

For DLS, protein nanoparticles were appropriately diluted (usually 30-40 times diluted to a concentration of 1 mg/mL) in phosphate buffer saline, pH 7.0 and were analysed using Zetasizer NS (Malvern, UK) for estimation of particle size distribution. Disposable polystyrene cuvettes (1.5 mL) were used. Preparations were equilibrated at 22°C for 90 seconds and light scattering data was collected using a laser of 633 nm wavelength at backscattering angle (173°) with auto settings for optimum location and attenuation. Usually, the attenuation factor of 6 to 10

and photon scattering rate of 150 kcps and above was considered as reliable for analysis. Instrument calibration was tested using 50 nm polystyrene nano-spheres (3050A, ThermoScientific, USA) NIST standards. Three runs were performed on each sample.

DLS measures the fluctuation of the scattered light over time and correlates the decay rate of initial scattering intensity to the Brownian motion of the particles by calculating the diffusivity (Carvalho *et al.*, 2018). Size of the particles is obtained from the estimated diffusivity values using the Stokes-Einstein equation assuming a spherical shape for the particles and using viscosity values for the solvent used (Kato, 2018). This analysis is automatically performed by the Zetasizer software and presented in form of a size distribution plot, mean particle diameter value and poly-dispersity index (PDI). Size distribution plot is usually presented in form of particle size as x-axis and % relative intensity of scattered light as the y-axis. The plot can also be transformed into % relative volume by converting the intensity distribution into volume distribution for spherical particles. The mean particle diameter is measured in form of intensity-weighted value, also known as Z-avg value and can also be measured in form volume weighted mean. The polydispersity index (PDI), which is an indication of the spread of the distribution of the particle size, is calculated from cumulant analysis by a standard method and can range from 0 to 1 for a sample. Samples with a PDI value below 0.2 are considered to be monodisperse i.e. with a narrow particle size distribution.

Nanoparticle tracking analysis (NTA) was also carried on protein nanoparticles and Adenovirus rich preparations using PBS buffer as diluent. Nanosight LM10 (Malvern, UK) with 532 nm laser was used for NTA measurements. A minimum of 3 and maximum of 5 measurements, each of 60 seconds was obtained for each sample, and proper detection limits were applied to analyse the raw data using the software provided with the machine. NTA also utilises light scattering by suspended particles but measures the Brownian motion i.e. mean free path by tracking the movement of scattering centre of each particle in the solution by analysing the video recordings of the illuminated sample obtained using a digital optical microscope. In this way, NTA can measure the number of particles in the sample along with particle size distribution, which is an advantage over DLS (Malloy, 2011).

3.3.4 Estimation of the yield of nanoparticles

The yield of nanoparticles was indirectly determined by measuring the amount of residual unmodified BSA in the final nanoparticle preparation. Protein-nanoparticle preparation was diluted using PBS, and 100 µL of diluted preparation was manually injected on to size exclusion column, Superose 6/12 300 (24 mL column volume). The column was pre-equilibrated using

PBS for 4-5 column volumes at 0.5 mL/min flow rate. BSA solutions of various concentrations were also injected into the column to obtain a standard calibration curve for BSA by measuring peak area at elution volume characteristic to BSA size. Amount of residual protein in diluted nanoparticle preparations was calculated from peak area at an elution volume of corresponding to BSA standard and calibration plot obtained for BSA solution **(see Appendix A2**). Net residual amount of BSA was calculated by considering the dilution factor and the total volume of nanoparticle preparation obtained. The yield of the nanoparticles was created using formula as below:

$$\text{BSA nanoparticles yield}(\%) = 100 * \left(\frac{\text{Total BSA used}(\text{mg}) - \text{Residual BSA (mg)}}{\text{Total BSA used}(\text{mg})}\right)$$

3.3.5 Zeta potential measurements

Zeta potential of nanoparticle preparation was measured using Zetasizer NS (Malvern, UK). Nanoparticle preparations were diluted in 10 mM NaCl, and pH of the solution was adjusted using 1M solutions of HCl and NaOH. pH values in the range of 3-10 were tested. Preparations were carefully loaded onto disposable polystyrene cells with electrodes, avoiding any air bubbles. Loaded cells were then equilibrated at 22°C for two minutes before measurements were started. Quality parameters such as conductivity (less than 5 mS/cm) and attenuation (between 5 and 10) were monitored to ensure the accuracy of measurements obtained. Three measurements were obtained for each sample. Scattering data was processed using software, Zetasizer. Calibration of the instrument was tested using zeta potential standard (47mV rating) supplied by the instrument manufacturer.

3.3.6 Analysis of the protein nanoparticles using Transmission Electron Microscopy (TEM)

Preparation of the protein nanoparticles was diluted 100-fold using 20mM Tris buffer (pH 7.5) and was negatively stained using uranyl acetate solution. The stained sample was spread onto a carbon grid with a mesh rating of 400 and was air-dried. The sample was then observed using a JEOL 1010 Transmission Electron Microscope (Jeol, MA, USA). Negative staining means that the sample or part of the sample would not be stained so would appear as a white feature in contrast to the surrounding black background.

3.3.7 Filtration studies to compare the filterability of protein-nanoparticle feed and Adenovirus feed

Filtration study comparing flux decline of BSA nanoparticles feed and Adenovirus feed was carried out in a stirred cell filtration set up using 100 nm rated commercial PAA membranes. Monodisperse preparation of 80 nm BSA nanoparticles was used and Adenovirus rich feed was obtained from mammalian cell culture and further processing.

3.3.7.1 Filtration set up

A cylindrical stirred cell device (Millipore, Amicon 8010) with a maximum working capacity of 10 mL and filter support area of 25 mm (as shown in **Figure 3-** 2) was used for this study. The device is equipped with a magnetic stirrer bar to provide tangential flow to the feed above the membrane surface. Filter support plate has distribution channels embedded in the plate and leading to the filtrate output with elastomeric tubing. Tubing volume was determined to be 0.3 mL. Membranes were wetted in water and mounted on to the filter support plate. The stirred cell was assembled as instructed by the manufacturer and filled with solution to be filtered with valve V2 closed (See **Figure 3-3**). The stirrer bar was carefully lowered into the cell by positioning the stirrer shaft in the centre and ensuring the stirrer bar is not pressed upon the membrane. The top plate of the stirred cell, connected to nitrogen supply was mounted on assembled stirred cell. Gas supply was turned on slowly by controlling gas flow using pressure regulator valve (V1) while gas relief valve (V3) on top plate kept open. After saturating the stirred cell with nitrogen gas relief valve on the top plate is closed.

Stirring rate is adjusted followed by adjustment of the feed pressure through valve V1 to the desired pressure. The collection vessel is kept on weighing balance and balance is blanked to zero. Valve V2 on filtrate tubing is then opened, and the filtrate is collected into 20 mL polystyrene tubes kept on weighing balance. To ensure that set up is leak proof, connections were routinely checked for gas leakage using leak detection liquids. Trans-membrane pressure is calculated as the difference of the applied feed side pressure and pressure in the filtrate tubing. In the case of the stirred cell, the applied gas pressure measured at valve V1 is considered equal to the effective transmembrane pressure as filtrate side is at atmospheric pressure. Pressure drop in the short filtrate line is assumed to be insignificant.

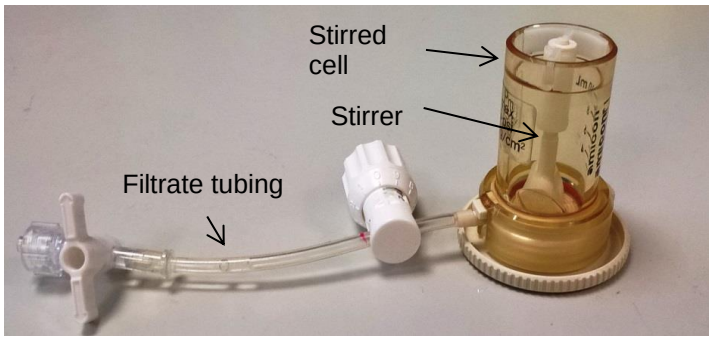

Figure 3- 2 Amicon stirred cell (8010, 10 mL) used in this study.

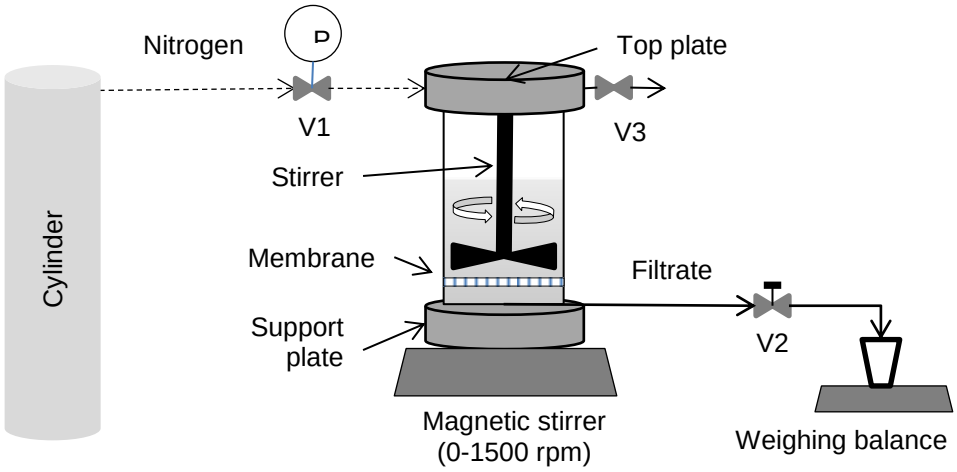

Figure 3-3 Illustration of the experimental setup for filtration studies using Amicon stirred cell device (8010, 10 mL).

V and P denote valves and pressure readout respectively. Nitrogen gas is used to create positive pressure in the stirred cell after closing valve V2 and V3. Valve V2 is opened after auto-zeroing the weighting balance and measurements are manually entered from the readout. Filtrate line is primed with buffer before addition of feed to the stirred cell so that immediate readings can be noted down.

3.3.8 Adenovirus production and filtration

Recombinant Adenovirus particles carrying the heterologous gene for enzyme ß-galactosidase were produced using adherent mammalian cell culture of Human Embryonic Kidney (HEK 293) cell line. All experiments related to viruses were performed in a biosafety level-2 chamber.

3.3.8.1 Mammalian cell culture

Fetal bovine serum (FBS) was heat inactivated at 56°C for no more than 30 minutes. Growth media was prepared by addition of 50 mL of heat-inactivated FBS, 5 mL of L-glutamine and 5.5 mL of antibiotic, Pen-Strep to 500 mL of DMEM media. HEK 293 cells were obtained from the European cell bank. Cells were cultured in tissue culture flasks with the treated surface. Cultures were incubated at 37°C at 5 % CO_2 incubator and routinely passaged after 80-90% confluency is achieved. During passages, cells were washed with PBS and treated with trypsin solution for 2-3 minutes to allow detachment. Trypsin was inactivated by addition of growth media and cells were centrifuged down at 100x g for 5 minutes. The cell pellet was re-suspended in fresh growth media and seeded in 75 cm^2 tissue culture flasks. Cells were used for Adenovirus production in HYPERFlask culture vessels or infectivity assay after 5^{th} passage and no more than 20^{th} passage.

3.3.8.2 Recombinant Adenovirus production using HEK293 cell lines

Recombinant Adenovirus, serotype 5, genetically engineered to contain genes for enzyme ß-galactosidase was produced using Human Embryonic Kidney cell line, HEK293. Cells were infected using a virus stock (10^9 virus particles/mL) to a final concentration of ~3 x 10^5 virus particles/mL in an HYPERFlask culture vessel. Cells were then incubated at 37°C at 5 % CO_2 incubator for five days. Cells were attached to a 500 mL capacity stacked tissue culture vessel, HYPERFlask with the treated surface. At the end of incubation, cells were observed to show the cytopathic effect (loosely bound to the vessel surface, round in the shape and smaller).

3.3.8.3 Preparation of Adenovirus feed for filtration studies

Infected cells loosely attached on the flask surface of HYPERFlask were detached by tapping the flask. Cells were then collected in 50 mL centrifugation tubes and centrifuges at 100xg for 5 minutes. The supernatant was discarded and cells were re-suspended in fresh growth media (DMEM + FBS). Cells were then exposed to one freeze-thaw cycle and stored at -70°C until further use. Growth media was added to enhance the stability of the virus particles during the long-term storage and shield the virus from stresses in freeze-thaw cycles. Frozen cells/ cell debris were further treated to two more freeze-thaw cycles, and subsequently, a suspension containing cell debris was filtered through 0.45 µm PVDF filter. The filtrate was collected and stored at -70°C.

3.4 Results and Discussion

3.4.1 Screening of the methods for synthesis of BSA nanoparticles

Three protocols from different literature (for details refer to **Table 3-1)** were selected for screening under local laboratory conditions. Operating conditions used were similar to those described for the synthesis of 100 nm nanoparticles in the original literature except for method C where the target size of 60 nm was cited.

Compared to target size, larger particle diameters were measured for preparations obtained through all the methods tested along with higher polydispersity (shown as polydispersity index, PDI) except for method C as displayed in **Figure 3-5**. Preparations with a polydispersity index of 0.2 and above are considered to be polydisperse solutions signifying that diverse class of sizes are present in the samples. However, the difference between target and measured particle diameter was smallest for method C. Particle size distribution plot of these preparations show clear differences in mean size and polydispersity of preparations (See **Figure 3-4**).

Method A, de-solvation using acetone, shows a variable particle size distribution even among repeat measurement of the same solution. Method A was thus found to be not suitable for the intended application considering highly poly-disperse preparation and high particle size along with the requirement of removal of acetone which will otherwise interfere with protein measurements using 280 nm absorbance assays.

Method B resulted in particles larger than targeted 100 nm particles and improved PDI over method A. However repetition of this method performed differently with large aggregates formed. It was also observed that ethanol consumption was much lower than what was reported by the reference literature (Paik *et al.*, 2013) possibly because of the differences in protein batches used in this study and authors.

Method C was found to result in monodisperse preparation with mean particle size at 82 nm compared to 60 nm targeted as per reference. Method C resulted in highly monodisperse preparation (PDI < 0.1) and particle size distribution was highly consistent with repeated measurement. Large standard deviations in PDI and intensity weighted particle diameter were observed for method A and B as shown above **in Table 3-2.** Thus method C was selected for further studies.

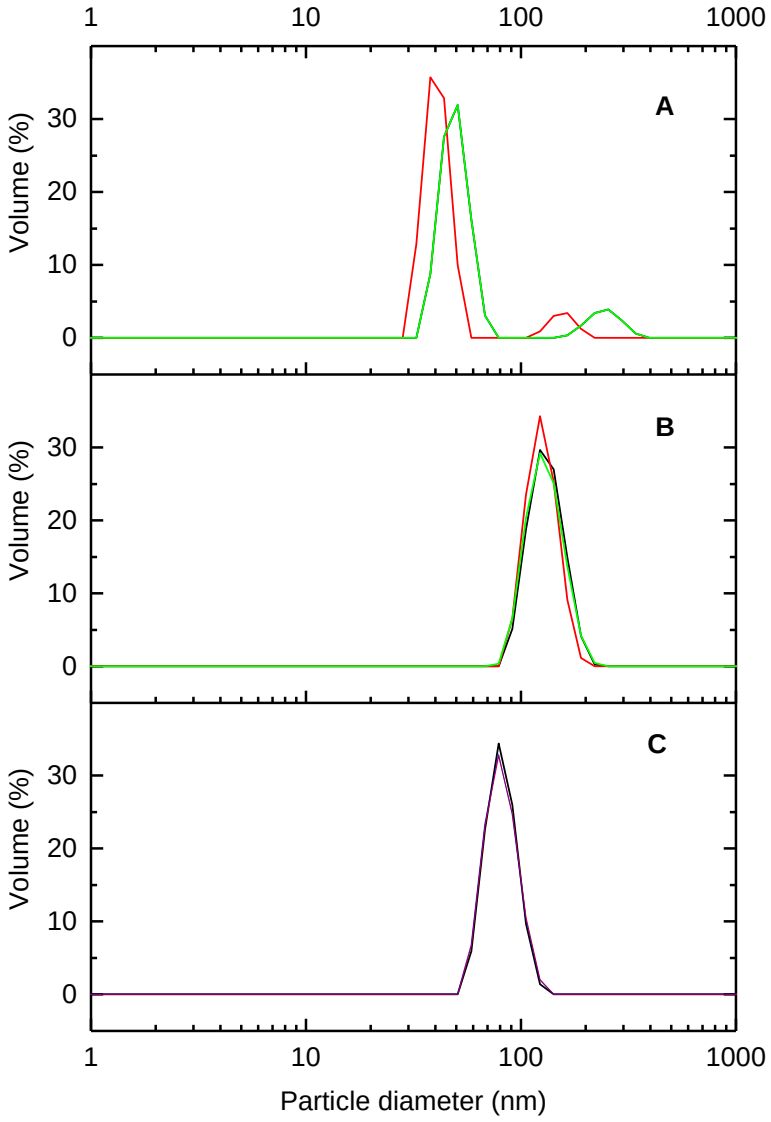

Figure 3-4 Particle size distributions for BSA nanoparticle preparations synthesised using three different methods A, B and C.

Samples were diluted with water to minimise interference due to de-solvating agents. Method A, B and C were adopted from Jun et al. (2011),Paik et al. (2013) and Storp et al. (2012) respectively. Triplicate measurements of each sample were carried out.

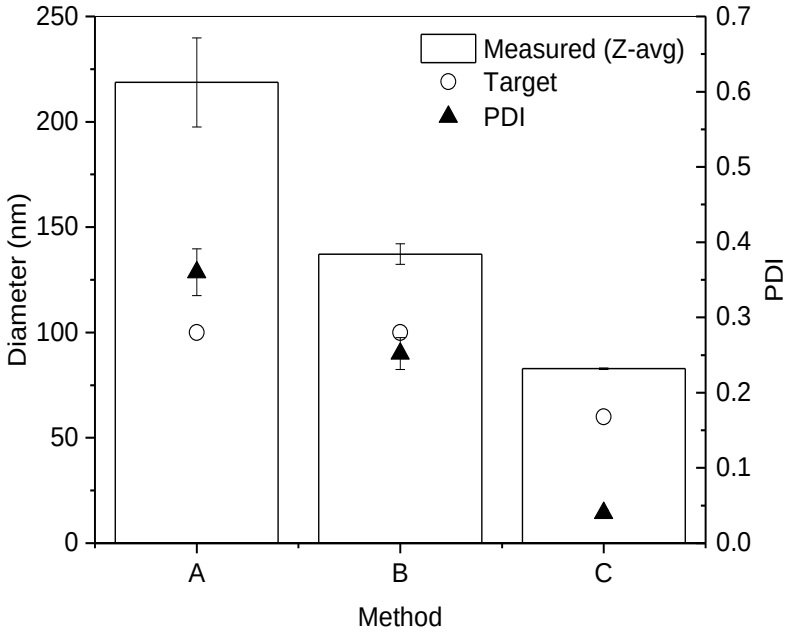

Figure 3-5 Nanoparticle diameter (bars) and polydispersity index, PDI (▲) of nanoparticle suspension prepared through three methods screened; Targeted size (○) is the diameter value published in the referenced literature.

Bars and symbols represent the average value of the measured diameter and PDI for three consecutive measurements of the nanoparticle solution. Error bars represent one standard deviation obtained for three measurements.

Method	Target size (nm)	Measured diameter (Intensity weighted) (nm)	PDI
A	100	219 ± 21	0.36 ± 0.03
B	100	137 ± 5	0.25 ± 0.02
C	60	83 ± 0.3	0.04 ± 0.004

Table 3-2 Particle size distribution obtained through three methods of nanoparticles synthesis, i.e. Method A (Jun *et al.*, 2011), Method B (Paik *et al.*, 2013) and Method C (Storp *et al.*, 2012).

Data displayed as average value ± one standard deviation for three measurements of the sample.

3.4.2 Manipulating nanoparticle size by varying the salt concentration in method C

Use of salt and pH to control particle size has been well established (Paik *et al.*, 2013, Langer *et al.*, 2008, Galisteo-Gonzalez and Molina-Bolivar, 2014) and trends are consistent in most of the reported literature. A variation of method C where the protein was dissolved in plain distilled water without any salt addition instead of 10 mM NaCl solution resulted in significantly lower particle size as shown in **Figure 3-6**.

Use of salt concentration to control the size was selected over the use of pH as it provided a more reliable parameter to adjust compared to pH where variability between electrode to electrode and effect of ageing of pH electrodes could affect the repeatability of preparation. Using salt as 'size controlling agent' does not have instrumentation risk except for the weighing of the salt and volume measurements. Salt helps to screen some of the charged groups on protein molecules thus reducing repulsion between molecules. Reduced repulsion increases the aggregation of protein molecules resulting in the formation of larger nuclei and hence larger nanoparticles.

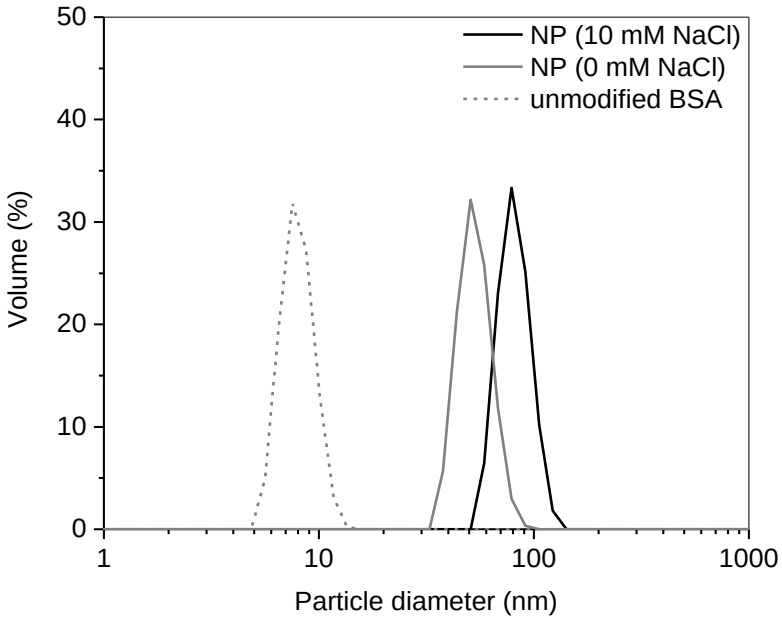

Figure 3-6 Volume based particle size distribution of BSA solution and nanoparticle (NP) preparation obtained using method C (Storp *et al.*, 2012) with varying concentration of NaCl (0 and 10 mM) in initial BSA solution.

3.4.3 Sources of variability in various methods screened

All three methods screened used different operating conditions for multiple parameters as detailed in **Table 3-1**. Thus a direct correlation with differences in protocols to the differences observed for particle size distributions of final nanoparticle preparation is not possible this experiment. However potential sources of variation could be speculated on the basis of differences in methods. A significant difference between the three methods was the de-solvating agent used. Storp et al, (2012) have observed smaller particle size and monodisperse preparations with methanol as compared to ethanol and acetone. Methanol having higher dielectric constant (polarity) results in slower and more controlled de-solvation of protein molecules thus resulting in smaller nano-particulates of uniform sizes. Method C utilised a mixture of methanol and ethanol in the ratio of 70:30 and resulted in smaller and more monodisperse preparations than method A and B where acetone and ethanol were used respectively. Nanoparticle size and polydispersity decreased in the order of method A > method B > method C whereas the polarity of solvent used in corresponding methods followed reverse trend i.e. highest polarity for methanol used in method C and lowest for acetone used in method A. High polarity of desolvating agent results in slower aggregation of protein thus minimising uncontrolled aggregation. This, however, does not explain why methods A and B could not be reproduced, unlike method C.

Another critical distinction between method C and other two methods was the explicit detail of the vessel and stirrer dimensions provided by the referenced literature for method C. Original authors did not publish such details for method A and B. For method C, though the original literature (Storp *et al.*, 2012) has reported no significant effect of the stirring rate above 500 rpm, it was suspected that mixing also plays a role in particle size distribution of final preparations. To test this, method B was performed with three different vessel dimensions with rest of the conditions being constant; it was found that volume of ethanol required for the onset of turbidity increased for the vessel with broader diameter along with foaming observed in stirred protein solution (For details refer to **Appendix B**). Vessel with dimension described by Storp *et al.*, (2012) was found to result in a lower polydispersity of preparation compared to other two vessels. Vessel with broader base was found to result in preparation with a high polydispersity (> 0.3). It appears that choice of the vessel could significantly alter size characteristics of nanoparticle preparation which suggests a strong influence of mixing characteristics of setup. Poorly defined mixing conditions for a simple beaker and stirrer system limit the study into the role of mixing in nanoparticle formation. A detailed study based on fluid dynamics to characterise shear zones and dead volumes and the effect of shear on protein molecules could help explain these observations. However, such study is beyond the scope of this research

work. Other significant differences such as protein concentration, 100 g/L for method C compared to 10 g/L for the other two methods could also be influencing.

The protein used itself could also be the source of variation. The protein used in these methods is bovine serum albumin. However, the commercial product used in this study and referenced literature are different. Manufacturing conditions, as well as final purity of lyophilised protein, may be different. In the case of method C, authors used human serum albumin, which though represents proteins with the same functionality but different sources and slightly different primary structure than bovine serum albumin. It is difficult to say how much of these changes impact toward non-reproducibility of these methods. BSA used in this study has been found to contain smaller protein aggregates (dimers and oligomers) when analysed using size exclusion chromatography (see **Figure 3-9**). It is possible that dimers and oligomers act as nucleation centres resulting in higher particle sizes than targeted. The composition of lyophilised protein material (such as impurity content, salt content and aggregates) has not been studied for its effect on protein nanoparticle synthesis.

3.4.4 Effect of cross-linking duration on particle size

Referred literature (Storp *et al.*, 2012) for method C used overnight incubation during cross-linking reaction. If a large amount of nanoparticles is to be generated, multiple reactions need to be set up thus smaller preparation time is strongly desired. Thus the minimum time required for cross-linking was investigated after which particle size distribution remains unchanged. With protocol C, particle size and PDI was tracked for 6 hours. Samples of 15 µL were taken immediately after addition of the crosslinker and then at 0.5, 2, 4 and 6 hours since the addition of the crosslinker. Samples were analysed using DLS within 15 minutes of collection time. Nanoparticle preparation was stirred at room temperature throughout the cross-linking process.

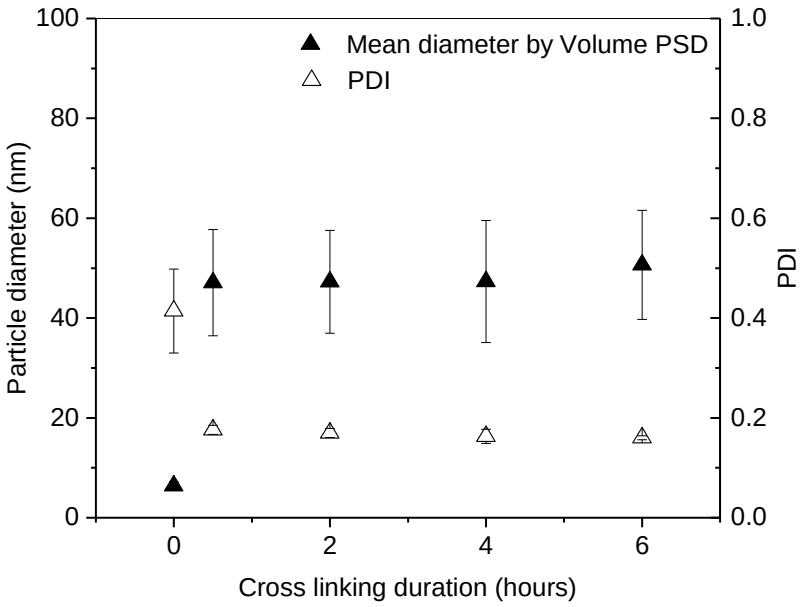

Figure 3-7 Effect of the cross-linking duration on particle size distribution (mean values of the particle diameter (▲) and PDI (△)) of nanoparticles preparation obtained using method C.

Error bars on particle diameter represent one standard deviation of the size distribution curve and one standard deviation of three measurements of the sample for PDI.

It was found that particle size distribution parameters (mean diameter and PDI) did not change significantly beyond 0.5 hours (as seen in **Figure 3-7**). Cross-linking time of 0.5 hours was thus sufficient for cross-linking. Conservatively, cross-linking duration of 2 hours was selected for future experiments. Two hours was selected to allow sufficient time for all of BSA to be converted to nanoparticles, and this was confirmed by yield calculated using size exclusion chromatography as shown in Section 3.4.6. Cross-linking time has been reported to have no significant effect on nanoparticle size distribution (Galisteo-Gonzalez and Molina-Bolivar,2014). On the other hand, the amount of glutaraldehyde added does influence particle size if used in smaller quantities. However, the amount of glutaraldehyde used in this method was higher and sufficient enough for cross-linking of all amino groups available on total protein used.

3.4.5 Repeatability of the selected method

It is essential that if method C is selected as a preferable method for generating nanoparticle material for filtration studies, it should be able to do so consistently. Thus, protocols for both preparations (for 50 and ~80 nm nanoparticles) were repeated four times to assess consistent performance.

Figure 3-8 shows mean particle diameter and polydispersity index for four different batches both two variations of method C targeting final particle size of 50 and 80 nm indicated by legends A and B respectively. For a targeted particle size of 50 nm, particle diameter ranged between 50 to 60 nm, and polydispersity was also below 0.1 for all of the batches. A similar trend was observed for a target size of 80 nm, except for batch 3, all other batches yielded nanoparticles with a diameter in the range of 80 to 90 nm and polydispersity index below 0.1. Batch 3 for both sub-methods showed higher particle sizes than particles sizes observed for other batches. This could be the result of an unknown contaminant as batch 3 for both preparations were synthesised on the same day using same protein stock. Overall, method C could be used consistently for nanoparticles synthesis.

Repeatability was not discussed in the original reference (Storp *et al.*, 2012) and since the method used the continuous addition of the de-solvating agent, these results were contrary to observations made by other authors (Paik *et al.*, 2013) where the continuous addition was reported to have poor repeatability. These authors, however, used ethanol or acetone as de-solvating agents contrary to the mixture of ethanol and methanol used in method C. Lower polarity of the de-solvating mixture would mean slower dehydration of protein molecules by a de-solvating agent. Slower dehydration should result in the formation of smaller nuclei despite higher local concentrations of de-solvating agents upon continuous addition. Thus the use of methanol appears to be a significant factor in controlling the size distribution of nanoparticles by reducing undesired precipitation

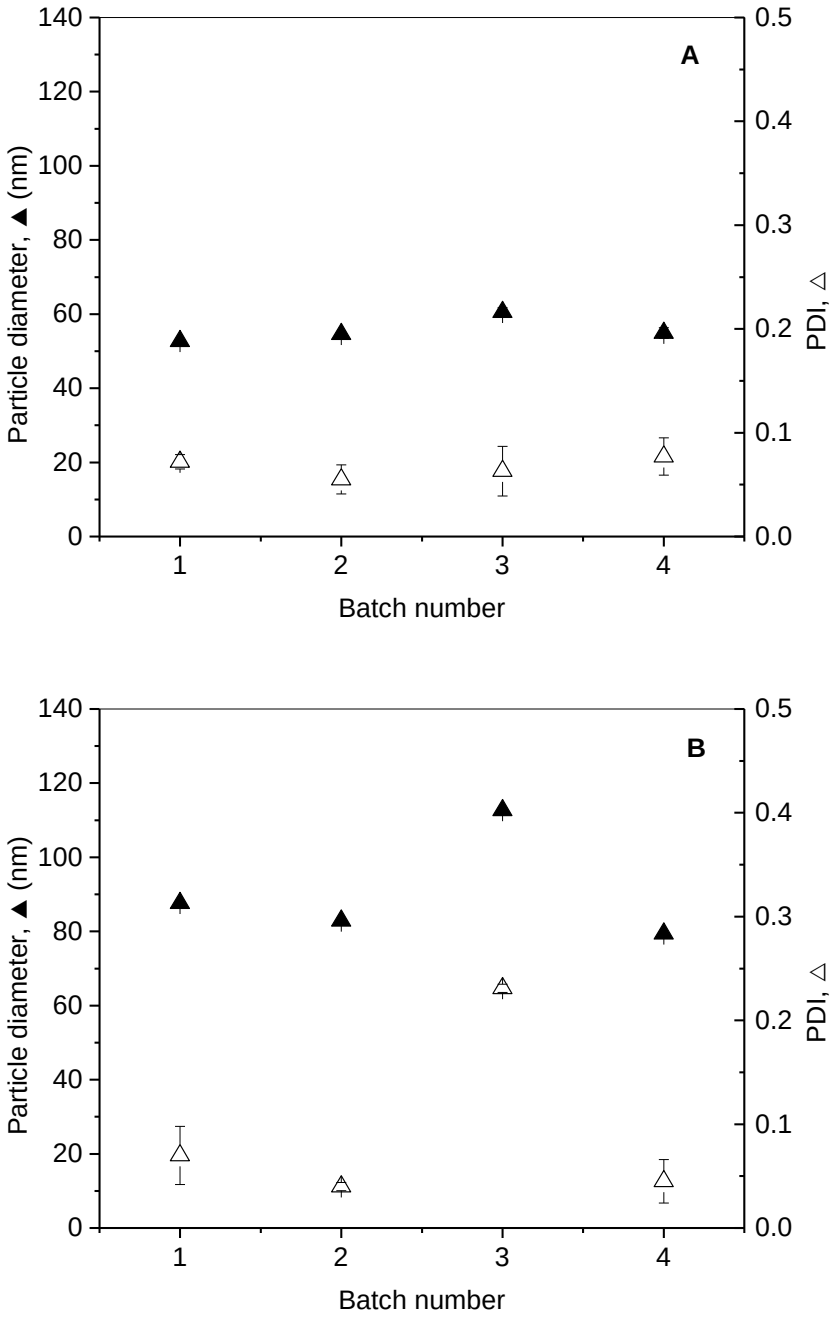

Figure 3-8 Repeatability of method C for the synthesis of BSA nanoparticles for consistent particle diameter (▲) and polydispersity index, PDI (△) studied using four batches of nanoparticles prepared with the target sizes of 50 nm (A) and 80 nm (B) with 0 and 10 mM NaCl in BSA solution respectively.

Symbols represent the average value of the particle diameter and PDI and error bars represent one standard deviation for triplicate measurements of the samples.

3.4.6 Nanoparticle yield for the selected method

An ideal method of synthesis is not only repeatable for consistent nanoparticle size distribution but also for its efficiency of converting BSA protein molecules into the nanoparticles. Method C was checked for the yield of nanoparticles by measuring the amount of residual unmodified BSA in final preparation using size exclusion chromatography (SEC) as described in the Section 3.3.4 of the chapter. Three batches of protein nanoparticles for both 50 and 80 nm preparations were tested with SEC. SEC is the method of choice for such quantitation due to its ability to resolve between larger nanoparticles and smaller unmodified protein molecules. Due to large size, nanoparticles were expected to elute earlier near void volumes as opposed to unmodified protein eluting later. As shown in **Figure 3-9**, nanoparticles were found to elute at an elution volume of 5-7 mL irrespective of size and unmodified BSA eluted later between 11 to 17 mL. Gel filtration protein standard with thyroglobulin eluting at 11 mL further confirmed that nanoparticles eluted in the void volume of the column implying large size of the particles (refer to the chromatogram in **Appendix A1).**

Chromatograms for these preparations (**Figure 3-9, B and C**) also show very small peak observed at retention time corresponding to unmodified BSA preparation indicating that most of the BSA molecules are aggregated into larger particles. Conversion percentage or yield of nanoparticles was calculated using the formula described in Section 3.3.4. Average yields of 99.4 ± 0.8 % and 97.5 ± 1.8 % were calculated for 50 nm and 80 nm nanoparticles preparations respectively. These values are average of three batches for each size. Results also validate that cross-linking duration of 2 hours is sufficient to achieve high conversion of protein into nanoparticles. It is important to recognise that conditions such as pH, salt concentrations as well as the amount of crosslinker added do influence the yield of nanoparticles (Galisteo-Gonzalez and Molina-Bolivar, 2014). These results could not be tallied with original reference as authors have not provided yield data.

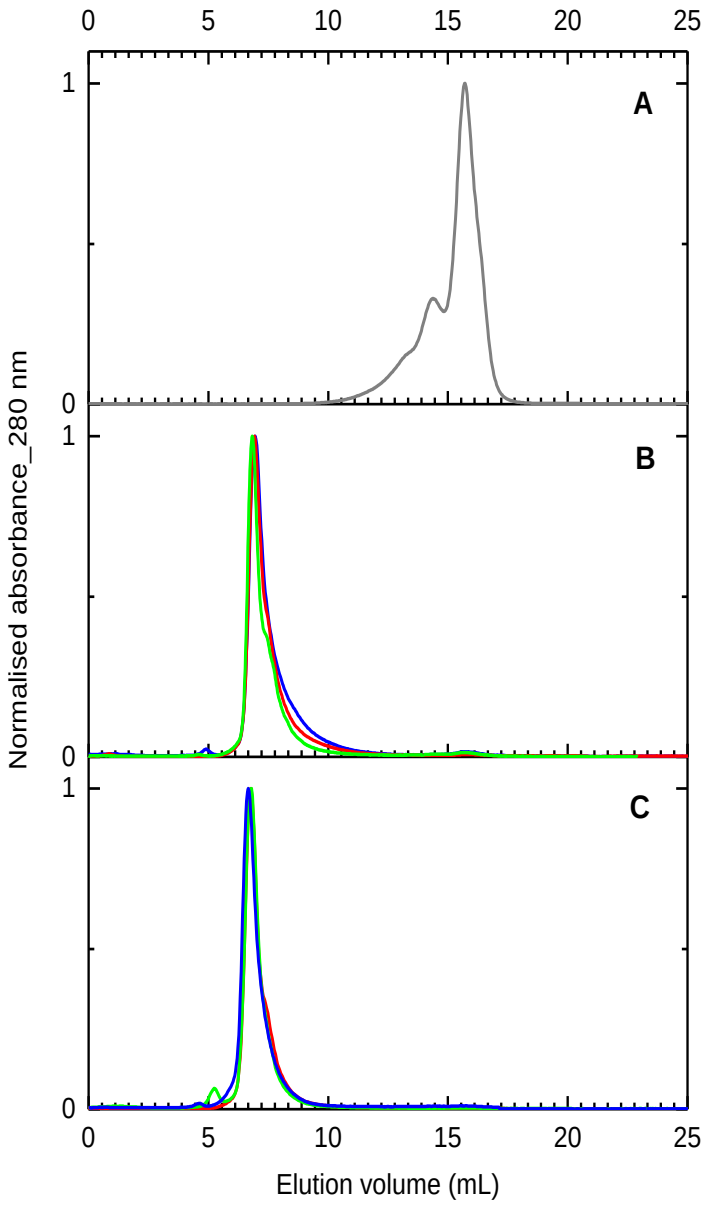

Figure 3-9 Size exclusion chromatograms for unmodified BSA solution (A) and BSA nanoparticle preparations, (50 nm (B) and 80 nm (C)) obtained using method C (Storp *et al.*, 2012)

Superose 6 10/300 column (CV 25 mL, 13 µm average particle size) was equilibrated and injected with 100 µL of samples. Isocratic elution was carried out with PBS (~10mM phosphate buffer with 143 mM NaCl and pH 7.4). The overlay shows chromatograms obtained for three nanoparticle batches of similar size. Consistent chromatograms were obtained for three repeats for BSA nanoparticle synthesis using the selected method C.

3.4.7 Characterisation of BSA nanoparticle preparation

It is essential to establish the means of measuring concentrations of the nanoparticles so that reproducible feeds could be prepared for future filtration experiments. Also, it should be ensured if such preparations are stable in the buffers used during filtrations along with long-term storage of nanoparticle samples.

For measuring the concentration, particle detection techniques such as dynamic light scattering or nanoparticle tracking analysis could be used. Dynamic light scattering (DLS) is a qualitative technique as it can only give information about particle size distribution of a bulk sample by analysis of change in intensity of backscattering from the sample. Nanoparticle tracking analysis (NTA) is another scattering based technique which uses a high-performance camera to observe the random motion of particle by tracking the scattering on individual particles. NTA is quantitative techniques and counts the number of particles in a defined sample volume along with size distributions.

However, NTA is a laborious technique as a single analysis cycle is around 10 minutes, and the sample chamber needs to be manually flushed after each repeat. Further, samples need to be diluted many folds before they can be analysed with NTA. A more convenient approach would be to use commonly used light absorption based protein quantification techniques for measuring nanoparticle concentrations in a sample as they are easier to perform and do not depend on sophisticated instrumentations unlike like DLS and NTA.

3.4.7.1 Absorbance characterisation of BSA nanoparticle preparations

Protein quantification for purified protein preparations is usually done by measuring absorbance at 280 nm where some amino acids are known to absorb light. BSA nanoparticles preparations in phosphate buffer saline were observed to have higher absorbance compared to BSA preparations of similar concentrations under similar conditions. Since most of the BSA was shown to get converted into nanoparticles, a nanoparticle preparation equivalent to 1 mg/mL of BSA was prepared by appropriately diluting nanoparticle preparation using mass balance calculations. Higher absorbance for nanoparticle preparation is the result of increased scattering by larger protein nanoparticles compared to much smaller BSA molecules. A visual inspection of nanoparticle preparation after synthesis against unmodified protein solution also shows high turbidity of the nanoparticle solution as can be seen in **Figure 3-10**.

Figure 3-10 Turbid BSA nanoparticles preparation (labelled NP) obtained after precipitation of 1 mL of 100 g/L unmodified BSA solution (labelled BSA) using a mixture of methanol and ethanol as de-solvating agent (prepared using method C).

The mean particle size of the preparation was measured to be ~80 nm using DLS in contrast to ~8 nm measured for BSA solution. The yellow colour of the preparation is the result of cross-linking reaction using glutaraldehyde.

The turbidity was quantified by measuring the absorbance of these preparations at 330 nm and 545 nm where proteins do not absorb light. Nanoparticles preparations showed higher absorbance than BSA solution even at these wavelengths. Increase in absorbance compared to BSA solution was more pronounced with an increase in the size of nanoparticles (see in **Figure 3-11**). The increase in absorbance at higher wavelengths is attributed to the dependence of scattering intensity on particle diameter by a power of 6 and increased ratio of the particle size particle and illuminating wavelength (Kato, 2018). Large particles would tend to scatter more and forward scattering is highly disproportional to size as particle size approaches light wavelength by the Mie theory (Tilley, 2011). The contribution of scattering in absorbance at 280 nm is difficult to predict as there is a possibility of change in the local environment around amino acids groups when protein is de-solvated and converted into nanoparticles. It has been shown that protein secondary structure is significantly altered in protein nanoparticles (Arroyo-Maya *et al.*, 2014).

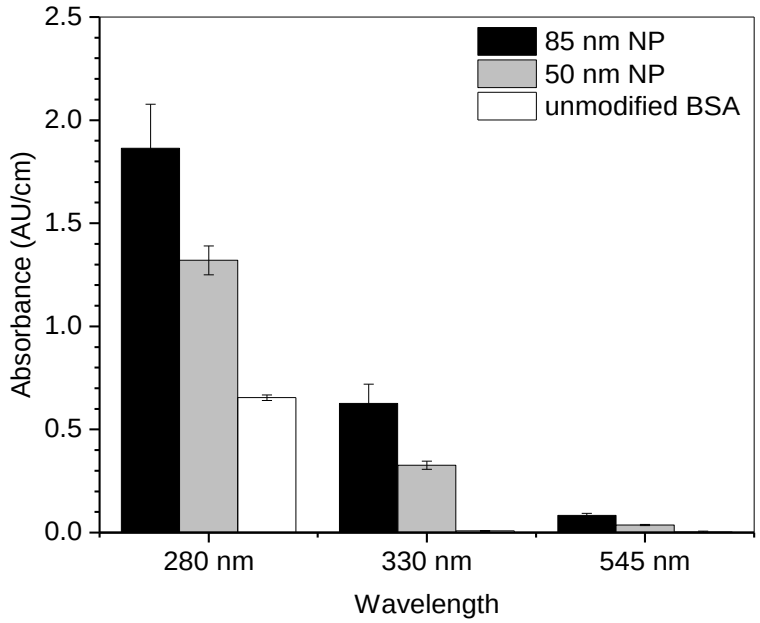

Figure 3-11 Light absorption characteristics at 280, 330 and 545 nm wavelengths for 1 g/L preparations of protein-nanoparticle (NP) preparations obtained through method C and unmodified BSA preparation in PBS, pH 7.0.

Error bars represent one standard deviation of absorbance measured for four protein preparations. Absorbance was measured using a quartz cuvette with 0.3 cm path length and Biomate 3S (ThermoScientific) spectrophotometer. High 330 nm absorbance for protein nanoparticles is likely due to increased scattering by the nanoparticles which also contributes to the net absorbance at 280nm.

Solute	**Extinction coefficients at 280 nm ($mL\ mg^{-1}\ cm^{-1}$)**
BSA	0.62
BSA NP (50nm)	1.23
BSA NP (80nm)	2.12

Table 3-3 Extinction coefficients for BSA and BSA nanoparticles calculated from dilutions of 1 g/L solutions of respective solutes.

Extinction coefficients (280 nm) for BSA and BSA nanoparticles preparation were calculated by measuring the absorbance of carefully diluted solutions of BSA nanoparticles. A strong dependence of the size of solute was observed with extinction coefficient for 50 nm preparation being ~1.7 times smaller than that of 80 nm preparation (See **Table 3-3**).

In some preparations, larger aggregates were formed and were eventually filtered out. Under such scenario, the mass balance equation could not be closed due to loss of the protein in large aggregates. This necessitated benchmarking filtered nanoparticle preparations against BSA solution based on a reliable criterion so that consistent feed of nanoparticles could be prepared. This was done by appropriately diluting the nanoparticles preparation to achieve a final absorbance at 280 nm equal to that of a solution of 1 g/L solution of unmodified BSA in the same buffer. This procedure avoids error-prone mass balance calculations against the use of a reliable spectrophotometer based reading to prepare appropriate dilutions. In similar particle size preparations, this method would likely result in feeds of similar particle titres if absorbance of 280 nm is similar.

It is easier to prepare a BSA solution of 1 mg/mL due to the availability of commercial lyophilised BSA powder. However, BSA nanoparticles are in suspension after their synthesis, and there is no direct method of quantification of nanoparticles except particle titre using NTA. Protein quantification using BCA based colourimetric assay resulted in lower absorbance for BSA nanoparticles solutions than that for an unmodified BSA solution of similar concentration prepared by mass balance. BCA assay detects protein by binding of the reagents to specific groups on the protein. Assay signal depends on the presence and density of these dye binding groups on the protein surface. Accessibility of these binding groups would decrease with a decrease in the total surface area of all protein molecules. Nanoparticle synthesis results in a decrease in this surface area as protein molecules aggregate to form larger particles. Reagent binding groups inside protein nanoparticles become inaccessible to the reagents thus resulting in lower signal output.

3.4.7.2 Surface charge characterisation of BSA nanoparticles

Proteins are charged molecules with multiple charge groups having different charge and valences. A sum of total surface charge results in a net charge on protein molecules which is affected by the ionic environment around proteins. The large size of protein nanoparticles increases their potential energy. Thermodynamically, such a system would attempt to reduce the surface area by collapsing into aggregates. However, the presence of charge on nanoparticles would result in a repulsive force to counterbalance aggregation. Thus aggregation of protein nanoparticles could be avoided by increasing repulsive forces among particles. This could be achieved by changing the pH of the solution.

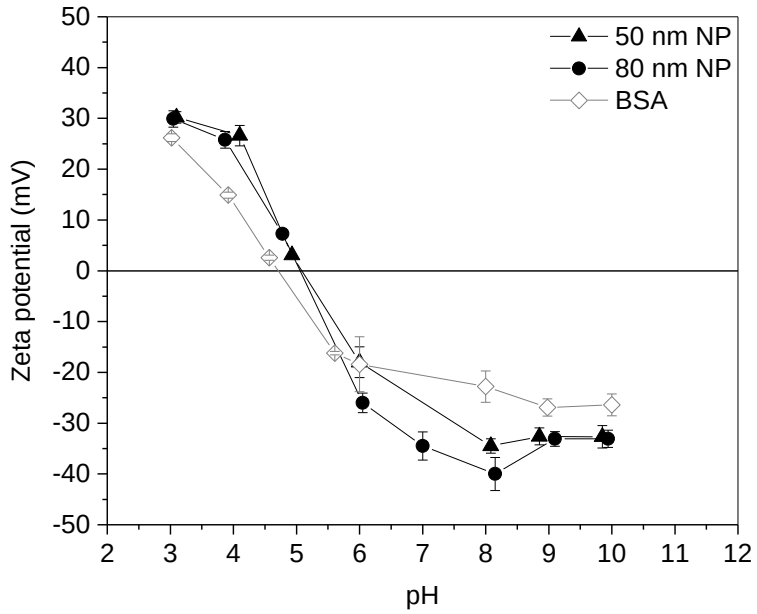

Figure 3-12 Zeta potentials of protein nanoparticles (50 and 80 nm NP) and unmodified BSA measured at various solution pH in 10 mM NaCl solution showing a shift of isoelectric point (pH where zeta potential = 0) of BSA nanoparticles to 5.2 from 4.8 for unmodified BSA. Both protein nanoparticles were prepared using method C.

Symbols and error bars represent mean values and one standard deviation respectively for three consecutive measurements of the sample at each pH value.

It has been reported that secondary and tertiary structure of protein undergoes drastic changes during the de-solvation process for nanoparticle synthesis. Thus surface charge distribution of the protein nanoparticles can be different from constituent proteins. This implies that protein nanoparticles could have different isoelectric points compared to their protein subunits. Nanoparticle preparations were tested for zeta potential at different pH from pH 3 to 10 and were found to have higher zeta potential compared to BSA solution. Isoelectric point (pI) was observed to be shifted from ~4.8 for BSA to ~5.2 for BSA nanoparticles (See **Figure 3-12**). This shift is likely due to cross-linking of terminal amino groups by the glutaraldehyde. Size of protein-nanoparticle did not have a significant effect on zeta potential values at different pH and isoelectric point. The difference in isoelectric point is significant but is inconsequential for storage of the protein nanoparticles. Both BSA and BSA nanoparticles should not be stored within 0.5 pH unit above or below the isoelectric points. Protein nanoparticles also showed higher zeta potentials than those of BSA at pH values away from isoelectric points. This could be attributed to the higher charge density of compact protein nanoparticles.

3.4.7.3 Stability of BSA nanoparticle preparation concerning storage temperature

It is essential to further studies that a nanoparticle preparation should be stable in the buffer used for a longer period. Most of the filtration experiments will be done at room temperature with nanoparticle preparations exposed to room temperature for at least a few hours. Further nanoparticle preparations are intended to be stable in the buffer for a few days at 4-8 °C to allow further analysis. **Figure 3-13** shows the change in particle diameter and polydispersity over the course of 72 hours (3 days) for storage at two temperature ranges. Intensity-weighted particle diameter, Z- avg was tracked as this parameter is highly sensitive to larger particles which may result from the aggregation of protein nanoparticles. Particle diameter and polydispersity index of preparation did not change significantly until 48 hours for preparations stored at 4-8°C. Compared to low temperature, particle size and polydispersity of preparations increased significantly after 24 hours of storage at room temperature. These changes, however, did not result from the aggregation of particles as the particle diameters increased by approximately 5 nm suggesting a change in nanoparticle density upon extended exposure to room temperature.

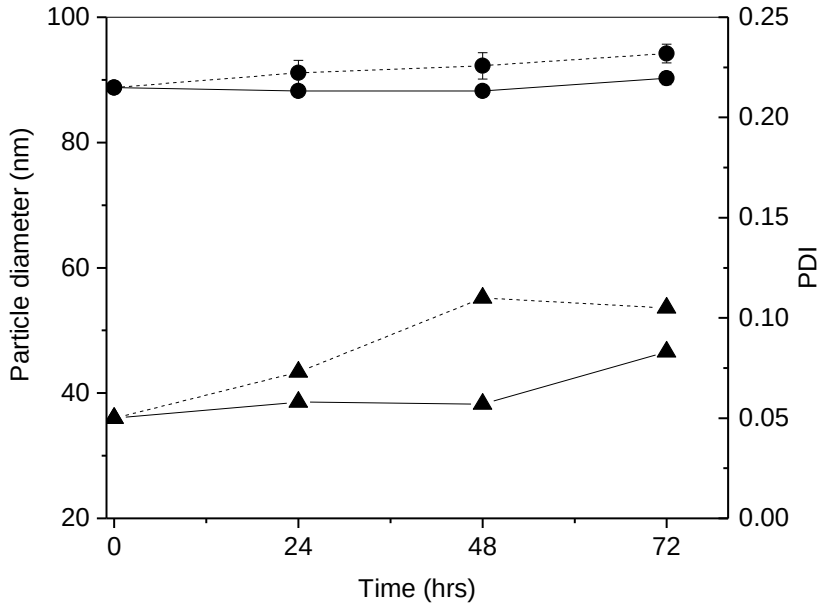

Figure 3-13 Stability of BSA nanoparticles preparations (obtained through method C) for storage at 4-8°C (—) and room temperature, 20-22°C (----) represented as time profile of particle diameter (●) and polydispersity index, PDI (▲).

Error bars represent one standard deviation around the average value for three measurements on the sample.

Presence of any significant fragmentation can also be ruled out from the observation of the polydispersity index in **Figure 3-13** as PDI remained below 0.1 which is expected to increase as partial fragmentation would make the solution more polydisperse. Further other parameters such as derived count rate, which is the total number of scattered photons collected from samples, remained constant throughout the storage duration. Numbers of photons scattered are sensitive to the composition of the sample.

Particle suspensions were also found to be stable for three months when stored at 4 °C in a mixture of ethanol and methanol as obtained after de-solvation. Particle size distribution did not change significantly after such prolonged storage despite the presence of glutaraldehyde indicating a complete cross-linking during preparation as also indicated by high yields. Galisteo-Gonzalez and Molina-Bolivar, (2014) have also reported no significant change in particle size distribution of preparations stored at 4 °C for as long as two months presumably after resuspension in water.

3.4.7.4 Particle titre measurement using NTA and TEM analysis of BSA nanoparticles

Particle size distributions and titres for nanoparticle preparation were measured by nanoparticle tracking analysis (NTA). A comparison of size distribution plots obtained through NTA and DLS, as shown in **Figure 3-14**, confirms similar size distribution for the nanoparticle preparations. NTA, however, shows a broader particle size distribution as it can track individual particles in real time while DLS deduces the particle size distribution from the bulk back-scattering characteristic of the solution.

No large aggregates beyond 200 nm were detected by any of these two techniques confirming that the sample is monodisperse. Particle titre for the nanoparticle solution was measured in the range of 1.4 – 2.1 x 10^{11} particles/ mL of 1 g/L (BSA absorbance equivalent) nanoparticle solutions in PBS when three different nanoparticle preparations were tested. This confirms that benchmarking nanoparticle solutions against 280 nm absorbance (equivalent to BSA absorbance) for denoting concentration is a reliable method to prepare a nanoparticle solution of particle titre of the defined range. This range, however, will be applicable for fixed particle size as particle titres would increase for lower particle size and vice versa assuming that packing density of nanoparticles does not change with particle size.

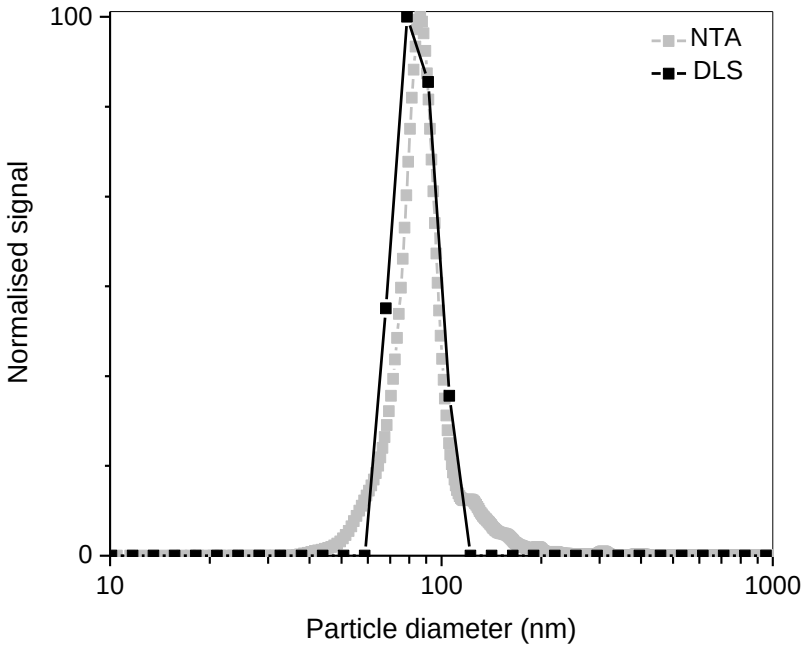

Figure 3-14 Comparison of particle size distribution of an 80 nm nanoparticle preparation prepared using method C using two orthogonal techniques DLS and NTA.

Both techniques showed similar particle size distributions and did not reveal any large aggregates.

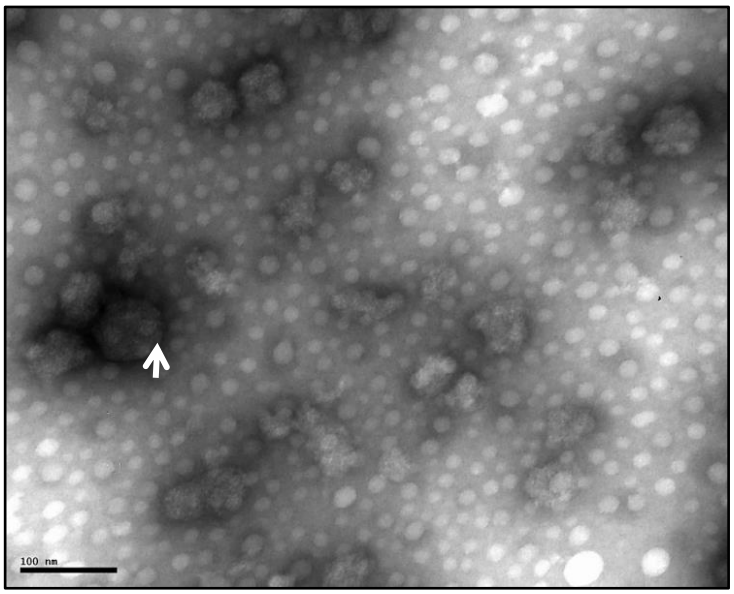

Figure 3-15 Analysis of 80 nm BSA nanoparticle preparation using Transmission Electron Microscopy after negative staining of nanoparticles indicated by white arrow.

Scale bar represents 100 nm and images were obtained at ~200,000x magnification factors. Non-spherical but globular nanoparticles were obtained using the method used.

Both DLS and NTA do not offer any insights into particle shape so nanoparticles were visualised using transmission electron microscope (TEM). Nanoparticle preparation, diluted in water and stained using uranyl acetate solution, was imaged under transmission electron microscope. **Figure 3-15** shows negatively stained nanoparticles. These nanoparticles are not perfectly spherical but rather a collection of smaller spherical nano-particulates which have dimensions around 20-50 nm. White spots are the grid artefacts.

3.4.8 Filtration: comparison of Adenovirus and 80 nm BSA nanoparticles

To investigate if nanoparticles could be used as a mimic for virus particles in purification studies, filterability of protein nanoparticles of 80 nm hydrodynamic diameter was performed using anodic alumina filters rated 100 nm for average pore size and compared with a similar experiment using partially purified Adenovirus feed. Similar stirring conditions were used using a stirred cell at 1000 rpm along with the same transmembrane pressure of 1 bar for both filtration experiments. Approximately similar filtrate volumes (7.5 - 8 mL) were collected for both nanoparticles as well as Adenovirus feed. Adenovirus feed showed lower filterability than nanoparticles which is likely due to the complex composition of Adenovirus feed.

Adenovirus feed showed slower filtration as the average cumulative flux of ~37 LMH was observed for filtration of ~7.5 mL feed as compared to ~80 LMH observed for filtration of ~8 mL of nanoparticles solution. However, the flux decline for both feed showed similar decay curve as shown in **Figure 3-16.** Adenovirus feed was found to have 4.9 ± 0.22 x 10^{10} particles/mL as compared to 2.1 ± 0.1 x 10^{11} particles/mL in BSA nanoparticles feed. Transmission of BSA nanoparticles was slightly higher 3.1 ± 1.9 % (n=3) compared to that of Adenovirus particles 1.5-2.2 ± 1.03 % (n=2). Lower flux for the Adenovirus feed could likely due to the fouling caused by particles with larger particle size as observed in the particle size distribution of the Adenovirus feed.

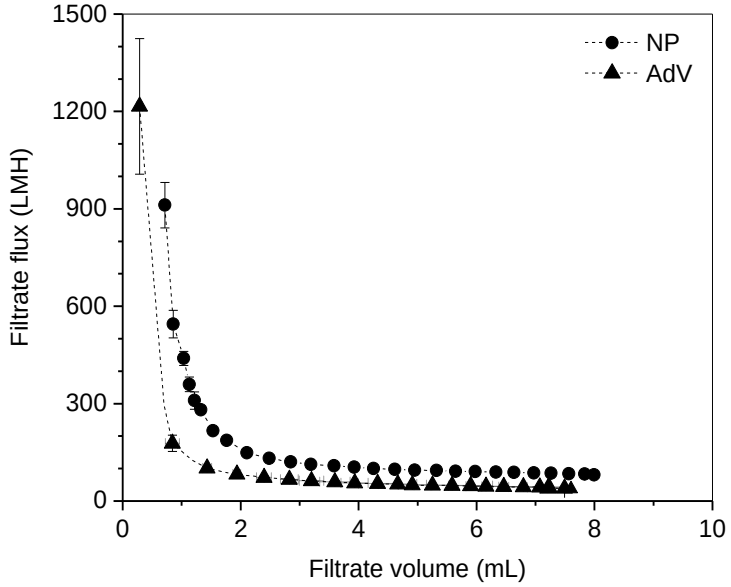

Figure 3-16 Comparison of filtrate flux (LMH) decline with filtrate volume (V) for Adenovirus feed (▲) and BSA nanoparticles feed (●) filtered through 2.83 cm^2 of 100 nm rated commercial PAA membrane (Anodisc) in stirred cell filtration.

Particle concentration of 10^{10}-10^{11} per mL was used for both feeds. Similar processing conditions (feed volume of 10 mL, transmembrane pressure of 1 bar and stirring rate of 1000 rpm) were used for both feeds. Error bars represent one standard deviation about the mean value of flux for triplicate filtration runs.

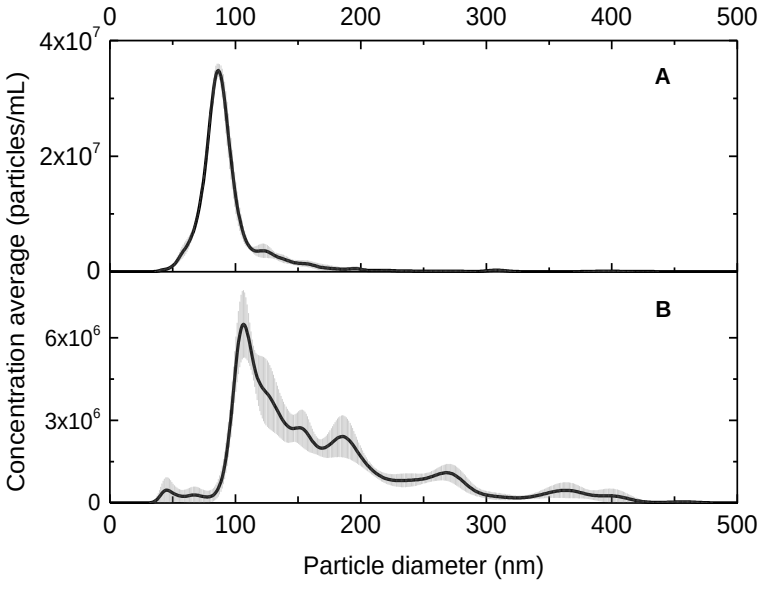

Figure 3-17 Comparison of particle size distribution of diluted protein nanoparticles feed (A), and Adenovirus feed (B) measured using NTA shows complex nature of Adenovirus feed with a major peak at 100 nm (similar to BSA nanoparticle preparation).

Both feeds were measured at 22-23°C and similar instrument setting. Grey bars represent one standard error about the mean (line) for 5 measurements of each sample.

Adenovirus feed is clarified supernatant obtained after cell disruption to release viruses. A centrifugation based clarification was used to remove debris. However, particles as large as 300-500 nm were still present in the feed (see **Figure 3-17**). They could be aggregates of virus itself as well as finner cell debris. Nanoparticles feed, however, showed narrower particle size distribution.

Adenovirus feed also shows particle sizes smaller than 100 nm likely which could be other protein aggregates, fragments of virus particles or exosomes. As far as transmission is concerned, transmission of particles from Adenovirus feed was lower compared to nanoparticles likely due to higher fouling by Adenovirus feed. However, in the case of Adenovirus feed, total particle count was used for transmission calculations. A fairer comparison would be to use highly purified Adenovirus particles with a titre equal to nanoparticles. Thus nanoparticles should be used cautiously as virus mimics and for only studying trends such as transmission or flux decline not for predicting absolute values of parameters.

3.4.9 Scale-up of BSA nanoparticle synthesis

In order to produce large amounts of protein nanoparticles, increasing volume of BSA solution from 1 to 2-3 mL was investigated for method C. Simply increasing volume, however, was found to alter size distribution characteristics of the final preparation. Preparations were found to have a significant amount of large aggregates and bimodal distributions in some cases **(for PSD plots refer to Appendix C).** In this study, synthesis was carried out at a smaller scale (1mL solution containing 100 mg BSA) with two preparations carried out simultaneously.

Since preparation time is ~3 hours and each preparation can usually be diluted to approximately 200 mL of the feed material with a titre of ~10^{11} particles/mL, sufficient nanoparticle preparation could be easily generated for small-scale experiments that were carried out in this research work. However, scale-up experiments do suggest that a simple volumetric scale up does not result in same particle size distributions as observed at smaller scales most likely due to altered mixing conditions. Thus, scale-up of nanoparticle synthesis needs to be studied in detail as it would be of crucial interest in various applications of protein nanoparticles such as therapeutics and food additives. Such a study, however, is not in the scope of this research work.

3.5 Conclusion

The objective of the chapter was to synthesise albumin nanoparticles and characterise them for the use as a mimic of virus particles for further filtration studies. A method was developed to synthesise albumin nanoparticles from bovine serum albumin under local laboratory conditions by controlled precipitation of the protein using organic solvents followed by cross-linking using glutaraldehyde. It was found that by altering the salt concentration in the initial protein solution the mean particle diameter can be tuned. Mixing in the vessel appears to be crucial in determining the particle size distribution and polydispersity of the nanoparticle preparations as the same protocol yielded different particle size distribution in vessels of different dimensions. Duration of the cross-linking step beyond 0.5 hours did not have any significant effect on the particle size distribution of the nanoparticle preparations (Section 3.4.4). Cross-linking duration of the method was optimised and was reduced to 2 hours compared to 12 hours as mentioned in the original literature. This resulted in a reduction of total preparation time to 3-4 hours without affecting the desired particle size distribution. Shorter preparation time is essential to generate a large amount of nanoparticle feed given that protocol was not found reproducible in a simple volumetric scale up (Section 3.4.9). The selected method was demonstrated to be repeatable by obtaining consistent particle size distribution and above 97% yield in four batches (Section 3.4.5).

High scattering due to the large size of nanoparticles was found to artificially increase the absorbance at 280 nm wavelength which is commonly used for protein concentration measurement. A benchmarking approach was thus devised to prepare the nanoparticle solution by diluting to a final absorbance equivalent to the BSA solution of 1 g/L. Benchmarking with the absorbance of BSA solution was useful in accurate quantification of protein nanoparticles and in preparation of consistent feeds for a particular particle size (Section 3.4.7.1). Nanoparticle preparations were found to be stable in buffer solutions for up to a day in room temperature and 2 days at 4°C to allow sufficient time for further analysis during filtration studies. Filterability of the nanoparticle preparation and Adenovirus feed was compared under similar processing conditions. Similar shape of flux decline curve was observed for both preparation, but membrane fouling was higher for Adenovirus feed possibly because of the polydisperse nature of the feed when compared to protein nanoparticles. The study shows the limitation of protein nanoparticles as a model mimic for viruses (Section 3.4.8). However, easy and economical production of protein nanoparticles makes them attractive models for preliminary experiments for a variety of studies targeted toward processing of large biomolecules such as viruses where morphology and biochemical characteristics of viruses could be ignored for initial developments such as screening of membranes for processing viral material.

CHAPTER 4 CHARACTERISATION OF POROUS ANODIC ALUMINA (PAA) MEMBRANES FOR FILTERABILITY OF PROTEIN SOLUTIONS OF SINGLE MODEL SOLUTES

4.1 Introduction and objective of the chapter

Polymeric membranes dominate ultrafiltration unit operations in biopharmaceutical processing (van Reis and Zydney, 2007). There have been significant improvements in the membrane as well module design for these applications. Primarily these membranes have been employed for concentration and buffer exchange rather than high-resolution separations unlike other DSP unit operations such as chromatography. This is due to the low selectivity of the membranes likely because of the presence of larger pores as defects (Urase *et al.*, 1994, Urase *et al.*, 1996). Thus membranes with uniform pore size distributions such as track etched membrane and anodised alumina membrane are attractive candidates for high-resolution separations of biologicals. Further, polymeric membranes have one drawback that they have limited solvent resistance especially to cleaning agents such as acids and bases and cannot be autoclaved. Ceramic membranes such as metal oxide membranes have better acid/base resistance and heat resistance. Porous anodic alumina (PAA) membranes are ceramic and offer quasi-uniform pore size distributions thus present an opportunity to design a new generation of ultrafiltration processes. However, little is known about their MWCO ratings, their filtration performance and fouling characteristics with a biological feed especially in comparison to the polymeric membranes.

The objective of this chapter is to screen commercial anodic alumina membranes of three different pore ratings for nanoparticles retention and subsequently compare selected membranes with commercial polymeric ultrafiltration membranes. PAA membranes are rated on the basis of pore size of the active side while polymeric UF membranes are usually rated by the molecular weight cut off (MWCO). The methodology used in this chapter is shown in **Figure 4-1** in the form of a flowchart.

This chapter will attempt to answer the following questions:

1. What is the pore size of the porous anodic alumina membrane potentially suitable for viral ultrafiltration?
2. How do porous anodic alumina membranes compare to polymeric UF membranes when rated using a standard dextran retention test for ratings?
3. How and if anodic alumina membranes differ in filtration performance and fouling susceptibility when compared to polymeric UF membranes?

4.1.1 Methodology used

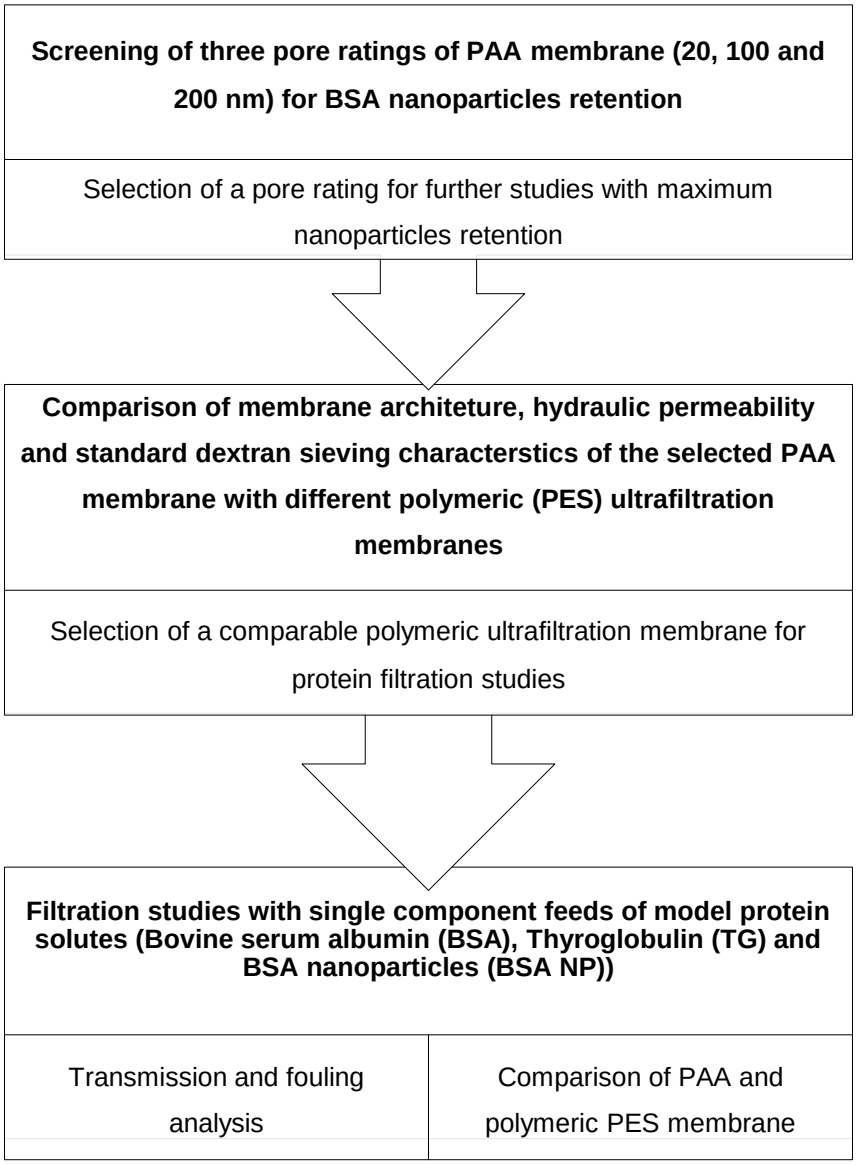

Figure 4-1 Schematics showing the methodology used and expected outcomes for objective 2 of the present work

PAA membranes of three ratings (20,100 and 200 nm) were screened for filterability and retention of 80nm protein nanoparticles. The membrane with the highest normalised process flux for nanoparticle solution and highest retention was selected for further experiments including dextran sieving and filtration studies with model protein solutes. Selected PAA membrane was compared with polymeric ultrafiltration membranes of three different MWCO ratings on the basis of hydraulic permeability, dextran sieving curves and membrane morphology using electron microscopy. Selected PAA membrane and a polymeric membrane with similar permeability and dextran sieving characteristics were then compared for filterability of protein solutions of single model solutes. Three model solutes were selected by the size of impurity and viral vectors. Transmission of the model solutes and fouling mechanisms were compared for the two membrane types.

4.1.2 Selection of the model protein solutes for filtration studies

A viral feed is a complex mixture of solutes containing virus particles as product and impurities such as host cell proteins, fragments of virus capsids as well as viral and host cell nucleic acids. All solutes except nucleic acids are proteinaceous. Nucleic acids can be ignored for the simplification of the present filtration studies as nucleic acids are usually degraded into smaller fragments (<100 base pairs) using commercial nucleases added after clarification of viral feed. Thus, a viral feed can be simplified to contain proteinaceous viral particles and protein impurities such as host cell proteins. Adeno-associated virus (AAV) and Adenovirus (AdV) are the most commonly used viral vectors, and their hydrodynamic sizes are reported to be 20-26 nm and 70-90 nm respectively (Burova and Loffe, 2005). Virus-like particles (VLPs) is another form of viral vectors and is reported to have dimensions in the range of 20 to 100 nm depending upon their composition. Thus, evaluation of ultrafiltration membranes for purification of AAV and AdV would necessitate two proteinaceous model solutes of two different sizes and another smaller proteinaceous solute to model as impurities or host cell proteins. For filtration studies, bovine serum albumin (BSA), bovine thyroglobulin (TG) and BSA nanoparticles were selected as model solutes representing smaller protein impurities or host cell proteins, AAV particles and AdV particles respectively. The basis of selection was average size either in terms of molecular weight or hydrodynamic size. Table 4-1 summarises the three model solutes used and the species of viral feed material they are intended to represent. The comparison is based on the size measurement of model solutes using DLS and the reported size of the major species encountered in the viral feed. BSA, to be used as model host cell impurity, is a monomeric protein of 67 kDa molecular weight. It has been reported that approximately 40 % of the host cell proteins produced in mammalian cell culture are in the range of 50-75 kDa molecular weight and more than 90% of all host cell proteins are within 25 to 100 kDa range with few proteins above 150 kDa (Jin *et al.*, 2010). Given that BSA monomer has a molecular weight of 67 kDa and BSA preparation used was found to have a significant amount of high molecular weight components (possible dimers and trimers), BSA can be used as a model impurity solute. Further, mammalian cell cultures also utilise serum-based media where albumin is the most abundant protein. Also, BSA is available in large quantities in lyophilised form at relatively lower costs compared to other proteins such as antibodies.

Thyroglobulin, a 660 kDa protein, was measured to have a hydrodynamic diameter of ~21 nm, similar to smaller viral particles such as AAVs. Protein nanoparticles of hydrodynamic diameter of 75-90 nm were selected to represent larger virus particles such as Adenovirus which are reported to have similar hydrodynamic size. BSA preparation, on the other hand, was measured to have an average hydrodynamic diameter of 8.1 nm, much smaller than both thyroglobulin and nanoparticles. Another variable in selection was availability and cost of the model solute. Larger proteins such as IgM (~900 kDa) can also be used, but limited availability and the high cost of these antibodies can be prohibitive for their use in experiments consuming large quantities of the protein.

Model solute for	**Reported particle diameter (nm) or molecular weight**	**Model solute used**	**Measured molecular weight or hydrodynamic diameter (nm)**
Impurities (HCP) (40% of HCPs)	25-75 kDa (Jin *et al.*, 2010)	**Bovine serum albumin (BSA)**	67kDa, ~8.1 nm
Adeno associated virus (AAV)	20-26 nm **(Burova and Loffe, 2005)**	**Bovine thyroglobulin (TG)**	21 nm
Adenovirus (AdV)	70-90 nm (Burova and Loffe, 2005)	**BSA nanoparticles (NP)**	74-90 nm

Table 4-1 Comparison of the reported solute size for common viral vectors and host cell proteins with measured hydrodynamic size of the model solutes used for filtrations studies. *Particle size distribution measured for three solutes are included in Appendix D.*

As all three model solutes have very close isoelectric points (in range of 4.6 to 5.1) the net surface charge (i.e. positive or negative) of the solutes at any given value of pH outside the above range will be same. Thus any effect of the surface charge could be ignored when comparing the filterability of different model solutes at a given pH value. Further, isoelectric points for Adenovirus and BSA protein nanoparticles were also closer at 4.7 and 5.0 respectively thus making BSA nanoparticles a reliable model solute. A limitation for the use of these model solutes is that they are intended to be physical mimics of viral particles and do not imitate the structural complexity and shape of the virus capsid. Thus these solutes can only be used for preliminary studies where the mechanism of separation is dominated by the size exclusion and to a limited extent electrostatic but not due to bio-specificity. Thus, the use of these model solutes cannot be extended to chromatography except size exclusion.

4.2 Materials and methods

4.2.1 Materials used

Bovine serum albumin, BSA (heat shock fraction, pH 7, > 98% purity, (A706)) and Bovine thyroglobulin, TG (> 90% purity, (T1001)) were purchased from Sigma-Aldrich, USA. PAA membrane discs of 25 mm diameter, Anodisc^{TM} of three pore ratings, 20 (6809-6002), 100 (6809-6012) and 200 nm (6809-6022) were procured from GE Healthcare, UK. Membrane discs of polymeric commercial ultrafiltration membranes, Biomax$^{®}$ of 100(PBHK02510), 300 (PBMK02510) and 500 kDa (PBVK02510) were obtained from EMD Millipore, MA, USA. Gel filtration protein standard (151-1901) from Biorad, CA, USA; Dextran from *Leuconostoc* sp, M_r 1500,000 -2800,000 (D5376), Dextran M_r 450,000 -650,000 (31392) and Dextran M_r 40,000 (31389) were procured from Sigma-Aldrich, Denmark while Dextran M_r 6,000 (31388) was obtained from Sigma-Aldrich, China. Gel permeation chromatography (GPC) grade dextran standards were purchased from Sigma-Aldrich, USA. Size exclusion columns (SEC), TSKgel3000SWXL (08541) and TSKgel5000PWXL (08023) were purchased from Tosho Biosciences GmBH, Germany. Size exclusion column, Bio SEC-5 (5190-2536) was obtained from Agilent, USA.

4.2.2 Filtration runs with solutions of model protein solutes

Filtration of the model protein solutes, BSA, TG and BSA nanoparticles was carried out in a 25 mm stirred cell module. Filtration set up used in the study is thoroughly described in materials and method of Chapter 3 (Section 3.3.7.1). All solutions, including buffers and protein solutions, were prepared using deionised water obtained from MilliQ water purification systems (Millipore) and the solutions were also subsequently filtered using 0.22 µm rated low protein binding PES filters. Only BSA nanoparticle solutions were filtered using 0.45 µm rated PES filters. All protein solutions were prepared in phosphate buffer saline (PBS, pH 7.4). Protein solutions with solute concentrations of 1.0 mg/mL were prepared for BSA and BSA nanoparticles. For TG solution, the concentration of 0.2 mg/mL was used. All solutions were prepared at room temperature conditions (21-23°C). Filtration was carried out using 25 mm membrane discs for both PAA (Anodisc) and polymeric PES membranes (Biomax). Available membrane diameter for discs was, however, smaller than 25 mm due to the presence of an impermeable seal (1 mm thickness) to be placed on top of the membrane while assembling the stirred cell. PAA membrane disc also had a 3 mm wide circular polypropylene support ring thermally bonded to the active side of the membrane, thus reducing effective membrane diameter to 19 mm. Thus the active filtration area for PAA membranes was 2.83 cm^2 compared to 4.15 cm^2 for a polymeric membrane like Biomax.

Both membranes were rinsed before assembling into the stirred cell. PAA membranes were washed with 20% ethanol solution for 3-5 minutes. Polymeric membranes were rinsed as per manufacturer's instructions, for 1 hour using pre-filtered, deionised water to remove any preservatives used for dry storage of the membranes. After assembling into the stirred cell membranes were first flushed with 20 L/m^2 of MilliQ water at different transmembrane pressures (in increasing order) to assess the hydraulic permeability. Subsequently, membranes were flushed with 20 L/m^2 of the buffer solution at similar transmembrane pressure as to be used for protein filtration. Time taken for filtration of 20 L/m^2 buffer was noted using a stopwatch and used to calculate the pre-filtration flux or initial buffer flux (J_o) for the clean membrane. While comparing two membrane types (PAA and PES), equal loading of protein solution (the volume of feed added per active filtration area, L/m^2) were applied, and similar filtrate outputs (the volume of the filtrate collected per active filtration area, L/m^2) were collected. Before loading protein solution into the stirred cell, any residual buffer solution was removed to avoid dilution of the protein solution. However, the buffer solution in the filtrate line was not removed to enable measurement of the filtration force (flow rate) for the initial period of the filtration. After filtration, the retentate solution was carefully aspirated out, stirred cell with the membrane and stirrer bar were rinsed with successive washes of 2, 5 and 5 mL of the buffer solution. Membranes were then flushed with the buffer solution as done before the protein filtration to measure the buffer fluxes after filtration. Recovery of the buffer permeability was calculated as a percentage of the initial buffer flux measured as post-filtration buffer flux at same transmembrane pressure.

For most of the experiments, a pressure of 0.6 bar is used with a stirring rate of 1500 rpm unless stated otherwise. The filtrate was collected in tubes kept on weighing balance. Readings from weighing balance were manually noted down at regular intervals (30 seconds) during the filtration runs. Filtration volumes were deduced from weighting balance reading by the assumption of the uniform fluid density of 1 g/mL for all solutions. This assumption is valid considering the low concentration of proteins in solution. Filtrate, retentate and feed samples were analysed for protein concentrations.

4.2.3 Dextran sieving characterisation of membranes

Dextran feed solution was prepared from a mixture of four dextrans (6, 40, 450 and 2000 kDa) with each dextran at 1 g/L final concentration except 0.5 g/L for 2000 kDa dextran. The solution was prepared in 20mM phosphate buffer (pH 7.0). Approximately 20 L/m^2 dextran feed solution was added to the stirred cell (10 mL capacity) with membranes mounted on the base of the stirred cell. This loading corresponded to 5.6 mL and 8.3 mL of feed solution for PAA and PES membranes respectively. The filtrate was recirculated to stirred cell through a tubing (Master flex, 1.6 x 500 mm) using a peristaltic pump (Watson Marlow 120U) as illustrated in **Figure 4-2**.

Filtrate flow rate was kept at 1.5-1.6 µm/s (5.5-5.8 LMH) by adjusting the pump rotation speed at 0.2 and 0.3 rpm for PAA (Anodisc) and PES (Biomax) membranes respectively. This was the minimum rotational speed for the pump. The filtrate was recirculated for 2 cycles (i.e. a total of 40 L/m^2 filtered through membranes) to ensure well steady state. This corresponded to 7.2 and 6.8 hours of total filtration time for PAA and PES membranes respectively.

Samples were collected from stirred cell and filtrate tubing at the end of 2 recirculation cycles. Samples were analysed using high-pressure size exclusion chromatography (HP-SEC) using TSKgelPW5000XL column (7.8 x 300 mm) operated at 0.3 mL/min in isocratic conditions using 20 mM phosphate buffer at pH 7.0. Injection volume for both filtrate and feed sample was 100 µL (<1 % of column volume). Since dextrans do not absorb any particular wavelength, diode array detector could not be used. Instead, refractive index detector (RID-20A, Shimadzu) was used to detect the dextrans. The column was well equilibrated using the same buffer for at least 10 column volumes. Calibration was carried out by injecting solutions of monodisperse gel permeation chromatography or GPC grade dextran standard (T5, T12, T25, T50, T80, T120, T250, T450 and T660) prepared at 1 g/L concentration in the same buffer as mobile phase. The calibration plot was obtained by plotting peak retention times against specified peak molecular weight for the GPC grade dextran standards. The calibration plot was used to transform the time axis of chromatograms for samples into molecular weight. Sieving curves are then obtained by normalising chromatograms for the filtrate samples with that of the feed sample as shown in **Figure 4-3** and the formula below the figure.

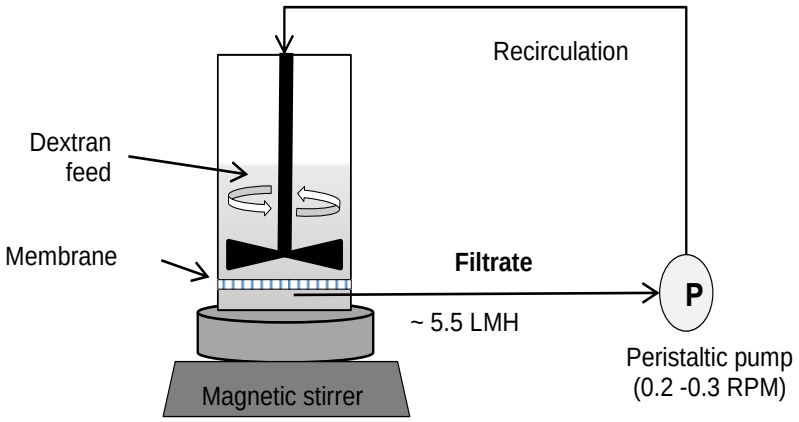

Figure 4-2 Illustration of the filtration set up for dextran sieving experiments.

Stirring speed is set at maximum of 1500 rpm after addition of the dextran and then pump is switched on. Recirculation is carried out for 2 recycles of total feed volume. At the end of recirculation, pump is stopped and samples from both stirred cell (feed) and filtrate line were collected and injected onto to size exclusion column. Sample is collected from this end of the filtrate line.

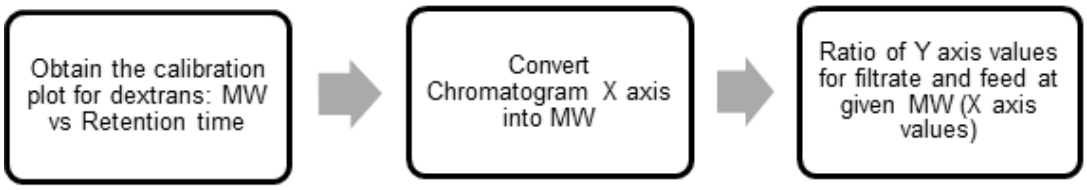

Figure 4-3 Schematic for analysis of the chromatograms of the dextran feed and the filtrate obtained using size exclusion chromatography to calculate sieving values

Sieving coefficient for a given molecular weight (MW) value of x was calculated using the following formula

$$Sieving\ coefficient_x = \frac{Signal\ amplitude\ for\ Filtrate\ at\ x\ MW}{Signal\ amplitude\ for\ Feed\ at\ x\ MW}$$

4.2.4 Scanning electron microscopy (SEM) of membranes

Membranes were fixed on aluminium stubs (13 mm diameter) using adhesive carbon discs and sealed on edge with conductive silver paint. Samples were then dried overnight in a closed chamber with moisture absorber pellets. Both alumina and PES being non-conducting materials could not be observed directly under electron microscope due to strong charging effects. Hence, samples were sputter coated with Platinum using sputter coater (Cressington 108auto) for a coating cycle of 24 seconds under helium. The coating thickness of 0.4 nm was achieved in this cycle. Platinum coated samples were then mounted on the stage and observed under field emission SEM (Zeiss Gemini, Sigma) using a secondary electron detector (InLens detector) in vacuum conditions. Low gun voltages of 3-5 kV were used at working distances between 3-7 mm with an aperture size of 30 µm.

4.2.5 Image analysis of SEM images for pore size distribution

Images acquired using SEM were analysed using software Image J (NIH, USA). Scale settings were fed into software by manually selecting the scale bar dimensions from raw images. Usually, 1.4 nanometres per pixel resolution was obtained for images of anodic alumina membranes obtained at 100,000-magnification factor. Images were then cropped to remove portions other than membrane features and normalised for enhanced contrast between pores and membrane wall. Images are smoothened to remove any noise or blur and then segmented. Segmentation of image refers to identifying a feature of the image by locating pixels of that feature in grey scale histogram. Greyscale value is representative of the light intensity stored in a pixel from 0 (black) to 255 (white). Threshold adjustment is made to segregate pore spaces from pore walls as former were usually black while latter brighter in intensity. Segmented

images only have information about pore space and are represented as two-dimensional particles. These particles are then counted, annotated with a number and area of the particle is measured. The equivalent circular diameter of the pore is obtained from the area of the particle in the segmented image. Debris (bright) on the membrane is recognised as the wall material and is not thus included as particles. **Figure 4-4** illustrates the various steps used in the image analysis with an example of the steps performed on a PAA membrane.

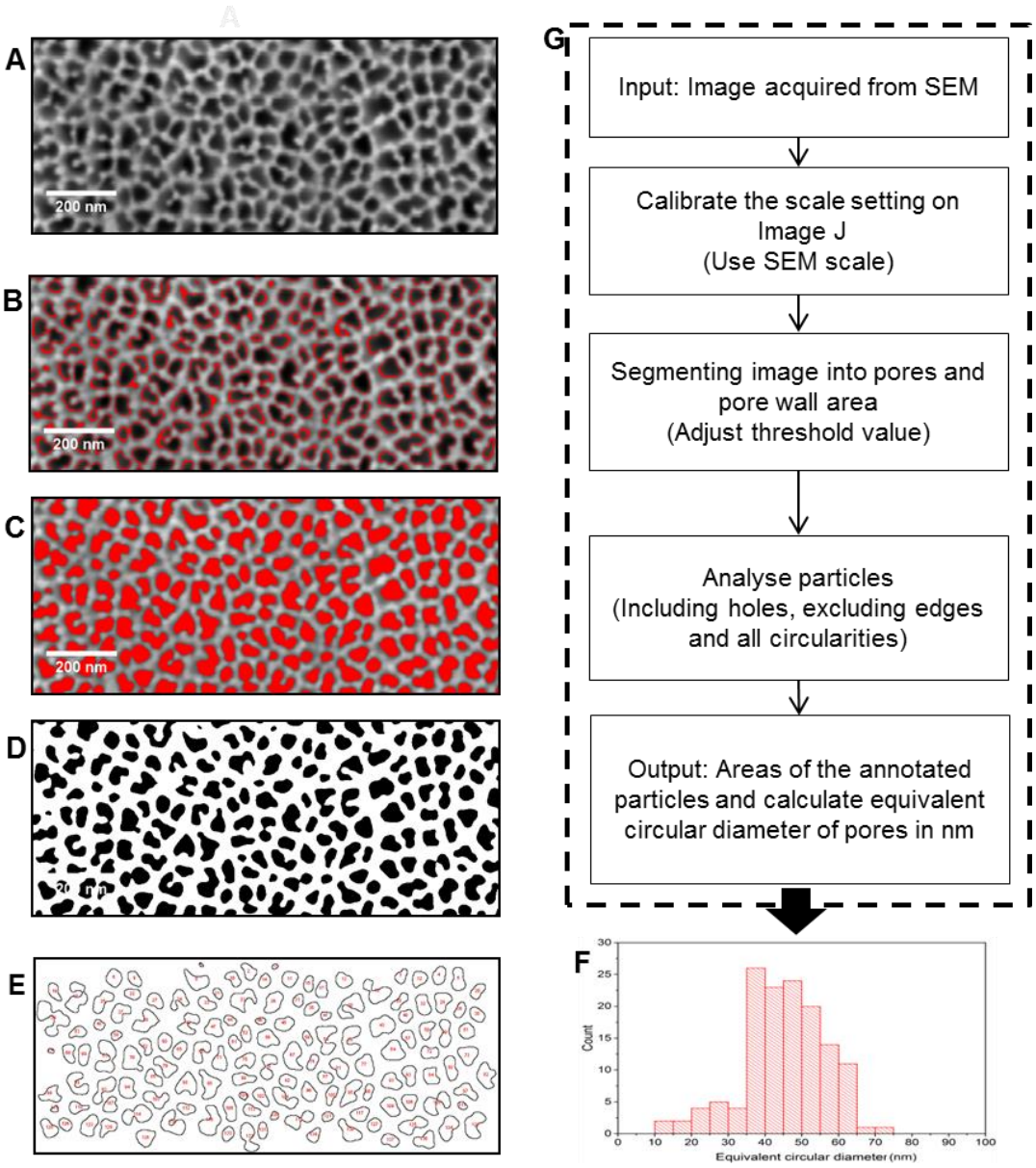

Figure 4-4 SEM image processing using Image J (NIH) software for evaluation of pore size distribution of membranes.

Step A. Original image with scale bar, B. Image with threshold adjusted to identify pore walls C. Image with threshold adjusted to include pore area D. Segmented image showing only pores as 2D particles, E. Pores annotated by software after identification of boundaries and subsequently analysed for area of pores. F. Pore size distribution obtained post-processing G. Process flow diagram for image processing.

4.2.6 Curve fitting for identification of the fouling mechanisms

Fouling mechanism for various protein filtrations runs was identified by fitting the experimental filtration data (initial buffer flux, filtrate volume and time) with well-established mathematical models (Bolton *et al.*, 2006) for four fundamental mechanisms (standard blocking, complete blocking, intermediate blocking and cake filtrations). These models are discussed in detail along with their mathematical expressions in Chapter 2 (see Section 2.4.2.1.1 and **Table 2-3**). For analysis of the fits, curve fitting tool of software, OriginPro (OriginLab Corp, USA) was used. Curve fitting tool is supplied with the mathematical expression and experimental filtration data to perform iterative fitting by assessing the goodness of the fit. Curve fitting tool initialised the value of the output parameter (blocking constant, k_x) and then predicts the values of volumes based on experimental time data. Residuals (the difference between predicted and experimental values of volume at same time point) of the volume-time curve are then squared and added to calculate the sum of the square of residuals (SSR). A least square algorithm known as chi-square minimisation is used to minimise the value of the chi-square (χ^2). The value of the output parameter is iteratively adjusted using Levenberg-Marquardt (LM) algorithm.

Experimental volume data was normalised with filtration area and converted to SI unit (m^3/m^2) for curve fitting. Initial buffer flux values in m/s units were used for input values of initial flux. Outputs from non-linear fittings were SSR, the adjusted regression coefficient (R^2) and blocking constant. R^2 and SSR values were used to compare fits with different mechanisms. The ideal fit would have SSR value of 0 and an R^2 value of 1. A mechanism where the best fit had highest R^2 and lowest SSR values were considered as dominant mechanism.

4.2.7 Estimation of protein transmission

Protein transmission in the filtrate samples was estimated by analysing filtrate and feed samples using size exclusion chromatography. For BSA and TG, 50 µL of sample was injected onto a 7.8 mm x 300 mm SEC column, TSKgel3000SWXL (Tosoh Biosciences GmBH) at 0.6 mL/min under isocratic conditions with PBS with Agilent 1260 Infinity HPLC system. For BSA nanoparticles, a 7.8 mm x 300 mm SEC column with larger pore sizes of 100 nm, BioSEC-5 (Agilent, UK) was used with 20 µL sample injection and 0.6 mL/min flow rate under isocratic conditions with PBS. Protein transmission and recoveries were calculated by using peak areas per injected volume of the sample as equivalent concentrations. Protein peaks were detected by measuring absorbance at 280 nm (characteristic absorption wavelength of some amino acids) or 214 nm (characteristic absorption wavelength of peptide bonds) using an inline UV detector.

4.3 Results and Discussion

4.3.1 Screening of various pore ratings of commercial PAA membrane for filterability of BSA nanoparticle preparation

Commercial PAA membrane, Anodisc is offered in three pore ratings viz. 20, 100 and 200 nm. These ratings refer to the nominal pore size of the thinner (<1 µm) active layer of the membrane supported by a thicker (~59 µm) layer of straight channel pores of larger diameter (~200 nm). These membranes would obviously have different filtration and retention properties for solutes. Three pore ratings were screened for filterability and retention of protein nanoparticles of ~90 nm diameter. Selection of BSA nanoparticles, a model system for Adenovirus particles, to screen three pore ratings is appropriate as the goal of the present work is to evaluate PAA membranes for viral separations. Equal volume (8 mL) of 1 g/L protein nanoparticles (of ~ 90 nm diameters) solution in PBS was filtered through membranes of three pore ratings at a trans-membrane pressure of 1 bar (±0.1 bar assuming 10% error in the analogue readout) and stirring rate of 1000 rpm. TMP of 1 bar selected on the basis of values reported in literature relevant to virus ultrafiltration. Nanoparticle concentration in the feed, filtrate and retentate were measured using nanoparticles tracking analysis. Log removal values were then calculated for nanoparticles removal in the filtrate solutions.

PAA membrane with 20 nm pore rating operated at higher steady-state flux percentage of 5% (process flux normalised to initial buffer flux through the membrane), compared to 100 and 200 nm membranes where process fluxes declined to less than 1% of the respective initial buffer fluxes. The flux decline was not as prominent for the membrane with 20 nm pore rating as seen in **Figure 4-5**. This was likely due to the lower accessibility of pores in 20 nm rated membrane where the majority of pores will be much smaller than the dimension of nanoparticles (80-90 nm). On the other hand, majority of pores in 100 and 200 nm membranes are likely to be in similar or larger size range as of nanoparticles size distribution thus increasing the chances of pore blockage by protein nanoparticles. Fouling susceptibility was also confirmed by comparison of recovery of buffer permeability (measured before and after the filtration) of the membrane for different pore ratings (**Table 4-2**). It was found that for 20 nm membrane approximately 22% of the permeability of the clean membrane could be recovered after the filtration of BSA nanoparticles. Recovery of the buffer permeability decreased with increase in the pore rating of the membrane with the 200 nm membrane being most fouled. The actual value of the average process flux was lower for 20 and 100 nm membrane compared to the 200nm membrane. The high value of the process flux for 200 nm is due to the high porosity of the membrane and high permeability value resulting in very high initial flux.

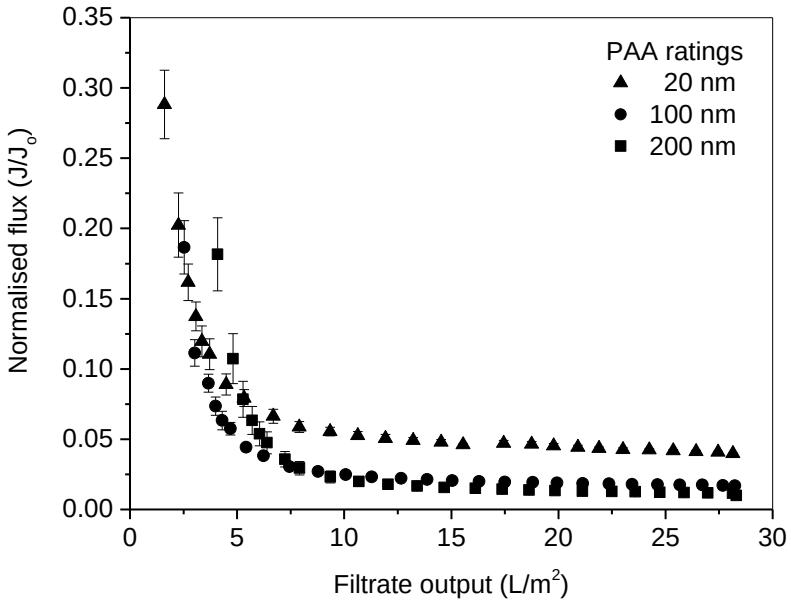

Figure 4-5 Flux decline for the filtration of 80 nm BSA nanoparticles solutions through different pore ratings (20,100 and 200nm) of the PAA membranes.

Fluxes were normalised by the initial buffer flux (J_o) for the respective membranes. BSA nanoparticles solutions (1 mg/mL) were filtered through membranes at 1 bar transmembrane pressure and stirring speed of 1000 rpm. Error bars represent one SD for three filtration runs using fresh membranes.

Pore rating	Process flux	Permeability (before filtration)	Permeability (after filtration)	Recovered permeability
	LMH	**LMH/bar**	**LMH/bar**	**%**
20 nm	81 ± 0	2003 ± 18	430 ± 29	22 ± 2
100 nm	81 ± 0	4897 ± 188	601 ± 144	12 ± 3
200 nm	94 ± 1	6583 ± 193	512 ± 124	8 ± 2

Table 4-2 Process flux, membrane permeability before and after filtrations and recovered permeability for different pore ratings after protein nanoparticle filtration (~28 L/m^2) at 1 bar pressure and 1000 rpm stirring (average values ± one SD for three filtration runs using fresh membranes)

As shown in **Table 4-2**, average process flux for ~28 L/m^2 filtrate output was highest for 200 nm rated membrane at ~94 LMH compared to ~80 LMH observed for both 20 and 100 nm rated membranes. Flux decay profiles were very similar for all three pore ratings. However, since the hydraulic permeability of different pore ratings is significantly different, it is more sensible to study normalised flux decay than absolute flux decay.

Transmission of the protein nanoparticles was also compared for different pore ratings. For virus filtrations, log removal values are often used to assess the ability of the membranes to remove virus particles from a virus-rich feed. Log removal values (LRVs) were obtained by negative log value of the ratio of BSA nanoparticles concentration in the filtrate to that in the feed solution as measured using nanoparticle tracking analysis. As expected, transmission of nanoparticles increased with pore ratings with 20 nm membrane capable of ~3 log removal as shown in **Figure 4-6**. Total protein recovery measured using 280 nm absorbance assay also showed the lowest transmission loss of protein nanoparticles with 20 nm rated PAA membranes.

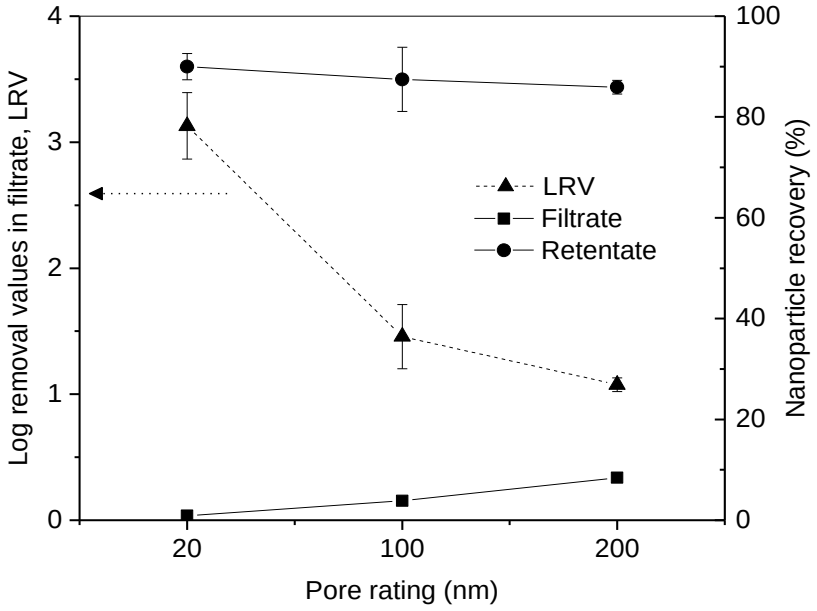

Figure 4-6 Log removal values (LRV, ▲) for BSA nanoparticles in the filtrate collected through different pore ratings of PAA membranes and nanoparticles recovery (% of feed) in the retentate and filtrate at different pore ratings.

Log removal values were calculated from particle titre values in the filtrates and feed solution as obtained using nanoparticle tracking analysis (NTA) and protein recovery was calculated on the basis of absorbance at 280 nm. Lot 1 of 20 nm rated PAA membrane (Anodisc) was used in this experiment.

Analysis of protein recovery in the retentate (using A280 absorbance assay) showed 90 ± 2.5 % of the protein retained by 20 nm pore ratings as opposed to 87± 6 % for 100 nm and 86 ± 1 % for 200 nm membranes. Net recoveries for all three membranes were between 90 to 95 %. PAA membrane with 20 nm pore rating was thus selected for further experiments as it showed better filterability, low fouling susceptibility and highest retention among three pore ratings of PAA membranes.

4.3.2 Comparison of membrane morphology of 20 nm rated PAA membranes and polymeric PES ultrafiltration membranes of various MWCO ratings

4.3.2.1 Comparison of the active layer surface of the membranes and pore size distribution obtained from image analysis

Commercial PAA membrane (Anodisc, 20 nm rating) and commercial polymeric PES ultrafiltration membranes (Biomax, 100, 300 and 500 kDa) were compared using scanning electron microscopy. Surface images of the active layer side of the membranes show non-uniform pore diameters, especially for 300 and 500 kDa polymeric membranes. Except for the 100 kDa PES membrane, all of the membranes were found to be highly porous. PAA membrane exhibited smaller pores and more uniform pore sizes across the membrane surface (See **Figure 4-7**)

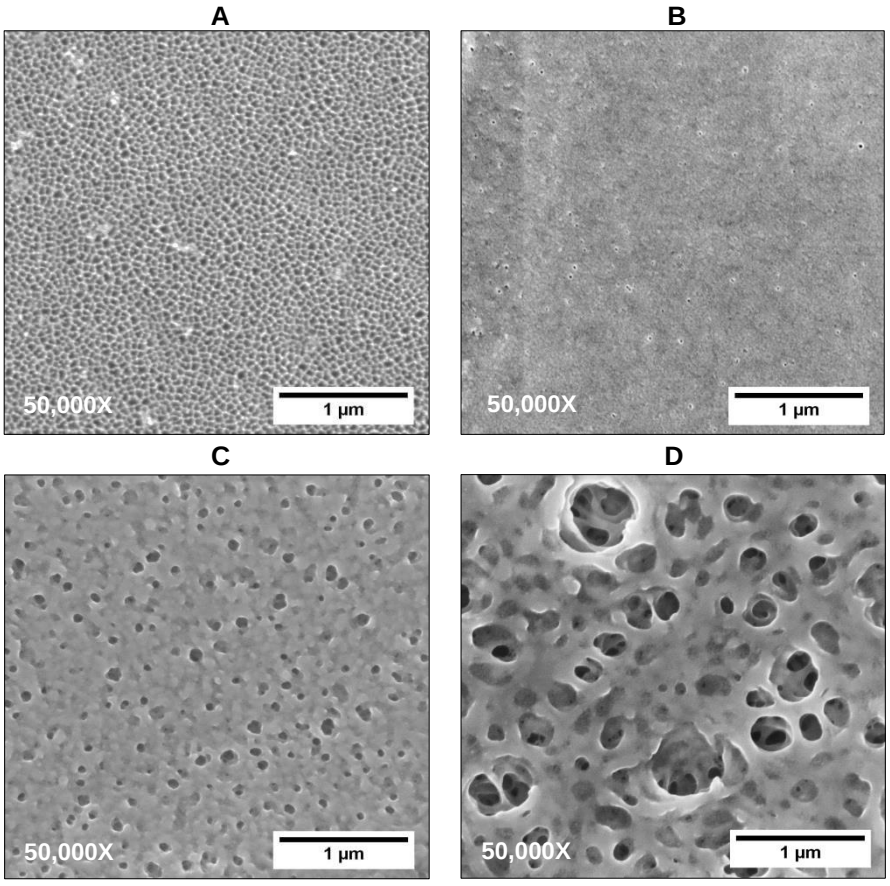

Figure 4-7 SEM images of the active side surface of a PAA membrane rated 20 nm (A) and PES membranes rated 100 kDa (B), 300 kDa (C) and 500 kDa (D) obtained at a magnification factor of 50,000X using FE-SEM (Leica Sigma). Scale bar corresponds to 1 µm distance.

All the images were obtained using InLens detector (secondary electron detector) with 30 µm aperture, the gun voltage of 4-5 kV and a working distance of 3-7 mm. Commercial PAA membrane, PAA (Lot 1) and PES membrane (Biomax) were used.

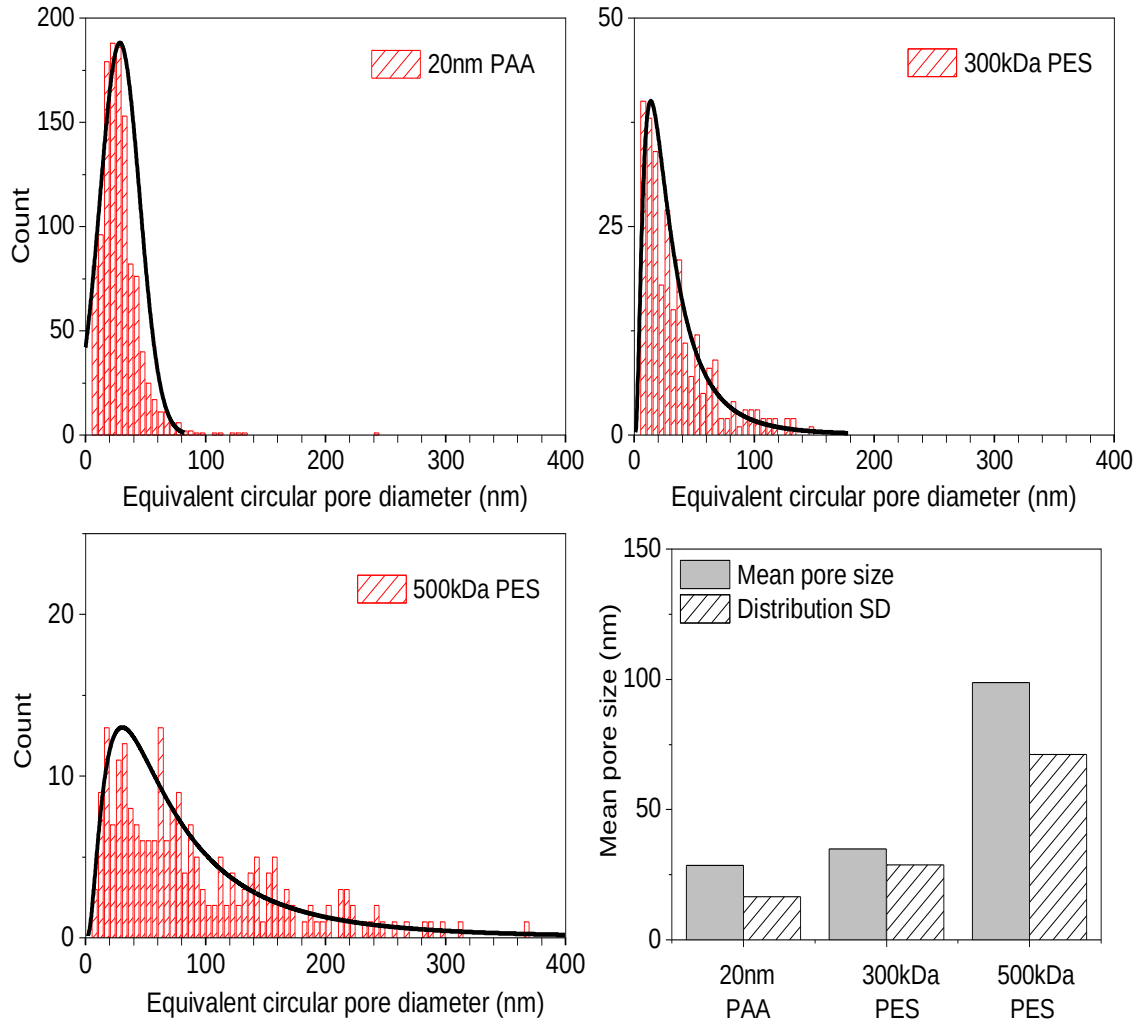

Figure 4-8 Surface pore size distribution for the active layer of PAA membrane rated 20 nm, and PES membranes rated 300 kDa and 500 kDa obtained by analysing SEM images.

Histograms are plotted for the equivalent pore diameters obtained using bin size of 5, and best fitting distribution curve (black line) was applied. The plot on the lower right side shows the mean pore size and distribution standard deviation as obtained from descriptive statistical analysis of the histograms.

Though the mean pore size for the 20 nm PAA and 300 kDa PES membranes were similar, the pore size distribution was narrower for 20 nm PAA membranes as highlighted by the lower value of the distribution standard deviation. However, distribution standard deviation, which is an indicator of the spread of the pore size values, was lowest for 20 nm rated PAA membrane with a value of 16.5 while values for 300 kDa and 500 kDa were calculated to be 28.8 and 71 respectively (shown in **Figure 4-8**). Pore size distribution of 100 kDa membrane could not be determined due to the poor quality of SEM scan for this membrane as well as the presence of a very low number of pores.

4.3.2.1.1 Comparison of commercial PAA membrane with custom fabricated PAA membranes reported for virus separation studies

It is apparent from **Figure 4-9** that such custom-made membranes have different pore shape and narrower pore size distributions compared to the commercial product used in the present study. This could be because of the differences in fabrication method employed by the manufacturer and by research groups fabricating in-house. Apart from pore size distribution, pore morphology is also different. Membranes used in a majority of the reported literature have circular, or near circular pores, however, commercial PAA membranes show a variety of pore geometries with most of the pores being polygonal.

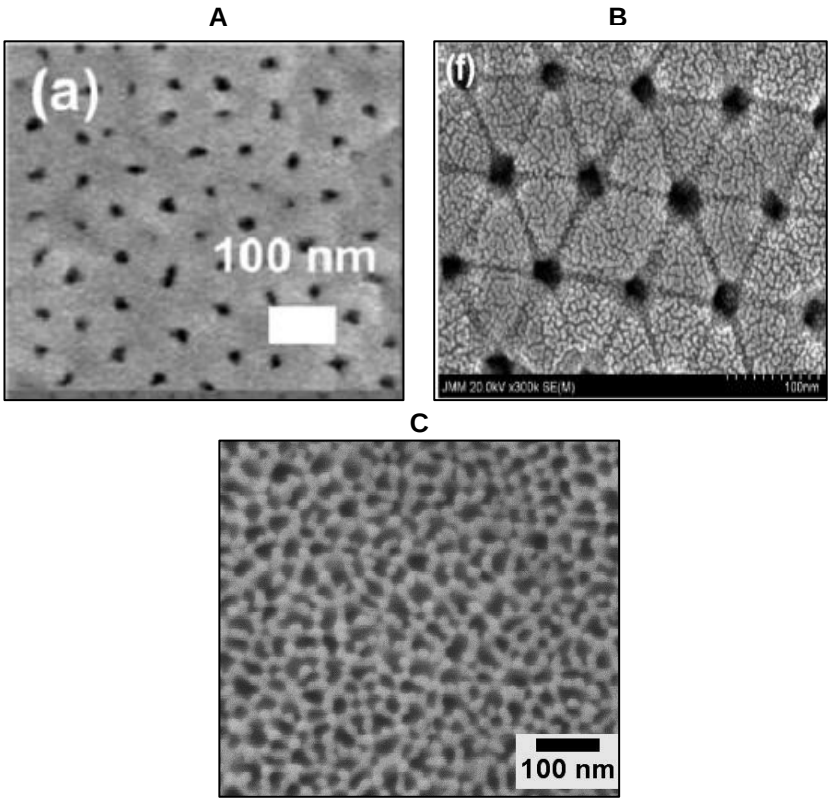

Figure 4-9 Comparison of the commercial PAA membrane used in the present study with reported in-house fabricated PAA membranes used in other viral separation studies.

A. AAM (pore size ~23±2 nm) used by Jeon et al,(2014) for enrichment of HCV , B. AAM (pore size ~25±3 nm) used by Moon et al,(2009) for separation of empty and filled capsids of bacteriophages and C. commercial PAA (Anodisc) membranes rated 20 nm by manufacturer (used in this study). Figure A and B reprinted with permissions.

4.3.2.2 Comparison of membrane architecture across the membrane thickness

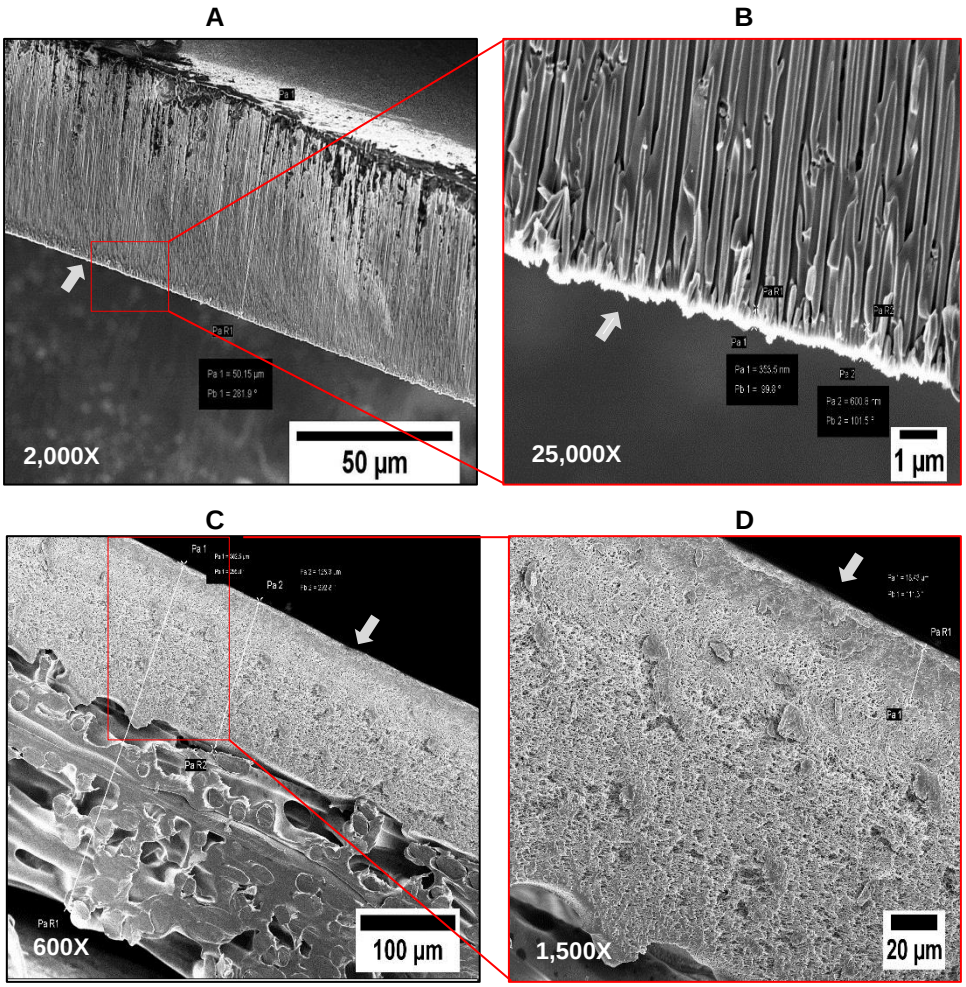

Figure 4-10 SEM images of the membrane cross-sections of the PAA membrane rated 20 nm (A, B), and PES membrane rated 300 kDa (C, D).

The white arrow indicates the active side of the membrane. Different magnifications were used for the two different types of membranes. Magnified sections of membranes are represented in red boxes.

Membrane morphology for polymeric ultrafiltration membrane and PAA membrane differs significantly across the membrane thickness. Both membranes are asymmetrical but different in tortuosity. Polymeric membranes show three distinct zones across the thickness exhibiting different porous structure as visible in **Figure 4-10** (C and D). The thickness of the active layer is very small (<1 µm) for PAA membrane compared to 18 µm for the polymeric membrane. Interconnectivity of the pores is also higher for the polymeric membrane. Low interconnectivity of the PAA membrane makes them more susceptible to fouling by pore plugging. Loss of membrane permeability could be correlated to the extent of surface pore plugging for such membrane. The tortuous channel along with interconnected channels may likely foul internally.

4.3.2.3 Membrane defects and debris observed on 20 nm rated PAA membranes

White amorphous structures were observed on top of the membrane surface for commercial PAA membranes (see **Figure 4-11**). This debris was confirmed to be aluminium oxide when observed for elemental analysis using energy dispersive X-ray spectroscopy (see **Appendix E** for the spectrum) and is likely the residual material left after chemical etching of oxidised porous structure from un-oxidised aluminium substrate. Distribution of debris across the membrane was uneven with some areas without any debris and some areas with abundant debris material.

PAA membranes were found to have a large number of structural defects on the active side of the membrane. Defects can be as large as 2-3 µm in dimension can be observed as shown in **Figure 4-11**. In all of the defects observed the active layer of the membrane was absent, exposing the support layer of larger pore diameter but no through holes were ever observed. The frequency of these defects could not be observed with electron microscopy, which is only useful to observe smaller areas at sufficient resolutions. Further, these defects appear to be randomly distributed hence require scanning a large membrane area to calculate the accurate frequency of these defects and their contribution to membrane permeability.

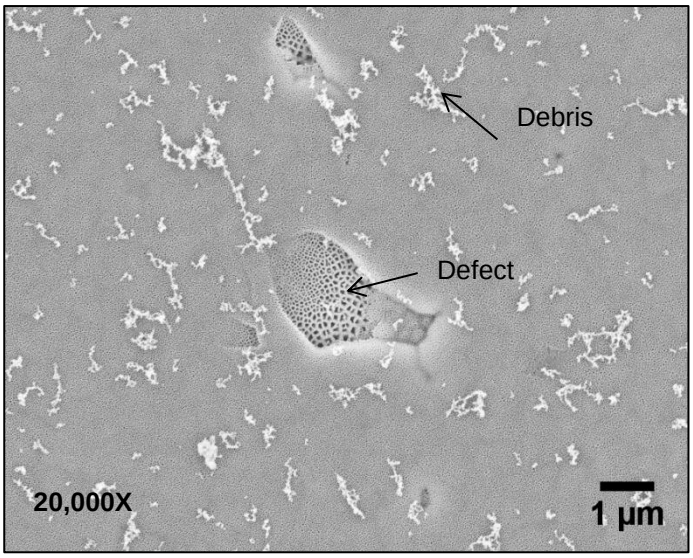

Figure 4-11 SEM image of the active surface of a PAA membrane showing defect (large area of peeled active layer exposing support layer of larger pores) and debris particles sitting on membrane surface.

No such debris or defect was found to be on the surface of polymeric membranes thus confirming debris to be related to membranes.

4.3.3 Comparison of the hydraulic permeability of 20 nm rated PAA membrane and polymeric UF membranes of various MWCO ratings

Hydraulic permeability of the membrane is strongly affected by pore size, bulk porosity, tortuosity and thickness of the membrane which is different for all the membranes.

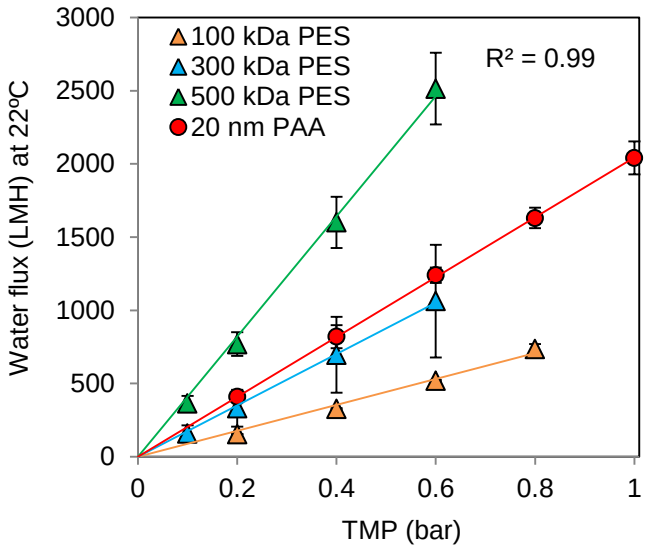

Membrane	Slope(LMH/bar)
20nm PAA	2046 + 93
100 kDa PES	885 + 27
300 kDa PES	1753 + 640
500 kDa PES	4104 + 416

Figure 4-12 Comparison of the hydraulic permeability (LMH/bar) of 20 nm PAA membranes (Anodisc), and PES membranes (Biomax) of three MWCO ratings.

Water (deionised, pre-filtered) flux data obtained at 22°C were obtained at different transmembrane pressures (TMP) for multiple membranes (n=3 for 100 and 500 kDa Biomax; n=9 for 20 nm PAA and 300 kDa PES). Linear fitting of the water flux and TMP data resulted in a regression coefficient of 0.99 and above. The slope of the data (in the table on the right) represents average hydraulic permeability. Error bars represent one standard deviation for multiple membrane discs. Lot#5 of PAA membrane was used for testing.

The variability in hydraulic permeability within the membrane lot is very high for polymeric membranes as compared to PAA membrane even within the same lot of the membranes tested. This is evident from large standard deviation (36.5% relative to the average value of permeability) observed for 300 kDa PES membrane as opposed to smaller (5%) standard deviation calculated for the 20 nm PAA membrane. The variability was also lower for 100 kDa and 500 kDa membranes with %RSD value of 3 and 10 % respectively. However, compared to PAA and 300 kDa PES membranes average values were calculated with only three membrane samples for each of 100 and 300 kDa membranes. Thus variation values could be underrepresented by the data collected for these membranes.

Hydraulic permeability of the PAA membrane (20 nm) was found to be higher than 100 and 300 kDa rated PES membranes but lower than that of 500 kDa PES membrane. Hydraulic

permeability of 2045 ± 93 LMH/bar was observed for 20 nm PAA membranes while for 300 kDa PES membranes value was estimated to be 1752 ± 640 LMH/bar. By hydraulic permeability, 20 nm PAA membrane was found to be similar in performance to 300 kDa PES membranes. Thus 300 kDa PES membranes were selected for comparison with 20 nm PAA membranes for filtration studies using protein solutes. Since PES membranes are marketed as high flux membranes, other commercial membranes were not considered.

4.3.3.1 Lot-to-lot variations in 20 nm rated PAA membranes: Correlating hydraulic permeability and mean pore sizes for various membrane lots

Since 20 nm rated PAA membranes were selected for further filtration studies, which resulted in the use of a large number of these membranes in this study. Ensuring the use of the same lot of the PAA membrane for all of the experiments done in this study was not feasible as often the same lot of membrane was not available from the suppliers on subsequent orders. Thus, six lots of PAA membranes used in this study were retroactively compared for their hydraulic permeability and pore size distributions.

Surface images of the active layer of PAA membranes were obtained using SEM and analysed to measure the pore size distributions. Lot variations observed in the membrane morphology are significant as shown in the comparison of the pore size distributions obtained after analysis of the images of the active layer surface of the membranes. Only lot #1 was found to be closer to manufacturer-specified pore ratings for this product. Since lot#1 was used for initial screening experiment and resulted in 3-log removal value for BSA nanoparticle removal in the filtrate. It is expected that similar experiment with lots such as lot#6 would result in lower log values. Hence achieving high viral retention or removal using these PAA membranes would depend upon the lot characteristics.

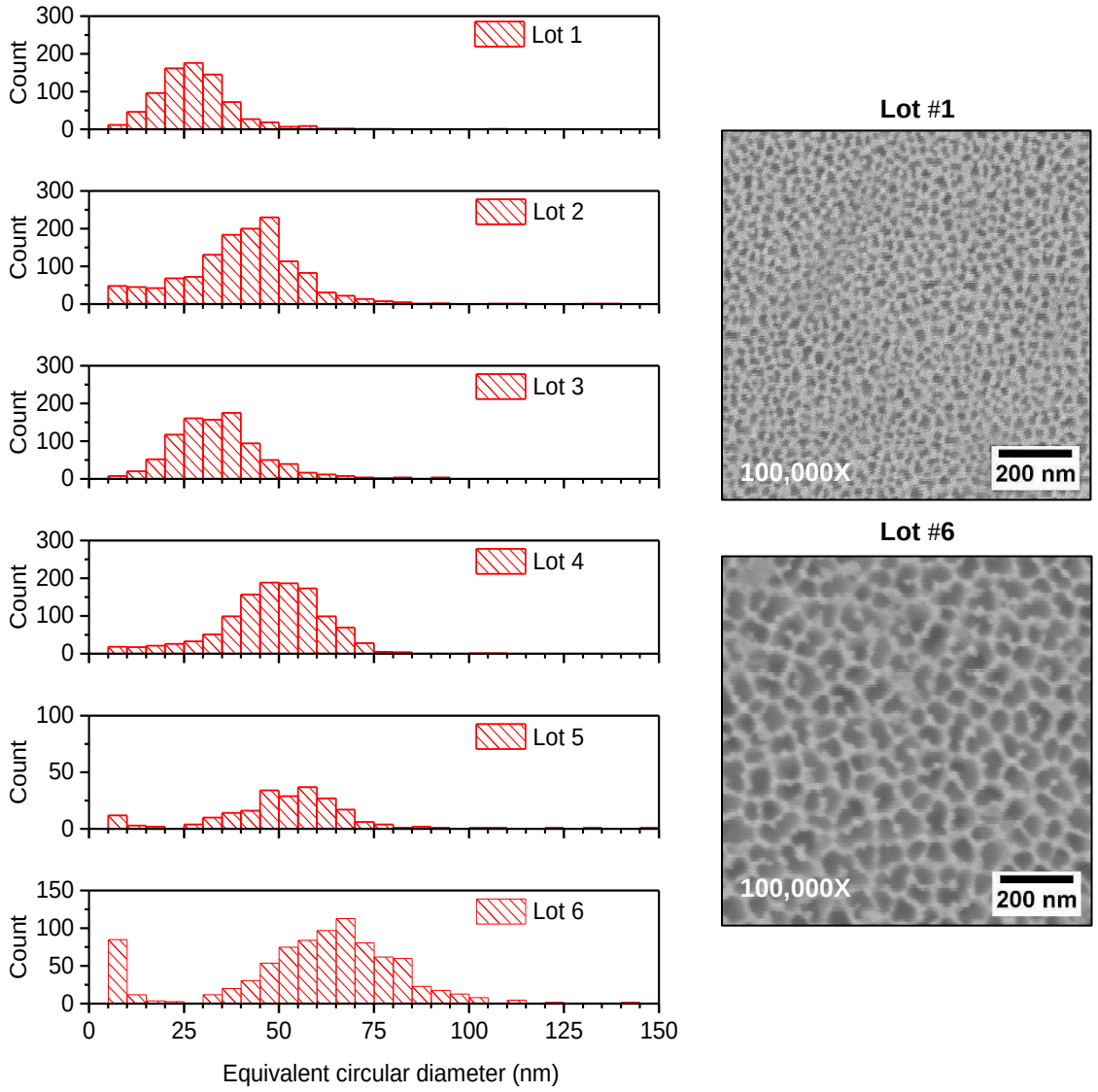

Figure 4-13 Lot variations observed in the pore size distribution of the commercial 20 nm rated PAA membrane shown in histogram overlays of pore size distribution of different lots as observed by SEM image analysis and SEM images (right side) of two lots of the membranes obtained at same magnification factor (100,000X) showing different pore sizes.

Mean pore size of these lots ranged from 26 to 60 nm along with variation in hydraulic permeability as shown in **Table 4-3**. Plotting mean pore diameter and hydraulic permeability suggested a linear correlation between the two parameters, though with a regression coefficient (R^2) of 0.84 only. A strong correlation is indicated by a higher value of correlation usually above 0.95. It is possible that accounting for the defect density (holes in the active layer) as shown previously, along with mean pore size could be used for a complete correlation. Calculation of such defect density is hindered by low scanning area of the electron microscopy.

Nonetheless, a significant change in mean pore size can impact the sieving of solutes especially with size in the range of 10 to 100 nm.

Lot No	Hydraulic permeability (LMH/bar)	Mean pore diameter (nm)	Pore size Distribution SD (nm)
#1	1540 ± 50	27 ± 2	10 ± 1
#2	1820 ± 150	45 ± 5	15 ± 3
#3	1570 ± 80	32 ± 4	14 ± 5
#4	1930 ±100	55 ± 7	19 ± 6
#5	2070 ± 100	49 ± 4	20 ± 2
#6	2250 ± 50	60 ± 4	19 ± 6

Table 4-3 Lot-to-lot variability in hydraulic permeability, mean pore diameter and pore size distribution standard deviation for 20 nm rated PAA membranes.

Mean pore diameter represents the mean equivalent circular diameter of pores size distribution when a normal distribution is applied to the pore size histogram. Distribution SD represents standard deviation or spread of the applied normal distribution. (Values ± one SD, n=3).

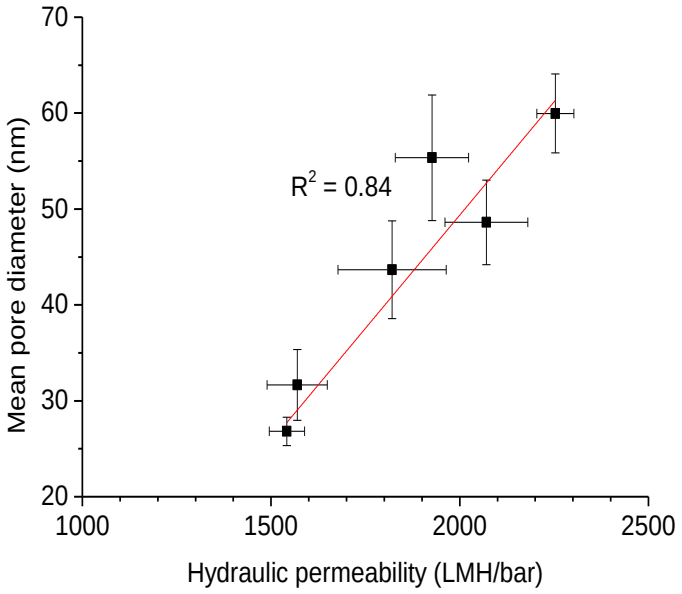

Figure 4-14 Linear correlation of the mean pore diameter measured using image analysis of SEM images and measured average hydraulic permeability of six different lots of the 20 nm rated PAA membranes.

Error bars represent standard deviations for measurements of three membrane samples for each lot.

4.3.4 Comparison of 20 nm rated PAA membranes and polymeric PES membranes of various MWCO ratings for dextran sieving characteristics

Dextran sieving analysis has been commercially used as a reliable test for rating membranes on the basis of molecular weight cut off (MWCO) or normal molecular weight limit (NMWL). Both MWCO and NMWL are used alternatively to specify the molecular weight of solutes rejected by membranes at a defined level or above. However, commercially available PAA membranes such as PAA are not rated on the basis of dextran sieving properties. Comparing PAA membranes with conventional polymeric membranes is thus necessary to answer the following questions :

1. Does the membrane architecture of PAA membranes have any impact on sieving characteristic of the membrane?
2. Which polymeric membrane rating should be used for comparison with 20 nm rated PAA for fouling and separation studies?

Hence, dextran sieving analysis of both PAA and PES membranes was carried out using a mixture of dextran with molecular weights ranging from 5 kDa to 2500 kDa. These experiments were performed at a very low flux rate (approximately 5 LMH) across the membrane and at a high stirring rate to avoid concentration polarisation at the membrane surface. Concentration polarisation of large solutes can form a layer on membrane surface which can reduce transmission of otherwise permeable smaller solutes. Thus the dextran sieving characteristics are near to the intrinsic sieving characteristics of the membranes and are not affected by any external phenomenon. Use of the dextran mixture instead of single dextran solution was favoured due to the similarity in the complexity of such a mixture with actual biological feeds used in fractionation applications. A detailed description of the method used is available in the section 4.2.3 of this chapter.

Analysis of the samples is crucial to study the dextran sieving characteristics for the membranes and compare different membranes. Chromatograms of feed and final filtrate samples were obtained using high-performance size exclusion chromatography (HP-SEC) with refractive index detector for detection of the dextrans. It is crucial the size exclusion chromatography is properly calibrated before the application of the samples. Calibration plot obtained using nine GPC-grade standard dextrans with molecular weights ranging from 5 to 670 kDa (T5-T670) is shown in graph B in **Figure 4-15**. A linear correlation was obtained between the log value of the molecular weight of the dextrans and peak elution volume as signified by a high value of the regression coefficient. Graph B in the same figure shows the peaks obtained with single dextrans solutions. Peak molecular weight specified by the manufacturer was used for the

calibration plot, though calibration plot with number average or weight averaged molecular weight also showed similar linear plot.

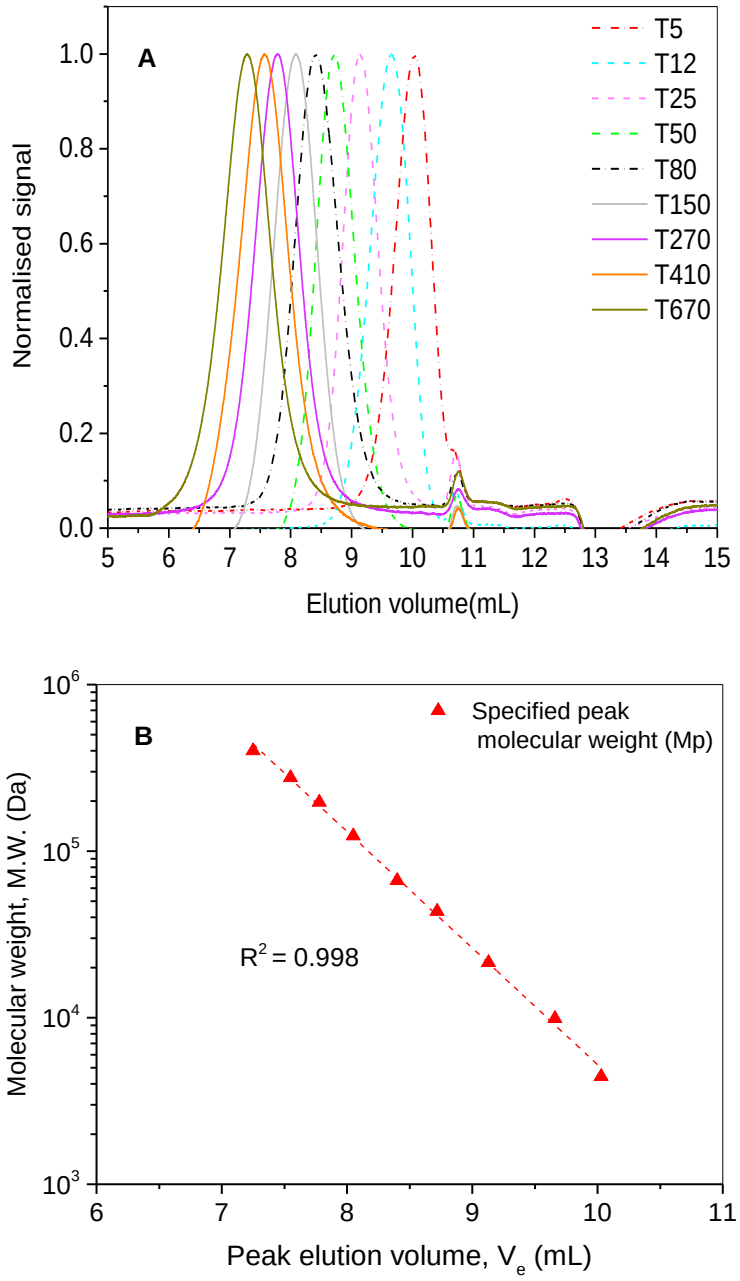

Figure 4-15 SEC chromatograms of various GPC grade dextran standards, 5 to 670 kDa (Top) on GPC column and semi-log calibration plot for dextran molecular weight and peak elution volume showing linear fit for the data.

Dextran standards in PBS were injected (100 µL) onto the GPC column TSKgel5000PWXL (7.8 X 300 mm) at 0.3 mL/min with PBS as mobile phase and detected using refractive index detector. The linear relationship shown in the calibration plot is described by the equation, log_{10} (M.W.) = (0.7 x V_e) + 10.7, which is used to transform the chromatograms obtained for samples obtained after dextran sieving experiments.

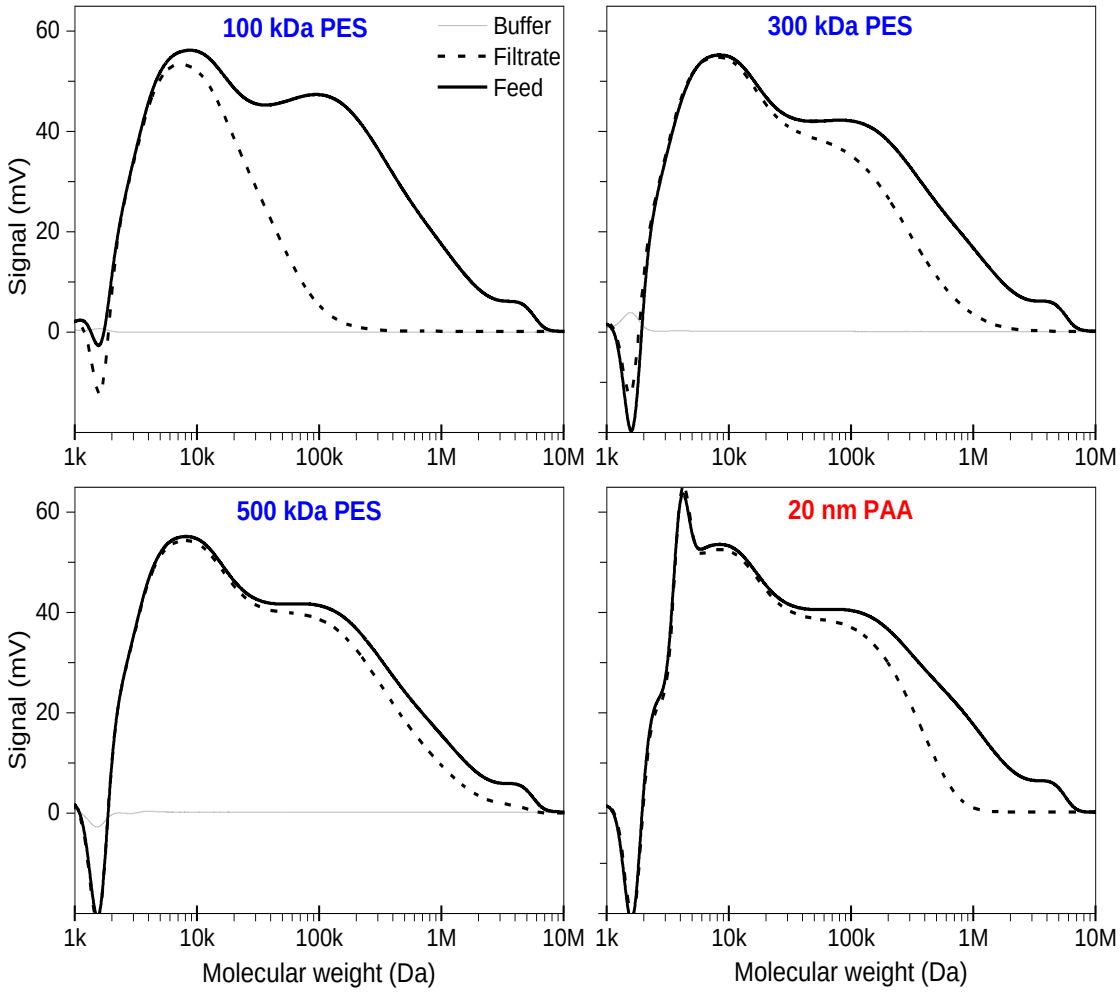

Figure 4-16 Transformed chromatograms for the dextran feed (solid line) and filtrate (dotted lines) samples obtained in the dextran sieving experiments using PAA membrane rated 20 nm and PES membranes rated 100,300 and 500 kDa.

Chromatograms were obtained by injection of 100 µL of the samples onto the GPC column, at conditions similar to those used to obtain the calibration plot. The x-axis (elution volume) of the initial chromatograms was transformed to molecular weight using the calibration equation.

Figure 4-16 shows gel permeation chromatograms of the polymeric membranes of three molecular weight cut-offs (100, 300 and 500 kDa) and 20 nm PAA membranes as selected during screening experiments. The feed was found to be highly polydisperse in composition with dextrans of molecular weights ranging from 3 kDa to approximately 6 MDa. However, a majority of the dextrans were in the range of 10 to 1000 kDa. It should be noted that since calibration plot was obtained in a range of 5 to 670 kDa and the linear range specified by the manufacturer for the elution of linear polymers such as polyethylene glycol and polyethylene oxide through the GPC column was in 10 to 800 kDa. Hence any significant extrapolation of the linear relationship of the calibration plot, especially above 1000 kDa should be used cautiously to make any experimental inference.

Feed solution curve was identical for all of the membranes as solutions of the same composition were used in all of the experiments. The additional peak observed at approximately 3 kDa molecular weight in the chromatogram of 20 nm rated PAA membranes. No such peak was observed with polymeric membranes. Since anodic alumina membrane does not have any leachates this is likely due to leachates from thermally bonded polypropylene support ring around the anodic alumina membranes. This was confirmed by analysing samples obtained after incubating a detached support ring (membrane removed except on bonded area) in buffer solution for a day. A similar spike was observed. Leachate was however found to be less than 5kDa and would be effectively removed during the filtration by the membrane.

Sieving curves for different membranes were calculated by normalising the filtrate signals with the feed signals as shown in the transformed chromatograms. Except for 100 kDa PES membranes, all of the membranes showed similar signals for both filtrate and feed solution for dextran molecules smaller than 20 kDa. As shown in **Figure 4-17**, PAA membrane exhibits a sharper sieving curve compared to PES membranes of all ratings. Among polymeric membranes, only 100 kDa membranes coincided with manufacturer specified ratings (~100 kDa) for 90% rejection (or 0.1 value of observed sieving coefficient). Both 300 and 500 kDa were found to have much higher MWCO compared to their original ratings from the manufacturer. Manufacturer's (Millipore) website appears to indicate that ratings for PES membranes are on the basis of proteins rather than dextrans. As proteins are charged molecules and globular in shape, their sieving across the membrane is likely to be influenced by a variety of factors other than the solute size such as protein-protein and protein-membrane interactions.

A rationale for using dextrans for sieving analysis is that these molecules are neutral, inert to the solvent environment to some degree and can be synthesised easily for a specified molecular weight, thus minimising the interference for solute-solute and solute-membrane interactions. However, there is no standard sieving test format for either dextran or protein-based testing. For dextran-based sieving analysis also it has been reported that factors such as the format of filtration i.e. stirred cell or cross-flow module, stirred cell diameter and composition of the dextran feed can strongly influence the retention ratings (Zydney and Xenopoulos, 2007, Bakhshayeshi *et al.*, 2011a). Thus dextran-based nominal molecular weight limits (NMWL) rating can vary for same membrane depending upon the procedure used. However, comparison of the membranes using same format or procedure can still be valid.

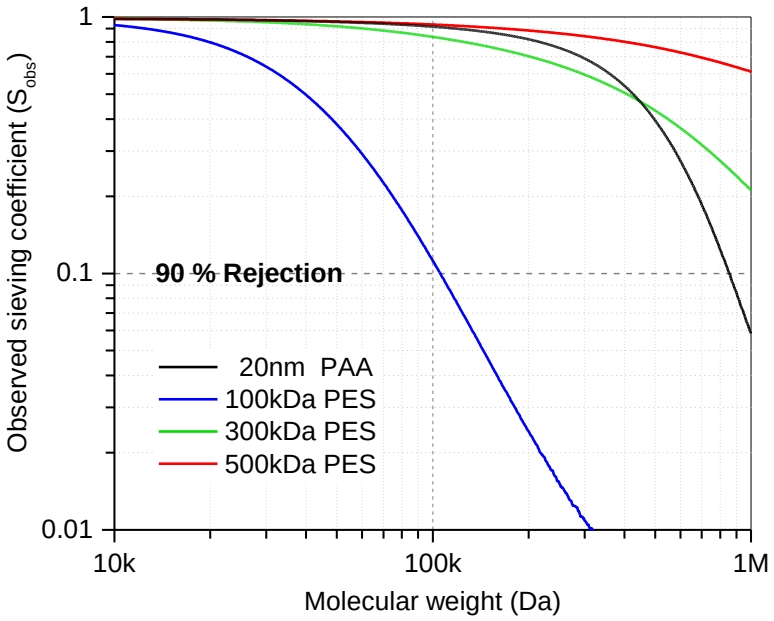

Figure 4-17 Dextran sieving curves for PAA membrane rated 20 nm and PES membranes rated 100,300 and 500 kDa.

Sieving coefficients were obtained by normalising signal obtained for filtrate to that obtained for feed solution at a particular elution volume, which represents a particular molecular weight of dextran as per calibration curve obtained using GPC grade standard dextrans. S_{obs} of 0.1 correspond to 90 % rejection of a dextran molecule of corresponding molecular weight. Lot 5 of PAA (Anodisc) membranes was used for this study.

Nominal molecular weight limits (NMWL) at 90% rejection were estimated to be 800-900kDa for PAA membrane. NMWL for 300 and 500 kDa PES membranes could not be accurately determined using the sieving curve obtained as the curve extended beyond the calibration limit and linear range of the size exclusion column. However, NMWL at 90% rejection can be speculated approximately 2000kDa for 300 kDa rated PES membrane. Zydney and Xenopolous, (2007) have reported 385 kDa value for 90 % rejection for 300 kDa rated PES membranes (same product) in a stirred cell experiment using a dextran solution. Authors favoured using 76 mm stirred cell diameter as they found smaller stirred cells to be very sensitive to operating conditions such as stirring speed as used in this study. A larger stirred cell could not be used in this study as the PAA membranes are not available at sizes larger than 43 mm. Use of similar format and size of the stirred cell was necessary to avoid the influence of different mass transfer of solutes with different stirred cell sizes. Nonetheless, out of three ratings of PES membranes, only 300 kDa membrane showed closest dextran sieving characteristics along with similarity in the mean pore size and hydraulic permeability established previously. Thus, 300 kDa PES membrane was selected for studying filterability of solutions of various proteins for comparison with PAA membrane.

4.3.5 Filterability of single solute solutions of selected protein model solutes through 20 nm rated PAA and 300 kDa PES membranes

Selected PAA membranes (Anodisc 20 nm rating) and PES membranes (Biomax 300 kDa) were compared for filterability of dilute feeds of single model solutes. BSA, Thyroglobulin and 90 nm BSA nanoparticles were filtered through both membranes are compared for transmission, average flux and fouling potential. Mechanisms of the fouling are deduced by statistically fitting the experimental data for filtration with the mathematical expressions for well-established mechanisms of fouling. Selection of these two membranes for comparison was by similar hydrodynamic permeability and dextran sieving characteristics as demonstrated in previous sections (4.3.3 and 4.3.4).

4.3.5.1 Flux decline for filtration of single model solute solutions

Equal feed volumes per unit membrane area were loaded (~26 L/m^2) and filtered (~20 L/m^2) through the two membranes to compare the performance for equal filtration output. Stirring conditions and pressure were the same for all filtration runs irrespective of solute and membrane. **Figure 4-18** shows the average (or cumulative) filtrate flux values for both membranes with three different model solutes.

For both membranes, average flux for 20 L/m^2 filtrate output decreases as solute size increases. Higher filtrate fluxes were observed for PAA membrane compared to PES membrane for each solute. However for BSA nanoparticles filtration difference of average process fluxes for two different membranes was marginal though still significant. Flux through PAA membrane was 20 LMH higher than that for PES membrane. Lot 5 of PAA membrane of 20 nm pore rating was used for these studies. Surprisingly, filtration of BSA through 300 kDa polymeric membrane (Biomax 300) resulted in lower process flux of ~500 LMH compared to that for PAA membranes. This could be due to lower mean pore size in 300 kDa PES membranes, i.e. 34 nm, compared to ~48 nm observed for the used lot of PAA membranes (lot 5).

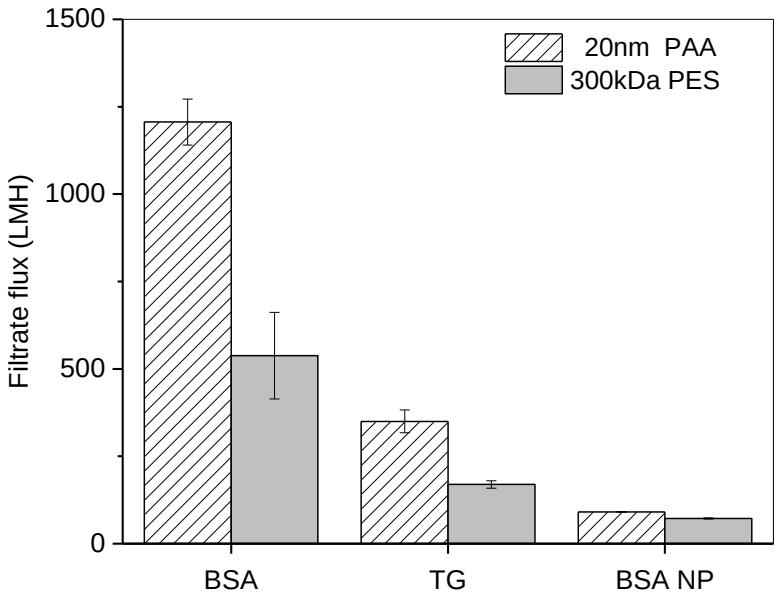

Figure 4-18 Filtrate fluxes through 20 nm rated PAA and 300 kDa PES membranes for solutions of model solutes (BSA, TG and BSA nanoparticles)

Solutions of all solutes were filtered for similar filtrate output (~20L/m^2) at a transmembrane pressure of 0.6 bar and a stirring rate of 1500 rpm was used in stirred cell-based filtration. BSA and BSA nanoparticles (90 nm) solutions were 1mg/mL and TG solution was 0.2 mg/mL, all prepared in PBS, pH 7.0 Lot 5 of PAA membranes was used for all filtration runs.

Filtrate fluxes normalised to the initial buffer flux (see **Figure 4-19**) highlight the differences for both membranes. A sharper flux decline was observed for PES membrane with BSA filtration resulting in membrane operating at ~60% of initial buffer flux instantaneously as filtration is started. PAA membranes however operated at ~90% value of the initial flux. Size exclusion chromatogram for BSA solution (see **Appendix A1**) used in this study shows that around 20 % of the total peak area is composed of dimers or trimers which would likely block some of the pores in 300 kDa rated PES membrane. Flux decline curves for TG were significantly different in shape for the two membranes which steeper decline observed for PES membranes indicating likely different mechanisms of fouling. For BSA nanoparticles, both membranes exhibited sharpest flux decline as filtration is started with membranes operating at ~20% of the initial buffer flux and the steady state is established very early in the filtration. This suggests immediate fouling or polarisation at the membrane surface. For all three solutes of different hydrodynamic sizes, PAA membranes operated at higher normalised flux rates throughout the course of the filtration indicating lower fouling. Large error bars for filtration runs with PES membranes show significant variation in filtration through membrane discs of the same lot as noted previously. Impacts of these variations were not though not significant for nanoparticle filtration.

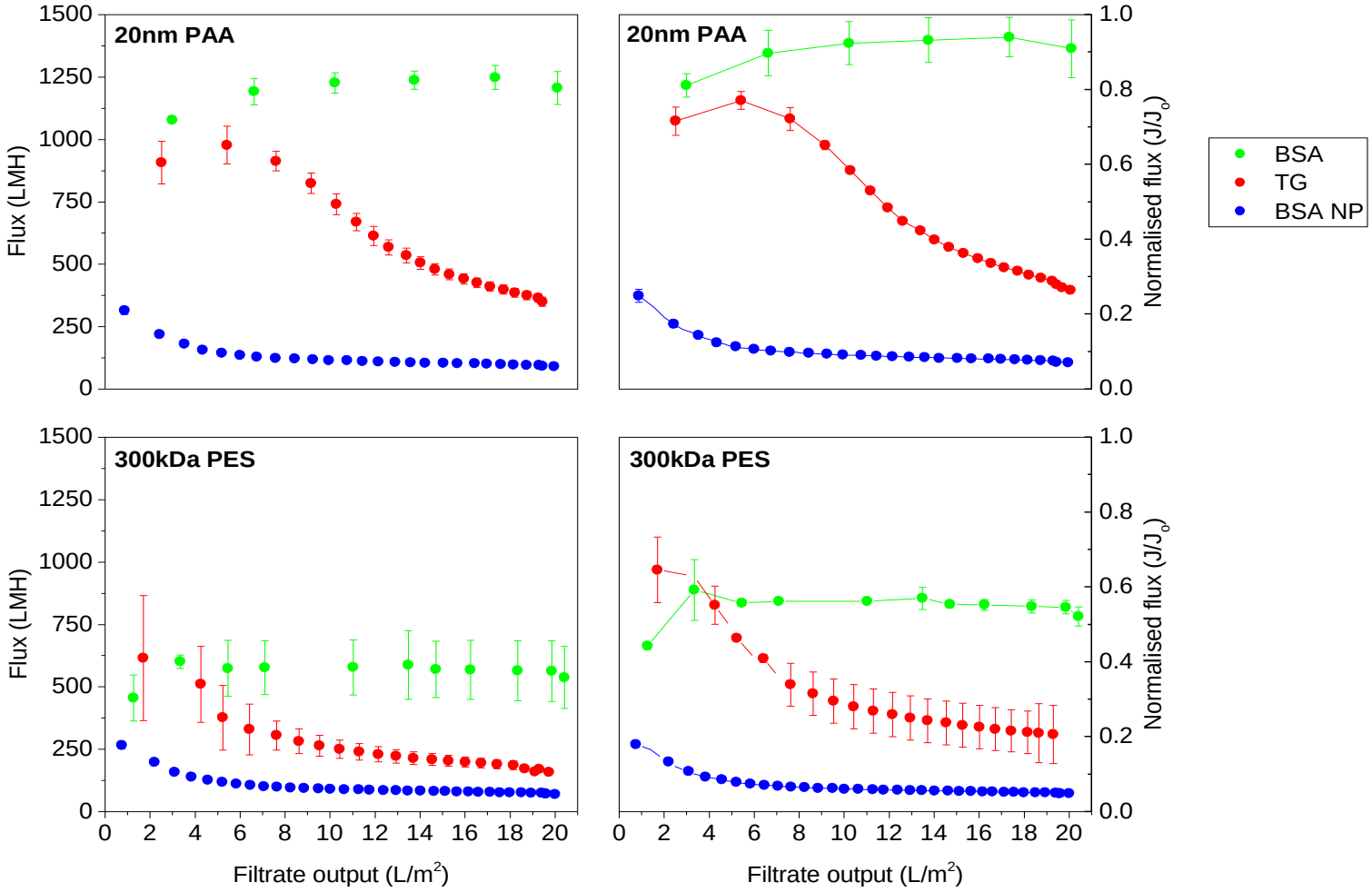

Figure 4-19 Flux decline for filtration of solutions of BSA, TG and BSA nanoparticles through 20 nm PAA and 300 kDa PES membranes.

Graphs on the left side show flux values normalised by the respective initial buffer flux (J_o) through the respective membranes. Error bars represent one standard deviation for flux data for triplicate filtration runs using fresh membranes discs.

4.3.5.2 Transmission of model solutes through membranes

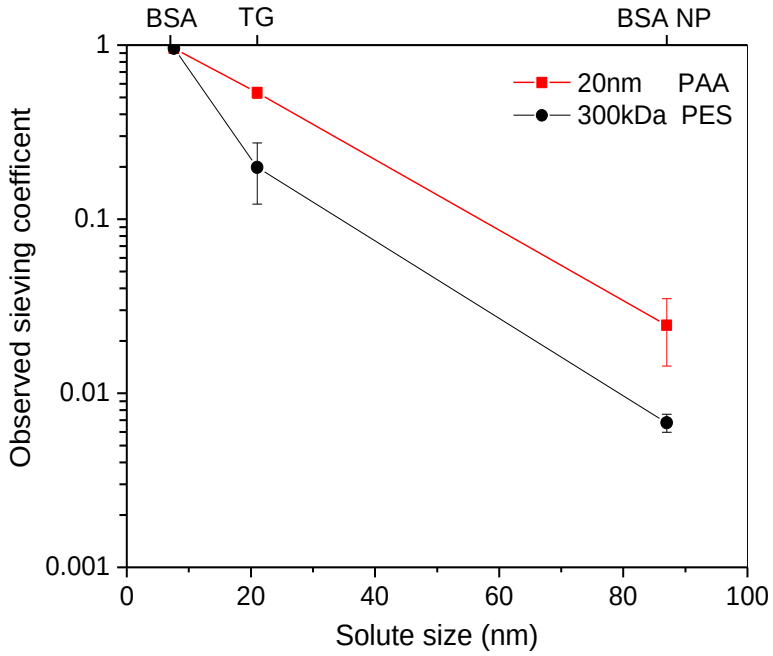

Figure 4-20 Observed sieving coefficients for three model protein solutes (BSA, TG and BSA NPs) of various hydrodynamic sizes filtered through 20 nm PAA and 300 kDa PES membranes.

Similar operating conditions (TMP, feed volume, stirring speed and filtrate output) were used for all filtration runs. The solute size was obtained from dynamic light scattering measurements for protein solutions. Error bars represent one standard deviation for triplicate filtration runs.

Figure 4-20 displays transmissions of the individual solutes through two membranes for equal filtrate output in the form of a ratio of final permeate concentration to the initial feed concentration denoted by observed sieving coefficient. Protein transmission for BSA was similar for both membranes. A remarkable difference is seen for TG transmission through two membranes. PAA membranes are partially retentive for the TG. Value of the observed sieving coefficient for PAA membrane was 3.6 times larger than that for the 300 kDa PES membrane. Overall both membranes were highly retentive for the nanoparticles of 80-90nm size as sieving coefficient was below 0.05 signifying less than 5% transmission for both membranes.

Sieving values for single solute filtration can be used to calculate selectivity or separation factor of the membrane for that particular solute. A selectivity permeability trade-off has been suggested and demonstrated for a variety of membrane ratings from 30 to 1000 kDa using BSA as model solute including a theoretical relationship between intrinsic selectivity and permeability estimated using applying some assumptions to the hydrodynamic model of sieving and stagnant film theory (Mehta and Zydney, 2005).

For BSA filtration in this study, the polarisation index (ratio of cumulative average flux and mass transfer coefficient for solute) was very high >100 for both membranes thus resulting in erroneously low values of actual sieving coefficient hence this analysis was not used. For TG and BSA nanoparticles, polarisation index was less than 15 for PAA membranes and less than 10 for PES membranes, so selectivity permeability analysis was conducted for these two solutes (Calculations for mass transfer coefficients and polarisation index are shown in Appendix F and G). Theoretical curves for selectivity-permeability trade-off were generated for two solutes by using same assumptions as used by Mehta and Zydney (2005), i.e. log normal pore distribution is assumed with a value of 0.2 for the ratio of the standard deviation of pore size distribution to mean value of pore radius (σ/μ). For thyroglobulin, PES membranes show lower selectivity and very close to the theoretical curve. PAA membranes exhibited higher selectivity and above the theoretical curve as displayed in **Figure 4-21**.

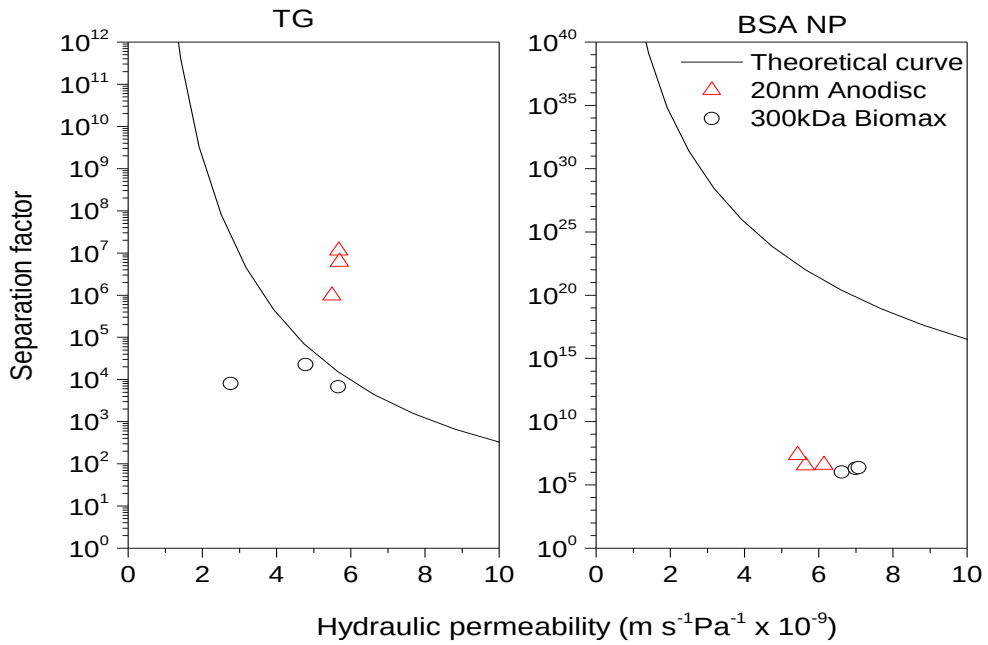

Figure 4-21 Comparison of 20 nm PAA and 300 kDa PES membranes for separation factors for Thyroglobulin and BSA nanoparticles under the theoretical selectivity-permeability framework (Mehta and Zydney, 2005).

Since the effect of fouling or concentration polarisation has not been factored in the theoretical calculation of selectivity. Nonetheless, such a framework is useful as in the actual application of the membranes non-ideal conditions such as high polarisation as well as fouling are very likely. Thyroglobulin can be used to compare the performance of two different membranes targeted for filtration of large molecules such as viral vectors. However, a thorough evaluation of fouling and other phenomenon is necessary to correlate such analysis with actual performance.

4.3.5.3 Mechanism of fouling

4.3.5.3.1 Thyroglobulin filtration

Fouling by thyroglobulin feed was more prominently due to intermediate blocking in PAA membranes while cake filtration mode was dominant for the PES membranes. **Figure 4-22** shows these two mechanisms being the best fit for the respective membranes. Regression coefficients of all of the model-fits for PAA membranes were above 0.95 with the intermediate model above 0.99 as shown in **Table 4-4**. Such high values for all the models make it difficult to identify a dominant mechanism of fouling. Thus, the values of the sum of squares of residuals (SSR) were compared and the intermediate blocking model was found to has the minimum value for SSR, 1/3rd of the value obtained for the standard blocking model, the next best fit. Short filtration window and a low number of data points collected is likely the reason for a good fit for all of the fouling models in PAA membranes. Short filtration time was unavoidable as membranes needed to be compared for similar filtrate output or capacity to compare the impact of fouling, process flux and transmission. For PES membrane, regression coefficients were above 0.9 only for cake filtration and intermediate blocking. Cake filtration was identified as the dominant mechanism as the regression coefficient was 0.99 and minimum SSR value that was 1/5th of SSR value for intermediate fouling.

For thyroglobulin, the initial period of the filtration (< 60 seconds) appear to fit standard blocking or complete blocking models for PAA membranes and intermediate blocking for the PES membranes indicating the presence of a different fouling mechanism in the initial window of filtration. A combined model approach was attempted to fit the filtration data with the reported combined models, but fitting was inconclusive due to over-parametrisation of the fits. Best fits for such combined models resulted in negative values of the kinetic parameters with large standard errors thus such fits were not considered valid. Likely reason could be the short time frame of initial mechanisms and very low number of data points captured in such a short period. Another possibility is that two participating mechanisms are consecutive and not concurrent and the combined models applied was developed assuming simultaneous fouling by two mechanisms. Initial pore blocking in the PAA membranes could be because of the thyroglobulin and aggregates blocking the pores similar to the size of solute (~20 nm) and as these pores are blocked, the more particles deposit on the blocked pores manifesting into intermediate blocking. Cake filtration in the polymeric membrane, however, indicates the inability of the particles to enter more in-depth into the membrane bed and deposition in the top active layer of the membrane could result in a cake-like layer. Such cake is likely to block large channels near membrane surface and result in lower transmission.

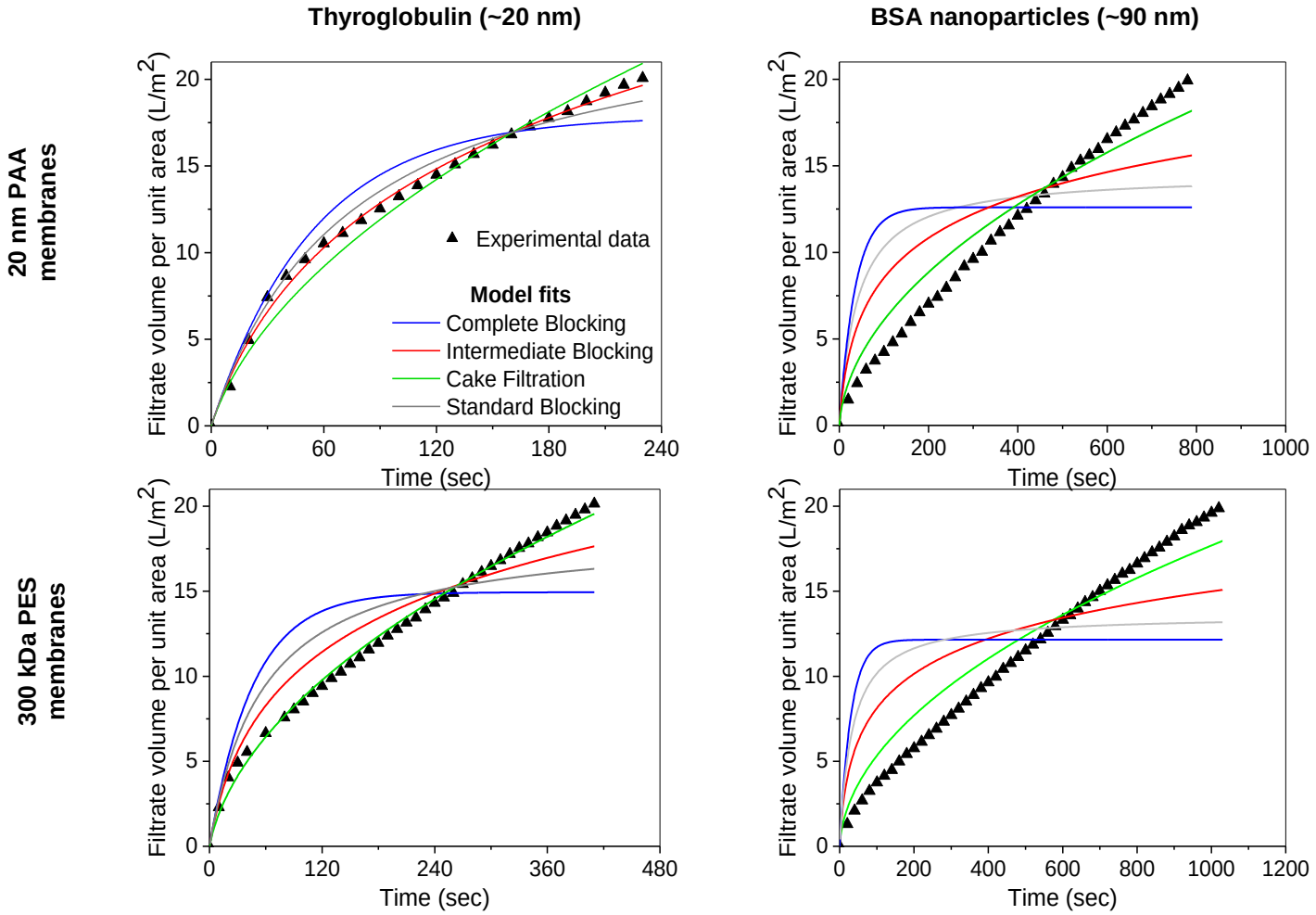

Figure 4-22 Fitting the experimental filtration data (triangles) obtained for filtration of thyroglobulin (TG) and 90nm BSA nanoparticles (NP) solutions through PAA and PES membranes using the well-established mathematical models for the fundamental mechanisms of fouling (predicted as solid curves).

Goodness of the fits were analysed and compared for the four mechanisms on the basis of adjusted R^2 and sum of square of residuals.

[140]

	Fouling mechanism	BSA nanoparticles			Thyroglobulin		
20 nm PAA		SSR (x 10^{-3})	R^2	Parameter	SSR (x 10^{-4})	R^2	Parameter
	Standard	1.24 ± 0.06	0.49	k_s = 137 ± 1	0.07 ± 0.04	0.99	k_s = 78 ± 2
	Complete	1.78 ± 0.78	0.27	k_b = 0.03	0.30 ± 0.11	0.95	k_b = 0.02
	Intermediate	0.65 ± 0.02	0.73	k_i = 278 ± 5	**0.02 ± 0.00**	**1.00**	k_i = 112 ± 4
	Cake	**0.13 ± 0.00**	**0.94**	k_c = 4.4 ± 0.2	0.15 ± 0.03	0.98	k_c = 0.64 ± 0.1
300 kDa PES		SSR (x 10^{-3})	R^2	Parameter	SSR (x 10^{-3})	R^2	Parameter
	Standard	1.83 ± 0.14	0.40	k_s = 145 ± 1	0.17 ± 0.05	0.85	k_s = 100 ± 7
	Complete	2.45 ± 0.16	0.20	k_b = 0.03	0.33 ± 0.07	0.71	k_b = 0.02
	Intermediate	0.95 ± 0.08	0.70	k_i = 321 ± 4	0.08 ± 0.03	0.94	k_i = 160 ± 20
	Cake	**0.17 ± 0.02**	**0.94**	k_c = 5.8 ± 0.3	**0.01 ± 0.01**	**0.99**	k_c = 1.7 ± 0.3

Table 4-4 Results of the curve fitting of experimental filtration data with well-established mathematical models for fundamental mechanisms of fouling for PAA and PES membranes

Parameters represent kinetic constants of the respective mechanisms, k_s (m^{-1}), k_b (s^{-1}), k_i (m^{-1}) and kc (sm^{-2} x 10^{-6}). Mathematical expressions of the fouling mechanisms are tabulated in Chapter 2 (Section 2.4.2.1.1).

4.3.5.3.2 BSA nanoparticles filtration

The goodness of fits for filtration data obtained for BSA nanoparticles solution was not as robust as observed for the thyroglobulin filtration. This was the case for both PAA as well as PES membrane. It could be argued that better goodness of fits observed for thyroglobulin solution is a result of shorter filtration time (200-500 sec) compared to filtration time observed for filtration of BSA nanoparticles. However, as fits show, even the best-fitted curves diverge from experimental data points in case of BSA nanoparticles. Hence it is likely that better goodness of fits in case of thyroglobulin is not because of the shorter filtration windows. The fundamental mechanism of fouling differs for two solutes. For both membranes, cake filtration model was observed to be the best-fitted model to experimental data collected for protein nanoparticles. Comparison of fitting for various models regarding R^2 and SSR is detailed in **Table 4-4.**

4.3.5.4 Recovery of the membrane permeability

Figure 4-23 shows the percentage of initial membrane permeability that could be recovered after a simple rinse of the fouled membranes. Interestingly, PAA membranes showed higher recovery for all three solutes compared to polymeric PES membranes. Higher recovery of the buffer permeability implies lower irreversible fouling, which can only be removed using chemical treatment and not using simple rinse or washing of the membranes with the buffer solution.

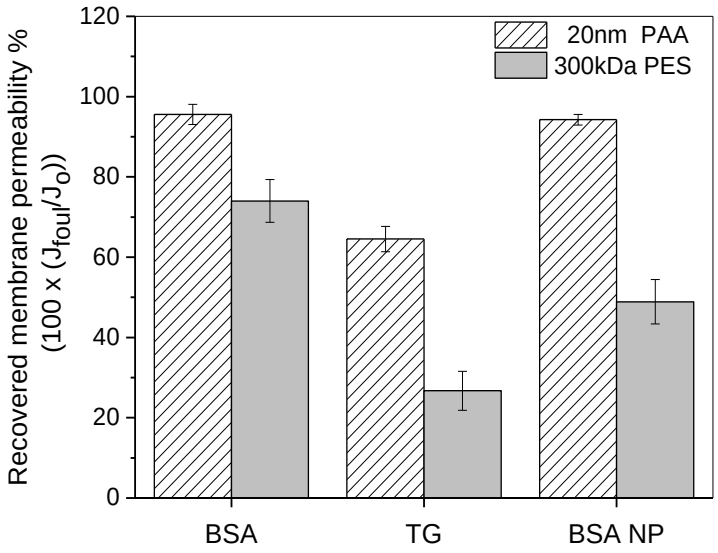

Figure 4-23 Recovered membrane permeability for 20 nm PAA and 300 kDa PES membranes after filtration of single solute solutions of three model solutes (BSA, TG and BSA nanoparticles).

Recovered membrane permeability is calculated as the buffer flux through the fouled membrane (J_{foul}) as a percentage of initial buffer flux (J_o) measured before protein filtration. Membranes along with stirred cells were gently rinsed three times before measuring the buffer flux through the fouled membranes. Measurement of buffer fluxes before and after the protein filtration was performed at similar operating conditions (0.6 bar TMP and 1500 rpm stirring rate). Error bars represent one standard deviation for triplicate filtration runs.

The difference is significant for BSA nanoparticles where more than 95 % of initial buffer permeability was restored for PAA membrane as opposed to only 40% for PES membranes. Recovery of the initial buffer permeability was lowest in case of TG for both membranes. For BSA solutions, PES membranes showed unexpectedly low recovery of the buffer permeability. This was likely due to the presence of dimers and oligomers of BSA proteins which would have molecular weights closer to the MWCO of the membrane.

TG can foul larger pores in the PES membranes and similarly sized pores available on PAA membrane. For protein nanoparticles, it appears that most of the particles are sieved on the membrane surface and did not plug a significant number of the membrane pores in PAA

membranes. Low transmission of nanoparticles (<0.1%) also concurs with this. Easy restoration of the initial membrane permeability is a known characteristic of concentration polarisation, which is known to be a pressure-dependent and reversible phenomenon (Porter, 1972). Loss of the hydraulic permeability of the membrane is typically a consequence of fouling of the membrane especially internal fouling or pore blockage which is usually an irreversible phenomenon. It can be argued that compression of the membranes during long filtration cycle could also be responsible for the reduced buffer permeability, especially in the case of polymeric membranes. However, the role of the compression can be ruled out as trend appears to be by the solute size and membranes were operated at lower transmembrane pressures than the maximum operating pressure specified by the manufacturers. PAA membranes being ceramic are not easily compressible.

Trends observed for the recovery of buffer permeability concerning different model solutes, and two different membranes were also visually verified using scanning electron microscopy of the active layer surface of the fouled membranes after rinsing. **Figure 4-** 24 and **Figure 4-25** show the surface images for unused membranes as well as fouled membranes for PAA and PES membranes respectively. Comparing two different membranes for the extent of the fouling caused by the same solute is difficult due to different mechanisms of fouling observed. A visual comparison of the membrane fouling on the surface of the PES membrane appears to suggest lower surface fouling if correlated with corresponding recovery data, thus suggesting the possibility of internal fouling which was not identified by curve fitting of the filtration data. Such fouling may be present on the thin active layer as well as thicker intermediate layer observed for the polymeric membranes. Imaging of the membrane cross-section using SEM was tried after cutting the membrane; however, images were inconclusive due to the damage caused to the layers during the cutting procedure.

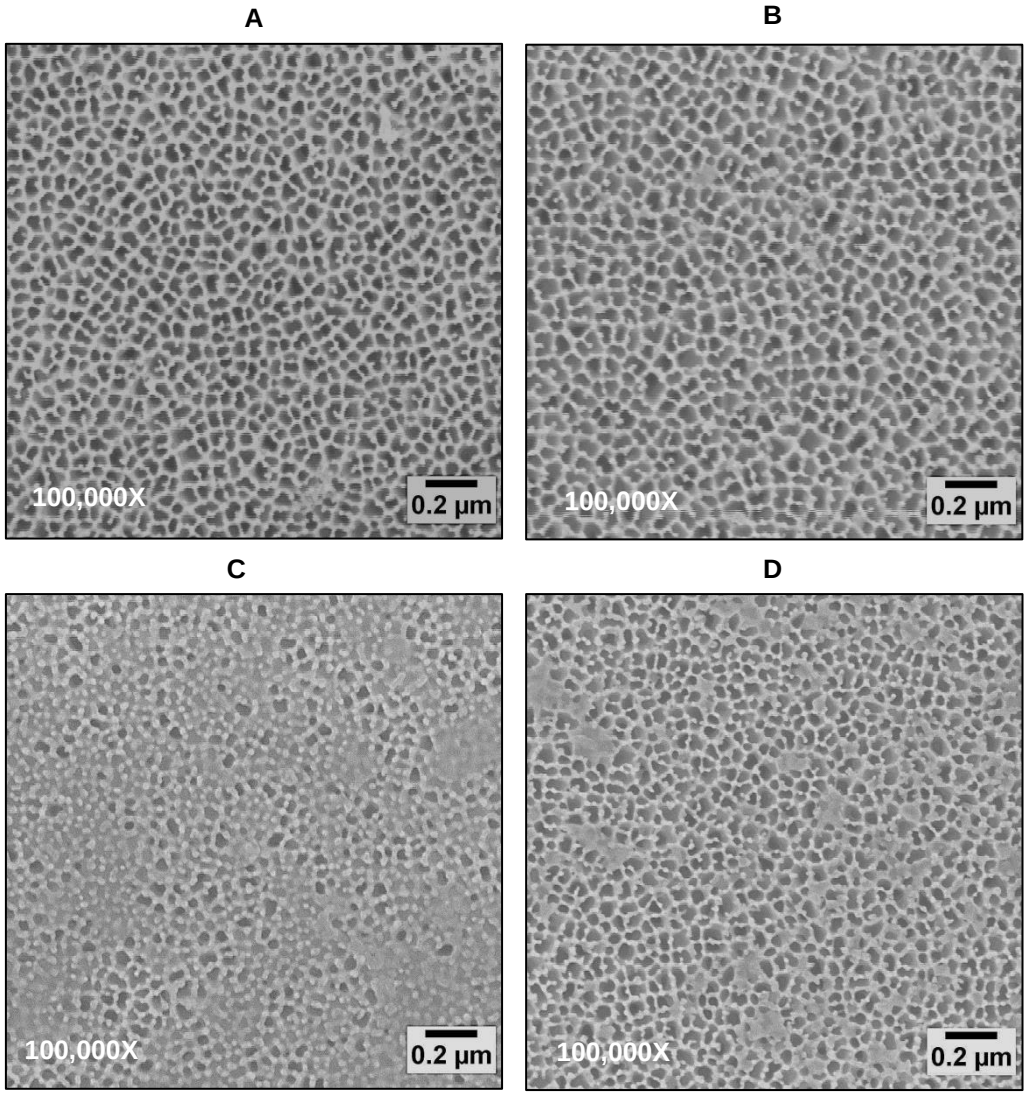

Figure 4- 24 SEM images showing fouling by different model solutes on the active layer surface of 20 nm rated PAA membranes. A- Unused membrane, B- BSA fouled, C- TG fouled and D- BSA nanoparticles fouled membrane.

Scale bar represents 0.2 µm and images were taken at a magnification of 100,000 for all of the samples. Images were obtained after drying and coating the membranes with ultrathin (<1 nm) and uniform layer of platinum using sputter coater and analysed using InLens detector with less than 5kV gun voltage.

On a visual comparison of the membrane surfaces fouled with different protein solutions, membranes appear to be fouled maximal with TG and least with BSA solution, confirming the recovery data obtained for buffer permeability through membranes. BSA nanoparticles appear to be deposited on the membrane surface as opposed to the TG molecules which appear to be embedded into the membrane bed. This cannot be ascertained with SEM, and other techniques such as atomic force microscopy need to be used which can give detailed information about the texture or surface roughness of the sample being investigated.

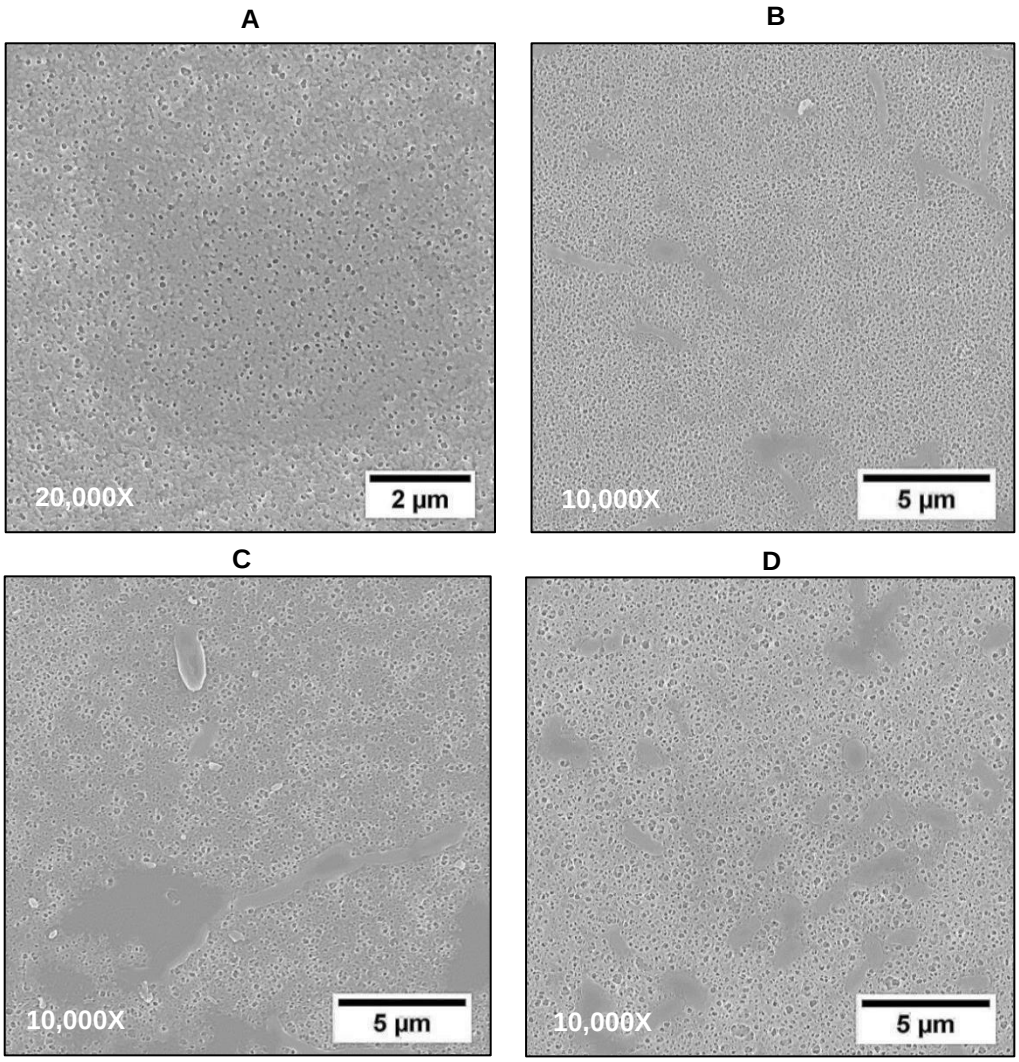

Figure 4-25 SEM images showing fouling by different model solutes on the active layer surface of 300 kDa PES membranes. A- Unused membrane, B- BSA fouled, C- TG fouled and D- BSA nanoparticles fouled membrane.

Scale bar represents 5 µm (except A) and images were taken at a magnification of 10,000 (except 20,000X for A) for all of the samples. Images were obtained after drying the membranes and coating with ultrathin (<1 nm) and uniform layer of platinum using sputters coater and analysed using InLens detector with less than 5kV gun voltage.

From SEM images of the active layer surface of the PES membranes, the trend observed in the recovery of buffer permeability concerning three model solutes is apparent. Darker non-porous solid mass characterises fouling or deposition of the protein in contrast to the lighter and porous membrane material. Fouling on the surface, however, did not seem to reflect the values of recovery of the buffer permeability when compared to PAA membranes. This suggests that internal fouling may also have played some role in fouling of the polymeric membranes. Gelatinous masses of protein observed on the surfaces of the membrane fouled by TG suggest cake formation on the membrane surface.

4.3.5.5 Confirming concentration polarisation for BSA nanoparticles filtration through 20 nm PAA membranes: effect of stirring speed on flux and transmission

High reversibility of membrane permeability with a simple rinse of membrane surface after BSA nanoparticle filtration and flux decline mechanism resembling to cake filtration and high retention of protein nanoparticles appear to suggest the presence of significant concentration polarisation in PAA membranes. Concentration polarisation is also known to increase transmission of polarising solute (Zydney, 1997, Narsaiah and Agarwal, 2007). This is likely due to diffusion of solute due to a high solute concentration above large membrane pores and defects. On the other hand in fouling, foulant solute molecules are trapped in membrane pores and are less likely to be transmitted to permeate side. Concentration polarisation can be confirmed by comparing different operational conditions where concentration polarisation is known to vary. Tangential flow across the membrane surface is known to reduce the polarisation by aiding in back-transport of the polarising solute from membrane surface to bulk solution. For stirred cells, tangential flow is controlled using the stirring rate. An experiment was designed to investigate the impact of stirring speed on the filtration performance of PAA membranes for BSA nanoparticle feed with all the other parameters (TMP, feed volume, filtrate output) kept constant.

Varying the stirring speed from 0 to 1500 rpm significantly increased the average filtrate flux from 59 to 87 LMH across the membrane for same filtrate output (as shown in **Table 4-5**). Changes in the clean membrane permeability were observed but were estimated to be statistically insignificant using ANOVA. Flux decline across the filtrate output as shown in **Figure 4-26** shows similar initial flux decline irrespective of the stirring speed. The steady-state region of the flux (beyond 10 L/m^2) however indicates improved steady state flux for 1500 rpm. As shown in the figure, the normalised steady state flux for 1500 rpm ranges from 0.075 to 0.1 of the initial buffer flux.

Analysing the flux decline for the mechanism of fouling; only cake filtration mechanism shows better fits out of four fundamental mechanisms of fouling with above 0.95 regression coefficient for all of the stirring speeds. As shown in **Table 4-6**, the cake filtration model showed better fits (low SSR and high regression coefficients) at lower stirring speeds (0 and 500 rpm) compared to 1000 and 1500 rpm. This is also reflected in the reduced value of the cake fouling constant at higher stirring speeds. Lower stirring speeds were expected to increase the concentration polarisation. It is also clear that 500 rpm is insufficient to create any significant improvement in flux as compared to unstirred filtration. Some improvement is seen for stirring speed of 1000 rpm and above. It is likely that the transition point is located somewhere between 500 and 1000 rpm.

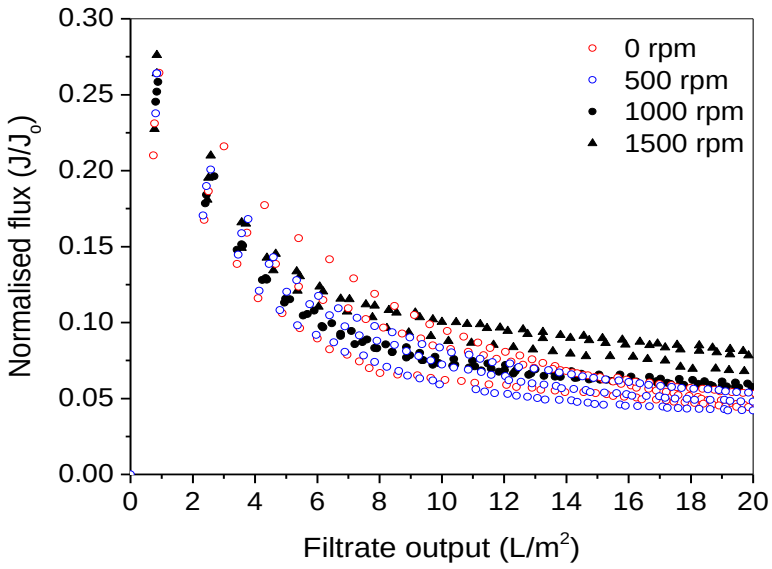

Figure 4-26 Effect of stirring rate on the flux decline for filtration of BSA nanoparticles through 20 nm PAA membrane (lot#6) at a constant transmembrane pressure of 0.6 bar.

Stirring speed (rpm)	Recovered membrane permeability %	Clean membrane permeability (LMH/bar)	Protein flux (LMH)
0	93 ± 1	2022 ± 87	59 ± 5
500	95 ± 1	1873 ± 74	57 ± 6
1000	96 ± 1	1938 ± 34	71 ± 3
1500	98 ± 1	1941 ± 105	87 ± 4
P-value (ANOVA)	0.001	0.22	0.0001

Table 4-5 Membrane permeability, protein flux and recovered membrane permeability for filtration of BSA nanoparticles at various stirring rates.

P-value (ANOVA) indicates the probability of error assuming the differences to be significant when they are not. A p-value less than 0.05 is assumed to indicate statistical significance. (Data: Average value ± one SD)

Stirring speed (rpm)	Adjusted R^2	SSR (x 10^{-5})	Cake constant, K_c (sm^{-2} x 10^6)
0	0.98 ± 0.01	4.13 ± 4.03	6.14 ± 0.65
500	0.98 ± 0.00	4.37 ± 1.47	7.02 ± 0.82
1000	0.96 ± 0.00	10.9 ± 0.75	5.91 ± 0.29
1500	0.96 ± 0.01	10.1 ± 1.96	4.54 ± 0.17
P-value (ANOVA)	0.001		0.004

Table 4-6 Fit parameters (Adjusted R^2, SSR and cake constant) for the model fit of cake filtration model to experimental filtration data for various stirring rates.

(Data : Average value ± one SD)

Additionally, more than 90% of the initial membrane permeability was recovered after rinsing the surface of the membranes post filtration of the feed. High reversibility of the membrane permeability is an indicator of concentration polarisation phenomena. Retentate solutions collected from stirred and unstirred runs were compared for particle size distribution using DLS to ensure if any aggregation of the nanoparticles is responsible for the different performance at extremes of the stirring rate. Particle size distributions of retentates were found similar to the initial feed solution.

Another characteristic associated with concentration polarisation is increased transmission of the polarising solute. **Figure 4-27** shows a decline in the sieving coefficient of BSA nanoparticles with an increase in the stirring rate. Filtration without stirring resulted in very high sieving coefficients of 0.13 compared to 0.04 observed for 1500 rpm. The lowest transmission was however observed at 1000 rpm instead of 1500 rpm. This could be due to reversible structural changes induced to nanoparticles at higher shears of 1500 rpm resulting in increased transmission through defects or could merely be due to higher defect density of the membranes used in 1500 rpm runs.

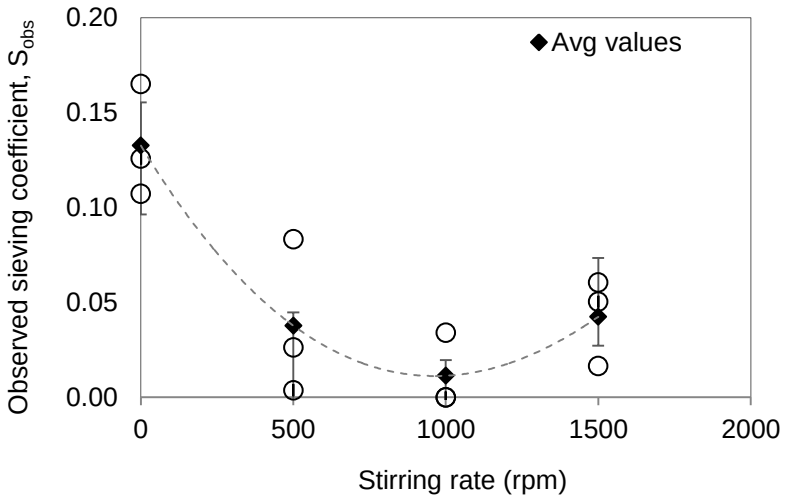

Figure 4-27 Effect of the stirring rate on observed transmission or sieving coefficients for BSA nanoparticle filtration through PAA membranes.

Solid symbols denote average values of the observed sieving coefficients for triplicate runs with error bars representing one standard deviation across the average and open symbols represent individual values for triplicate runs.

Trends observed for protein transmission, filtrate flux and consistently high reversibility of the membrane permeability upon withdrawal of transmembrane pressure for all stirring rate confirm that concentration polarisation is the dominant mechanism for flux decline in BSA nanoparticles filtration through PAA membranes.

An analysis of the variation of the momentum boundary layer above the membrane surface explains the effect of the stirring speed. The momentum boundary layer is a hypothetical zone above the membrane surface where the velocity of the fluid is less than the mean fluid velocity of the bulk liquid with the fluid velocity approaching zero near the membrane surface. The solute transport within the boundary layer region is dominantly diffusive. Diffusion is the primary mode of the back-transport of the polarised solutes which are pushed towards the membrane surface by strong convection of the pressure applied to the solvent. Diffusion is small for large macromolecules and significantly smaller for macromolecular assemblies such as nanoparticles and viruses. The boundary layer thickness is a characteristic of the bulk properties of the liquid (viscosity and density) and the bulk fluid velocity.

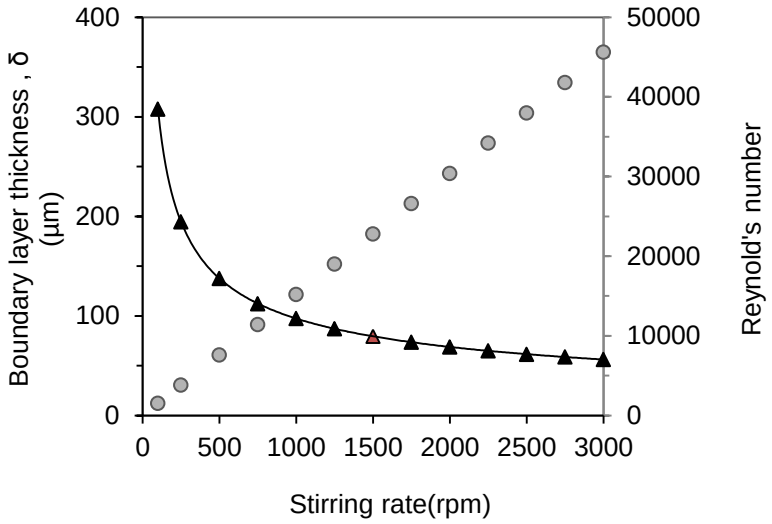

Figure 4-28 Boundary layer thickness and Reynold's number over a range of stirring rate in 25 mm stirred cell. Calculated using the equations described by Becht *et al.,* (2008).

The polarising solute needs to overcome significant boundary layer thickness to come back to the bulk solution. Calculation of the boundary layer thickness suggests a non-linear relationship with the stirring speed as shown in **Figure 4-28**. Stirring aids in the back transport of solutes from the membrane surface to the bulk solution. It was also found that the tangential flow of the liquid in the stirred cell under the stirring rates used is laminar as the Reynolds' number at 1500 rpm is calculated to be 22,800 while the transitional Reynold's number for stirred cells is determined to be 32,000 by Smith and Colton, (1972). Operating at a higher stirring rate (above 2000 rpm) approaching the transitional or turbulent flow regimen will likely improve the filtration performance and will further reduce the transmission. The higher stirring rate was not possible due to the instrumentation limitation. A characterisation study using cross-flow filtration could be helpful to reduce the concentration polarisation.

4.3.6 Proposed sieving mechanisms in PAA and PES membranes

PAA (20 nm rating) and PES (300 kDa rating) membranes tested in this study show different fouling resistances and different protein transmissions for same model solutes despite having similar hydraulic permeability and closer dextran sieving curves. Higher transmission of 80 nm BSA nanoparticles through PAA membrane and almost complete recovery (>90%) of the initial membrane permeability is in stark contrast with the PES membrane indicating lower retention for BSA nanoparticles but higher fouling resistance (Section 4.3.5.1 and 4.3.5.2). Data shows that PES membranes are more susceptible to fouling by large protein solutes. Since analysis of fouled membrane surfaces showed low coverage of surface fouling on PAA membrane and PES membrane, along with data on recovery of membrane permeability, it can be concluded that PES membranes have a significant internal fouling. Since identical feed and filtration conditions were used for testing of both membranes, the different performance of the two membranes can be attributed to the differences in the membranes themselves. As discussed earlier (Section 4.3.2), the two membranes have radically different porous architectures. This section attempts to explain the difference in solute transmission and fouling resistance of PAA and PES membranes on the basis of their morphology resulting in different solute transport mechanisms for the two membranes.

Large solutes such as BSA nanoparticles are excluded from the smaller pores on the membrane surface. Pores larger than the solutes are however accessible to the nanoparticles. Once particles enter pores, solute transport within the pores is dominated by diffusion, given that the particle diameter is close to the pore diameter. Diffusive transport is affected by the pore length and tortuosity. Effective diffusion length is increased with the membrane thickness and tortuosity of the pore channels. BSA nanoparticles are able to penetrate the large pores observed on the surface of the PES membranes but the transport is hindered by tortuous pore channels in the interconnected porous membrane bed. Particles are thus entrapped in the inside the membrane bed. Since used PES membranes are asymmetric membranes, it is likely that entrapment occurs in active or intermediate layer zone. Thus particles are effectively screened inside the membrane bed preventing them to be transverse membrane bed into the filtrate resulting in lower sieving coefficients and low recovery of the membrane permeability after a surface wash with the buffer solution. Smaller pores of the active layer of the PAA membrane along with narrow pore size distribution are not penetrated and plugged by the BSA nanoparticles thus avoiding any internal fouling and screening solutes above the membrane surface. Such a mechanism is expected to also result in completely which was not observed in the experiments. Higher transmission is likely due to diffusion of the BSA nanoparticles through large support layer pores exposed by the surface defects. Since PAA membranes have thinner

membrane bed (by a factor of 2 compared to the PES membranes) and have straight pore channels (very low tortuosity), the effective diffusional path length for the solute to sieve through the PAA membranes would be significantly smaller than that in thicker and tortuous channels of PES membranes. Since surface defects offer low hindrance to the solute transport they are unlikely to be plugged. The presence of small number of surface defects thus explains the higher sieving coefficients for BSA nanoparticles along with the high recovery of the membrane permeability in PAA membranes.

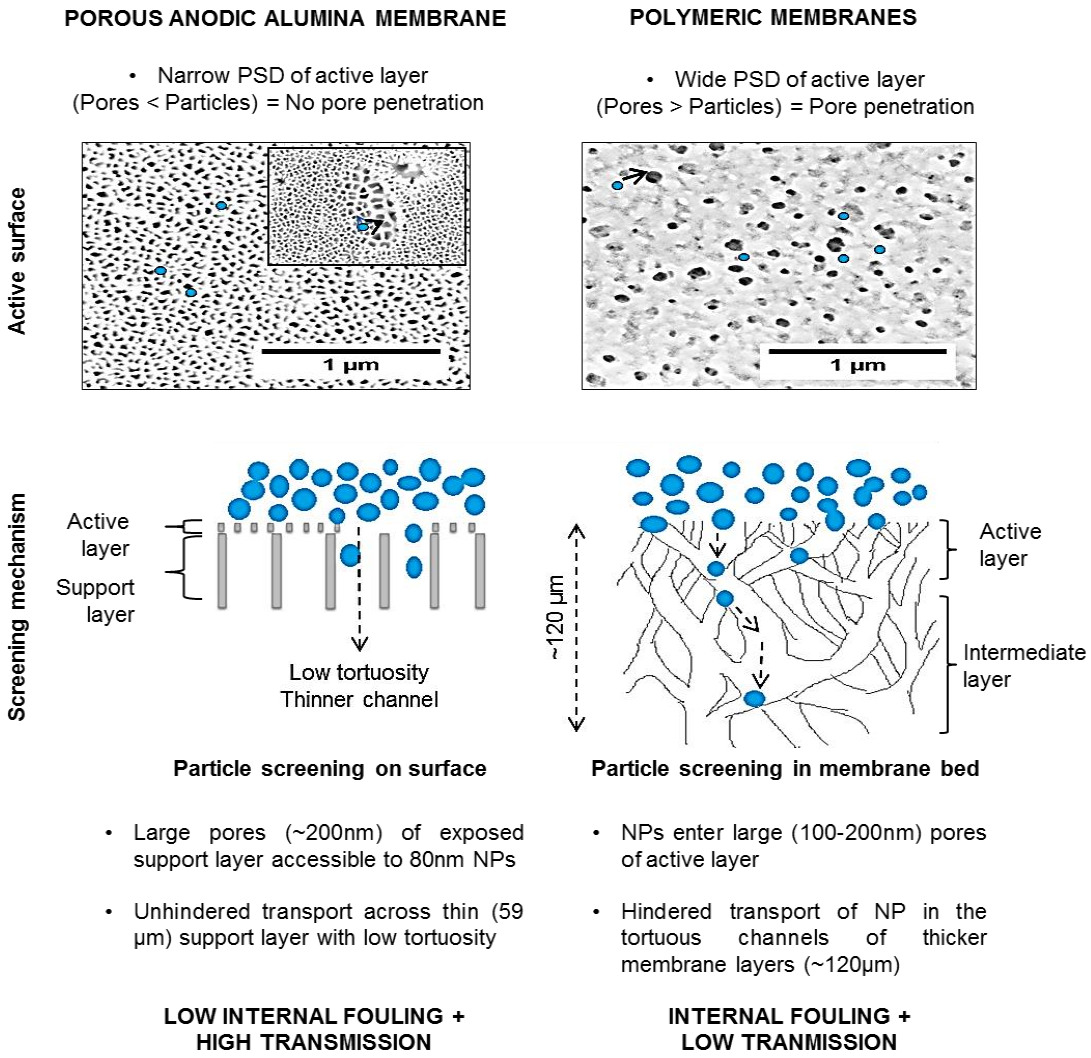

Figure 4-29 Illustration of the proposed mechanisms of fouling and screening/retention of BSA nanoparticles through 20 nm rated PAA, and 300 kDa rated polymeric ultrafiltration membranes.

Differences in the extent of internal fouling and NP transmission between the two membranes are attributed to the differences in the pore size distribution of the active layers, the presence of the surface defects, tortuosity and length of the pore channels in two membranes. SEM images of the active layer surface of the membrane show the differences in pore size distribution of the two membranes. Surface defect exposing the support layer of large pores in the PAA membrane is shown in the inset.

4.4 Conclusion

The objective of this chapter was to characterise the porous anodic alumina membranes for its filtration performance using model protein solutes, primarily 20 nm thyroglobulin and BSA nanoparticles used as mimics of virus particles, compare the performance with traditionally used polymeric ultrafiltration membranes and understand the role of membrane architecture in the filtration performance of the membranes.

Suitability of the 20 nm rated PAA membranes among three available ratings (20, 100 and 200nm) was demonstrated for highest retention of 80 nm BSA nanoparticle and lowest fouling among all ratings (Section 4.3.1). Different methods and units of ratings used for PAA (pore diameter using electron microscopy or porosimetry) and the polymeric membranes (molecular weight cut off using tracer molecules of different molecular weight) presented a challenge to select the polymeric membrane with an appropriate rating to compare with the selected membrane. Comparisons on the basis of hydraulic permeability and dextran sieving characteristics were utilised for the selection of the polymeric membrane rating and among three available ratings for polymeric membranes, 300 kDa rated PES membrane was shown to exhibit hydraulic permeability and dextran sieving curves closest to those of the 20 nm PAA membranes (Section 4.3.3 and 4.3.4).

A structural characterisation of the two different membrane types was also performed using scanning electron microscopy and image analysis highlighting a porous morphology with narrow pore size distribution, straight pore channels and surface defects in PAA membranes as opposed to wider pore size distribution and interconnected tortuous bed with thicker membrane bed in the polymeric membrane (Section 4.3.2). The presence of the surface defects and straight pore channels in PAA membranes was found to make PAA membranes susceptible to leaky transmission of solutes as higher transmission of large model solutes (thyroglobulin and BSA nanoparticles) were observed compared to the polymeric membranes. Higher solute transmission along with lower irreversible membrane fouling was observed in PAA membranes, especially for BSA nanoparticles. Overall, the filterability of protein-nanoparticle solutions was found to be superior for 20 nm rated PAA membranes and was dominated by concentration polarisation of the nanoparticles above the membrane surface. Superior fouling resistance (1.5-2.5 folds higher) of PAA membranes for protein-nanoparticles makes them attractive membrane material for concentration and buffer exchange applications of larger viral vectors such as Adenovirus. The impact of concentration polarisation and other fouling mechanisms observed in this chapter on protein fractionation needs to be examined.

CHAPTER 5 SEPARATION PERFORMANCE OF POROUS ANODIC ALUMINA (PAA) MEMBRANES FOR BINARY MIXTURES OF THE MODEL SOLUTES

5.1 Introduction and objective of the chapter

In bioprocessing, membranes are mainly used in concentration and diafiltration of protein solutions and for fractionation of a protein mixture of various sizes of proteins. So far bioseparation properties of anodic alumina membranes have been studied using diffusion cells where solute transport is diffusion dominated (Osmanbeyoglu *et al.*, 2009) or lab-scale centrifugation filtration (Jeon *et al.*, 2014, Moon *et al.*, 2009) which is not easily scalable to pilot or manufacturing scales. These studies involved the separation of bovine serum albumin and haemoglobin through an ultrathin anodic alumina membrane by alteration of buffer pH and separation of hepatitis C virus using anodic alumina membranes in centrifugal filter format. These membranes were custom made and did not represent the commercially available membranes used in this study. Ultrafiltration operations at lab, pilot or manufacturing scales are pressure driven processes, and solute transport is mainly convective. Thus to utilise the potential advantages of anodic alumina membranes evaluation of their separation performance should be carried out at conditions similar to industrial format.

In chapter 4, anodic alumina membranes were compared with commercial polymeric ultrafiltration membranes for MWCO ratings, hydraulic permeability and transport of model protein solutes in pressure driven filtrations. These studies, however, did not include the investigation of the separation ability of the membranes. What happens if a mixture of these model solutes is filtered through membranes instead of solutions of single model solute? How can separation performances of anodic alumina membranes be affected by process conditions such as pH and salt concentrations? Are these commercial anodic alumina membranes capable of separating virus particles without loss of infectivity? These are some of the questions that will be addressed in this chapter. Separation performance of the PAA membranes was studied using mixtures of model solutes in two combinations 1.) TG + BSA and 2.) BSA NP + BSA. BSA used as a model impurity or host cell protein and TG and BSA nanoparticles used as model mimics for virus particles of Adeno associated virus and Adenovirus, two most commonly used viral vectors in gene therapy.

5.1.1 Methodology used

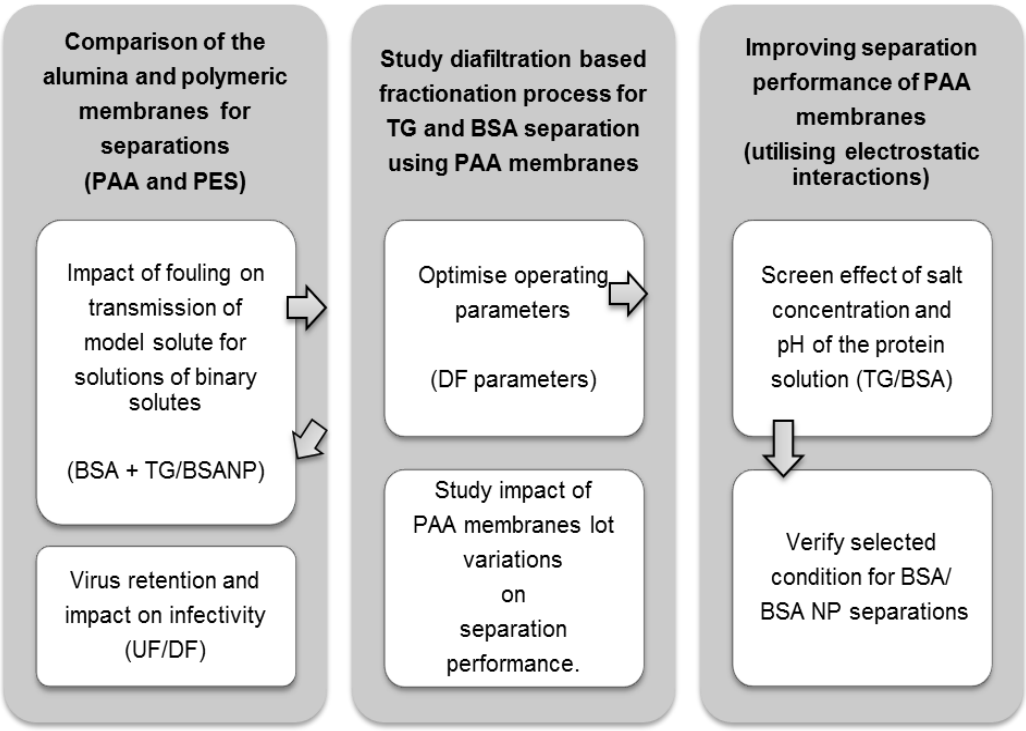

Figure 5-1 Illustration of the methodology followed and various experiments conducted to study separation performance of commercial PAA membrane (20 nm rating).

Various experiments are grouped into three major groups. Initial studies involved evaluating the filterability of binary mixtures of three model solutes (BSA, TG and BSA NP) through PAA and PES membranes and comparison with single solute filtrations as discussed in Chapter 4. Impact of fouling on the transmission of two solutes was assessed. A diafiltration based fractionation process was studied to increase separation of model solutes. TG/BSA system was used for the majority of separation studies for studying the impact of process parameters during diafiltration based fractionation process. Improvement in separation factor was studied by utilising electrostatic interactions of the solutes and membranes. Optimised processing parameters and conditions were applied to the separation of BSA and BSA nanoparticles mixtures. Finally, filterability of Adenovirus rich clarified cell culture filtrate was studied and performance of two membrane types was compared for impact on infectivity. Arrows show a sequence of studies conducted.

5.2 Materials and Methods

5.2.1 Materials used

All the materials used for experiments using model solutes (BSA and TG) reported in this chapter are described in detail in Section 4.2.1 of Chapter 4. Materials used for the production of Adenovirus feed are described in detail in Section 3.3.1 of Chapter 3. Infectivity assay for the Adenovirus was performed using ß-galactosidase reporter cell staining kit from Sigma Aldrich, USA and flat bottom Costar® 96-wells cell culture plates obtained from Corning Inc., USA. Poly-L-lysine (0.01% solution) was also obtained from Sigma Aldrich, USA.

5.2.2 Filtration setup and experiment

All of the filtration experiments reported in this chapter are carried out using 25 mm stirred cell module. Except few, most of the experiments were conducted in a UF/DF format in discontinuous diafiltration mode. Discontinuous diafiltration is discussed in detail in the section below (5.2.3). A detailed protocol for assembly of the stirred cell and filtration runs are discussed in Section 3.3.7.1 and Section 4.2.2 of Chapter 3 and 4 respectively.

5.2.3 Discontinuous/Sequential diafiltration

Fractionation/separation experiments were carried out in UF/DF format. A fixed volume of feed was loaded into the assembled stirred cell with the membrane. Feed conversion ratio (ratio of collected filtrate volume to feed volume) of 0.75 was used for all steps including an initial concentration step and diafiltration steps. After concentration to a volumetric concentration factor (VCF) of 4, permeate was removed and retentate was diluted back to original feed volume using PBS. The final retentate (obtained at the end of the final diafiltration cycle) was not diluted. Permeates collected for the different steps (initial concentration and DF cycles) and final retentate sample was analysed for protein concentration. **Figure 5-2** shows an illustration of a discontinuous diafiltration process after an initial concentration step.

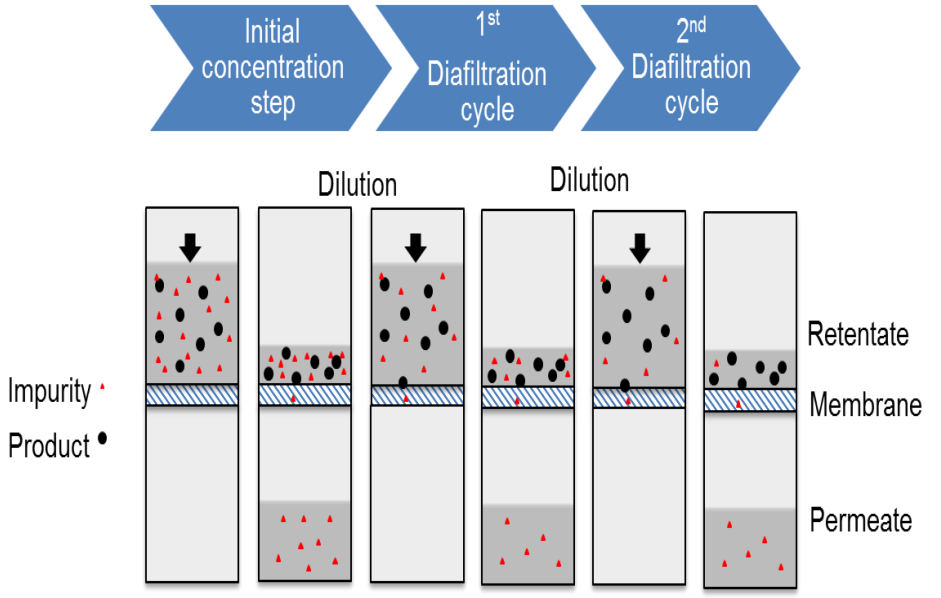

Figure 5-2 Illustration of a discontinuous ultrafiltration/diafiltration (UF/DF) process.

The discontiounous diafitration process is a series of alternating concentration and dilution steps. The retentate is diluted back to the original feed volume using diafiltration buffer after each concentration step. One diafiltration cycle involves dilution of the retentate obtained after previous step/cycle to original feed volume and subsequent 4 fold concentration of the diluted retentate. Impurity (low MW solute) will pass through membranes and product (larger solute) will be retained through all of the steps.

5.2.4 Calculation of yields and purification factors for protein model solutes

Yields or recoveries of model solutes in permeate, retentate, rinse or wash samples were estimated by quantification of the peak area of the solute in HP-SEC chromatograms. A detailed description of the HP-SEC methods used for separation of protein solutes and estimation of peak areas is discussed in Section 4.2.7 of Chapter 4. The purity of the samples is interpreted from the relative peak area % for the desired solute (product) in a given sample.

Yield or recovery of any solute s in a filtration fraction (permeate or retentate)

$$\% \, Y_s = \left(\frac{C * V}{C_f * V_f} \right) * 100$$

C and V, represent concentration (peak area per injection volume) of the solute and total volume of the sample (retentate or permeate) respectively. C_f and V_f, represent concentration (peak area per injection volume) of the solute in the feed and total volume of the feed respectively.

The yield of impurity is also referred to as % removal in permeate and residual % in the retentate. The yield of the product to be retained is referred as % retained in retentate and % loss in permeates.

Purification factor (PF) is calculated for the retained product as the ration of the yield of product to the yield of impurity in retentate (since model solutes for viruses, TG and BSA NP are completely or partially retained by the membranes).

$$PF = \left[\frac{Y_{product}}{Y_{impurity}}\right]$$

5.2.5 Filtration experiments to investigate electrostatic effects on the separation performance of PAA membranes for fractionation of a mixture of protein solutes.

All initial filtration studies were performed using PBS buffer which can have a high salt concentration (~150 mM) hence high conductivity (~18 mS/cm as measured from the conductivity detector of FPLC). The first experiment was to measure the impact of salt concentration on the fractionation of BSA and TG from a binary mixture. Hence phosphate buffer solution (10 mM Na_2HPO_4, 2.3 mM KH_2PO_4 and 2.7 mM KCl) were prepared with varying NaCl concentrations (0, 50, 100, 150 and 300 mM). Final pH of every buffer preparation was adjusted to 7.4, and final pH did not change after protein addition to the buffer. Solutions were then filtered through 20 nm PAA membranes in a discontinuous diafiltration mode with one diafiltration cycle (3 diavolumes filtered after the initial concentration step). The transmembrane pressure of 0.5 bar and a stirring speed of 1500 rpm was used throughout the filtration.

Impact of pH was studied in a similar manner with protein solutions prepared using the phosphate buffer system (10 mM) and final pH adjusted to 3.5, 4.6, 6.5, 7.4 and 9.0. Phosphate buffer system of H_3PO_4, NaH_2PO4, Na_2HPO_4 and Na_3PO_4 was used. For example pH 3.4 and 4.6 solutions were obtained by addition of 10mM of H_3PO_4 to 10mM solution of NaH2PO4. Buffer solutions of pH 6.5 and 7.4 were obtained by mixing defined volumes of 10mM solutions of NaH_2PO_4 and Na_2HPO_4. A buffer solution of pH 9.0 was obtained by addition of 10mM Na_3PO_4 to 10 mM solution of Na_2HPO_4. Final solution pH of the protein solutions was adjusted to the required pH levels (3.5, 4.6, 6.5, 7.4 and 9.0) using either H_3PO_4 or Na_3PO_4. Similar buffer system was required for all pH to eliminate the effect of different ion species (citrate, acetate, tris etc.) which may manifest from the use of different buffer systems for different pH levels. Filtration of protein solutions was carried out at a transmembrane pressure of 0.5 bar, stirring speed of 1500 rpm and for one diafiltration cycles using corresponding buffers.

5.2.5.1 Batch adsorption of protein solutes on PAA membranes

Protein solutions of BSA and TG at 1.0 and 0.2 mg/mL concentrations respectively were prepared in phosphate buffer system (10 mM) for two final pH values of 5.2 and 8.4. The low ionic strength of buffer components, as well as lack of any salt, was to avoid charge screening effect of salts. Fresh, unused anodic alumina membranes (20 nm Anodisc) were wrapped in clean aluminium foil and crushed to small pieces (< 3 mm). Pieces of crushed membranes were added to 2 mL polypropylene centrifugal tubes. Tubes with membrane pieces (referred to as treatment) and tubes without membranes (referred to as control) were washed with 1 mL of pre-filtered buffer to remove any dust and buffer solution was aspirated out. Following washing, 0.5 mL of protein solution was added to both control and treatment tubes. Samples were incubated at room temperature for 1.5 hours. After incubation, protein solutions were carefully aspirated out of both control and treatment tubes and the absorbance of the solutions was measured. The absorbance of protein solutions was measured at 280 nm using 100 µL of the sample in a quartz cuvette and UV-Vis spectrophotometer (Biomate 3S). The same procedure was repeated for all four protein solute-solution pH combinations. An equal amount of anodic alumina material was used for all experiments.

5.2.6 Virus UF/DF

5.2.6.1 Preparation of Adenovirus feed for Ultrafiltration/Diafiltration experiments

Adenovirus particles were produced in mammalian cell culture and subsequent processing of the cell culture as described earlier in Section 3.3.8 of Chapter 3.

5.2.6.2 Filtration of clarified Adenovirus feed

Feed material diluted in PBS (clarified Adenovirus -rich supernatant) was filtered through the PAA membranes. To compare these two membranes with different filtration areas, the load on the membrane was adjusted accordingly to keep the constant load per unit area (L/m^2). Similar conversion ratio hence similar filtrate output per unit area (~20 L/m^2) was used for filtration experiments with both membranes. Three diafiltration cycles (each of 3 diavolumes) were applied to the retentate obtained after the initial concentration step. Each diafiltration cycle consisted of 20 L/m^2 of filtrate collected. PBS was used as the diafiltration buffer.

5.2.6.3 Infectivity assay for Adenovirus

Infectivity assay for the recombinant Adenovirus (with ß-gal gene) was based on observing the number of HEK293 cells infected by the virus and thus transformed to produce ß-galactosidase enzyme intracellularly. The assay was composed of following three major steps:

Step 1: Preparation of samples and tissue culture plates

Tissue culture plates with 96 wells were coated with 30 µL of 0.01% poly-L-lysine solution in each well and incubated for 10 minutes at room temperature. The solution was aspirated out and discarded. Wells were then subsequently washed twice with 50 µL of Dulbecco's PBS solution for each well per wash. PBS solution was aspirated out and discarded. Wells were then seeded with 100 µL HEK293 cell suspension at a seeding density of 4×10^4 viable cells per well. The cell suspension was repeatedly mixed by inverting to ensure uniform seeding in each well and all the plates. Plates were incubated overnight at 37°C until 70 % confluency is observed. Dilutions of samples containing virus particles were prepared on the same day in growth media and stored at 4°C. It was ensured that all the samples are stored for an approximately equal amount of time in similar buffer conditions. For each sample, four dilutions were prepared with dilution factors ranging from 100 to 1×10^6 depending upon the nature of the sample.

Step 2: Infecting cells

Following day, plates were seeded with 100 µL of samples at various dilutions and incubated at for 1 hour. At the end of incubation, wells were carefully aspirated and 100 µL of fresh growth media was added. Plates were then incubated overnight at 37°C. Each sample was seeded in four dilutions with triplicates per dilutions. As a negative control, 100 µL of growth media was also plated in triplicate wells in each plate. As a positive control, similar dilutions of feed material were plated in each plate.

Step 3: Staining and counting

Following overnight incubation, the growth medium is carefully aspirated out of the wells. Cells are washed twice with 50 µL of 1X PBS per well in each wash. Cells were then fixed using 50 µL of 1x fixation buffer (2% formaldehyde + 0.2% glutaraldehyde in PBS) per well for 10 minutes at room temperature. Following fixation, cells were further washed twice with PBS as described above. 30 µL of staining solution containing $MgCl_2$, Potassium ferricyanide, Potassium ferrocyanide and substrate, X-gal was added to each well. Plates were sealed with parafilm and covered with aluminium foil before incubating for 24 hours at 37°C. Cells infected and transformed by recombinant Adenovirus would produce the recombinant ß-galactosidase enzyme. This enzyme can aid in the hydrolysis of glycosidic bonds in carbohydrate like ß-galactosides into monosaccharides. Staining kit uses X-gal (5-bromo-4-chloro-3-indolyl ß-D-galactopyranoside) as a substrate, an organic compound with indole group attached to galactose through the glycosidic bond. The substrate can penetrate the cells. Bond cleavage

catalysed by recombinant ß-galactosidase in infected cells results in the release of indole group which results in indigo-blue colour. Infectivity was measured by counting the number of blue formation unit (BFU) in the well under an optical microscope with a 10X objective lens. Dilutions where 30-200 BFUs per well were observed were used for calculations of titres.

5.3 Results and Discussion

5.3.1 Choice of binary model solute solutions for separation or fractionation studies

As described earlier in Section 4.1.2 of Chapter 4, three model solutes; BSA, TG and BSA nanoparticles were selected for their size similarity with most abundant host cell proteins, smaller Adeno-associated viruses and larger Adenoviruses respectively. A typical virus-rich feed from mammalian cell culture contains host cell proteins (impurity) and virus particles (product). The objective of any separation process is to remove impurities from the product. TG (~20 nm) and BSA nanoparticles (~80-90nm) have hydrodynamic sizes similar to common viral vectors, adeno-associated viruses and Adenovirus respectively. BSA, a 67kDa protein is used as a model impurity solute for average size range for the host cell proteins produced by mammalian cell culture. Hence two types of feeds were used in these experiments, i.e. BSA + TG mixture and BSA + BSA nanoparticles mixture. The idea is to simulate a partially purified virus-rich feed for two different virus particle sizes (i.e. TG for 20 nm AAV and BSA nanoparticles for 90 nm AdV). The mixture of TG and BSA nanoparticles was not tested. However, such preparations could be tested if the intention is to study the effect of virus feed containing aggregated virus particles.

5.3.2 Comparison of filtration of single solute and binary solute solutions of protein model solutes through 20 nm PAA and 300 kDa PES membranes

Following from Section 4.3.5 from Chapter 4 where filtration of single solute solutions of three model solutes was studied, this section attempts to compare the performance of two membrane types (PAA and PES) for the filtration of binary solute feed (mixtures of two solutes). Membrane performance (flux decay, transmission and recovery in buffer permeability) were compared with that observed during single solute filtrations to assess the impact of the binary solute system.

To draw a direct comparison with single solute filtrations, the same values of various process parameters such as transmembrane pressure (0.6 bar), stirring speed (1500 rpm), membrane loading (~25 L/m^2) and filtrate output (~20 L/m^2) were used except the feed composition. However, final concentrations of each solute in the mixed solute feed were similar to the concentrations of solute used in single solute filtrations. Filtrations were carried out with two

types of binary feeds 1). BSA and TG mixture in PBS with final concentrations of 1.0 and 0.2 mg/mL respectively and 2). BSA and BSA nanoparticles mixture in PBS with final concentrations of 1mg/mL for both solutes. Same membrane lots were used for filtration of the binary solute feeds as used for single solute filtrations as discussed in Chapter 4.

5.3.2.1 Comparing flux decline and fouling mechanisms

Flux decline through both membranes showed similar trends as observed with filtration of a solution of single solutes (reported in Chapter 4) indicating that mechanism of fouling has not changed significantly with the addition of a smaller solute. For single solute filtrations, BSA alone did not result in significant flux decline for PAA membranes where filtrate flux was above 80% of the initial buffer flux throughout the filtration run. However, 300 kDa membranes filtered BSA solution at a relatively lower fraction (50 %) of the initial buffer flux through these membranes. Larger solutes, i.e. TG and BSA nanoparticles were concluded to be the fouling solutes for both membranes.

Comparison of filtration of binary and single solute solutions did not show any appreciable differences in the filtrate fluxes or change in the flux decline curves as shown in **Figure 5-3**. Flux decline curves were normalised with initial buffer fluxes for the respective membranes to include the differences in the membrane permeability between several membranes used for single solute and binary solute filtrations. Compared to single solutes, membranes filtered the mixed feeds at slightly higher normalised fluxes. This effect appears to be high for polymeric membranes for both TG and BSA nanoparticles containing feeds. Another reason for elevated normalised fluxes for BSA NP + BSA feed in polymeric membranes could be reduced NP penetration in membrane pores which are now completed by relatively smaller high molecular weight components of BSA in the mixed feed. However, large standard deviations represented by large error bars also imply higher variations in membrane performance for polymeric membranes. Large standard errors for polymeric membranes meant that the average values of fluxes could vary significantly over the course of filtration using different membranes. For PAA membranes, flux decline curves for solutions TG alone and TG with BSA were similar for PAA membranes. Similarly, flux decline curves for BSA nanoparticles solutions with and without BSA were also found to be identical. Fouling mechanisms identified for filtration binary solute solutions were found similar to those identified for single solute solutions of foulant solutes.

When comparing the filtrations of single solute and binary solute solution of TG or BSA nanoparticles, the same membrane lots were used for both membrane types. Comparison of hydraulic permeability of membranes used for such pairs (TG/ TG+BSA or BSA NP/ BSA NP+BSA) for both membranes concluded no significant differences (p-values > 0.05 for all

pairs). Similarly, process fluxes and recovery of buffer permeability also didn't change significantly (**Table 5-1**).

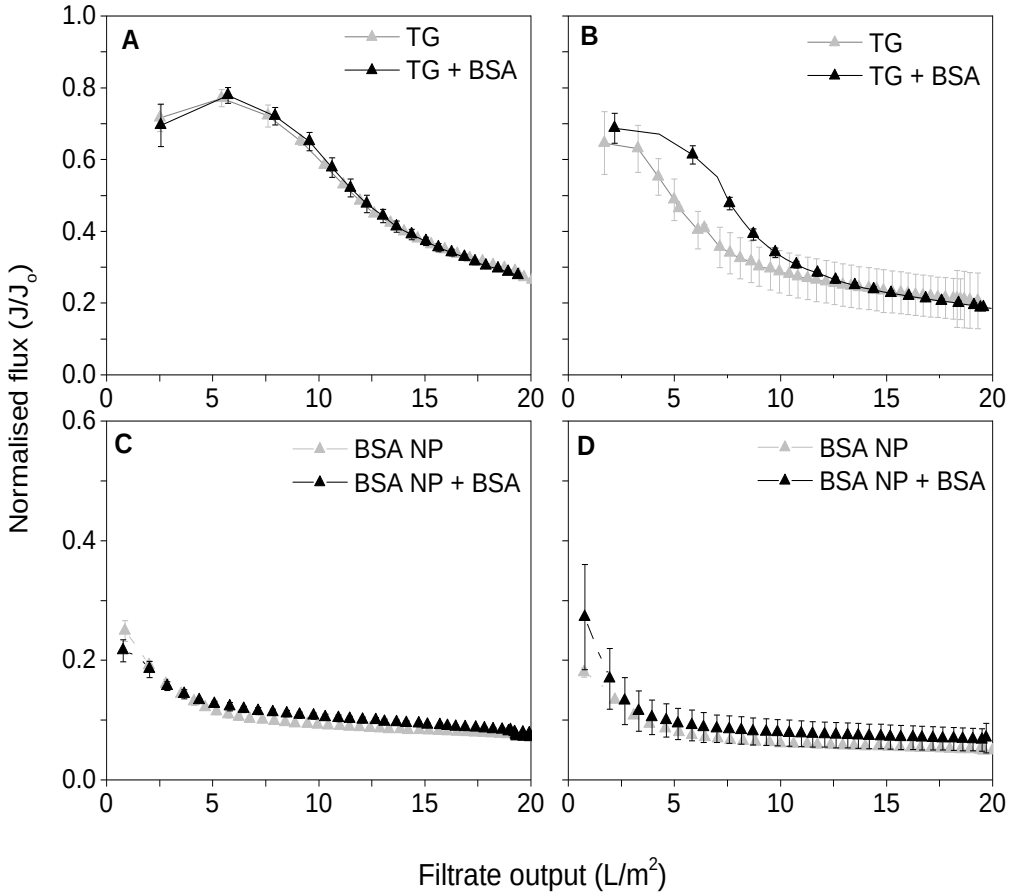

Figure 5-3 Comparison of flux decline for protein solutions through PAA membranes (A, C) and 300 kDa PES membranes (B, D) for single solutes feeds (TG and BSA nanoparticles) and binary solute mixtures of TG and BSA nanoparticles with BSA.

The comparison shows no difference in the filterability of single solute or binary solute systems. Similar filtration conditions (TMP 0.6 bars, stirring speed of 1500 rpm) and feeds (both single and binary solutes) were prepared in PBS with 0.2 mg/mL for TG and 1 mg/mL for BSA and BSA nanoparticles as final concentrations in both single solute and binary solute feeds.

Membrane	Solute	Hydraulic permeability (LMH/bar)	Filtrate flux, (LMH)	Recovered membrane permeability %
20 nm PAA	**TG**	2030 ± 40	350 ± 20	65 ± 3
	TG + BSA	2100 ± 150	360 ± 40	60 ± 0
	BSA NP	1990 ± 40	90 ± 01	94 ± 1
	BSA NP + BSA	2080 ± 80	110 ± 10	97 ± 2
300 kDa PES	**TG**	1590 ± 540	170 ± 10	27 ± 5
	TG + BSA	1930 ± 120	220 ± 20	26 ± 1
	BSA NP	2480 ± 90	72 ± 02	43 ± 6
	BSA NP + BSA	1790 ± 460	70 ± 02	52 ± 6

Table 5-1 Comparison of single solute and binary solute filtrations by the hydraulic permeability of clean membranes, cumulative filtrate flux for protein solutions and recovered membranes permeability(%) after protein filtration.

No significant changes in process fluxes for protein solutions and recovery of buffer permeability after filtrations irrespective of single or binary solute composition of the feed (Values ± SD for triplicate runs)

5.3.2.2 Comparing transmission of the model solutes

Feed	Solutes	Observed sieving coefficients, S_{obs}	
		20 nm PAA	**300 kDa PES**
Single solute	BSA	0.96 ± 0.03	0.96 ± 0.02
	TG	0.60 ± 0.04	0.21 ± 0.08
	BSA NP	0.03 ± 0.01	0.01 ± 0.00
Binary solutes BSA + TG	BSA	0.89 ± 0.03	0.76 ± 0.01
	TG	0.67 ± 0.09	0.43 ± 0.03
Binary solutes BSA + BSA NP	BSA	0.68 ± 0.03	0.54 ± 0.06
	BSA NP	0.18 ± 0.03	0.00 ± 0.00

Table 5-2 Comparison of single solute and binary solute filtrations through PAA and PES membranes by observed sieving coefficients for various solutes.

Similar process conditions and similar solute concentrations were used for filtration of single solute and binary solute solutions. (Mean value ± one SD for triplicate runs)

Impact of the fouling by TG and BSA nanoparticles was significant for transmission of the smaller solute, BSA. For both membranes, transmission of BSA was lower in the presence of the fouling solutes. In the absence of these solutes, both membranes showed high transmission (~96%) of BSA molecules. Impact of the fouling by TG and BSA was more prominent on the transmission of BSA through the polymeric membrane as compared to PAA membranes. Relative to the high transmission of BSA in a pure BSA solution, transmission of BSA dropped by 7% and 20% for PAA and PES membranes respectively in the presence of TG in the feed. Similarly, BSA transmission reduced by 29% and 44% respectively in PAA and PES membranes in the presence of BSA nanoparticles. These changes were found to be statistically significant with a p-value of less than 0.05 when means were compared using two-tailed t-tests. Surprisingly, for both membranes transmission of the larger fouling solutes (TG or BSA nanoparticles) when filtering their mixtures with BSA was found to be increased as compared to filtration of single solute solutions of these fouling solutes. For thyroglobulin, transmission through the polymeric membrane was found to be doubled which could be attributed to the higher hydraulic permeability of the PES membranes used for filtration of TG+BSA mixture as compared those used for TG alone. Increased transmission of TG was also observed through PAA membranes, but the increment was modest and not statistically significant. BSA nanoparticles transmission, on the other hand, was significantly high for PAA membranes when a mixture of nanoparticles and BSA was filtered through it.

No transmission of BSA nanoparticles was observed in size exclusion chromatogram of the permeate samples collected after filtration of a mixture of BSA nanoparticles and BSA through polymeric membranes. Presence of BSA is unlikely to increase the permeability of larger solutes through membranes. Thus, likely explanation for increased transmission across PAA membrane could be due to different defect densities in the membranes or change in particle size. Reduced transmission of BSA nanoparticles in BSA + BSA NP filtrations through PES membranes is consistent with fouling hypothesis that the high molecular weight component of BSA are competing with protein nanoparticles for access to the pores. Thus preventing nanoparticles' penetration into the pores which also leads to membranes operating at higher normalised fluxes when compared to filtration of BSA nanoparticles alone. Another possibility for the variations observed in transmission is the sampling error or analytical measurement errors. Nonetheless, PAA membranes were observed to result in significant leakage of larger solutes (TG and BSA nanoparticles) whether single solute solutions or a mixture of these solutes with BSA were used. High sieving of BSA NP through PAA membranes in the binary mixture was considered as an anomalous reading and was not observed in further experiments.

5.3.3 Fractionation of mixtures of protein model solutes using discontinuous diafiltration through PAA membranes

PAA membranes were evaluated for fractionation of protein mixtures of model solutes (TG + BSA or BSA NP + BSA). For the experiments conducted so far only 4 to 5 fold concentration step was used for protein separation which could only remove 40 to 60 % of the total BSA in the feed. The retentate obtained were still not purified to satisfactory levels. Thus, a diafiltration step was carried out in addition to the initial concentration step to remove BSA from the retentate further. Since these are not comparison studies with polymeric membranes, thus filtrations for greater feed loadings (35 L/m^2) and greater filtrate output (26 L/m^2) were carried out. These parameters were constrained by the loading capacity of the stirred cell and different active filtration areas of the membranes used in previous experiments.

5.3.3.1 Fractionation of BSA and TG mixture

5.3.3.1.1 Effect of diafiltration cycles on flux through the membranes and fouling

The goal of the fractionation process is to remove the maximum amount of impurities (BSA) and retain the maximum amount of product (TG) from a feed with a mixture of two proteins. Discontinuous diafiltration is alternating between concentration and dilution of feed in a stirred cell by filtration and then the addition of buffer to retentate. Protein solution (TG+BSA) in PBS buffer was initially 5 fold concentrated from 10mL to a retentate volume of 2mL. Each diafiltration step was then carried out by dilution of the retentate using PBS and further concentration by 4-5 fold.

Flux decline during diafiltration steps and initial concentration steps were compared. Both diafiltration steps have similar flux decline and same final filtrate flux at the end of the filtration cycle. Flux decline curve was steeper for the initial concentration step as the fresh membrane was exposed to the fouling solutes. Final filtrate flux for the initial concentration step and diafiltration steps was found to be similar suggesting no significant fouling occurring in diafiltration steps. For diafiltration steps, initial filtrate fluxes (at 0 L/m^2) are slightly higher than the filtrate fluxes observed at the end of the initial concentration step. This was possibly due to an interruption in the applied pressure across the membrane between the diafiltration and initial concentration steps. The interruption was because of the manual dilution of the retentate before proceeding for the next filtration step. This resulted in the diluted feed on membrane surface thus reducing the concentration polarisation above the membrane. Internal fouling which occurred during the first step or initial concentration step remains un-mitigated by such dilutions and upon the application of the pressure concentration polarisation manifest again on the surface of the fouled membrane. A control experiment was also performed where the feed was only processed for the initial concentration step without any subsequent diafiltration.

Analysis of the total permeate collected for initial concentration and diafiltration steps revealed 74% BSA monomers removal as opposed to 47% for the control run without diafiltration. Total loss of TG, on the other hand, was similar for both with and without diafiltration. These trends were also reflected for retentate solutions with low residual BSA measured in retentate obtained after the diafiltration process. Recovery of the initial membrane permeability (of the clean membrane) was marginally lower for runs with diafiltration (48 ± 1 %) than the control run (57 ± 5 %). The slight decrease was expected for the runs with diafiltration as pores were exposed to longer filtration cycles and more transmission of the smaller solute, BSA. This proved that fractionation yield could be improved using a diafiltration process without significant loss in the flux after the initial concentration step.

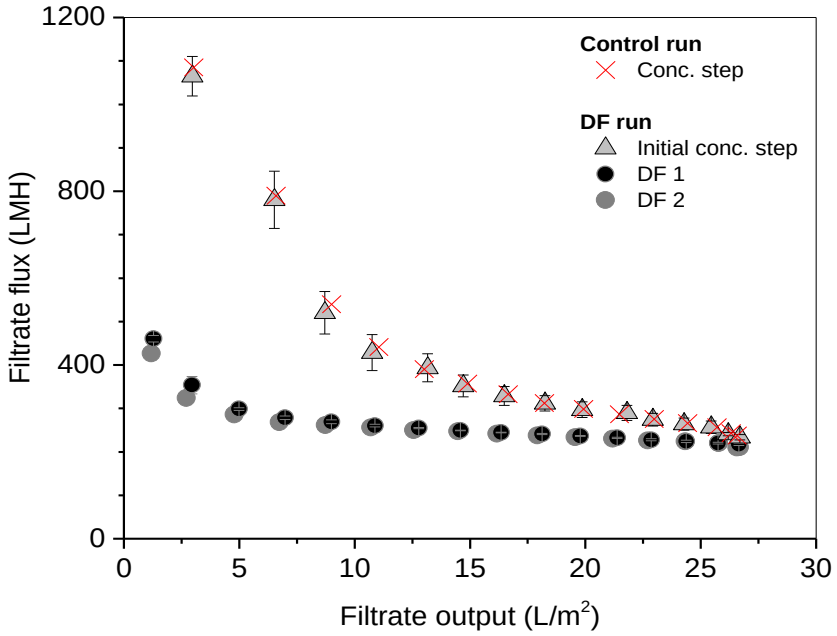

Figure 5-4 Flux decline during the initial concentration step and two subsequent diafiltration (DF1 and 2) steps for TG/BSA fractionation by PAA membranes in ultrafiltration-diafiltration process.

Error bars represent one standard deviation for triplicate runs. Control run included only the initial concentration step without subsequent diafiltration steps. Filtrations are carried out at TMP of 0.6 bar and 1500 rpm in a stirred cell. Feeds were concentrated 4-fold in initial concentration step followed by two diafiltration steps (4 fold dilution of the retentate followed by ~4 fold concentration). Dilutions were carried out manually. Cumulative filtrate fluxes (at the end of filtrations) for DF steps and initial concentrations steps were similar indicating no further fouling in diafiltration steps.

5.3.3.1.2 Effect of diafiltration cycles or diavolumes on fractionation

It is desirable that maximum fractionation could be carried out with minimal time and volume of the diafiltration buffer used. The previous experiment established the role of diafiltration in increasing removal of BSA for only two diafiltration cycles (with approximately 4 diavolumes of the buffer used per cycle). An experiment was thus conducted to study the impact of the number of diafiltration cycles or diavolumes on the removal of BSA. The protocol was slightly modified for this experiment with 7.5 mL filtrate collected per filtration run instead of 8 mL collected in the previous experiments. This meant that retentate volume is 2.5mL with the modified protocol compared to 2mL collected previously. Significant frothing was observed in the stirred cell when the liquid volume was below 2mL resulting in loss of some of the retentate volume thus such modification was necessary. For diafiltration, each DF cycle now represented 3 diavolumes. A total of 4 DF cycles or 12 diavolumes were applied with samples collected after each diafiltration cycle (3 DVs).

Cumulative filtrate flux did not change significantly for the diafiltration cycles as shown in **Figure 5-4** but was slightly lower than that for the initial concentration step (at 0 diavolume). No loss of TG was observed in any diafiltration cycle. BSA removal increased with increase in the diavolumes in a non-linear fashion. BSA removal was highest for the initial concentration step and first diafiltration cycle. A maximum of 80 % of the BSA could be removed at the end of 12 diavolumes of the diafiltration process. Removal achieved per DF reduced from 0 to 12 diavolumes, and it was confirmed by a reduction in the peak area of the BSA monomer in size exclusion chromatograms of the permeate collected after each step. Such non-linear removal was expected because the concentration of BSA left after each diafiltration cycle reduces and since the constant volume of the filtrate is processed for each cycle the amount of the BSA removed will decrease. This is assuming that the sieving coefficient of the BSA is similar for all of the filtration runs which is possible as no change in the fouling was observed with diafiltration steps. This can be remedied by either increasing the volume concentration factor or reducing the dilution factor during the diafiltration steps. However, such action means reducing the number of diavolumes per cycle thus requiring more frequent manual interventions for dilutions. A continuous diafiltration strategy could be used to further minimise the diavolumes as well as the process time by maintaining a constant volume of retentate by continuous addition of buffer and simultaneous filtration. It should be noted that TG transmission in permeate was found to be ~10% in this experiment while it was approximate ~50% for previous experiments (Section 5.3.2). A possible reason was that the current experiment used lot 3 of the membrane but previous experiments used lot 5 of the PAA membranes. Mean pore size of the lot 3 membrane was significantly smaller (~30 nm) compared to that of lot 5 membranes (~50 nm). Further,

diafiltration experiments were conducted with higher protein feed loading of 35 L/m^2 compared to 20 L/m^2 in previous experiments.

Optimising the diafiltration process in a UF/DF operation is critical to minimise the amount of buffer and processing time. Since UF/DF operations are run in batch mode, a longer process can delay the processing of subsequent batches of the feed resulting in longer hold times. Longer hold time increase risk of contamination, reduce protein stability and occupy facility space. Increasing filtration area or adding more filtration system increases capital cost and the facility space.

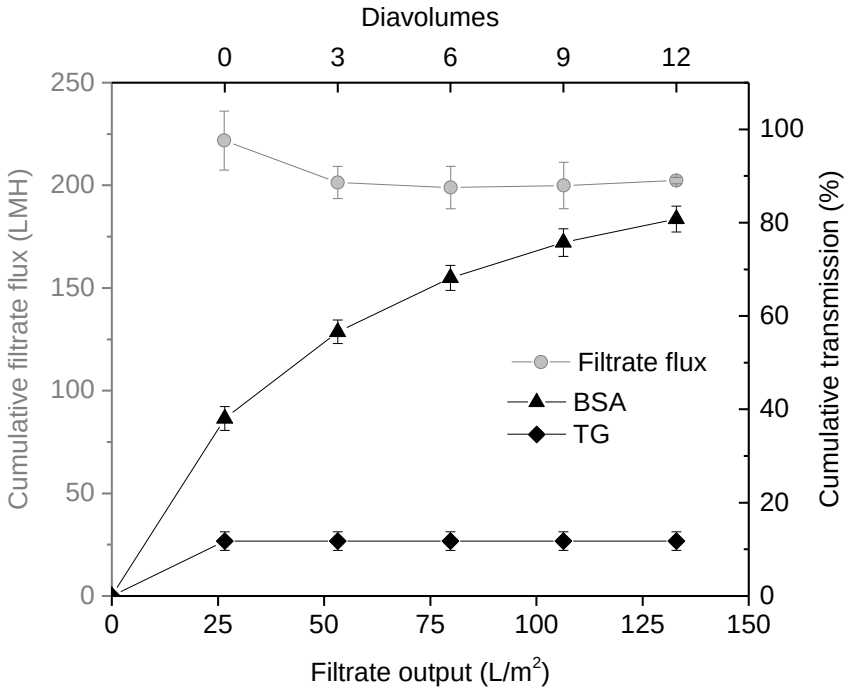

Figure 5-5 Effect of dia-volumes on the transmission of BSA and TG through 20 nm PAA membranes (Lot 3) when 5 cycles of discontinuous diafiltration (1 cycle = 3 diavolumes) were carried out on initially 4 fold concentrated samples.

Error bars represent one standard deviation for triplicate runs. Cumulative transmission of BSA starts to level off after 2 DF cycles. TG loss is observed only for the initial concentration step (at DV=0). Cumulative filtrate flux (shown is grey) remains constant through diafiltration indicating no significant fouling in DF phase.

Purification factor for TG increased from 1.5 ± 0.1 without diafiltration to 3.0 ± 0.5 and 4.1 ± 0.6 after 2nd and 4th DF step respectively. Analysis of both permeate and retentate collected after 0, 2nd and 4th DF cycles show no change in TG recovery but significant differences for BSA recovery as shown in **Figure 5-6**. Effect of diafiltration is also observed in retentate with a reduction in the peak area of BSA as shown in **Figure 5-7**.

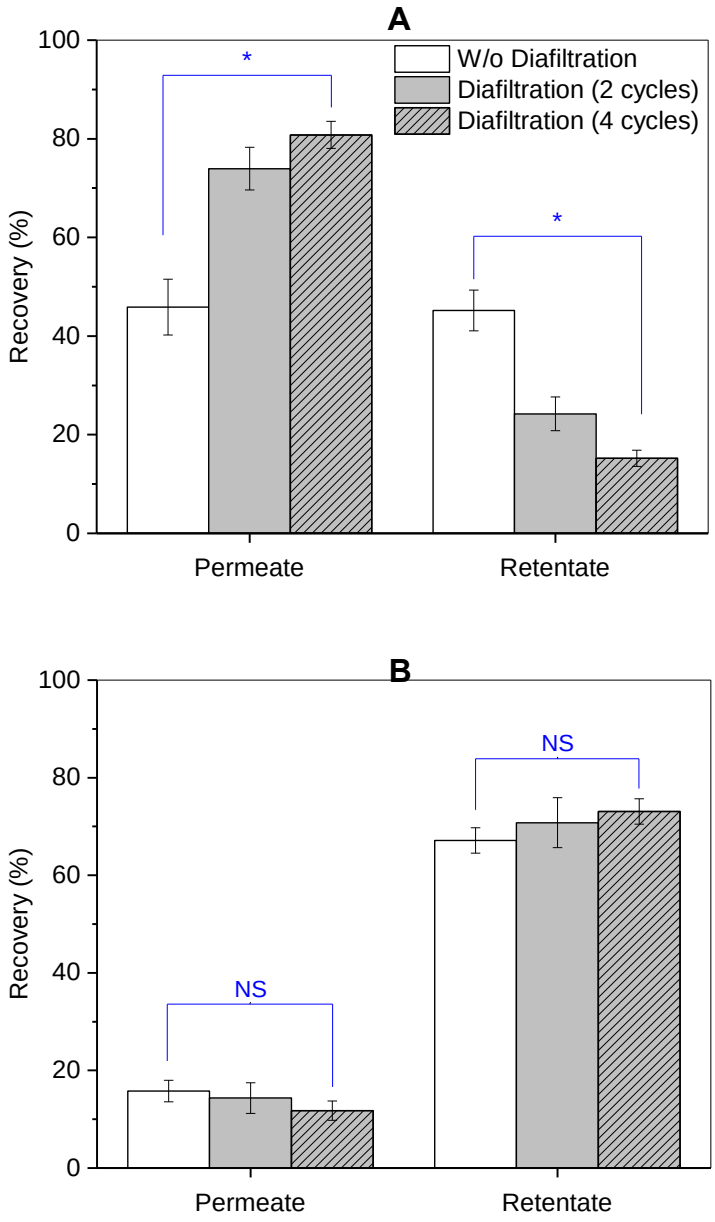

Figure 5-6 Effect of diafiltration (DF) and the number of DF cycles (0, 2 and 4) on fractionation of BSA (A) and TG (B) in permeate and final retentate obtained after processing through 20 nm PAA membranes.

*W/o diafiltration represents the control (i.e. 0 DF cycles/ initial concentration step only). Error bars represent one standard deviation for triplicate runs. Blue bars indicate statistical significance among data columns where NS represents no significant differences (ANOVA p> 0.05 and * represents significant differences (ANOVA p<0.01) among the data columns.*

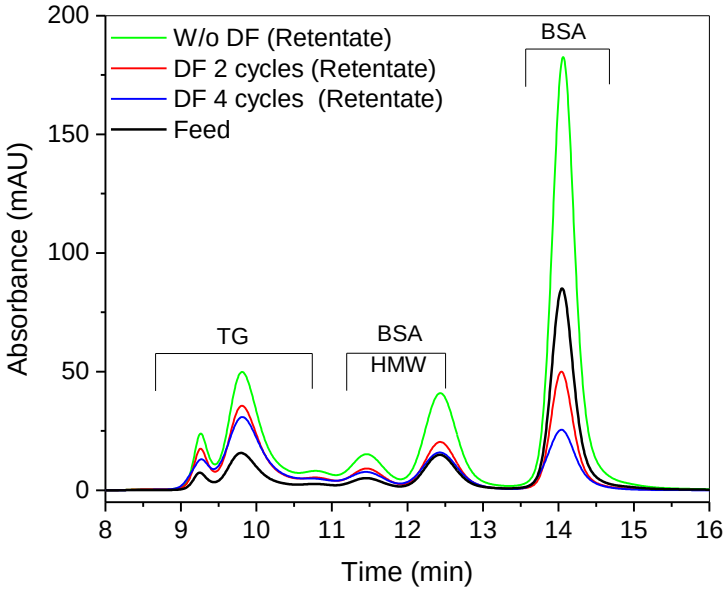

Figure 5-7 Overlay of HP-SEC chromatograms of retentate collected after 0, 2 and 4 cycles of diafiltration for fractionation of TG and BSA using PAA membranes showing effect of diafiltration on residual BSA.

Chromatograms were obtained by injecting 50µL of samples on to TSKgel3000SWXL (7.8 x 300 mm) column at flow rate of 0.6 mL/min and under isocratic elution with PBS. Retentate samples are 4 fold concentrated compared to the feed sample. Peaks were detected using 280 nm wavelength.

For future experiments, DF up to 2 cycles, with 3 DVs per cycle will be used since any effect of the treatment will likely be visible into 1st or 2nd DF cycle and from the results obtained for DV studies, 1 DF cycle can achieve a modest 60 % removal of BSA. Using more DF cycles does not result in a significant increase in BSA removal, however, increases the total processing time. Most of the experiments in the following sections used one diafiltration step of 3 diavolumes for fractionation experiments.

5.3.3.1.3 Effect of TG concentration and stirring speed on fractionation of BSA and TG

Three TG concentrations (0.2, 0.4 and 1.0 mg/mL) were tested in UF/DF mode with one diafiltration cycle (3 DVs) at 1500 rpm. Feed consisted of TG at selected concentration level along with 1mg/mL of BSA in PBS. Purification factor for TG decreased from 3 to 1.3 with an increase in TG concentration. This was due to increased fouling by a higher concentration of TG as evident by reduction in recovery %age of initial membrane permeability of the membranes from 48 % at 0.2 mg/mL TG to 36 % at 1.0 mg/mL TG concentration. Increased fouling resulted in reduced BSA transport through the membrane with only 20 % of total BSA measured in permeate at 1.0 mg/mL TG concentrations as opposed to 80% BSA removal observed at 0.2 mg/mL.

Effect of stirring was studied at three stirring levels (0, 500 and 1500 rpm) with a feed containing 0.2 mg/mL TG and 1.0 mg/mL of BSA filtered at 0.5 bar transmembrane pressure. Recovery %age of initial buffer flux of membranes improved with increasing stirring rate. Greater stirring speed leads to reduced concentration polarisation at the membrane surface thus lowering effective concentration at the membrane surface. Purification factor for TG increased from 2.8 to 5.7 with a reduction in stirring speed from 1500 to 0 rpm. Increased purification factor was due to differentially BSA removal (>92%) at 0 rpm but at the expense of TG loss with only 37 % yield in the retentate. Stirring helped retain both TG and BSA molecules. For low volume and high-value products such as viral vectors, operating conditions would be prioritised on the basis of the yield of the product in ultrafiltration. Thus the use of higher stirring rate is justified for any future experiments.

5.3.3.1.4 Effect of the PAA membrane lot variability on separation performance

In the previous chapter (Chapter 4), six lots of 20 nm PAA membranes were tested for hydraulic permeability and pore morphology using SEM. It was found that the hydraulic permeability of lots varied from 1500 to 2200 LMH/bar. This was correlated with the morphology of the active surface of the membranes when observed under SEM. SEM data revealed significant variations in the pore size distribution with only lot #1 and #3 having a mean pore size less than 30 nm (**Table 5-3**). Fractionation of BSA and TG was compared for different PAA lots to assess the impact of lot variability on the purification factor for TG.

Lot No.	Mean pore diameter (nm)	% BSA removal	% TG loss	Purification factor (for TG)
#1	27 ± 2	62 ± 8	14 ± 4	2.0 ± 0.5
#2	44 ± 5	74 ± 3	38 ± 3	2.5 ± 0.5
#3	32 ± 4	62 ± 8	16 ± 6	2.5 ± 0.7
#4	55 ± 7	72 ± 3	43 ± 8	2.4 ± 0.3

Table 5-3 Transmission of BSA (removal) and TG (loss) in permeate collected after UF/DF based fractionation of BSA and TG from four different lots of 20 nm PAA membranes and mean pore diameter of different lots of membrane were estimated by analysis of SEM images of the membrane surface.

Similar filtration conditions (TMP =0.5 bar, 1500 rpm, membrane loading of 35 L/m^2 with 1 diafiltration cycle of 3 dia-volumes). The composition of feed used for all of the filtrations was similar, i.e. 0.2 and 1.0 mg/mL of TG and BSA in PBS solution. (Average values ± one SD for triplicate runs).

Lot #1 and #3 have similar performance and lowest TG losses in permeate (less than 20 %). These lots had narrower pore size distribution as well as lower mean pore size (<32 nm), which

is close to the hydrodynamic size of TG protein (~21 nm). Fractional losses of the total thyroglobulin in permeate for different lots were found to be in linear correlation with the hydraulic permeability of the membrane lots (as shown in **Figure 5-8**). On the other hand, both lot#2 and #4 showed significantly high TG losses (40-50 %) and higher mean pore sizes (40-55 nm). The contribution of large structural defects in higher transmissions could not be factored in due to non-uniform distribution and low frequency of such large defects. Since transmission of both BSA and TG increased with increase in the hydraulic permeability, the purification factor for thyroglobulin did not change significantly and ranged from 2 to 3 for all four lots (See **Table 5-3**).

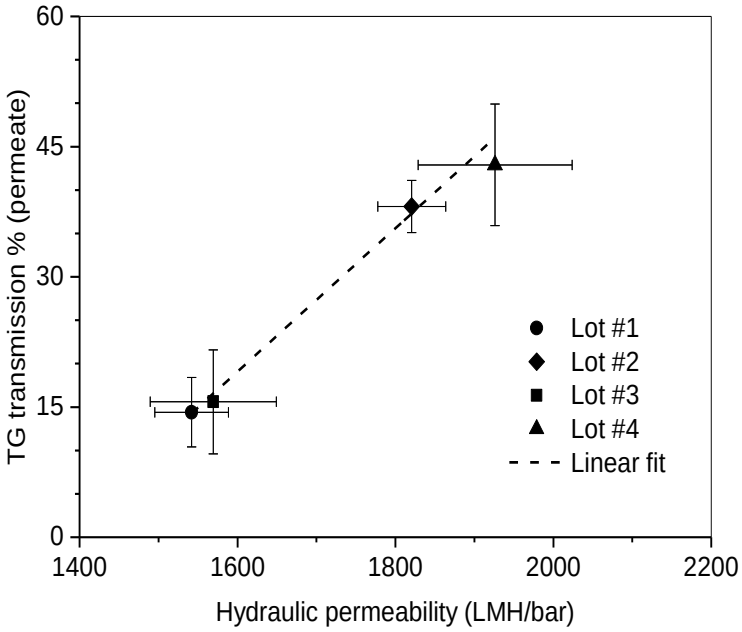

Figure 5-8 Effect of PAA membrane lot variations on TG loss through the membrane during TG/BSA fractionation: correlation of the hydraulic permeability and TG transmission (%) into the permeate for four different lots of the membrane.

Error bars represent one standard deviation for triplicate runs (3 membranes of each lot). A linear fit was attempted to describe the correlation between the TG transmission and the hydraulic permeability with a regression coefficient (R^2) of 0.99 for the fit.

Thus lot selection is crucial if the yield of retained product (TG in this case) is a priority rather than the purity of the final product. A difference of 300 LMH/bar in hydraulic permeability of PAA membranes could lead to 2-3 times higher losses of product.

5.3.3.2 Fractionation of BSA and BSA nanoparticles mixture

A mixture of 80 nm BSA nanoparticles and BSA (both 1 g/L) was tested for fractionation using 20 nm PAA membranes. Conditions similar to those used for TG/BSA fractionation were used. The high stirring rate was used to ensure low concentration polarisation hence low nanoparticle loss. Discontinuous mode diafiltration was carried out for 1 diafiltration cycle (3 diavolumes) and resulted in a purification factor of 3.5 ± 0.5 for BSA nanoparticles. **Figure 5-9** shows the effect of diafiltration on residual BSA in the retentates collected after a fractionation process with and without a diafiltration step. BSA levels in retentate were lower when diafiltration was used.

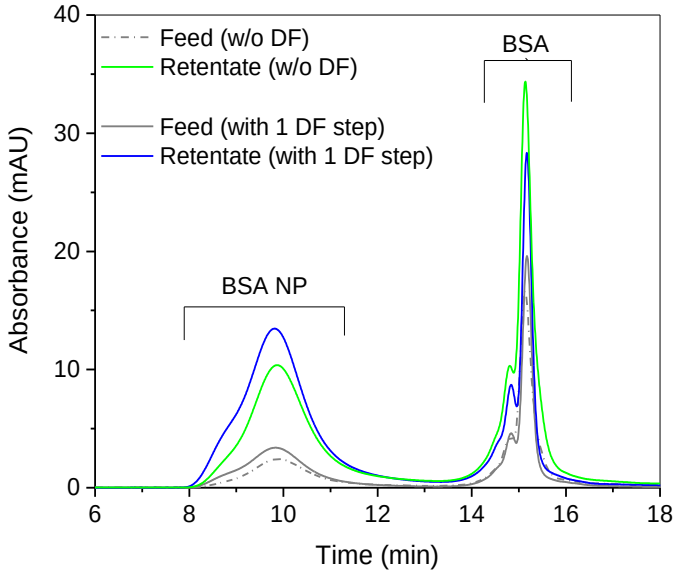

Figure 5-9 Overlay of HP-SEC chromatograms of retentate collected after 0 (w/o DF) and 1 step of diafiltration for fractionation of BSA nanoparticles and BSA using 20 nm rated PAA membranes showing residual BSA peaks. Retentate samples are ~4 fold concentrated compared to the feed samples.

Chromatograms were obtained by injecting 20µL of samples on to BIOSEC 5 (7.8 x 300 mm) column at flow rate of 0.8 mL/min and under isocratic elution with PBS. Peaks were detected using 280nm wavelength. Similar processing (TMP and membrane loading) were used for both runs. However, feed composition for both runs was slightly different.

Though the diafiltration step was able to remove more BSA from BSA NP and BSA mixture, the residual amount of BSA in the retentate is still high when compared to diafiltration runs for TG and BSA mixture as shown in **Figure 5-8**. One reason for low removal is that only one DF step was used for BSA NP and BSA fractionation compared to 2 or 4 used. In Section 5.3.2.2, it was observed that the concentration polarisation due to BSA NP results in the lower transmission of BSA than the transmission observed with fouling by TG. Hence, more DF steps are required for fractionation of BSA NP and BSA. However, a single DF step was used for most of the experiments in this thesis because of time constraints for performing experiments in triplicate.

5.3.4 Approaches to improve separation performance of the 20 nm rated PAA membranes

5.3.4.1 Influence of electrostatic interactions on the separation performance of fractionation using PAA membranes

Membrane performance is a function of solute interactions with the membrane material. Both steric and ionic interactions can affect the sieving of solutes through membrane pores. Variations in pH and salt concentration of protein solution were investigated for their effects on flux and separation performance of the PAA membranes for fractionation of BSA and larger solutes, TG and BSA nanoparticles. Initial screening experiments (for salt concentrations and solution pH) were performed with TG/BSA fractionation, and the selected conditions were later verified for BSANP/BSA fractionation.

5.3.4.1.1 Effect of salt concentration in protein solution on the fractionation of BSA and TG through PAA membranes

Fluxes for the solutions of protein mixture were not significantly affected by high salt concentration. However, cumulative filtrate flux was significantly higher for solutions without any NaCl than with NaCl added despite having the same protein concentrations (See **Figure 5-10**). Recovery of the initial membrane permeability was also similar (~50 %) for all salt concentrations. Buffer composition itself did not have any effect on membrane permeability as the buffer fluxes for different buffers (varying salt concentrations) were similar. Thus, any difference in the fluxes for protein solutions could be attributed to the solute-salt interaction and not to any change in hydraulic permeability of the PAA membrane due to the salt solution.

Removal of BSA in permeate was considerably higher (~80%) for the feed solution without any NaCl as compared to those solutions with NaCl added. However, varying the concentration of NaCl from 50 to 300 mM in the protein solution did not change the removal of BSA in permeate (~60%) or amount of BSA remaining in the final retentate (See **Figure 5-11**). Increasing salt concentration resulted in higher TG transmission into the permeates thus higher loss of TG. Loss of TG in the permeate increased from ~10% to 20% as salt concentration is increased from 0 to 300 mM. Opposite trend was reflected when TG recovery was estimated in final retentate solutions. In terms of purification factor of TG in the final retentate, at 0mM NaCl concentration the purification factor was 4.8 ± 0.7 compared to 2.2 ± 0.3 for all of the other solution. Recovery was estimated by ‘mass’ balancing of the peak areas of TG and BSA in various samples and taking into account the respective volumes.

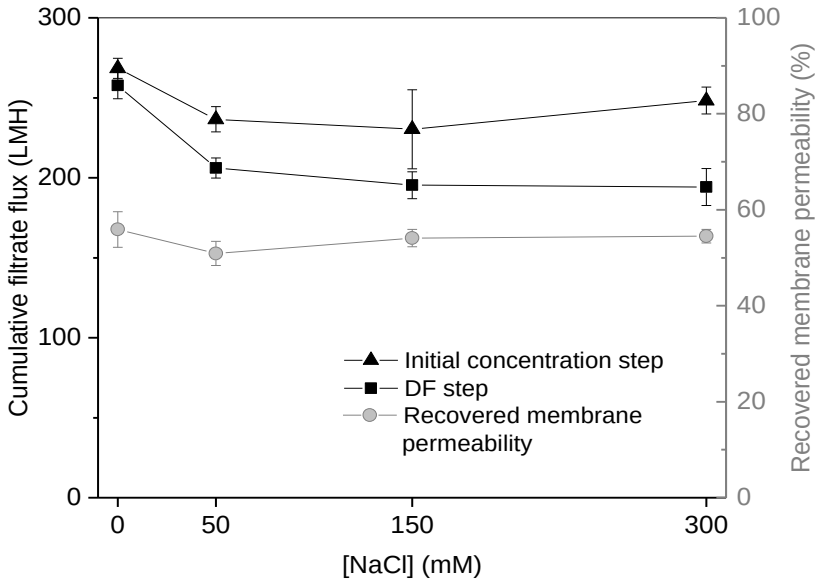

Figure 5-10 Cumulative flux for filtrates collected after initial concentration and DF step and recovered membrane permeability (%) after filtration of solutions of BSA and TG mixture with different salt concentrations through 20 nm PAA membranes.

Protein solutions were filtered at a TMP of 0.5 bar and 1500 rpm stirring rate in a stirred cell. Lot #3 of the PAA membranes were used. All solutions were prepared in phosphate buffer, pH 7.4. Error bars indicate one standard deviation for triplicate runs.

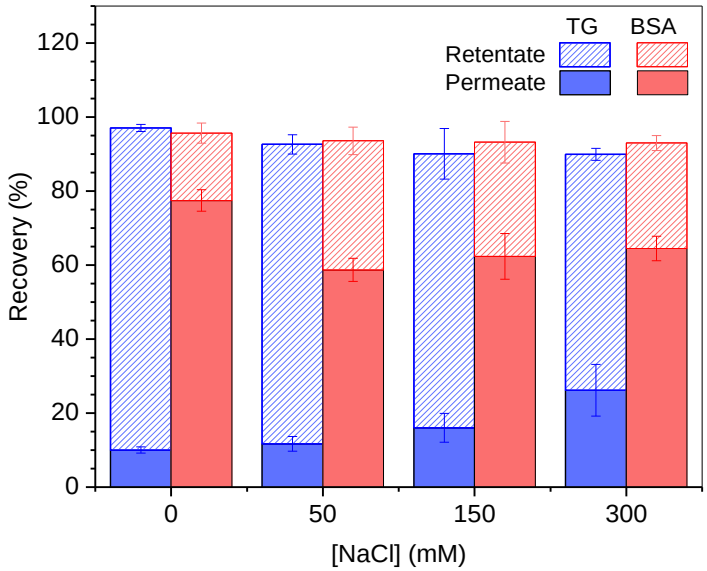

Figure 5-11 Recovery of BSA and TG solutes in permeates and retentate collected after UF/DF using 20 nm PAA membranes with different NaCl concentration in the protein solution and diafiltration buffer solutions.

TG transmission (permeate) increased with increasing salt concentration. BSA removal was significantly high (~80%) for 0mM NaCl concentration compared to 60% removal for other higher salt concentrations. PF for TG was highest (4.8) without salt, compared to 2.2 for solutions with salt. Error bars indicate one standard deviation for triplicate runs.

It was suspected that high salt concentration could lead to aggregation of the protein solutes, especially TG. However, such a process would reduce the flux and transmission of the protein at higher salt concentrations. Further, no such aggregation was observed in HP-SEC chromatograms and particle size analysis using DLS. For HP-SEC analysis, to avoid non-specific protein binding to the resin, samples with lower salt concentrations were appropriately diluted to adjust a final salt concentration of 150mM before injection. This ensured that all peak analysis of all of the samples was not affected by the different sample conditions. Dilutions were appropriately accounted for when 'mass' balancing for each of the protein solutes.

Cheang and Zydney (2003), have reported similar findings for protein fractionation using 100 kDa polymeric membranes and attributed it to electrostatic interactions. At low concentrations of salt, the thickness of the electric double layer (also referred to as Debye's length) around charged solutes and surfaces increases. The increased thickness of the electric double layer increases the effective sizes of solutes and reduces the effective pore diameter assuming anodic alumina membrane are charged. Increase in the salt concentration leads to screening of the surface charge and reduces the thickness of the electric double layer as illustrated in **Figure 5-12.** Solute permeability will be affected for solutes such as TG with dimensions (~20 nm) near the pore size (20-40 nm).

Low salt concentration results in loss of charge screening or masking by salt thus increase in electrostatic forces between solute molecules and between solutes and membrane surface. These electrostatic forces can affect the sieving of solutes depending upon the nature (repulsive or attractive) and the magnitude of the electrostatic forces. For both TG and BSA, the isoelectric point is similar (~4.8). At buffer pH 7.4, both proteins would be highly negatively charged. In the absence of salt ions, this charge is not screened thus resulting in high repulsion forces between TG and BSA as well as among the molecules of same proteins. Increased effective size of TG and similar pore size results in the electrostatic exclusion of the TG from the pores as the electrical double layer of protein and pore surface would tend to overlap. Assuming that membrane is also negatively charged at this pH, very high potential energy would be required for TG molecules to overcome the energy barrier to disrupt the repulsion in the overlapping the electric double layers, which would be thermodynamically unfavourable. BSA molecule, on the other hand, is much smaller than the pore diameter and can escape the repulsive forces between pore wall and solute surface as the electrostatic forces are inversely proportional to the distance between the charges. A weak membrane surface charge or weak BSA charge can also explain the increased transmission of BSA.

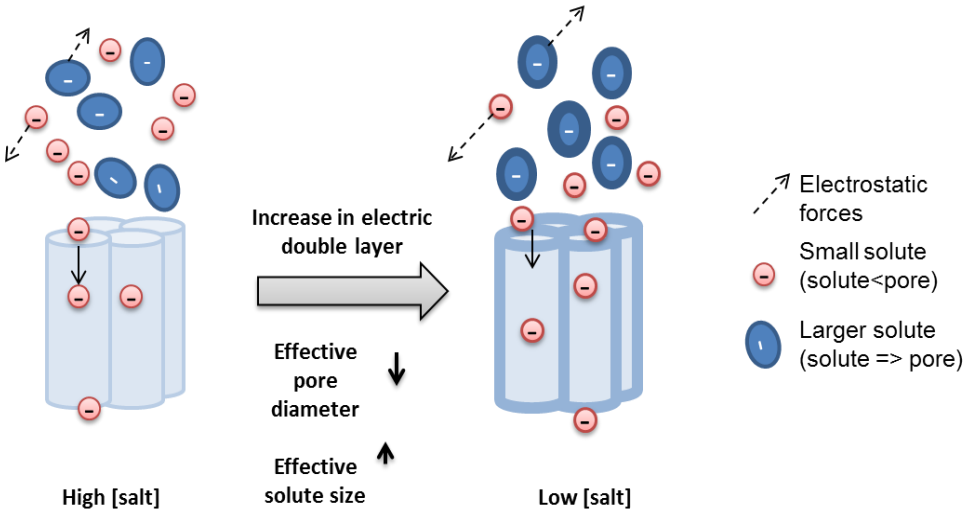

Figure 5-12 Illustration of the effect of salt concentration on solute-membrane interactions and solute-solute interactions showing the impact of the increased electric double layer (shown as thicker boundaries on solute and pores) at very low salt concentrations resulting in reduced effective pore radius and increased effective solute radius and increased repulsion forces among solutes. In case of BSA, TG and BSA nanoparticles all of the solutes will have similar charge (though different magnitudes) at any given pH due to similar isoelectric points.

Another factor could be loose polarisation layer of the TG molecules above membrane surface (after initial fouling) due to large surface charge on TG resulting in TG-TG repulsions but increased permeability as evident by high filtrate flux. Zeta potential measurements for BSA and TG show larger surface charge for TG molecules for various pH values on either side of pI points (see **Appendix H**). Repulsion from TG rich loosely polarised region at the membrane surface also contributes to increased BSA transmission through pores. An accurate modelling of these effects, however, would require measurement of surface charge of the membrane pore surface.

5.3.4.1.2 Effect of pH of protein solution on the fractionation of BSA and TG

Low salt concentration solutions were selected for studying the effect of solution pH on separations as screening by salt will mask the effect of surface charges of pore walls and solutes on separation performances as observed in the previous section (5.3.4.1.1). Effect of solution pH was more pronounced on process flux than the effect of salt concentration. Flux decline, as shown in **Figure 5-13**, was most prominent for the feed solution with pH 5.2. Process fluxes were similar for pH 6.5, 7.4 and 8.4 but higher than the fluxes at pH 3.7 and 5.2. Lowest process flux was observed with pH 5.2 which indicates interactions between solute or solute and membrane.

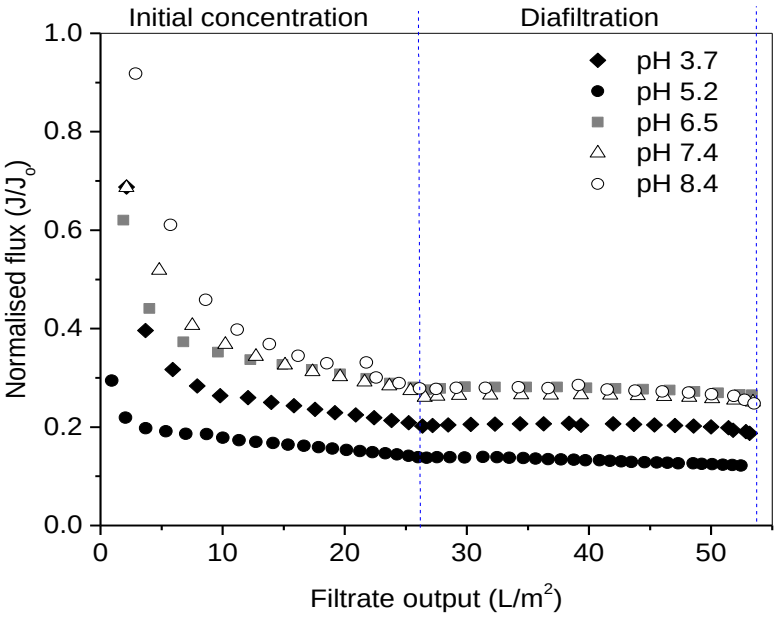

Figure 5-13 Effect of pH of feed and buffer solution on flux decline during initial concentration and diafiltration step during fractionation of TG and BSA using 20 nm PAA membrane.

Flux is normalised with the initial buffer (1115 ± 34 LMH at 0.5 bar) flux. The solution with pH 5.2 shows the fastest flux decline. Filtrate output is collected filtrate volume normalised with filter area at TMP of 0.5 bar and stirring rate of 1500 rpm in a stirred cell. Lot#3 of the PAA membrane was used.

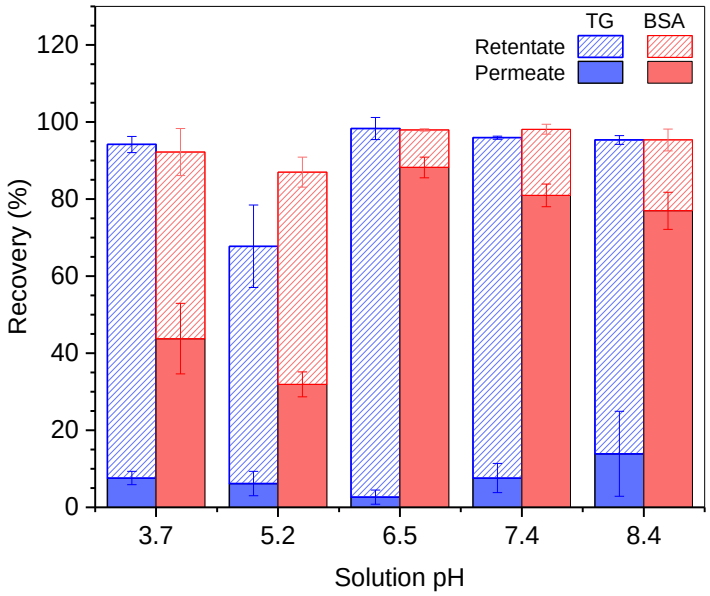

Figure 5-14 Effect of pH on the recovery of TG and BSA in the retentate and permeate fractions displayed in a stacked chart showing highest separation performance of PAA membrane at pH 6.5 and loss of proteins at pH 5.2.

Error bars indicate one standard deviation for triplicate runs.

Significant differences were observed in protein transmission as well with higher % of total BSA in permeate for pH levels equal and above 6.5 (see **Figure 5-14**). TG transmission was found the minimum (~2.4%) at pH 6.5 and increased significantly at pH levels below and above the pH of 6.5. This leads to maximum purification factor of 10 being observed at pH 6.5. Effect of pH on separation is visible from the chromatograms of retentates collected at different pH (See **Appendix I-1**). Net recovery (permeate and retentate) of both BSA and TG was found to be minimum (<70%) for pH 5.2 indicating loss of protein. This was unexpected as the PAA membranes are marketed as negligible protein binding material. Due to similar isoelectric points, electrostatic interaction between the two solutes (TG and BSA) is always going to be repulsive. An electrostatic attraction between larger solute and membranes can result in higher fouling by ionic adsorption, especially with the larger solute. Adsorption will also reduce the total protein recovery after UF/DF experiment. Abnormally high BSA transmission at pH 6.5 and very low TG transmission can be possible if the membrane does not have any net surface charge at that pH resulting in increased permeability for smaller BSA molecules due to lack of repulsive forces between BSA and pore walls but significant steric hindrance to the larger TG molecules which are charged and have thick electric double layer.

Based on the trend observed in transmission and fluxes at various pH values it could be speculated that the isoelectric point (pI) of the 20 nm rated PAA membranes is approximately 6.5 which is also what has been reported by Pedimonte *et al.* (2014b) for custom made PAA membranes with a similar rating (15nm). This was however contradictory to the isoelectric point of 3-4 observed by Bowen and Hughes, (1991) for 100nm rated commercial PAA membrane. Impact of the fabrication conditions has been shown to influence the pore size as well as the surface charge on anodic alumina membranes strongly (Pedimonte *et al.*, 2014b). Bowen and Hughes, (1991) also reported different isoelectric points for 100 and 200 nm rated PAA membranes. Incorporation of anions using acidic organic electrolytes such as oxalic acid, the phosphoric acid used for fabrication of anodic alumina membranes have been shown to shift membrane pI (Chen *et al.*, 2005). Membrane pI was also found to be lower than that expected for amorphous alumina (pI 8-9) and varied with the pore size of the anodic membranes. Membrane pI has not been reported for 20 nm rated commercial PAA membrane used in the present experiment. Unlike TG and BSA, membrane pI could not be estimated form DLS based electrophoretic measurements due to a different format of the equipment required for measurements for solid samples.

Assuming the isoelectric point of the membrane is 6.5, the low recovery of both proteins at pH 5.2 could be attributed to the adsorption loss of proteins on membrane surface as proteins and membrane will have opposite charges at pH 5.2. To verify this, batch adsorption studies carried

out at two pH values (8.4 and 5.2) confirming the presence of ionic interactions between membrane and solutes. Loss of free protein was observed in the solution when membranes were incubated with a protein solution with pH 5.2 at room temperature (See **Figure 5-15**). Proteins (BSA and TG) are negatively charged at pH 5.2 so the loss of protein is due to the binding of protein molecules to the positively-charged membrane at pH 5.2. Protein solution at pH 8.4, where both solutes and membrane will be negatively charged did not result in loss of the protein from solution. To ensure that loss of protein is not due to protein binding to the container (PP tubes), control with the same volume of the protein solution in the container was also incubated. Control solutions did not show protein loss at any of the pHs tested.

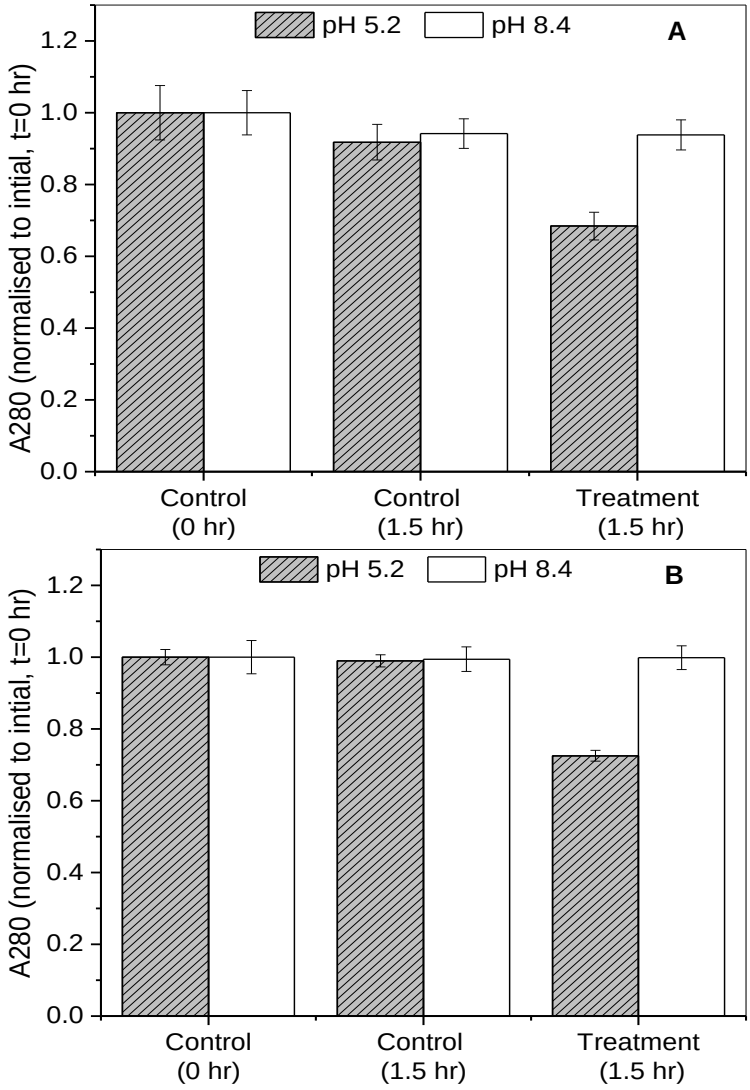

Figure 5-15 Batch adsorption of TG (A) and BSA (B) solutions at different solution pH (5.2 and 8.4) showing loss of protein in solution incubated with porous anodic alumina material in PP tubes (Treatment) compared to protein solution incubated in PP tubes without alumina material (Control) after incubating for 1.5 hours at room temperature.

Error bars represent one standard deviation for trpilicate measurements of absorbance of the sample.

A (at pH 7.4)	
NaCl (mM)	**PF (TG)**
0	4.8 ± 0.7
50	2.3 ± 0.3
150	2.4 ± 0.5
300	2.2 ± 0.2

B (at 0 mM NaCl)	
pH	**PF (TG)**
3.7	1.8 ± 0.4
5.2	1.1 ± 0.2
6.5	9.9 ± 0.4
7.4	5.2 ± 0.2
8.4	4.4 ± 0.3

Table 5-4 Effect of salt concentrations (A) and solution pH (B) on purification factors of TG during fractionation of BSA and TG mixture (in 10mM phosphate buffers) using 20 nm PAA membrane. Data are presented as average value ± one standard deviation for triplicate runs.

5.3.4.1.3 Effect of electrostatic interactions on fractionation of BSA and BSA nanoparticles

Based on trends observed for electrostatic effects on BSA and TG fractionation and since the isoelectric point of BSA nanoparticles is similar to that of BSA and TG, only selected buffer conditions were tried for BSA nanoparticles. Trends observed in TG/BSA fractionation experiments indicate that operating at membrane pI of 6.5 results in best fractionation performance compared to other pH levels. Thus, comparing the performance of separation of BSANP and BSA at pH 6.5 with pH 7.4 would be sensible. To investigate if the pH effect is observed at high salt concentrations, separation performance was compared for solutions in 10 mM phosphate buffer at pH 7.4 and pH 6.5 both with 150 mM NaCl. Finally, the effect of salt concentration was studied at pH 6.5 with two salt levels, 0 and 150 mM. Flux through the membrane was found to be higher for protein solution without any NaCl when compared to the same for with 150 mM NaCl. This effect was observed throughout the filtration including diafiltration steps.

Membranes used for both filtration experiments were from the same lot but showed the difference in initial buffer fluxes, varying by ~ 70 LMH (~ 5%). It is possible that this difference in the membrane permeability resulted in differences in flux observed with the protein solution. As seen in **Figure 5-16**, normalised flux decline curves for both protein solutions with 0 and 150 mM NaCl are identical in shape, but membranes used for 0mM NaCl operated at higher normalised fluxes from the initial period of the filtration. It is also possible that the differences in membrane permeability are not significant for the flux decline but solute charge and repulsive forces played a role in variations in fluxes. High repulsion between protein nanoparticles at 0mM NaCl could result in a loose concentration polarisation layer resulting in lower resistance to the convective flow of the liquid.

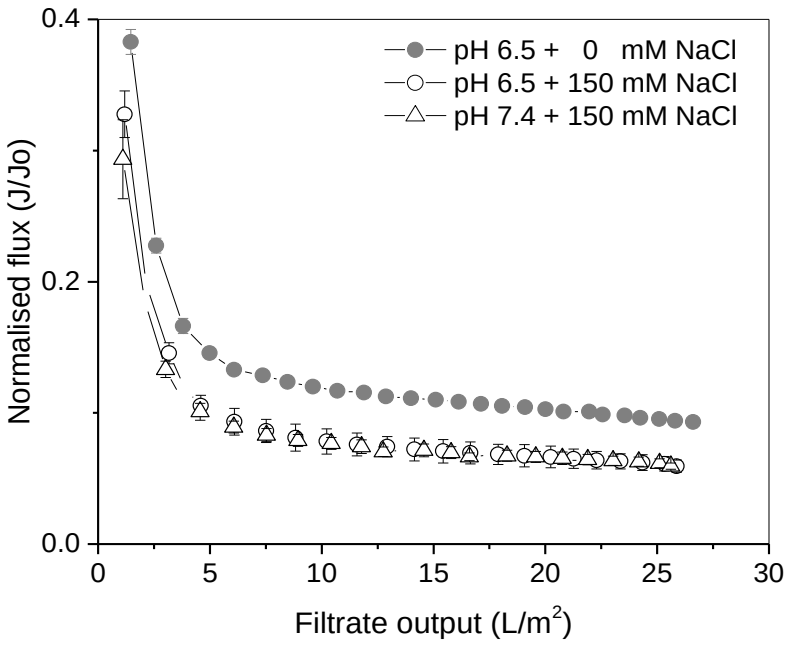

Figure 5-16 Effect of solution pH and salt concentration on flux decline during the initial concentration step of UF/DF based fractionation of BSA NP and BSA through 20 nm PAA membrane.

Process flux normalised with initial buffer flux (Jo) through membranes and all of the protein solutions were prepared using 10mM phosphate buffer. Same membrane lot and the same operating conditions (TMP and stirring) and feed were used for all solutions. Error bars indicate one standard deviation for triplicate runs.

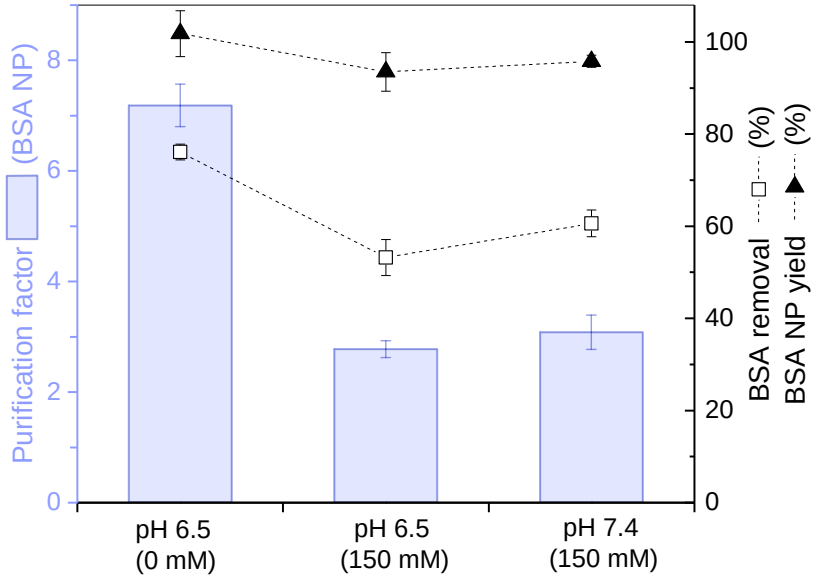

Figure 5-17 Effect of solution pH and salt concentration on purification factor and yield of the BSA nanoparticles and BSA removal in the fractionation of BSA NP and BSA mixture using 20 nm PAA membranes.

Purification factor for BSA NP decreased with the addition of salt even at membrane pI (pH 6.5) indicating the role of solute-solute interactions. Error bars represent one standard deviation of triplicate runs.

Improvement in purification factor (PF) was observed for separation of BSA nanoparticle from BSA at pH 6.5 and 0 mM salt concentration. PF of 7.2 was found for feed without NaCl as compared to 2.5 seen for feed with 150 mM NaCl as shown in **Figure 5-17**. The improvement was driven by an increase in BSA transmission and a decrease in transmission of BSA nanoparticles (for chromatogram overlays see **Appendix I-2**). This resulted in improved purity (60%) of BSA nanoparticles in the final retentate solution at 0mM NaCl compared to 40% purity observed at 150 mM NaCl. The purity of BSA nanoparticles in the feed was 21.5%. The decrease in the effective diameter of the pore at low salt concentrations would significantly reduce transmission of large protein nanoparticles. However, the reduction is not significant enough for smaller solutes like BSA. The absence of any significant steric hindrance and lack of electrostatic interactions results in high BSA transmission. However, low BSA transmission for a 150mM solution cannot be explained. However, it should also be noted that electrostatic repulsion would be higher among protein solutes at 0 mM NaCl as compared to repulsion forces at higher salt concentrations where solute charges will be masked. Since BSA nanoparticles cannot enter pore due to steric hindrance and charge repulsion of BSA and BSA nanoparticles would likely result in BSA transmission through neutral pores.

5.3.4.2 Effect of permeate backpressure on separation performance of 20 nm PAA membranes for BSA/TG fractionation

Applying pressure on the permeate line resulted in high BSA removal without loss of TG when compared to similar filtration runs but without any permeate backpressure. Permeate tubing was pinched with a manual pinch valve to apply a back pressure on permeate as shown in **Figure 5-18**. The purification factor for TG increased by 85%, from 1.4 for control to 2.6 with the application of backpressure while applying the same feed pressure (**Table 5-5**).

Figure 5-18 Manual pinch valve on the permeate line of stirred cell setup used for applying back pressure on the permeate line

Treatment	Filtrate flux	BSA removal %	Retained TG %	Purification Factor (TG)
Control	230 ± 15	39 ± 2	74 ± 9	1.4 ± 0.3
Backpressure (BP)	156 ± 35	60 ± 3	74 ± 3	2.6 ± 0.3

Table 5-5 Filtrate flux and separation performance (% of BSA removed in permeate, % of TG retained and purification factor for TG) upon application of permeate backpressure on permeate in comparison to control (without backpressure) at similar operating conditions (applied feed pressure =0.5 bar, 1500 rpm, and same feed).

Only initial concentration step was carried out for both control and backpressure treatment without any diafiltration step. Data represented as average value ± one standard deviation for triplicate runs.

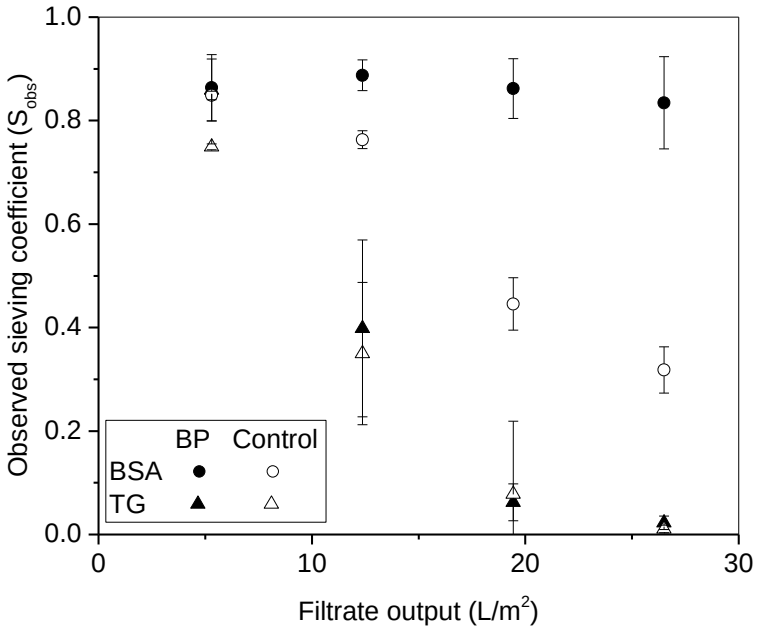

Figure 5-19 Enhancement in the sieving of BSA through 20 nm PAA membranes upon application of backpressure on permeate line during fractionation of TG and BSA.

Backpressure runs (BP) show a sustained sieving coefficient (~0.9) for BSA throughout the filtration run (up to 26 L/m^2) as compared to reducing sieving coefficient in control. Sieving of TG remained unaffected by backpressure. Error bars represent one standard deviation for triplicate runs.

HP-SEC analysis of fractions collected throughout filtration run shows high and sustained transmission of BSA when permeate backpressure was applied. **Figure 5-19**, above, shows enhancement of the observed sieving coefficient for BSA (concentration ratio of permeate and

feed) when backpressure was applied in contrast to reducing trend in control runs. TG sieving was not affected by the application of backpressure. A possible explanation for enhanced BSA transmission could be a change in the nature of fouling layer of TG due to the reduction of the effective transmembrane pressure (as the filtrate flux was also reduced) upon to pressurisation of permeate line in the vicinity of the membrane. It is also possible that permeate backpressure creates a transient backflow through the pores resulting in increased turbulence at pore inlet which increases BSA permeability. This hypothesis is not tested in the present study but could be explored further for a better understanding of enhancement observed with backpressure experiment. Such an approach has been described for hollow-fibre TFF based purification of Adenovirus (Weggeman, 2013), where low TMP control was not possible without permeate backpressure due to the requirement of high minimum feed pressure. Authors reported high recovery of the virus particles using permeate backpressure approach and suggested it as an alternative to chromatography.

5.3.4.3 Effect of transmembrane pressure on fractionation of BSA nanoparticles and BSA

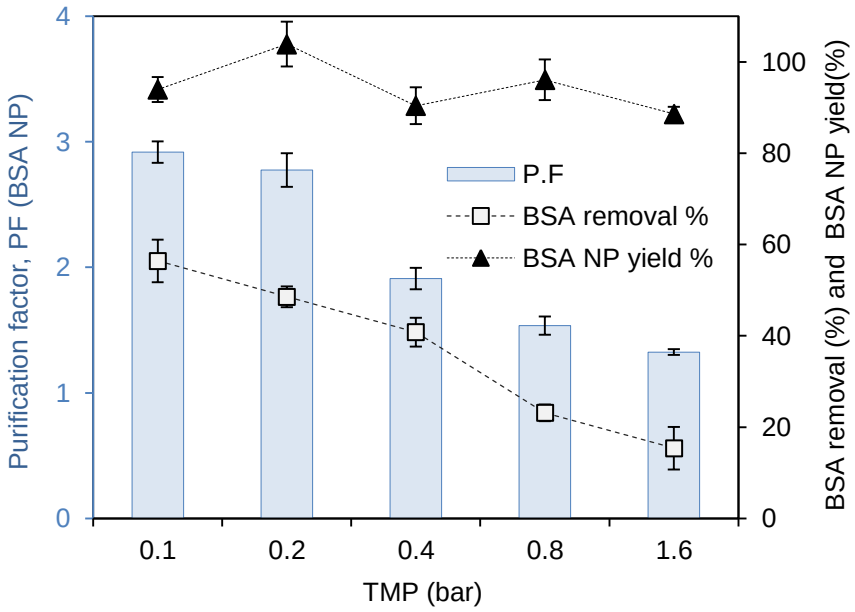

Figure 5-20 Effect of the transmembrane pressure (TMP) on fractionation of BSA nanoparticles and BSA during the initial concentration step using PAA membranes.

Except for TMP, the same operating conditions were used for all of the filtration runs including the membrane lots. Diafiltration step was not used in this experiment. Error bars represent one standard deviation for triplicate runs.

As discussed in the last section, the permeate backpressure effect could be due to the reduced effective transmembrane pressure. Concentration polarisation is strongly dependent upon applied transmembrane pressure and more prevalent for highly retained large solutes such as BSA nanoparticles. It was found that the purification factor of BSA nanoparticles can be

improved by reducing the transmembrane pressure applied as shown in **Figure 5-20.** Enhanced purification factors were primarily because of increased removal of BSA with decreasing TMP.

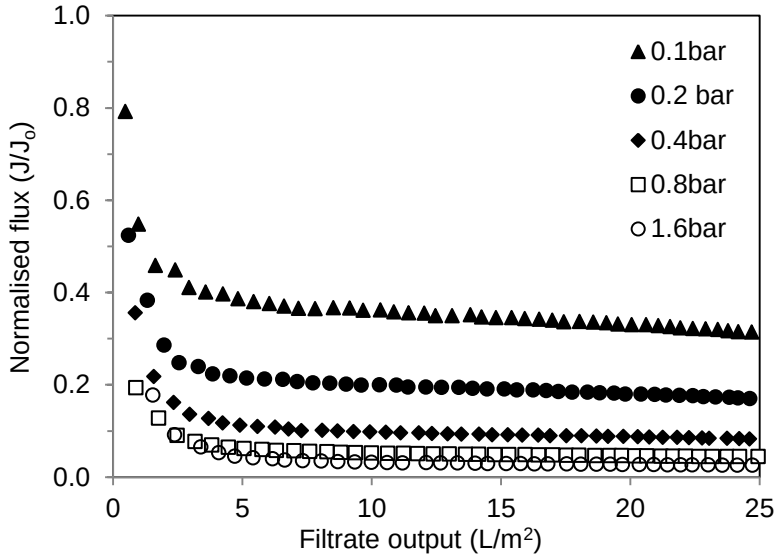

Figure 5-21 Effect of transmembrane pressure on flux decline during fractionation of BSA nanoparticles and BSA mixture using 20 nm PAA membranes.

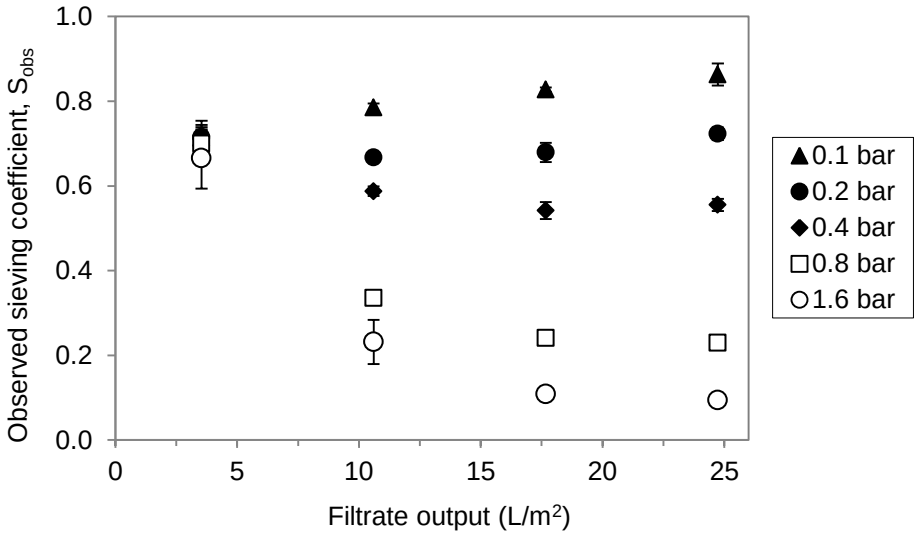

Figure 5-22 Effect of transmembrane pressure on sieving of BSA monomer through 20 nm PAA membranes during fractionation of BSA nanoparticles and BSA. BSA nanoparticles sieving was below 0.1 for all TMPs.

Error bars represent one standard deviation for triplicate runs.

The yield of BSA nanoparticles or retention of BSA nanoparticles did not change significantly. Likely reason is that the nature of the concentration polarisation layers such as layer thickness or density changes with increasing TMP which alters the permeability of the polarised layer for BSA molecules. This is also evident from the flux decline curves for different pressures. At low

pressures (<0.4 bar) membranes operated at a very high value of normalised flux as shown in **Figure 5-21**. The layer is more permeable at lower TMPs resulting in the high removal of BSA. Sieving coefficient for BSA was high for lower TMPs (0.4 bar or lower) as shown in

Figure 5-22. Lower TMPs also showed uniform sieving throughout the course of filtration (up to 25 L/m2) when fractions of filtrate were analysed for BSA. BSA sieving dropped significantly during filtration when higher TMPs (0.8 and 1.6 bar) were used. This shows more permeable polarisation layer at lower TMPs. Recovery %age of initial membrane permeability also decreased to 88% at highest TMP indicating some irreversible solute-membrane interaction with high concentration polarisation. Actual process fluxes only increased marginally from 66 to 76 LMH with an increase in TMP.

5.3.4.4 Membrane performance over extended UF/DF process for complete fractionation of BSA nanoparticles and BSA: comparison of 20 nm PAA and 300 and 500 kDa PES membranes

A robust membrane performance in UF/DF based fractionation should result in maximum separation with minimum processing time, minimum buffer consumption and minimum irreversible fouling of the membranes. A UF/DF process at pilot and manufacturing scale would normally be operated in a continuous diafiltration mode to achieve robust performance. For most of the experiments conducted so far in the thesis, the discontinuous mode has been used with 1 or 2 diafiltration cycles with each cycle consisting of 3 diavolumes. Limitation of the small volume capacity of the stirred cell, handling and risk of spillage and lack of automation for stirred cell filtration makes it challenging to use it in continuous mode. However, using smaller DVs per diafiltration cycle in discontinuous mode will simulate a separation performance closer to that of the continuous mode by increasing the convective transport of the impurities per cycle.

Hence, a UF/DF process with 12 discontinuous DF cycles each of 1 diavolume (i.e. manual 2-fold dilution of the retentate with buffer followed by 2-fold concentration step) was carried out for fractionation of feed mixture of BSA nanoparticles and BSA. The goal was to observe differences in cumulative flux, protein transmission through DF steps to maximise fractionation and see if membrane fouling increases with DF steps. As functionally the operation is still discontinuous, requiring the repeated manual addition of the diafiltration buffer, pressurisation and depressurisation of the setup, only single fractionation runs were studied for each membrane. Equal protein loading per membrane area (~28 L/m^2), filtrate output (~20 L/m^2), transmembrane pressure (0.6 bar) and stirring rate (1500 rpm) were used for all of the membranes. **Figure 5-23** A shows the diafiltration cycle with 1 diavolume (retentate volume) across the time for 12 diavolumes UF/DF process. The time required for manual dilution was not

accounted in the process time for data analysis. No further flux decline was observed for any of the membranes during the DF step up to 12 dia-volumes as seen in **Figure 5-23 B**.

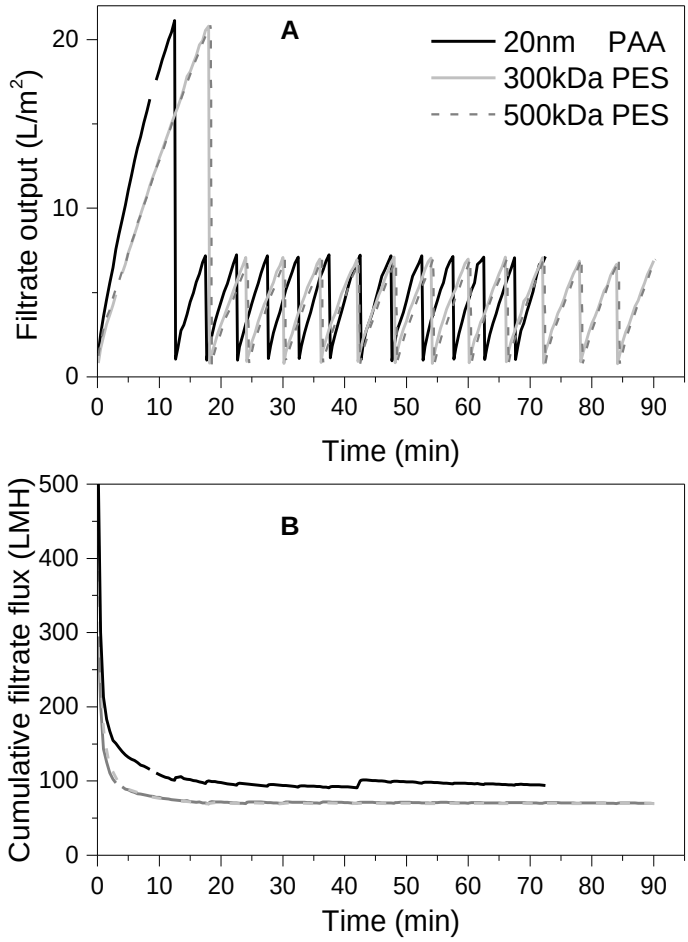

Figure 5-23 Extended UF/DF process (with 12 DF steps each of 1 diavolume) for fractionation of a mixture of BSA nanoparticles and BSA using 20 nm PAA, 300 and 500 kDa PES membranes showing filtrate output for the discontinuous DF mode (A) and flux decline (B) during UF/DF process for different membranes.

Time taken for 12 dia-volumes filtration is significantly shorter for PAA membranes due to higher average flux compared to PES membranes.

Membrane	Retained NP (%)	Residual BSA (%)	PF (BSA NP)
20 nm PAA	86.0	0.04	2170
300 kDa PES	99.6	0.13	780
500 kDa PES	82.2	0.08	990

Table 5-6 Purification factor, BSA nanoparticle retention and residual BSA after BSANP/BSA fractionation using PAA and PES membranes in extended UF/DF process (12 DF cycles)

Analysis of the final retentates collected after 12 diavolumes of UF/DF process using HP-SEC shows very low residual BSA for all of the membranes with a minimum for PAA membrane as shown in **Table 5-6**. Retention of the protein nanoparticles was least for 500 kDa PES membrane and maximum for 300 kDa PES membrane. The 300 kDa PES membrane was, however, more retentive to BSA as well (for chromatogram overlays see **Appendix J**). The purification factor for BSA nanoparticles was maximum for PAA membranes (2170 ± 220), almost three times of that for 300 kDa membrane. Based on the final purity of retentate, PAA membranes were suitable for achieving high purity BSA nanoparticles preparations at a modest yield of 86% in the retentate. This shows that PAA membranes may be suitable in applications where the focus is mainly on high purity, and faster processing and yield can be traded off to some extent. PAA membrane also maintained higher process flux than both PES membranes throughout the process which resulted in the shortest processing times of ~70 minutes in comparison to 90 minutes using PES membranes.

Previously PAA membranes have been shown to exhibit very low irreversible fouling compared to the PES membranes. However, those experiments were done for limited processing times. Thus recovery of the membrane permeability after extended UF/DF process was measured as a percentage of initial buffer flux recovered after a buffer rinse of membrane surface and module. PAA membranes did not show any loss of membrane permeability with 96% of the initial permeability recovered after rinsing of the membrane surface, thus requiring no further cleaning procedure as shown in **Figure 5-24**. PES membranes, on the other hand, showed poor recovery of the membrane permeability with a buffer rinse. Only 33 and 14% of the initial membrane permeability could be recovered for 300 and 500 kDa PES membranes respectively. For similar membrane loadings, the recovery of the membrane permeability value was 50% and 97% for 300 kDa PES and 20 nm PAA membrane respectively when no diafiltration process was used (refer to **Table 5-1** in Section 5.3.2.1). Thus extended UF/DF processes have more impact on the fouling of the polymeric membrane. Thus a cleaning step for the regeneration of the membrane permeability is required for the polymeric membranes.

Various chemical treatments were applied to the two polymeric membranes starting with soaking in a salt solution of high concentrations, backflushing, alkaline soak and protein degrading enzymes. Despite these treatments, only 45 to 68% of the membrane permeability could be recovered (as shown in **Figure 5-24**). It should also be noted that 500 kDa membranes were fouled the most by protein nanoparticles as only 14% and 45% of the initial membrane permeability was restored after protein filtration and subsequent chemical cleaning. This was despite the fact that 500 kDa PES membranes had a hydraulic permeability of ~5000 LMH/bar, more than twice of that of 300 kDa PES or 20 nm PAA membranes. This is likely due to large

pores observed in 500 kDa membranes allowing more pore penetration by fouling nanoparticles.

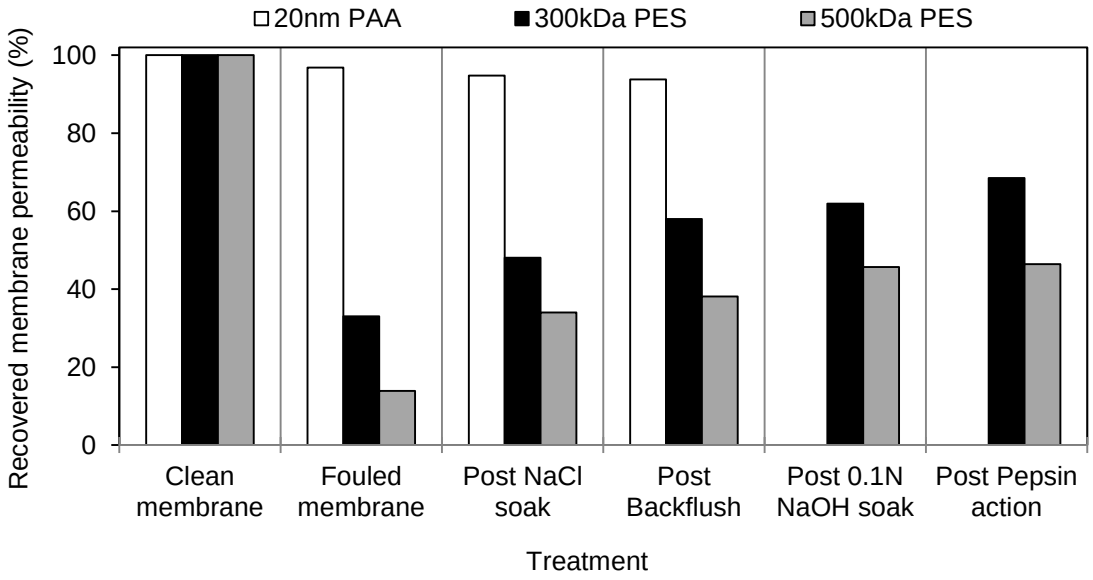

Figure 5-24 Recoverable membrane permeability (% of membrane permeability for fresh membranes) for PAA membrane and PES membranes after an extended UF/DF experiment (12 DF cycles each of one diavolume) for fractionation of a mixture of BSA and BSA nanoparticles and effect of various chemical treatments to remove fouling.

Membranes were treated (in sequence) with 1M NaCl soak for 24 hours; buffer backflush (2 x TMP used in protein filtration), 0.1 N NaOH soak for an hour and proteolytic enzyme treatment for 18 hours at room temperature). PAA membrane showed ~96% of initial buffer flux recovered after rinsing with buffer. Polymeric membranes could not be restored to similar levels even with the chemical treatments.

Tedious and time-consuming chemical cleaning can take significantly increase total processing time of a UF/DF cycle and can only restore membrane permeability to a limited extent for PES membranes. Other harsher treatment such as alkaline solution mixture of proteases and detergents (for example Tergazyme, a commercial product) or sodium hypochlorite may be required for complete cleaning. These treatments, however, can result in leachates and need to be validated for low carryovers of the fouling protein as well as the cleaning chemicals. PAA membranes did not require such treatments and thus can be used to further reduce the processing times by a much easier buffer wash procedure to regenerate the membrane. Thus, PAA membrane could be used in single-pass UF/DF processes or processes requiring quicker turnaround for the filtration system to process multiple batches and minimise hold time for the batches. The later can be useful in processing large volumes of low titre viral feeds where hold time can be significant for viral infectivity.

5.3.5 UF/DF of clarified Adenovirus feed: comparison of 20 nm PAA and 300 kDa PES membranes

Commercial PAA membranes have not been tested for virus separation applications so far. A major concern during such separations is a loss of virus particles in permeate and loss of infectivity of the virus particles thus affecting recovery of infectivity. Impact of the material (chemistry, surface roughness) on virus infectivity needs to be examined.

5.3.5.1 Characterisation of the virus feed

Low particle and infectious titres were observed for the feed used in this study. Total particle titre (~10^{10} particle per mL) in the feed was obtained using nanoparticles tracking analysis (NTA) and was found to be much higher than the infectivity titres (~$6x10^{8}$ IFU per mL) which could be due to protein aggregates or exosomes present in the clarified Adenovirus feed. Though titres are improving for Adenovirus and AAV, for viral vectors like Lentiviruses (another 100nm sized virus) such low titres are the current scenario. Membrane loading of 26 L/m^2 similar to that used in the limited literature available for Adenovirus ultrafiltration (Nestola *et al.*, 2014a) was used in this experiment.

5.3.5.2 Flux decline for the filtration of crude clarified virus feed and growth media

For similar membrane loading and conversion ratio (fraction of the feed filtered), cumulative flux was found to be higher for PAA membranes (116 ± 6 LMH) by more than 20 LMH (93 ± 1 LMH for PES membranes), and the difference was statistically significant. **Table 5-7** shows the cumulative filtrate fluxes for two membranes at the end of each step of the UF/DF process. A similar trend was observed in the previous experiments when the two membranes types were compared for filtration of BSA nanoparticles solution (~$1x10^{11}$ particles per mL of 80 nm nanoparticles) with similar membrane loading (26 L/m^2). Both membranes showed the identical shape of flux decline curves for viral feed as shown in **Figure 5-25**, and fouling mechanism was also identified to be cake filtration dominated. The impact of fouling by viral feed was more pronounced for polymeric membrane than for the PAA membrane.

	PAA membrane	PES membrane
UF/DF steps	**Cumulative filtrate flux (LMH)**	
Initial conc. step	116 ± 6	93 ± 1
DF cycle 1 (3 DVs)	113 ± 6	85 ± 7
DF cycle 2 (6 DVs)	111 ± 7	99 ± 1
	Fouling resistance	
Initial buffer flux (LMH at 0.6 bar)	1266 ± 32	1110 ± 48
Recoverable membrane permeability (%)	27 ± 1	18 ± 3

Table 5-7 Cumulative filtrate fluxes for various UF/DF steps, initial buffer fluxes of the membranes used, recoverable membrane permeability of PAA and PES membranes used for UF/DF processing of crude and clarified Adenovirus feed.

Data presented as average value ± one standard deviation for multiple filtration runs (n=3 for PAA and n=2 for PES membranes).

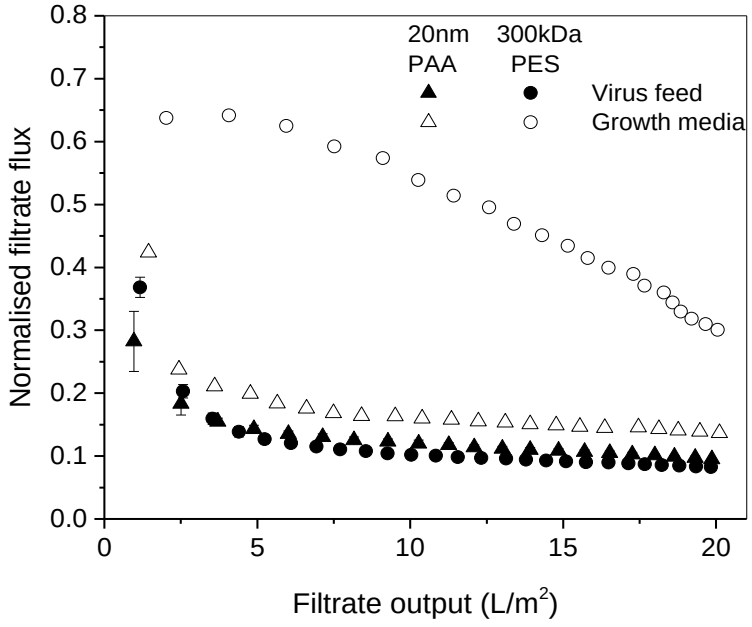

Figure 5-25 Flux decline for filtration of crude, clarified Adenovirus feed in growth media and growth media alone through 20 nm PAA and 300 kDa PES membranes.

Filtrations were carried out at TMP of 0.6 bar and stirring speed of 1500 rpm in a stirred cell. Flux decline is shown for the initial concentration step. Error bars on the virus flux data represent one standard deviation for multiple filtration runs (n=3 for PAA and n=2 for PES membranes). Lot #5 of PAA membranes was used.

Filterability of the serum-rich growth media was also evaluated. It was observed that serum-rich media contributes to a significant proportion of the flux decline observed for viral filtration through PAA membrane as similar flux declines were observed for filtration of growth media and clarified virus feed (see **Figure 5-25**). For PES membranes, flux decline was not significant for

the growth media alone, but the viral feed significantly fouled these membranes with membranes operating below 15% of the initial buffer flux. PAA membranes were observed to be more susceptible to fouling by growth media as compared to the PES membranes. Though a chief component of growth media is bovine albumin at 4-5 g/L concentration, it would appear that something else may be responsible for the fouling observed as filtration of a similar volume of BSA solution of 5 g/L through PAA membranes has shown the meagre effect on flux decline and transmission.

Recoverable membrane permeability after virus filtration was also found higher for PAA membranes compared to the PES membrane, as shown in **Table 5-7**, indicating higher fouling resistance exhibited by PAA membrane for similar protein loading. Differences in the recoverable membrane permeability between two membranes were found to be statistically significant (with ANOVA p-values less than 0.01). Values of the recovered membrane permeability for virus feed, however, are lower than those observed for the filtrations of 80nm BSA nanoparticles where more than 90% of initial membrane permeability was recovered for PAA membranes (see Section 5.3.1). Lower recovery was observed due to the compositional differences among two different feeds. Virus feed used in the study is a crude, complex mixture of multiple host cell proteins, undigested viral and host cell nuclear acids, exosomes, lipids, protein aggregates, serum media components and fragments of virus capsids along with intact virus particles. Some of these particles can be in a very low amount below detection limits of UV detector in HPLC and may be masked by light scattering of larger virus particles when analysed in light scattering based size and titer analytical techniques such as NTA.

5.3.5.3 Transmission of the proteins through the membranes

HP-SEC chromatograms of feed, retentate and permeate samples were analysed for both experiments (filtration of virus-rich feed and growth media only). Filtration of growth media through membrane showed better protein transmission of serum albumin through PES than PAA membrane, indicated by higher peak area for serum albumin in permeate collected through former (Shown in **Figure 5-26 B**). Interestingly, a high molecular weight (HMW) peak (> 660 kDa) of the growth media feed was absent from permeate collected through PAA membrane but present in permeate from PES membrane. This suggests a role of this HMW component in the flux decline for PAA membrane. For viral filtration, however, this HMW peak was absent from the permeate collected from both membranes suggesting another foulant also playing a role (**Figure 5-26 C**). A thorough characterisation of virus feed will be necessary to identify the foulant species. Intact Adenovirus particles will be unlikely to result in the internal fouling of PAA membranes but more likely for PES membranes due to increased pore accessibility of such membranes with broad pore size distributions. Adenovirus particles could not be observed on

HP-SEC chromatogram due to low titre. Transmission of virus particles was studied using more sensitive infectivity assay. Removal of serum albumin (BSA) was approximately 47±2% and 58 ±4% for PAA and PES membranes respectively when measured from permeate collected. Residual serum albumin in retentates (**Figure 5-26D**) were also measured to higher (35±4%) for PAA membrane than PES membrane (29±3%). The lower difference in residual levels of albumin is because of difficulty in retrieving all of the retentates from the stirred cell, especially for PAA membrane. Proteins smaller than albumin were removed to a high extent (>80%) and residual levels were not detected in SEC.

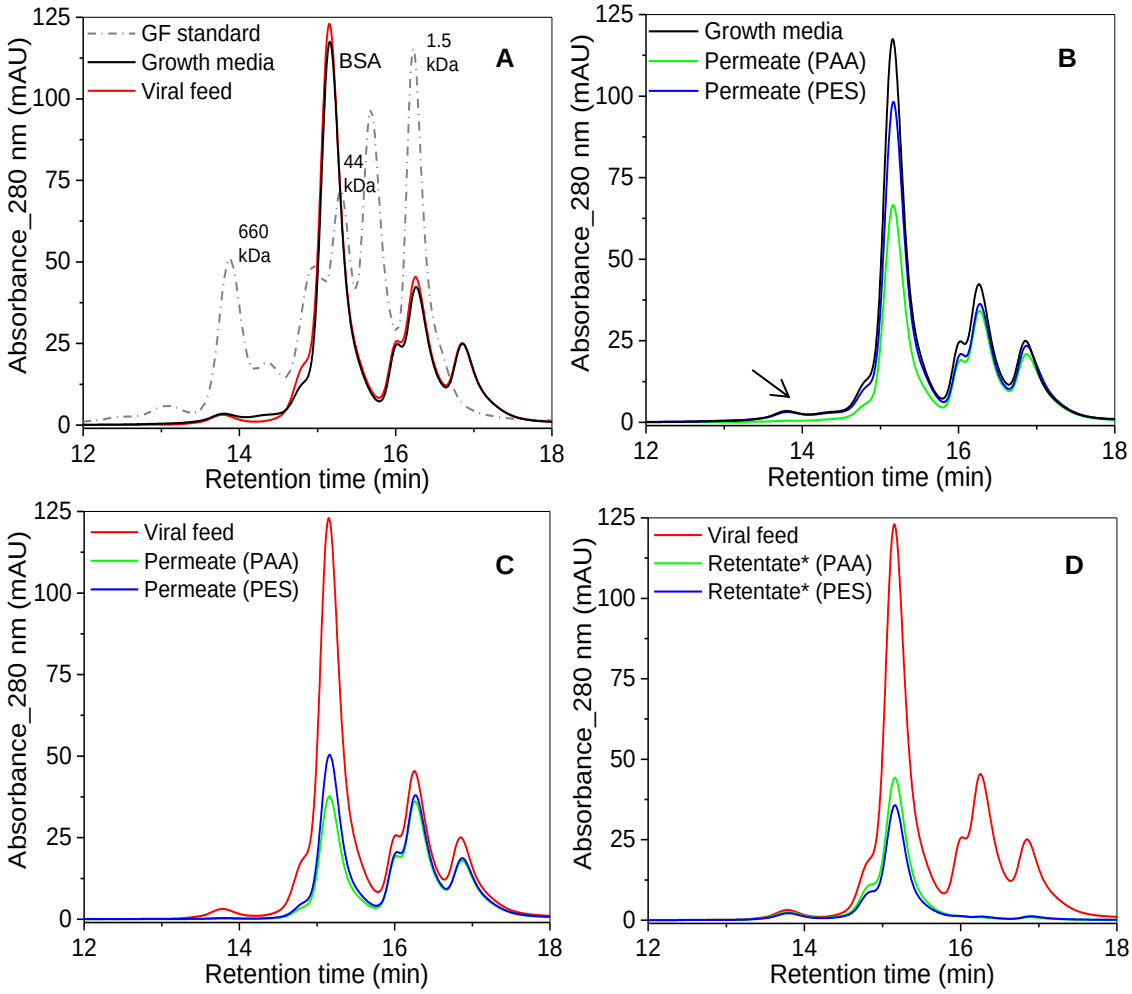

Figure 5-26 Comparison of HP-SEC chromatograms viral feed and serum rich growth media (A), and permeates collected for growth media filtration (B) and permeates (C) and retentates (D) collected for viral filtrations through PAA and PES membranes.

**Retentates were diluted (~4 fold) to the level of initial feed volume. PAA membrane show reduced transmission of growth media components compared to PES membrane. Notice the HMW peak (arrow in B) absent form PAA permeate of growth media filtration. Same peak was absent from permeates from both membranes for viral feed filtrations indicating impact of other components of viral feed on membrane performance including reduction of serum albumin (main peak, ~15 min) removal. Chromatograms were obtained by injecting 50µL of the samples onto BioSEC-5 size exclusion column (7.8x300 mm) at 0.8 mL/min with PBS as mobile phase.*

5.3.5.4 Recovery of virus infectivity

PAA membranes were found to be leaky with less than 2% of the total infective titre of the feed was recovered in permeate. This could be because of the defects in the active layer of the membrane. The effect was more pronounced in one of the three PAA membranes used where significant losses (~0.7%) were observed for concentration and each DF step. Losses were prominent for DF steps using all three PAA membranes. PES membrane showed almost no leakage or particle passage into the permeate. The total number of virus particles observed in the undiluted permeate solutions were very low (less than 5) per sample hence not significant sample size for accurate estimation of the titre.

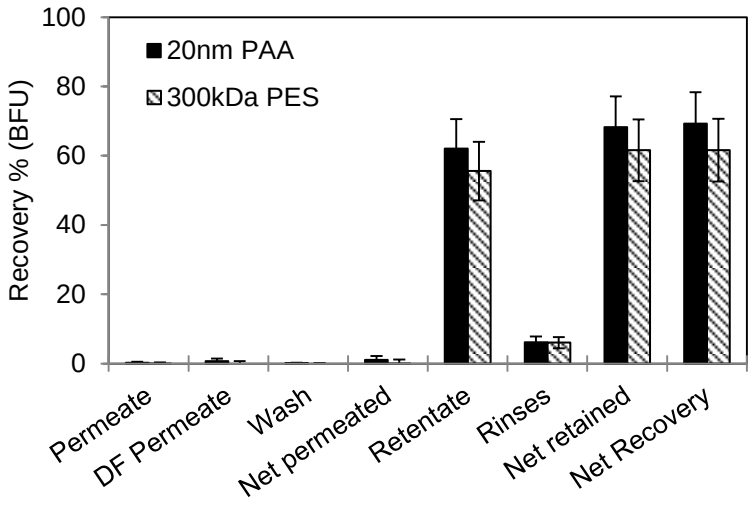

Figure 5-27 Recovery of infectious recombinant Adenovirus (ß-galactosidase gene) particles in different fractions collected during UF/DF of crude and clarified Adenovirus feed using PAA and PES membranes.

Blue forming units (BFUs) are formed upon staining of recombinant virus-infected (transfected) HEK293 cells producing ß-galactosidase enzyme breaking assay substrate to release blue coloured compound.

For both membranes, most of the invective particles were recovered in the retentate and the rinse solution after cleaning the membrane surface. Around 61 ± 10 % and 68 ± 11 % of the total infective units (BFU) of the feed were retained (retentate + rinse solution) by the PES and PAA membranes respectively. Differences in the infectivity recoveries between two membranes were found to be statistically insignificant (ANOVA p values >0.1) due to large standard deviations. Net recoveries of the infective titre (in all the fractions) were similar to recoveries found in the retained volume. Loss of total infective units (15 to 40 %) could be due to the exposure to shear due to stirring conditions in the stirred cell. **Figure 5-28** shows blue forming

units formed on monolayers of cells by infective virus particles leaked through membranes into the permeate solutions.

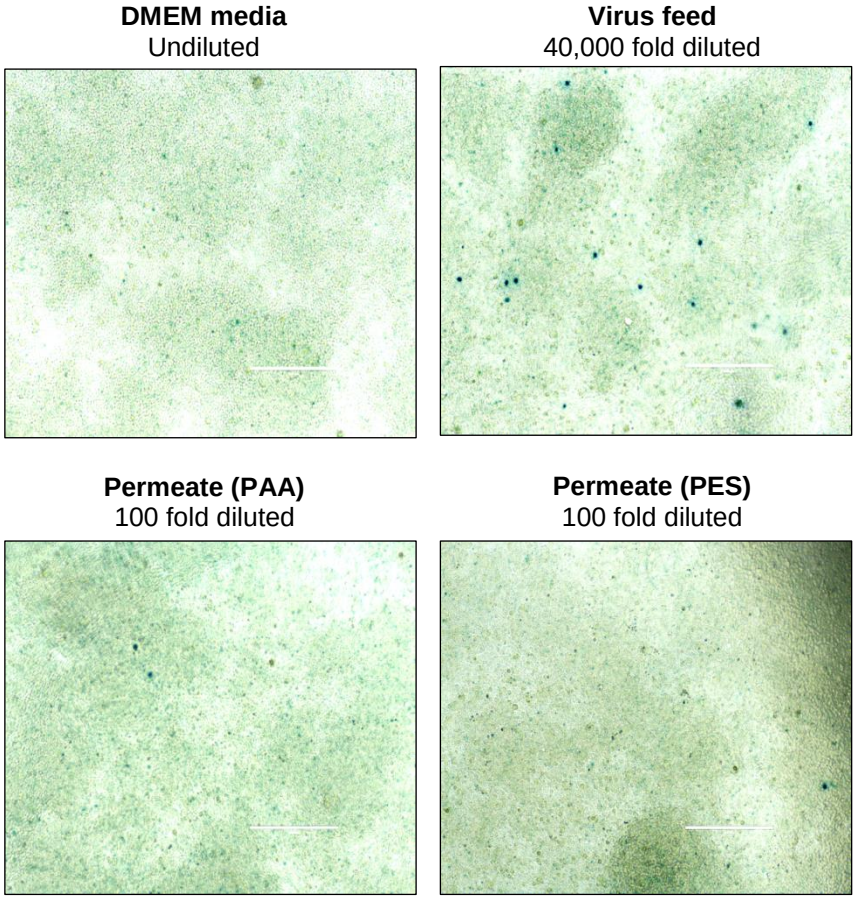

Figure 5-28 Infected HEK 293 cells (observed as dark green dots using the infectivity assay) for the sterile growth media, virus rich feed and permeates collected after filtration of the viral feed through 20 nm PAA and 300 kDa PES membranes.

Images from light microscopy were obtained for the plate wells after staining the infected cells in the wells. All the spots for each well were counted using a grid to avoid duplicate counting of same spots. More dots can be seen in permeate collected using PAA than permeate collected for PES membranes. AdV infected and transformed cells produce the enzyme , galactosidase which converts substrate releasing green colored dye.

These results indicate compatibility of PAA membrane material for processing of viruses like Adenoviruses as similar recoveries of infectivity was observed as seen with the traditionally used membrane materials such as PES. Further work could be extended to test the compatibility of this membrane material for more delicate, enveloped viruses like lentiviruses. Results also show that trends observed for various process outputs such as process flux, transmission of solutes and fouling resistance when comparing PES and PAA membranes using protein nanoparticles are valid for virus feeds but not in absolute values of these process

outputs. Given the fouling observed with growth media and viral feed, it should be noted that studies for protein nanoparticles filtrations are more likely to better simulate a UF/DF step after an initial chromatography-based purification step rather than direct UF/DF of a crude viral preparation. Modelling a complex mixture such as protein nanoparticles mixture with the addition of growth media as well as other model impurities such as bacterial and bacteriophage DNA could be useful for a crude viral preparation.

5.4 Conclusion

The objective of the chapter was to study the separation performance of the 20 nm rated PAA membranes using binary solute mixtures of the larger model solutes for viral vectors (TG or BSA nanoparticles) with BSA as a model solute for impurities such as host cell proteins. Fractionation experiments comparing 20 nm rated PAA membrane with 300 kDa polymeric membrane revealed different separation performance with PAA membranes showing leaky transmission of BSA nanoparticles resulting in lower selectivity as compared to the polymeric membranes (Section 5.3.2.2). It was observed that the presence of a large solute in the feed hinders the transmission of smaller solutes such as BSA resulting in lower selectivity.

A diafiltration aided process was found to be effective for removal of residual BSA thus improving purification factors for the large solutes by 2-3 folds (Section 5.3.3). Fine tuning of the ionic environment of the protein solution was found to be the most effective strategy for improvement of the purification factors. Operating at isoelectric point (pH 6.5) of the membrane and very low salt concentrations in protein solutions dramatically improved the separation performance (Section 5.3.4.1). This demonstrates the potential for improvement in separation by tailoring membrane surface possibly reducing risks posed by the membrane defects. Operating at low transmembrane pressure also improved the purification factors without any significant reduction in the flux. This demonstrates that PAA membranes can be used as effective ultrafiltration membranes if operating parameters are optimised.

Adenovirus UF/DF runs demonstrated biocompatibility of the PAA membranes for virus ultrafiltration as the net recovery of the infectious virus particles was found to be similar to traditionally used polymeric membranes (Section 5.3.5.4). Comparison of the two membranes for Virus UF/DF runs also showed similar trends of performance parameters as observed using BSA nanoparticles such as higher particle transmission, higher flux and superior fouling resistance for PAA membranes. Thus protein nanoparticles could be successfully used for the studies such as comparison of membranes for potential use for viral separation.

CHAPTER 6 CONCLUSIONS AND FUTURE WORK

6.1 Conclusions

A systematic approach to the study of porous anodic alumina membranes for viral separations was presented in this thesis.

Objective 1: Preparation and characterisation of the BSA nanoparticles as a mimic of virus particles

Lack of sufficient viral material and the associated requirements for the sophisticated analytical and containment facilities for such studies were addressed by establishing the use of protein nanoparticles as a mimics for virus particles. Synthesis of such protein nanoparticles was described in chapter 3. A protocol for the preparation of 80-90nm albumin nanoparticles was developed from previously reported literature. The resulting method was shown to be both reproducible, and high yielding with more than 97% of BSA converted into nanoparticles. The time required for synthesis was further from overnight to under 4 hours by studying the impact of the length crosslinking step on particle size characteristics of the nanoparticles. Preparations were highly monodisperse with polydispersity index as low as 0.04 as measured by the dynamic light scattering and confirmed using nanoparticle tracking analysis. Particle shape was however not ideal spherical instead of globular structures formed from 2-3 smaller spherical nano particulates when observed under transmission electron microscope. This observation warrants the cautious use of the nanoparticles as physical mimics to highly symmetrical virus particles. A filtration study comparing 90nm protein nanoparticles and Adenovirus rich feed showed similarity in shape of the flux decline curve but lower values of the average fluxes for Adenovirus which was ascribed to the presence of other impurities such as host cell protein, DNA, protein aggregates, virus fragments and aggregates in the viral feed.

Objective 2: Characterisation of porous anodic alumina (PAA) membranes for filterability of protein solution of single model solutes

A systematic approach was followed to screen different ratings of the PAA and polymeric membranes and compare the selected membranes for filterability studies with protein model solutes of different sizes (8nm BSA as model protein impurity, 22 nm TG as model for smaller virus particles such as AAV and 80-90 nm BSA nanoparticles as model for larger viral particles such as AdV). PAA membrane rated 20 nm (lowest pore rating available) and polymeric membrane rated 300 kDa were selected among three different ratings for each membrane material. The selection was on the basis of comparable hydraulic permeability, similar mean pore size, and dextran sieving characteristics. PAA membrane rated 20 nm showed approximately two-fold lower 90% rejection value of 850 kDa than that observed for the 300 kDa polymeric membrane. However, dextran sieving curve for the PAA membrane was sharper than

that of the polymeric membranes. For protein solute filtrations, sieving coefficients for solutes decreased with increasing model solute size for both membranes, as was expected. Both membranes were highly retentive (with observed sieving coefficient being less than 0.05) to protein nanoparticles however PAA membranes showed ~3.6 times higher transmission. The leaky transmission was attributed to the presence of the large surface defects (> 1 um in dimensions) on the active layer surface of PAA membranes which were observed using SEM. These large defects exposed the underlying support layer with large pores. Unexpectedly, PAA membranes also showed higher fouling resistance exhibiting restoration of >90% of initial membrane permeability after a simple buffer rinse while polymeric membranes could only be restored to 50% of their initial permeability.

It is hypothesised that fundamental differences in the membrane architecture are responsible for these observations. Polymeric membranes show wide pore size distribution where pores larger than solutes are accessible to the solutes. However, the tortuous pore channels and thicker membrane bed causes the entrapment of the solute particles resulting in internal fouling and low transmission. Higher transmission of BSA nanoparticles, on the other hand, is the result of the presence of the surface defect exposing large highly permeable support layer pores and straight channels in thinner membrane bed (2 times lower than polymeric membranes). Majority of the pores in narrow pore size distribution of the PAA membranes are smaller than solute particles and hence are not accessible to the solutes resulting in very low internal fouling. This hypothesis explains the differences in transmission and fouling behaviour of the two membranes. The hypothesis could not be verified as internal fouling and its location in the membranes could not be discernibly observed in the electron microscopy and would require alternative methods such as confocal laser fluorescence microscopy.

Objective 3: Separation performance of porous anodic alumina (PAA) membranes for binary mixtures of the model solutes

Filtration of the binary solute mixtures of large model solutes and smaller impurity (BSA) showed similar flux decline, cumulative flux, and restoration of membrane permeability as observed for the filtration single solute solutions of large solutes. However, fractionation was low for both polymeric and PAA membranes due to the fouling by large solute reducing the transmission of the model impurity by 10-45 % compared to complete transmission of the BSA in pure BSA solution. Hence different approaches to aid in the removal of BSA were further investigated using PAA membranes. Addition of discontinuous diafiltration steps was found to be effective in increasing the BSA removal from 40% to 70% with 3-diavolumes of buffer exchange and improved purification of TG by 2- fold. Improvement in purification factor of BSA

nanoparticles was also observed upon addition of diafiltration steps. A continuous diafiltration would likely be more effective but could not be used with the current experimental setup. An extended UF/DF process with 12 diavolumes for fractionation of BSA NP and BSA showed complete removal of BSA with both PAA and polymeric membranes. PAA membranes showed higher flux, 3-fold higher purification factors, however, lower BSA NP recovery. PAA membranes also did not foul significantly with only 10% loss of membrane permeability compared to a 67 % loss observed for the polymeric membrane. Fractionation was also enhanced by operating at low feed conductivity and pH near determined isoelectric point (6.5) of the PAA membranes. Highest purification factors of 9.9 and 7.3 for TG and BSA NP were observed at such feed conditions which were 4 and 2 fold higher than those observed at pH 7 and high salt concentrations. Operating at low transmembrane pressures also improved the purification factors without significant loss in flux. With suitable surface modifications, PAA membranes can be used for separation of viral particles and host cell protein impurities by utilising the ionic environment of the feed.

For Adenovirus purification from a crude, clarified mammalian cell culture feed, both PAA, and polymeric membranes showed similar recovery of 60-70% of the infective virus particles, primarily retained by the membranes, thus demonstrating the compatibility of the PAA membranes for viral processes. Similar to experiments with BSA nanoparticles, PAA membranes showed leaky transmission of the infective virus particles while polymeric membranes did not show any leakage. As predicted with filtration experiments with BSA nanoparticles, trends observed in the comparison of the two membranes were also observed for virus filtration such as higher recovery of membrane permeability and flux for PAA membranes although absolute values were different. Removal of the host cell impurities was slightly higher for the PES membrane (58%) compared to PAA membrane (47%), but the final purification factor of infective virus particles in the retentate was found to be similar at 3.0.

Studying commercial PAA membrane limited the scope of the present work as limited commercial products are available with formats compatible with stirred cells and modules compatible for cross-flow filtration are not yet developed for PAA membranes. Custom built modules could be developed, but such work is constrained by lack of membrane sheets and brittle nature of the membranes. Large membrane lot to lot variability in the commercial product also complicated the study, which was characterised in Chapter 4 and its effect of separation performance studied in Chapter 5. Most of the previous studies exploring bioseparation applications including virus purifications used custom-made membranes which are more refined membranes compared to the commercial product used in this thesis. Membranes used in this study were not as refined.

Despite these limitations, the present study is the first study conducted so far to evaluate commercial PAA membranes for viral separations especially using model systems and offering a parallel comparison with traditional polymeric membranes for filterability of these model systems. Useful insights gained in this study will help to improve the fabrication of PAA membranes and design new membranes for viral separations.

6.2 Future work

Various issues regarding the porous anodic alumina membranes and their UF applications were identified in this study. Findings from this study can be used as guidelines for future developments of these membranes as ultrafiltration membranes for viral vector separations. Based on the observations made in the present study, following different studies are suggested for further work in this area:

6.2.1 Optimising protein nanoparticles synthesis for better model solutes

Protein nanoparticles produced in the current work were found to be non-spherical in shape formed of aggregates of smaller globular nano-particulates (Chapter 3). These particles despite having similar hydrodynamic size as of viral vectors are far from the highly organised and symmetrical structures of viruses. Influence of the shape of protein nanoparticles in sieving through membranes was not considered in the present study. To obtain spherical nanoparticles, the greater understanding of the impact of process parameters on particle shape and size as well as distribution is crucial. To this end, the present study identified gaps in current literature where factors such as reaction vessel dimensions, mixing and quality of the protein feed (presence of impurities such as lipids, protein dimers, and higher molecular weight aggregates) are not evaluated. Use of multivariate data analysis such as principal component and partial least square analysis could be used to identify the crucial factors, and these factors could be optimised through the design of experiment approach.

6.2.2 Confocal light scattering microscopy experiments to prove the differences in mechanism of retention of nanoparticles by quasi-isoporous PAA membranes with cylindrical pores and conventional polymeric membranes with tortuous pores and broad pore size distribution

Confocal microscopy could be used to study how fluorescently labelled protein nanoparticles traverse through membrane bed. Resistance faced by protein nanoparticles could be studied by

estimating penetration depth and time for fluorescent nanoparticles through the bed, and these estimates could be used in modelling of the sieving process.

Fouling of the various membrane layers could be studied by measuring fluorescence intensity across the membrane bed after filtration of protein solutions. The build-up of the fluorescence above the membrane surface could be studied to estimate the thickness of the concentration polarisation layer. Solute build-up across the membrane thickness and above it could be helpful to prove the differences in retention mechanisms. This is a challenging task as it requires operation under flowing conditions thus requiring fabrication of a flow cell capable of replicating flow and shear conditions observed in a stirred cell. Another challenge is to use this flow cell for brittle PAA membranes. These challenges require a significant investment of time and efforts in the fabrication of flow cell and were thus not in the scope of the present study.

6.2.3 Addressing the lot to lot variations in membranes

The present study reports significant variations in hydraulic permeability and pore size distribution of all the PAA membranes lots used in this study (Chapter 4) and its impact on protein losses (Chapter 5). Besides differences in pore size distributions, large structural defects were also observed, however, their contribution towards hydraulic permeability could not be calculated due to their low frequency and random distribution. However, such large defects can still contribute to a significant fraction of total hydraulic permeability as well as protein transmission. Electron microscopy fails to accurately measure the density of such defects due to low scanning area usually in few μm^2.

Mutually complementary characterisation techniques such as small angle X-ray spectroscopy (SAXS), high-resolution X-ray computerised tomography (CT) scanning and porosimetry could be used to scan a large area of membranes to identify and quantify the defect density. Correlation of such defect density along with mean pore size of the membrane with more commonly used and non-destructive techniques such as integrity testing of membranes will thus be crucial for any further studies or applications of these membranes. Well established characterisation methods and fundamental understanding of the mechanisms of the defect formation is thus necessary to fabricate defect-free membranes. Optimisation of fabrication procedure and control strategy needs to be undertaken to minimise deviations in mean pore sizes and defects.

6.2.4 Thyroglobulin as a model solute for selectivity permeability analysis of UF membranes targeted for separations of large biomolecules

Increasingly membranes with MWCO rating of 300 kDa and above are being marketed by some manufacturers for the applications in virus separations. These relatively new products are not tested for virus related applications. Membrane ratings by manufacturers can vary significantly due to the lack of standardised characterisation methods. Mehta and Zydney (2005) have proposed a selectivity permeability curve, similar to Robeson plot used for gas separation membranes, to compare different membranes for the trade-off in separation performance and permeability. However, these authors have used BSA as the model solute to generate this curve for a range of membranes. Larger solutes such as TG which is similar in dimensions to smaller viral vectors such as AAVs can be used instead of BSA to compare membranes targeted towards virus separations. The current study shows that TG transmission was sensitive to the variations in lots of commercial anodic alumina membranes.

A caveat in such analysis is that theoretical curve generated does not account for actual feed properties and impact of fouling associated which is inevitable in real-world applications of membranes. Impact of the module, feed properties and fouling on deviations from the theoretical selectivity permeability curve needs to be explored further.

6.2.5 Performance of PAA membranes in cross-flow conditions

Stirred cell module used in this study is an excellent tool to study the effect of various treatments to feed or membrane. However, mass transfer properties of the stirred cell module are not at par with cross-flow or tangential flow filtration modules. At the industrial scale, the cross-flow mode is almost unanimously preferred over stirred cell filtration due to the ease of automation and control available in the former. The present study could not test PAA membranes in cross-flow conditions due to lack of availability of commercial membrane in flat sheet or hollow fibre format. A spiral cross-flow module which could accommodate circular discs of PAA membranes is thus highly desirable. XFlo76 (TangenX Corp., USA) is such a marketed module designed for membrane screening in cross-flow mode but using 76 mm circular discs. This module is however fabricated for compressible polymeric membranes and not for brittle ceramic membranes. Further, the commercial PAA membranes are only available up to 43 mm disc diameter.

Cross-flow mode is a more appropriate module to study the scalability of the separations of both model solutes and viral vectors using PAA membranes. Thus the designing of custom-built cross-flow modules compatible with brittle membranes is crucial. Fabrication of large sheet of

PAA membranes would also need to be studied. Another workaround is fabricating tubular anodic alumina membranes, which have been reported in the literature (Lee and Mattia, 2013, Attaluri *et al.*, 2009). However, challenges to fabrications of such membranes are not discussed, and no such product is commercially available. In theory, these tubular membranes could be used as hollow fibres in TFF mode. However, limitation of fabrication methods on the internal diameter and length of the membrane tubes would need to be investigated.

6.2.6 Fine tuning of membrane morphology of PAA to enhance separation performance

Commercial PAA membranes used in the present study are offered in limited pore ratings (20, 100 and 200 nm), which restrict their applications for a variety of viral vectors ranging from 20 to 500 nm in size. PAA membranes with more pore size ratings will be helpful in selecting and studying ultrafiltration of viral vectors or model solutes with optimal pore ratings. Another commercial product from InRedox LLC (USA) has been marketed with a broader range of pore ratings and even customised pore ratings. Studying viral separations using these membranes would be useful to design better ultrafiltration processes.

Pore morphology itself can affect separation performance. It is well known that slit-like pores have better selectivity-permeability characteristics compared to circular pores (Feinberg *et al.*, 2018, Kanani *et al.*, 2010). Fabrication of porous anodic alumina membranes with different pore shapes such as triangular pores has been reported (Smith *et al.*, 2008) but not yet studied for their separation performances, especially for viral vectors. Besides the commercial product had quasi-isoporous pore size distribution with polygonal pores rather than circular pores. Custom fabricated membranes reported in the literature (Ni *et al.*, 2014) though have highly uniform pore size distributions. It would be interesting to see if higher selectivity could be obtained for viral vector separations using these non-commercial but refined membranes.

Another interesting aspect could be functionalisation of the porous anodic alumina membranes using chemical groups. Functionalisation can be done to minimise the fouling (Lee *et al.*, 2005), tune effective pore size of the membrane through polymer groups on internal pore surfaces such as PEG coating (Popat *et al.*, 2004) and aid separation of large biomolecules from smaller impurities by providing differential steric and electrostatic repulsions by functionalising only the pore entrance with a mesh of polymer brushes such as polyacrylic acid brushes as described in literature (Nagale *et al.*, 2000). The goal of such an approach is to improve separations without compromising the permeability thus processing time. The inclusion of surface charge groups on membrane surface such as hydroxyl groups (Jeong and Yi, 2013) and manipulation of

isoelectric point of membranes with respect to targeted bio-separation such as different viruses and impurities can also be investigated.

These approaches have been illustrated in **Figure 6-1**. It would be interesting to see how these modified membranes could be used with complex feeds containing viral particles.

6.2.7 Studying iso-porous polymeric membranes

Challenges with the fabrication of brittle, porous anodic alumina membranes could be avoided if membranes offering uniform surface pore size distribution are available in the polymeric material. Block co-polymeric (BCP) membranes are a newer class of polymeric membranes which are fabricated by manipulating the self-assembly of the residues during the polymerisation process. BCP membranes have surface topology similar (shown in inset D of **Figure 6-1**) to that of PAA membranes with narrow pore size distributions. BCP membranes have highly interconnected support layer unlike PAA membranes but similar narrow pore size distributions (Yu *et al.*, 2016). BCP membranes with slit-like lamellar pores have also been reported. These membranes are worth investigating to see if they operate with similar separation mechanisms such as PAA membranes and have similar or superior fouling resistance.

From the issues and potential solutions discussed above, it is clear that a multi-disciplinary approach would be necessary for the development of these membranes as viable commercial products for bio-manufacturing. These challenges call for synergies of material scientists, inorganic chemists, module fabrication engineers and bioprocess engineers. Some of these approaches are illustrated in **Figure 6-1**. All of these approaches for designing new or improved membranes will require a cost-benefit analysis to assess the commercial feasibility of these membranes by comparison to traditional polymeric membranes currently used for viral vector purifications.

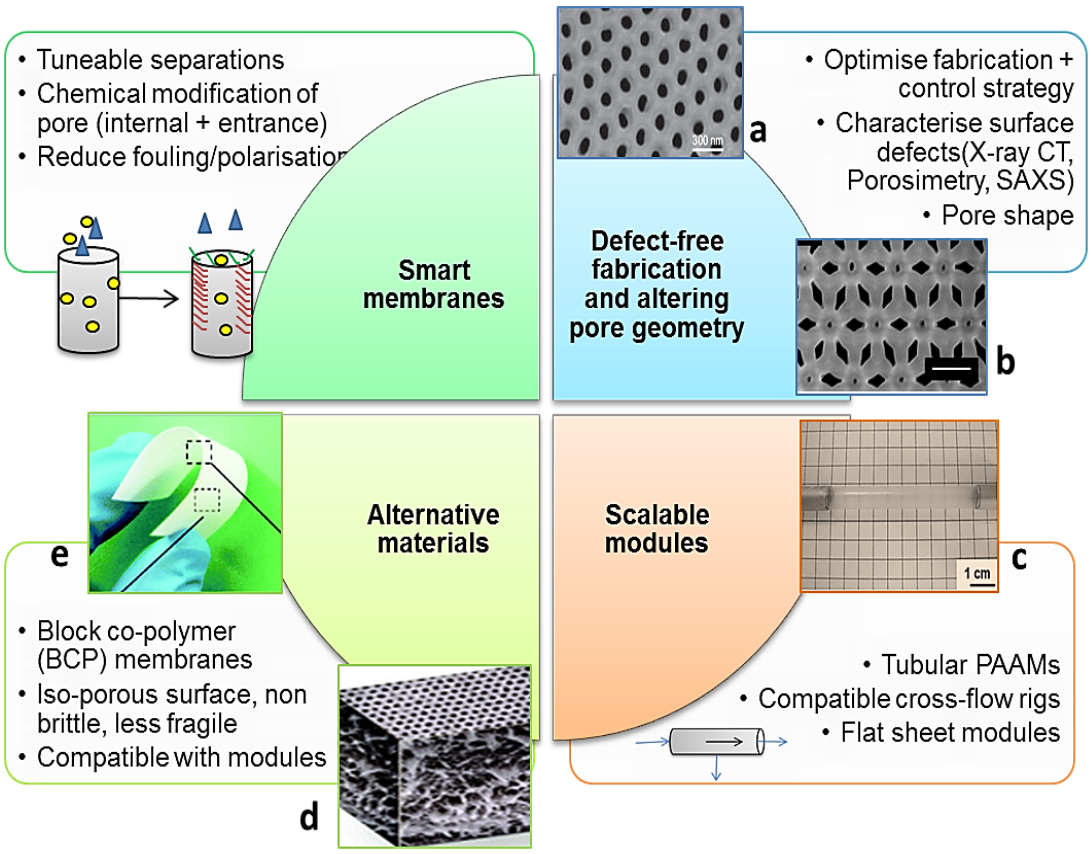

Figure 6-1 Future work: Various approaches to developing new membranes for viral vector separations.

Fabrication of defect-free PAA membrane with narrower pore size distribution (inset a reproduced from (Ni et al., 2014) than the commercial membranes used in this study, would require an understanding of the fabrication process and better characterisation tools for defects.

Use of different pore geometry such as triangular pores (as in inset b reproduced from (Smith et al., 2008) can also be studied for improved separation performance.

Scalable modules with the cross-flow mode of operations can be studied by fabricating tubular PAA membranes, as shown in inset C reproduced from(Lee and Mattia, 2013) or flat sheets membranes.

Smart membranes with multiple mechanisms of sieving can be created by chemical alteration of pore surface and entrance for selective transport of impurities without compromising permeability including fouling remediation.

Finally, using alternative materials such as polymeric BCP membranes, shown in inset e and d, reproduced from (Yu et al., 2016) could help bypass the fabrication issues faced with PAA membranes. All the images were reused with permissions from cited sources.

BIBLIOGRAPHY

ANHORN, M. G., MAHLER, H. C. & LANGER, K. 2008. Freeze drying of human serum albumin (HSA) nanoparticles with different excipients. *International Journal of Pharmaceutics,* 363**,** 162-9.

ARKHANGELSKY, E. & GITIS, V. 2008. Effect of transmembrane pressure on rejection of viruses by ultrafiltration membranes. *Separation and Purification Technology,* 62**,** 619-628.

ARROYO-MAYA, I. J., HERNANDEZ-SANCHEZ, H., JIMENEZ-CRUZ, E., CAMARILLO-CADENA, M. & HERNANDEZ-ARANA, A. 2014. alpha-Lactalbumin nanoparticles prepared by desolvation and cross-linking: structure and stability of the assembled protein. *Biophysical Chemistry,* 193-194**,** 27-34.

ATTALURI, A. C., HUANG, Z., BELWALKAR, A., VAN GEERTRUYDEN, W., GAO, D. & MISIOLEK, W. 2009. Evaluation of nano-porous alumina membranes for hemodialysis application. *ASAIO Journal,* 55**,** 217-23.

AURICCHIO, A., HILDINGER, M., O'CONNOR, E., GAO, G. P. & WILSON, J. M. 2001. Isolation of highly infectious and pure adeno-associated virus type 2 vectors with a single-step gravity-flow column. *Human Gene Therapy,* 12**,** 71-6.

BAKER, R. W. 2012. Overview of Membrane Science and Technology. *Membrane Technology and Applications.* Third ed. United Kingdom: John Wiley & Sons Ltd.

BAKHSHAYESHI, M., KANANI, D. M., MEHTA, A., VAN REIS, R., KURIYEL, R., JACKSON, N. & ZYDNEY, A. L. 2011a. Dextran sieving test for characterization of virus filtration membranes. *Journal of Membrane Science,* 379**,** 239-248.

BAKHSHAYESHI, M., ZHOU, H. Y., OLSEN, C., YUAN, W. & ZYDNEY, A. L. 2011b. Understanding dextran retention data for hollow fiber ultrafiltration membranes. *Journal of Membrane Science,* 385**,** 243-250.

BECHT, N. O., MALIK, D. J. & TARLETON, E. S. 2008. Evaluation and comparison of protein ultrafiltration test results: Dead-end stirred cell compared with a cross-flow system. *Separation and Purification Technology,* 62**,** 228-239.

BINABAJI, E., RAO, S. & ZYDNEY, A. L. 2014. The osmotic pressure of highly concentrated monoclonal antibody solutions: effect of solution conditions. *Biotechnology and Bioengineering,* 111**,** 529-36.

BO, H., CHEN, J., LIANG, T., LI, S., SHAO, H. & HUANG, S. 2015. Chromatographic purification of adenoviral vectors on anion-exchange resins. *European Journal of Pharmaceutical Sciences,* 67**,** 119-125.

BOLTON, G., LACASSE, D. & KURIYEL, R. 2006. Combined models of membrane fouling: Development and application to microfiltration and ultrafiltration of biological fluids. *Journal of Membrane Science,* 277**,** 75-84.

BOWEN, W. R. & HUGHES, D. T. 1991. Properties of microfiltration membranes - the surface electrochemistry of anodic film membranes. *Journal of Colloid and Interface Science,* 143**,** 252-265.

BOYD, R. F. & ZYDNEY, A. L. 1998. Analysis of protein fouling during ultrafiltration using a two-layer membrane model. *Biotechnology and Bioengineering,* 59**,** 451-60.

BRAAS, G. M. F., WALKER, S. G. & LYDDIATT, A. 2000. Recovery in aqueous two-phase systems of nanoparticulates applied as surrogate mimics for viral gene therapy vectors. *Journal of Chromatography B: Biomedical Sciences and Applications,* 743**,** 409-419.

BURDEN, C. S., JIN, J., PODGORNIK, A. & BRACEWELL, D. G. 2012. A monolith purification process for virus-like particles from yeast homogenate. *Journal of Chromatography B,* 880**,** 82-9.

BUROVA, E. & LOFFE, E. 2005. Chromatooraphic purification of recombinant adenoviral and adeno-associated viral vectors: methods and implications. *Gene Therapy,* 12**,** S5-S17.

CAO, W., OU, S., LIN, W. & TANG, C. 2016. Food protein-based phytosterol nanoparticles: fabrication and characterization. *Food & Function,* 7**,** 3973-3980.

CARVALHO, P. M., FELÍCIO, M. R., SANTOS, N. C., GONÇALVES, S. & DOMINGUES, M. M. 2018. Application of Light Scattering Techniques to Nanoparticle Characterization and Development. *Frontiers in Chemistry,* 6**,** 1-17.

CELGENE. 2015. *FULL PRESCRIBING INFORMATION ABRAXANE® for Injectable Suspension (paclitaxel protein-bound particles for injectable suspension)* [Online]. USA: Celgene. Available: http://media.celgene.com/content/uploads/abraxane-pi.pdf [Accessed 24-04 2018].

CHAHAL, P. S., AUCOIN, M. G. & KAMEN, A. 2007. Primary recovery and chromatographic purification of adeno-associated virus type 2 produced by baculovirus/insect cell system. *Journal of Virological Methods,* 139**,** 61-70.

CHATURVEDI, P., RODRIGUEZ, S. D., VLASSIOUK, I., HANSEN, I. A. & SMIRNOV, S. N. 2016. Simple and versatile detection of viruses using anodized alumina membranes. *ACS Sensors,* 1**,** 488-492.

CHEANG, B. & ZYDNEY, A. L. 2003. Separation of alpha-lactalbumin and beta-lactoglobulin using membrane ultrafiltration. *Biotechnology and Bioengineering,* 83**,** 201-9.

CHEN, C. C., LAI, Z. L., WANG, G. J. & WU, C. Y. 2016. Polymerase chain reaction-free detection of hepatitis B virus DNA using a nanostructured impedance biosensor. *Biosensor and Bioelectronics,* 77**,** 603-8.

CHEN, W., YUAN, J. H. & XIA, X. H. 2005. Characterization and manipulation of the electroosmotic flow in porous anodic alumina membranes. *Analytical Chemistry,* 77**,** 8102-8.

CHERYAN, M. 1998. Membrane chemistry, structure and function. *In:* CHERYAN, M. (ed.) *Ultrafiltration and Microfiltration Handbook.* 2nd ed. USA: CRC Press.

CHOI, H., ZHANG, K., DIONYSIOU, D. D., OERTHER, D. B. & SORIAL, G. A. 2005. Influence of cross-flow velocity on membrane performance during filtration of biological suspension. *Journal of Membrane Science,* 248**,** 189-199.

CHOUDHARY, E. & SZALAI, V. 2016. Two-Step Cycle for Producing Multiple Anodic Aluminum Oxide (AAO) Films with Increasing Long-Range Order. *RSC Advances,* 6**,** 67992-67996.

CZERMAK, P., GRZENIA, D. L., WOLF, A., CARLSON, J. O., SPECHT, R., HAN, B. & WICKRAMASINGHE, S. R. 2008. Purification of the densonucleosis virus by tangential flow ultrafiltration and by ion exchange membranes. *Desalination,* 224**,** 23-27.

DENG, J. J. & TOH, C. S. 2013. Impedimetric DNA biosensor based on a nanoporous alumina membrane for the detection of the specific oligonucleotide sequence of dengue virus. *Sensors,* 13**,** 7774-7785.

DENG, L., KIM, J., CHANG, T., ZHANG, H., MOHAN, T., CHAMPION, J. & WANG, B. 2017. Protein nanoparticle vaccine based on flagellin carrier fused to influenza conserved epitopes confers full protection against influenza A virus challenge. *Virology,* 509**,** 82-89.

DODS, S. R., HARDICK, O., STEVENS, B. & BRACEWELL, D. G. 2015. Fabricating electrospun cellulose nanofibre adsorbents for ion-exchange chromatography. *Journal of Chromatography A,* 1376**,** 74-83.

DREIS, S., ROTHWELLER, F., MICHAELIS, A., CINATL, J., KREUTER, J. & LANGER, K. 2007. Preparation, characterisation and maintenance of drug efficacy of doxorubicin-loaded human serum albumin (HSA) nanoparticles. *International Journal of Pharmaceutics,* 341**,** 207-214.

FALLAHIANBIJAN, F., GIGLIA, S., CARBRELLO, C. & ZYDNEY, A. L. 2017. Use of fluorescently-labeled nanoparticles to study pore morphology and virus capture in virus filtration membranes. *Journal of Membrane Science,* 536**,** 52-58.

FEINBERG, B., HSIAO, J., PARK, J., ZYDNEY, A., FISSELL, W. & ROY, S. 2018. Slit pores preferred over cylindrical pores for high selectivity in biomolecular filtration. *Journal of Colloid and Interface Science,* 517**,** 176-181.

FERNANDES, C. S., GONCALVES, B., SOUSA, M., MARTINS, D. L., BARROSO, T., PINA, A. S., PEIXOTO, C., AGUIAR-RICARDO, A. & ROQUE, A. C. 2015. Biobased monoliths for adenovirus purification. *ACS Applied Materials & Interfaces,* 7**,** 6605-12.

GALISTEO-GONZALEZ, F. & MOLINA-BOLIVAR, J. 2014. Systematic study on the preparation of BSA nanoparticles. *Colloids and Surfaces B-Biointerfaces,* 123**,** 286-292.

GE HEALTHCARE LIFE SCIENCES. 2018. *Anodisc circle with support ring : Overview* [Online]. GE Life Sciences. Available: https://www.gelifesciences.com/en/gb/shop/whatman-laboratory-filtration/membranes-circles-sheets-and-reels/anopore-membranes/anodisc-circle-with-support-ring-p-05830 [Accessed 02/11/2018 2018].

GINN, S., AMAYA, A., ALEXANDER, I., EDELSTEIN, M. & ABEDI, M. 2018. Gene therapy clinical trials worldwide to 2017: An update. *The Journal of Gene Medicine***,** 16.

GRZENIA, D. L., CARLSON, J. O., CZERMAK, P., HAN, B., SPECHT, R. K. & WICKRAMASINGHE, S. R. 2006. Purification of densonucleosis virus by tangential flow ultrafiltration. *Biotechnology Progress,* 22**,** 1346-53.

GRZENIA, D. L., CARLSON, J. O. & WICKRAMASINGHE, S. R. 2008. Tangential flow filtration for virus purification. *Journal of Membrane Science,* 321**,** 373-380.

GULFAM, M., KIM, J., LEE, J., KU, B., CHUNG, B. & CHUNG, B. 2012. Anticancer drug-loaded gliadin nanoparticles induce apoptosis in breast cancer cells. *Langmuir,* 28**,** 8216-8223.

HARDICK, O., DODS, S., STEVENS, B. & BRACEWELL, D. G. 2013. Nanofiber adsorbents for high productivity downstream processing. *Biotechnology and Bioengineering,* 110**,** 1119-28.

HO, C. C. & ZYDNEY, A. L. 1999. Effect of membrane morphology on the initial rate of protein fouling during microfiltration. *Journal of Membrane Science,* 155**,** 261-275.

HO, C. C. & ZYDNEY, A. L. 2000. A combined pore blockage and cake filtration model for protein fouling during microfiltration. *Journal of Colloid and Interface Sciences,* 232**,** 389-399.

HO, C. C. & ZYDNEY, A. L. 2001. Protein fouling of asymmetric and composite microfiltration membranes. *Industrial & Engineering Chemistry Research,* 40**,** 1412-1421.

JEON, G., JEE, M., YANG, S. Y., LEE, B. Y., JANG, S. K. & KIM, J. K. 2014. Hierarchically self-organized monolithic nanoporous membrane for excellent virus enrichment. *ACS Applied Materials & Interfaces,* 6**,** 1200-1206.

JEONG, Y. & YI, C. 2013. Novel light reinforced materials using surface modified alumina using silane coupling agents. *Journal of Ceramic Processing Research,* 14**,** 213-216.

JIN, M., SZAPIEL, N., ZHANG, J., HICKEY, J. & GHOSE, S. 2010. Profiling of host cell proteins by two-dimensional difference gel electrophoresis (2D-DIGE): Implications for downstream process development. *Biotechnology and Bioengineering,* 105**,** 306-16.

JOHNSTON, S. T., SMITH, K. A. & DEEN, W. M. 2001. Concentration polarization in stirred ultrafiltration cells. *AIChE Journal,* 47**,** 1115-1125.

JONES, D. S., ROWE, C. G., CHEN, B., REITER, K., RAUSCH, K. M., NARUM, D. L., WU, Y. & DUFFY, P. E. 2016. A method for producing protein nanoparticles with applications in vaccines. *PLoS One,* 11**,** e0138761.

JUN, J., HOANG, H., PAIK, S., CHUN, H., KANG, B. & KO, S. 2011. Preparation of size-controlled bovine serum albumin (BSA) nanoparticles by a modified desolvation method. *Food Chemistry,* 127**,** 1892-1898.

KALASHNIKOVA, I. V., IVANOVA, N. D., EVSEEVA, T. G., MENSHIKOVA, A. Y., VLAKH, E. G. & TENNIKOVA, T. B. 2007. Study of dynamic adsorption behavior of large-size protein-bearing particles. *Journal of Chromatography A,* 1144**,** 40-7.

KANANI, D., FISSELL, W., ROY, S., DUBNISHEVA, A., FLEISCHMAN, A. & ZYDNEY, A. 2010. Permeability-selectivity analysis for ultrafiltration: Effect of pore geometry. *Journal of Membrane Science,* 349**,** 405-410.

KATO, H. 2018. Size determination of nanoparticles by dynamic light scattering - Nanomaterials - Wiley Online Library. *In:* SINGH, S. C. & ZENG, H. (eds.).

KELLY, S. T. & ZYDNEY, A. L. 1997. Protein fouling during microfiltration: comparative behavior of different model proteins. *Biotechnology and Bioengineering,* 55**,** 91-100.

KOSIOL, P., HANSMANN, B., ULBRICHT, M. & THOM, V. 2017. Determination of pore size distributions of virus filtration membranes using gold nanoparticles and their correlation with virus retention. *Journal of Membrane Science,* 533**,** 289-301.

LADD EFFIO, C., WENGER, L., OTES, O., OELMEIER, S. A., KNEUSEL, R. & HUBBUCH, J. 2015. Downstream processing of virus-like particles: single-stage and multi-stage aqueous two-phase extraction. *Journal of Chromatography A,* 1383**,** 35-46.

LANGER, K., ANHORN, M. G., STEINHAUSER, I., DREIS, S., CELEBI, D., SCHRICKEL, N., FAUST, S. & VOGEL, V. 2008. Human serum albumin (HSA) nanoparticles: reproducibility of preparation process and kinetics of enzymatic degradation. *International Journal of Pharmaceutics,* 347**,** 109-17.

LANGER, K., BALTHASAR, S., VOGEL, V., DINAUER, N., VON BRIESEN, H. & SCHUBERT, D. 2003. Optimization of the preparation process for human serum albumin (HSA) nanoparticles. *International Journal of Pharmaceutics,* 257**,** 169-80.

LEE, C., KANG, H., CHANG, Y. & HAHM, Y. 2000. Thermotreatment and chemical resistance of porous alumina membrane prepared by anodic oxidation | SpringerLink. *Korean Journal of Chemical Engineering,* 17**,** 266-272.

LEE, K. P. 2013. *Fabrication and applications of nanoporous alumina membranes.* Ph.D., University of Bath.

LEE, K. P. & MATTIA, D. 2013. Monolithic nanoporous alumina membranes for ultrafiltration applications: Characterization, selectivity-permeability analysis and fouling studies. *Journal of Membrane Science,* 435**,** 52-61.

LEE, S., SHANG, H., HAASCH, R., PETROVA, V. & LEE, G. 2005. Transport and functional behaviour of poly(ethylene glycol)-modified nanoporous alumina membranes. *Nanotechnology,* 16**,** 1335-1340.

LEE, W. & PARK, S. 2014. Porous Anodic Aluminum Oxide: Anodization and Templated Synthesis of Functional Nanostructures. *Chemical Reviews,* 114**,** 7487-7556.

LEI, Y., CAI, W. & WILDE, G. 2007. Highly ordered nanostructures with tunable size, shape and properties: A new way to surface nano-patterning using ultra-thin alumina masks. *Progress in Materials Science,* 52**,** 465-539.

LIN, T., ZHAO, P., JIANG, Y., TANG, Y., JIN, H., PAN, Z., HE, H., YANG, V. C. & HUANG, Y. 2016. Blood-brain-barrier-penetrating albumin nanoparticles for biomimetic drug delivery via albumin-binding protein pathways for antiglioma therapy. *ACS Nano,* 10**,** 9999-10012.

LOCK, M., MCGORRAY, S., AURICCHIO, A., AYUSO, E., BEECHAM, E., BLOUIN-TAVEL, V., BOSCH, F., BOSE, M., BYRNE, B., CATON, T., CHIORINI, J., CHTARTO, A., CLARK, K., CONLON, T., DARMON, C., DORIA, M., DOUAR, A., FLOTTE, T., FRANCIS, J., FRANCOIS, A., GIACCA, M., KORN, M., KORYTOV, I., LEON, X., LEUCHS, B., LUX, G., MELAS, C., MIZUKAMI, H., MOULLIER, P., MULLER, M., OZAWA, K., PHILIPSBERG, T., POULARD, K., RAUPP, C., RIVIERE, C., ROOSENDAAL, S., SAMULSKI, R., SOLTYS, S., SUROSKY, R., TENENBAU, L., THOMAS, D., VAN MONTFORT, B., VERES, G., WRIGHT, J., XU, Y., ZELENAIA, O., ZENTILIN, L. & SNYDER, R. 2010. Characterization of a recombinant adeno-associated virus type 2 reference standard material. *Human Gene Therapy,* 21**,** 1273-1285.

LOOK, J., WILHELM, N., VON BRIESEN, H., NOSKE, N., GUNTHER, C., LANGER, K. & GORJUP, E. 2015. Ligand-modified human serum albumin nanoparticles for enhanced gene delivery. *Molecular Pharmaceutics,* 12**,** 3202-13.

LUCERO, A. T., MERCADO, S. A., SANCHEZ, A. C., CONTADOR, C. A., ANDREWS, B. A. & ASENJO, J. A. 2017. Purification of adenoviral vector serotype 5 for gene therapy against alcoholism using anion exchange chromatography. *Journal of Chemical Technology and Biotechnology,* 92**,** 2445-2452.

LUECHAU, F., LING, T. C. & LYDDIATT, A. 2011. Recovery of B19 virus-like particles by aqueous two-phase systems. *Food and Bioproducts Processing,* 89**,** 322-327.

LUTZ, H., ARIAS, J. & ZOU, Y. 2017. High concentration biotherapeutic formulation and ultrafiltration: Part 1 pressure limits. *Biotechnology Progress,* 33**,** 113-124.

MALLOY, A. 2011. Count, size and visualize nanoparticles. *Materials Today,* 14**,** 170-173.

MARTINEZ, F., MARTIN, A., PRADANOS, P., CALVO, J. I., PALACIO, L. & HERNANDEZ, A. 2000. Protein adsorption and deposition onto microfiltration membranes: the role of solute-solid interactions. *Journal of Colloid and Interface Science,* 221**,** 254-261.

MASUDA, H. & FUKUDA, K. 1995. Ordered metal nanohole arrays made by a two-step replication of honeycomb structures of anodic alumina. *Science,* 268**,** 1466-1468.

MEHTA, A. & ZYDNEY, A. L. 2005. Permeability and selectivity analysis for ultrafiltration membranes. *Journal of Membrane Science,* 249**,** 245-249.

MI, X. & HELDT, C. L. 2014. Adsorption of a non-enveloped mammalian virus to functionalized nanofibers. *Colloids and Surfaces B: Biointerfaces,* 121**,** 319-24.

MIAO, R., WANG, L., ZHU, M., DENG, D., LI, S., WANG, J., LIU, T. & LV, Y. 2017. Effect of hydration forces on protein fouling of ultrafiltration membranes: the role of protein charge, hydrated ion species, and membrane hydrophilicity. *Environmental Science and Technology,* 51**,** 167-174.

MILLESIME, L., DULIEU, J. & CHAUFER, B. 1996. Fractionation of proteins with modified membranes. *Bioseparation,* 6**,** 135-45.

MINGOZZI, F. & HIGH, K. 2013. Immune responses to AAV vectors: overcoming barriers to successful gene therapy. *Blood,* 122**,** 23-36.

MOON, J. M., AKIN, D., XUAN, Y., YE, P. D., GUO, P. X. & BASHIR, R. 2009. Capture and alignment of phi29 viral particles in sub-40 nanometer porous alumina membranes. *Biomedical Microdevices,* 11**,** 135-142.

MORENWEISER, R. 2005. Downstream processing of viral vectors and vaccines. *Gene Therapy,* 12 Suppl 1**,** S103-10.

MU, L.-J. & ZHAO, W.-Z. 2009. Hydrophilic modification of polyethersulfone porous membranes via a thermal-induced surface crosslinking approach. *Applied Surface Science,* 255**,** 7273-7278.

MULHERKAR, P. & VAN REIS, R. 2004. Flex test: a fluorescent dextran test for UF membrane characterization. *Journal of Membrane Science,* 236**,** 171-182.

MULLER, B. G., LEUENBERGER, H. & KISSEL, T. 1996. Albumin nanospheres as carriers for passive drug targeting: an optimized manufacturing technique. *Pharmaceutical Research,* 13**,** 32-7.

MULLIN, E. 2017. *Tracking the Cost of Gene Therapy* [Online]. USA: @techreview. Available: https://www.technologyreview.com/s/609197/tracking-the-cost-of-gene-therapy/ [Accessed 04/05 2018].

NAGALE, M., KIM, B. & BRUENING, M. 2000. Ultrathin, hyperbranched poly(acrylic acid) membranes on porous alumina supports. *Journal of the American Chemical Society,* 122**,** 11670-11678.

NARSAIAH, K. & AGARWAL, G. 2007. Transmission analysis in ultrafiltration of ternary protein mixture through a hydrophilic membrane. *Journal of Membrane Science,* 287**,** 9-18.

NEMATI, M., SANTOS, A., KUMERIA, T. & LOSIC, D. 2015. Label-Free real-time quantification of enzyme levels by interferometric spectroscopy combined with gelatin-modified nanoporous anodic alumina photonic films. *Analytical Chemistry,* 87**,** 9016-24.

NEMATI, M., SANTOS, A., LAW, C. S. & LOSIC, D. 2016. Assessment of binding affinity between drugs and human serum albumin using nanoporous anodic alumina photonic crystals. *Analytical Chemistry,* 88**,** 5971-80.

NESTOLA, P., MARTINS, D. L., PEIXOTO, C., ROEDERSTEIN, S., SCHLEUSS, T., ALVES, P. M., MOTA, J. P. B. & CARRONDO, M. J. T. 2014a. Evaluation of novel large cut-off ultrafiltration membranes for adenovirus serotype 5 (Ad5) concentration. *PLoS ONE,* 9**,** 22.

NESTOLA, P., SILVA, R. J., PEIXOTO, C., ALVES, P. M., CARRONDO, M. J. & MOTA, J. P. 2014b. Adenovirus purification by two-column, size-exclusion, simulated countercurrent chromatography. *Journal of Chromatography A,* 1347**,** 111-21.

NESTOLA, P., VILLAIN, L., PEIXOTO, C., MARTINS, D. L., ALVES, P. M., CARRONDO, M. J. & MOTA, J. P. 2014c. Impact of grafting on the design of new membrane adsorbers for adenovirus purification. *Journal of Biotechnology,* 181**,** 1-11.

NI, S., LI, C., NI, S., CHEN, T. & WEBSTER, T. 2014. Understanding improved osteoblast behavior on select nanoporous anodic alumina. *International Journal of Nanomedicine,* 9**,** 3325-3334.

NOBBMANN, U., CONNAH, M., FISH, B., VARLEY, P., GEE, C., MULOT, S., CHEN, J., ZHOU, L., LU, Y., SHENG, F., YI, J. & HARDING, S. E. 2007. Dynamic light scattering as a relative tool for assessing the molecular integrity and stability of monoclonal antibodies. *Biotechnology and Genetic Engineering Reviews,* 24**,** 117-128.

O'SULLIVAN, J. P. & WOOD, G. C. 1970. The morphology and mechanism of formation of porous anodic films on aluminium. *Proceedings of the Royal Society of London. Series A, Mathematical and Physical Sciences,* 317**,** 511-543.

ORR, V., ZHONG, L., MOO-YOUNG, M. & CHOU, C. P. 2013. Recent advances in bioprocessing application of membrane chromatography. *Biotechnology Advances,* 31**,** 450-465.

OSMANBEYOGLU, H. U., HUR, T. B. & KIM, H. K. 2009. Thin alumina nanoporous membranes for similar size biomolecule separation. *Journal of Membrane Science,* 343**,** 1-6.

PAIK, S., NGUYEN, H., RYU, J., CHE, J., KANG, T., LEE, J., SONG, C. & KO, S. 2013. Robust size control of bovine serum albumin (BSA) nanoparticles by intermittent addition of a desolvating agent and the particle formation mechanism. *Food Chemistry,* 141**,** 695-701.

PALACIO, L., HO, C. C. & ZYDNEY, A. L. 2002. Application of a pore-blockage--cake-filtration model to protein fouling during microfiltration. *Biotechnology and Bioengineering,* 79**,** 260-70.

PEDIMONTE, B. J., MOEST, T., LUXBACHER, T., VON WILMOWSKY, C., FEY, T., SCHLEGEL, K. A. & GREIL, P. 2014a. Morphological zeta-potential variation of nanoporous anodic alumina layers and cell adherence. *Acta Biomaterialia,* 10**,** 968-974.

PEDIMONTE, B. J., MOEST, T., LUXBACHER, T., VON WILMOWSKY, C., FEY, T., SCHLEGEL, K. A. & GREIL, P. 2014b. Morphological zeta-potential variation of nanoporous anodic alumina layers and cell adherence. *Acta Biomaterialia,* 10**,** 968-74.

PEIXOTO, C., FERREIRA, T. B., SOUSA, M. F., CARRONDO, M. J. & ALVES, P. M. 2008. Towards purification of adenoviral vectors based on membrane technology. *Biotechnology Progress,* 24**,** 1290-6.

PONDER, K. P. 2002. Vectors in Gene Therapy. *In:* KRESINA, T. F. (ed.) *An Introduction to Molecular Medicine and Gene Therapy.* New York,USA: Wiley-Liss, Inc. .

POPAT, K., MOR, G., GRIMES, C. & DESAI, T. 2004. Surface modification of nanoporous alumina surfaces with poly(ethylene glycol). *Langmuir,* 20**,** 8035-8041.

PORTER, M. C. 1972. Concentration polarization with membrane ultrafiltration. *Industrial & Engineering Chemistry Product Research and Development,* 11**,** 234-&.

POTTER, M., LINS, B., MIETZSCH, M., HEILBRONN, R., VAN VLIET, K., CHIPMAN, P., AGBANDJE-MCKENNA, M., CLEAVER, B. D., CLEMENT, N., BYRNE, B. J. & ZOLOTUKHIN, S. 2014. A simplified purification protocol for recombinant adeno-associated virus vectors. *Molecular Therapy - Methods & Clinical Development,* 1**,** 14034.

PRADANOS, P., ARRIBAS, J. I. & HERNANDEZ, A. 1994. Retention of proteins in cross-flow UF through asymmetric inorganic membranes. *AIChE Journal,* 40**,** 1901-1910.

PRADANOS, P., HERNANDEZ, A., CALVO, J. I. & TEJERINA, F. 1996. Mechanisms of protein fouling in cross-flow UF through an asymmetric inorganic membrane. *Journal of Membrane Science,* 114**,** 115-126.

QU, G., BAHR-DAVIDSON, J., PRADO, J., TAI, A., CATANIAG, F., MCDONNELL, J., ZHOU, J., HAUCK, B., LUNA, J., SOMMER, J. M., SMITH, P., ZHOU, S., COLOSI, P., HIGH, K. A., PIERCE, G. F. & WRIGHT, J. F. 2007. Separation of adeno-associated virus type 2 empty particles from genome containing vectors by anion-exchange column chromatography. *Journal of Virological Methods,* 140**,** 183-92.

QU, W., WANG, M., WU, Y. & XU, R. 2015. Scalable downstream strategies for purification of recombinant adeno-associated virus vectors in light of the properties. *Current Pharmaceutical Biotechnology.*

RADER, R. A. 2018. *Overcoming The Manufacturing Hurdles Of Cell Gene Therapy* [Online]. BioProcessOnline. Available: https://www.bioprocessonline.com/doc/overcoming-the-manufacturing-hurdles-of-cell-gene-therapy-0001 [Accessed 10/03/2018].

RODRIGUES, T., CARVALHO, A., CARMO, M., CARRONDO, M. J., ALVES, P. M. & CRUZ, P. E. 2007. Scaleable purification process for gene therapy retroviral vectors. *Journal of Gene Medicine,* 9**,** 233-43.

RUSCIC, J., PERRY, C., BRACEWELL, D. G., MUKHOPADAYA, T. & TAKEUCHI, Y. Nanofiber based lentiviral vector production. *In:* CHEN, W., BORTH, N. & GRAMMATIKOS, S., eds. Biochemical and Molecular Engineering XX, July 17-20 2017 Newport Beach, CA, USA. ECI Symposium Series.

SEGURA, M. M., PUIG, M., MONFAR, M. & CHILLON, M. 2012. Chromatography purification of canine adenoviral vectors. *Human Gene Therapy Methods,* 23**,** 182-97.

SHI, W., SHEN, Y. Q., GE, D. T., XUE, M. Q., CAO, H. H., HUANG, S. Q., WANG, J. X., ZHANG, G. L. & ZHANG, F. B. 2008. Functionalized anodic aluminum oxide (AAO) membranes for affinity protein separation. *Journal of Membrane Science,* 325**,** 801-808.

SHI, W., SHEN, Y. Q., JIANG, H. R., SONG, C. F., MA, Y. Y., MU, J., YANG, B. Y. & GE, D. T. 2010. Lysine-attached anodic aluminum oxide (AAO)-silica affinity membrane for bilirubin removal. *Journal of Membrane Science,* 349**,** 333-340.

SHIMIZU, K., KOBAYASHI, K., THOMPSON, G. E. & WOOD, G. C. 1992. Development of porous anodic films on aluminium. *Philosophical Magazine A,* 66**,** 643-652.

SHUKLA, R., BALAKRISHNAN, M. & AGARWAL, G. P. 2000. Bovine serum albumin-hemoglobin fractionation: significance of ultrafiltration system and feed solution characteristics. *Bioseparation,* 9**,** 7-19.

SKELDON, P., THOMPSON, G. E., GARCIA-VERGARA, S. J., IGLESIAS-RUBIANES, L. & BLANKO-PINZON, C. E. 2006. A tracer study of porous anodic alumina. *Electrochemical and Solid-State Letters,* 9**,** 47-51.

SMITH, J., HANG, Q., FRANKLIN, A., JANES, D. & SANDS, T. 2008. Highly ordered diamond and hybrid triangle-diamond patterns in porous anodic alumina thin films. *Applied Physics Letters,* 93.

SMITH, K. A. & COLTON, C. K. 1972. Mass transfer to a rotating fluid : Part I. Transport from a stationary disk to a fluid in Bodewadt flow. *AIChE Journal,* 18.

SMITH, R. H., LEVY, J. R. & KOTIN, R. M. 2009. A simplified baculovirus-AAV expression vector system coupled with one-step affinity purification yields high-titer rAAV stocks from insect cells. *Molecular Therapy,* 17**,** 1888-96.

SORCI, M., GU, M., HELDT, C. L., GRAFELD, E. & BELFORT, G. 2013. A multi-dimensional approach for fractionating proteins using charged membranes. *Biotechnology and Bioengineering,* 110**,** 1704-13.

STEINHAUSER, I., LANGER, K., STREBHARDT, K. & SPANKUCH, B. 2008. Effect of trastuzumab-modified antisense oligonucleotide-loaded human serum albumin nanoparticles prepared by heat denaturation. *Biomaterials,* 29**,** 4022-4028.

STORP, B., ENGEL, A., BOEKER, A., PLOEGER, M. & LANGER, K. 2012. Albumin nanoparticles with predictable size by desolvation procedure. *Journal of Microencapsulation,* 29**,** 138-46.

STROBEL, B., MILLER, F. D., RIST, W. & LAMLA, T. 2015. Comparative analysis of cesium chloride- and iodixanol-based purification of recombinant adeno-associated viral Vectors for preclinical applications. *Human Gene Therapy Methods,* 26**,** 147-57.

STROEVE, P. & ILERI, N. 2011. Biotechnical and other applications of nanoporous membranes. *Trends in Biotechnology,* 29**,** 259-266.

SUBRAMANIAN, S., ALTARAS, G. M., CHEN, J., HUGHES, B. S., ZHOU, W. & ALTARAS, N. E. 2005. Pilot-scale adenovirus seed production through concurrent virus release and concentration by hollow fiber filtration. *Biotechnology Progress,* 21**,** 851-9.

SULKA, G. D. 2008. Highly ordered anodic porous alumina formation by self-organized anodizing - nanostructured materials in electrochemistry. *In:* EFTEKHARI, A. (ed.) *Nanostructured Materials in Electrochemistry.* Weinheim: Wiley-VCH Verlag GmbH & Co. KGaA.

SYEDAIN, Z. H., BOHONAK, D. M. & ZYDNEY, A. L. 2006. Protein fouling of virus filtration membranes: effects of membrane orientation and operating conditions. *Biotechnology Progress,* 22**,** 1163-9.

TANDON, A., GUPTA, S. K. & AGARWAL, G. P. 1994. Modelling of protein transmission through ultrafiltration membranes. *Journal of Membrane Science,* 97**,** 83-90.

THAMIDA, S. K. & CHANG, H. C. 2002. Nanoscale pore formation dynamics during aluminum anodization. *Chaos,* 12**,** 240-251.

THAO LE, Q., BYEON, H. J., LEE, C., LEE, S., LEE, E. S., CHOI, Y. W., CHOI, H. G., PARK, E. S., LEE, K. C. & YOUN, Y. S. 2016. Doxorubicin-bound albumin nanoparticles containing a TRAIL protein for targeted treatment of colon cancer. *Pharmaceutical Research,* 33**,** 615-26.

TILLEY, R. J. D. 2011. Colour due to scattering. *Colour and the optical properties of materials : An exploration of the relationship between light, the optical properties of materials and colour.* 2nd ed. United Kingdom: John Wiley & Sons.

TRILISKY, E. I., KOKU, H., CZYMMEK, K. J. & LENHOFF, A. M. 2009. Relation of structure to performance characteristics of monolithic and perfusive stationary phases. *Journal of Chromatography A,* 1216**,** 6365-6376.

TRILISKY, E. I. & LENHOFF, A. M. 2007. Sorption processes in ion-exchange chromatography of viruses. *J Chromatogr A,* 1142**,** 2-12.

TSANG, M. K., YE, W., WANG, G., LI, J., YANG, M. & HAO, J. 2016. Ultrasensitive detection of ebola virus oligonucleotide based on upconversion nanoprobe/nanoporous membrane system. *ACS Nano,* 10**,** 598-605.

URASE, T., YAMAMOTO, K. & OHGAKI, S. 1994. Effect of pore-size distribution of ultrafiltration membranes on virus rejection in cross-flow conditions. *Water Science and Technology,* 30**,** 199-208.

URASE, T., YAMAMOTO, K. & OHGAKI, S. 1996. Effect of pore structure of membranes and module configuration on virus retention. *Journal of Membrane Science,* 115**,** 21-29.

VAN REIS, R., GOODRICH, E. M., YSON, C. L., FRAUTSCHY, L. N., WHITELEY, R. & ZYDNEY, A. L. 1997. Constant Cwall ultrafiltration process control. *Journal of Membrane Science,* 130**,** 123-140.

VAN REIS, R. & ZYDNEY, A. 2007. Bioprocess membrane technology. *Journal of Membrane Science,* 297**,** 16-50.

VELASCO, C., OUAMMOU, M., CALVO, J. I. & HERNANDEZ, A. 2003. Protein fouling in microfiltration: deposition mechanism as a function of pressure for different pH. *Journal of Colloid and Interface Science,* 266**,** 148-52.

VIJAYARAGAVAN, K. S., ZAHID, A., YOUNG, J. W. & HELDT, C. L. 2014. Separation of porcine parvovirus from bovine serum albumin using PEG-salt aqueous two-phase system. *Journal of Chromatography B,* 967**,** 118-26.

VINCENT, D., KRAMBERGER, P., HUDEJ, R., STRANCAR, A., WANG, Y., ZHOU, Y. & VELAYUDHAN, A. 2017. The development of a monolith-based purification process for Orthopoxvirus vaccinia virus Lister strain. *Journal of Chromatography A,* 1524**,** 87-100.

WAEHLER, R., RUSSELL, S. J. & CURIEL, D. T. 2007. Engineering targeted viral vectors for gene therapy. *Nature Reviews Genetics,* 8**,** 573-87.

WANG, Y., CHEN, W., WU, J., GUO, Y. & XIA, X. 2007. Highly efficient and selective enrichment of phosphopeptides using porous anodic alumina membrane for MALDI-TOF MS analysis. *Journal of American Society of Mass Spectrometry,* 18**,** 1387-95.

WEBER, C., KREUTER, J. & LANGER, K. 2000. Desolvation process and surface characteristics of HSA-nanoparticles. *International Journal of Pharmaceutics,* 196**,** 197-200.

WEGGEMAN, M. 2013. *Virus purification using ultrafiltration*. 11/909,955. Nov. 5, 2013.

WICKRAMASINGHE, S. R., CARLSON, J. O., TESKE, C., HUBBUCH, J. & ULBRICHT, M. 2006. Characterizing solute binding to macroporous ion exchange membrane adsorbers using confocal laser scanning microscopy. *Journal of Membrane Science,* 281**,** 609-618.

WICKRAMASINGHE, S. R., KALBFUSS, B., ZIMMERMANN, A., THOM, V. & REICHL, U. 2005. Tangential flow microfiltration and ultrafiltration for human influenza A virus concentration and purification. *Biotechnology and Bioengineering,* 92**,** 199-208.

WILSON, J. M., AURICCHIO, A., HILDINGER, M. & PENNSYLVANIA, T. T. O. T. U. O. 2003. *Method for purification of viral vectors having proteins which bind sialic acid*.

WU, M. T., LEU, I. C. & HON, M. H. 2002. Effect of polishing pretreatment on the fabrication of ordered nanopore arrays on aluminum foils by anodization. *Journal of Vacuum Science & Technology B,* 20**,** 776-782.

WU, Y., ABRAHAM, D. & CARTA, G. 2016. Comparison of perfusion media and monoliths for protein and virus-like particle chromatography. *Journal of Chromatography A,* 1447**,** 72-81.

WU, Y., SIMONS, J., HOOSON, S., ABRAHAM, D. & CARTA, G. 2013. Protein and virus-like particle adsorption on perfusion chromatography media. *Journal of Chromatography A,* 1297**,** 96-105.

XIE, R., CHU, L.-Y., CHEN, W.-M., XIAO, W., WANG, H.-D. & QU, J.-B. 2005. Characterization of microstructure of poly(N-isopropylacrylamide)-grafted polycarbonate track-etched membranes prepared by plasma-graft pore-filling polymerization. *Journal of Membrane Science,* 258**,** 157-166.

YAMASHITA, T., KODAMA, S., KEMMEI, T., OHTO, M., NAKAYAMA, E., MURAMOTO, T., YAMAGUCHI, A., TERAMAE, N. & TAKAYANAGI, N. 2009. Separation of adenine, adenosine-5'-monophosphate and adenosine-5'-triphosphate by fluidic chip with nanometre-order diameter columns inside porous anodic alumina using an aqueous mobile phase. *Lab Chip,* 9**,** 1337-9.

YU, H., QIU, X., BEHZAD, A., MUSTEATA, V., SMILGIES, D., NUNES, S. & PEINEMANN, K. 2016. Asymmetric block copolymer membranes with ultrahigh porosity and hierarchical pore structure by plain solvent evaporation. *Chemical Communications,* 52**,** 12064-12067.

YU, M., LI, Y., ZHANG, S., LI, X., YANG, Y., CHEN, Y., MA, G. & SU, Z. 2014. Improving stability of virus-like particles by ion-exchange chromatographic supports with large pore size: Advantages of gigaporous media beyond enhanced binding capacity. *Journal of Chromatography A,* 1331**,** 69-79.

YUAN, J. H., HE, F. Y., SUN, D. C. & XIA, X. H. 2004. A simple method for preparation of through-hole porous anodic alumina membrane. *Chemistry of Materials,* 16**,** 1841-1844.

ZARASKA, L., SULKA, G. D. & JASKULA, M. 2011. Anodic alumina membranes with defined pore diameters and thicknesses obtained by adjusting the anodizing duration and pore opening/widening time. *Journal of Solid State Electrochemistry,* 15**,** 2427-2436.

ZAVECKAS, M., SNIPAITIS, S., PESLIAKAS, H., NAINYS, J. & GEDVILAITE, A. 2015. Purification of recombinant virus-like particles of porcine circovirus type 2 capsid protein using ion-exchange monolith chromatography. *Journal of Chromatography B,* 991**,** 21-8.

ZHANG, W. & ZHONG, Q. 2009. Microemulsions as nanoreactors to produce whey protein nanoparticles with enhanced heat stability by sequential enzymatic cross-linking and thermal pretreatments. *Journal of Agricultural and Food Chemistry,* 57**,** 9181-9.

ZHEN, X., WANG, X., XIE, C., WU, W. & JIANG, X. 2013. Cellular uptake, antitumor response and tumor penetration of cisplatin-loaded milk protein nanoparticles. *Biomaterials,* 34**,** 1372-1382.

ZHOU, J., YANG, X., WRIGHT, J. F., HIGH, K. A., COUTO, L. & QU, G. 2011. PEG-modulated column chromatography for purification of recombinant adeno-associated virus serotype 9. *Journal of Virological Methods,* 173**,** 99-107.

ZOU, L., ZHENG, B., ZHANG, R., ZHANG, Z., LIU, W., LIU, C., XIAO, H. & MCCLEMENTS, D. 2016. Food-grade nanoparticles for encapsulation, protection and delivery of curcumin: comparison of lipid, protein, and phospholipid nanoparticles under simulated gastrointestinal conditions. *RSC Advances,* 6**,** 3126-3136.

ZYDNEY, A. L. 1997. Stagnant film model for concentration polarization in membrane systems. *Journal of Membrane Science,* 130**,** 275-281.

ZYDNEY, A. L. & HO, C. C. 2003. Effect of membrane morphology on system capacity during normal flow microfiltration. *Biotechnology and Bioengineering,* 83**,** 537-43.

ZYDNEY, A. L. & XENOPOULOS, A. 2007. Improving dextran tests for ultrafiltration membranes: Effect of device format. *Journal of Membrane Science,* 291**,** 180-190.

APPENDICES

APPENDIX A

Size exclusion chromatography used for calculation of residual BSA in final protein nanoparticle preparations

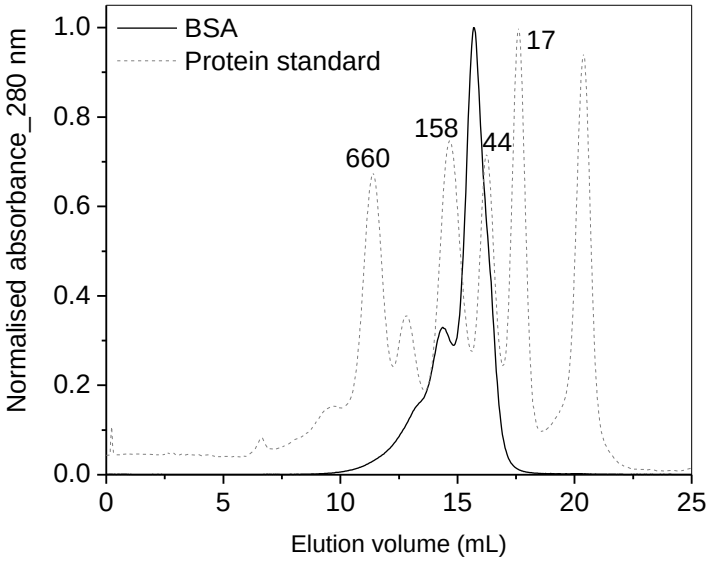

Appendix A-1: Protein molecular weight standards and BSA preparation used for nanoparticles preparations on a size exclusion column, Superose 6/12 (with a column volume of 24 mL). Equilibration and elution were carried out using PBS. A sample volume of 100µl was injected. Peak labels represent the molecular weight (kDa) of the peak protein.

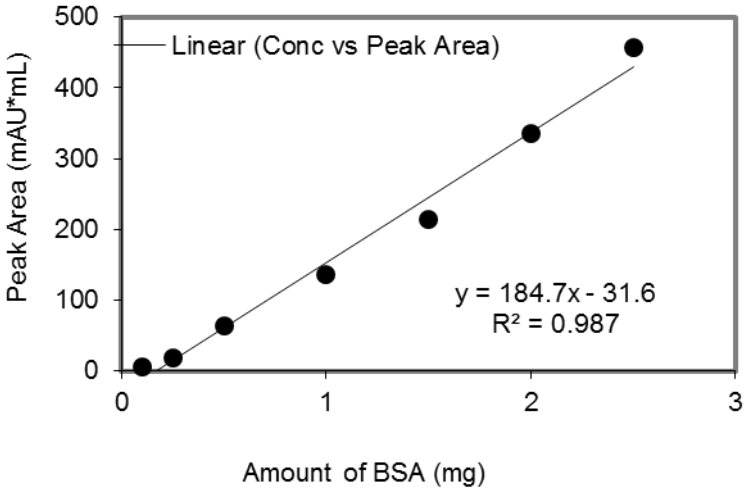

Appendix A-2: Standard curve for BSA on SEC column at 0.5 mL/min flow rate in isocratic elution under PBS as the mobile phase. Superose 6/12 column (column volume of 24 mL) was used to plot a standard curve for BSA. The plot was used to measure residual BSA concentration in nanoparticle preparations.

APPENDIX B

Effect of vessel dimensions on nanoparticle preparation

Parameters	Beaker 50 mL	Beaker 30 mL	Beaker 100 mL
Vessel Height /Diameter mm/mm (Ratio)	60/31 (1.93)	40/30 (1.33)	66/45 (1.43)
Effective Height /Diameter (with liquid level of 20mL solution)	24/31 (0.80)	24/30 (0.80)	15/45 (0.33)
Initial BSA concentration (% w/v)	1	1	1
Initial BSA volume (mL)	20	20	20
Stirring (rpm)	1000	1000	1000
Volume of ethanol added (mL)	15	14	30
Foaming observed	NO	NO	YES
Particle diameter, nm (after 15 mL addition)	129 ± 6	100 ± 1	71 ± 2
Polydispersity index, PDI	0.14 ± 0.05	0.25 ± 0.01	0.48 ± 0.01
Particle diameter, nm (Final, after crosslinking)	129 ± 6	100 ± 1	139 ± 17
Polydispersity index, PDI	0.137 ± 0.05	0.245 ± 0.007	0.334 ± 0.018

APPENDIX C

Effect of volumetric scale-up of BSA nanoparticle synthesis using method C

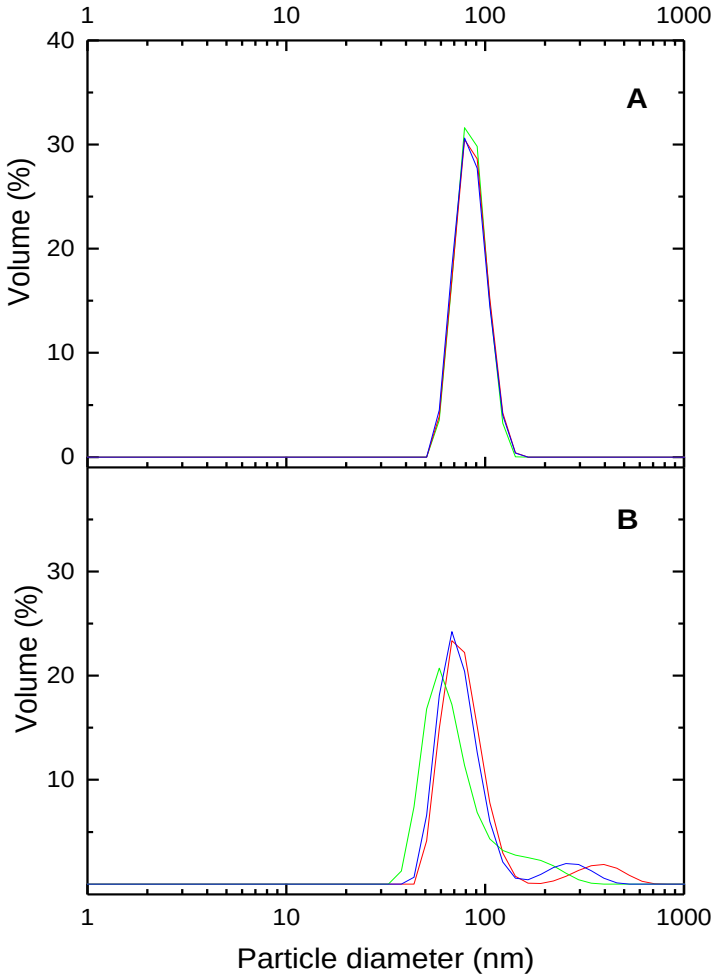

Differences in the particle size distribution between nanoparticle preparations prepared with an original volume of 1 mL (A) and scaled-up volume of 3 mL (B) for method C.

APPENDIX D

Particle size distribution of various model solutes used in filtration studies and latex size standard

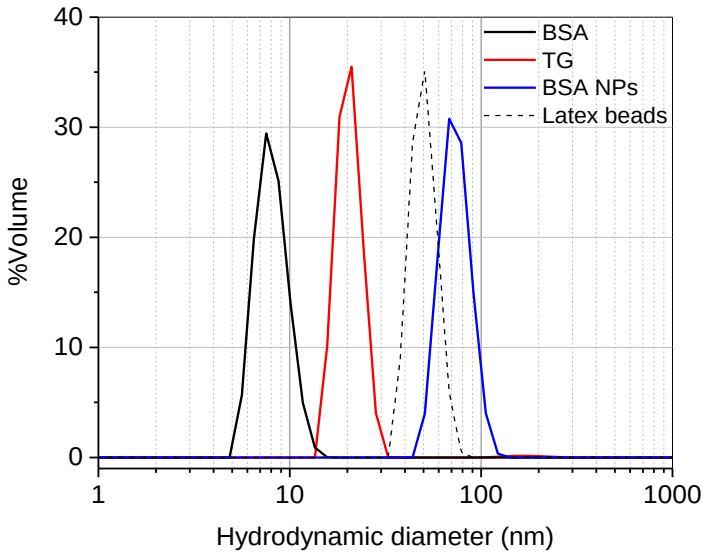

Protein solutions in PBS with concentrations 1.0, 0.5 and 1.0 mg/mL for BSA, TG and BSA nanoparticles were used for measurement of particle size using dynamic light scattering (Zetasizer, Malvern UK) Monodisperse solution of latex nanoparticles (46 nm, Nanosphere, ThermoScientific) was used as size standard to check calibration of the equipment**.**

APPENDIX E

Debris observed on the surface of PAA membranes

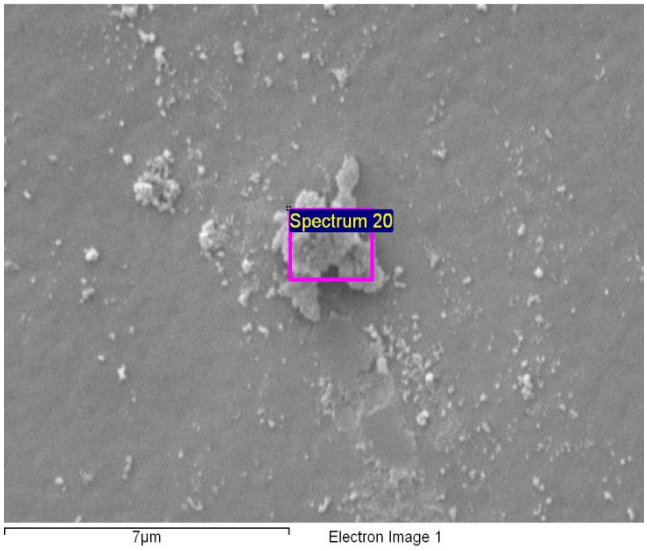

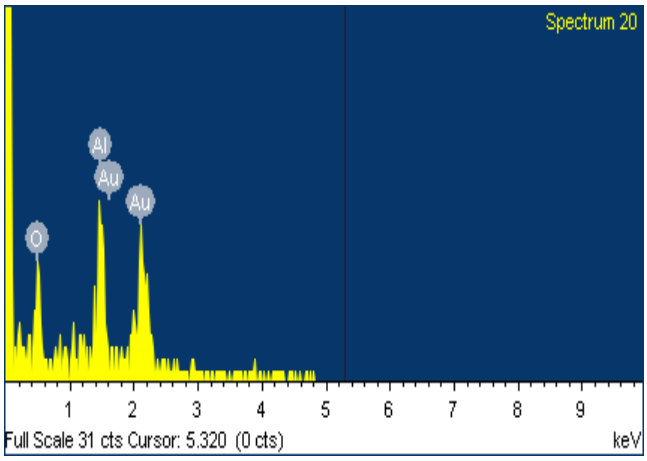

Elemental analysis of the debris observed on the surface of anodic alumina membrane using energy dispersive X-ray spectroscopy (EDS). Elements identified are Al-Aluminium, O-Oxygen and Au-Silver deposited during sputter coating.

APPENDIX F

Calculation of mass transfer coefficient for a solute in stirred cell filtration

Mass transfer coefficient (k_m) for a solute of a given bulk diffusivity (D) in solution with given bulk properties (viscosity, μ, and density ρ) can be calculated in a stirred cell of a given diameter (T) operating at a given rotation speed (ω) using following equations (as described by Smith and Colton, 1972):

Calculate Reynold's number for the stirred cell and the bulk solution

$$Re = \frac{\rho\omega\left(T/2\right)^2}{\mu}$$

Calculate Sherwood number for the stirred cell using empirical relationship described for Sherwood number and Reynold's and Schmidt number

$$Sc = \frac{\mu}{\rho D}$$

$$Sh = 0.285Re^{0.567}Sc^{0.33}\ ;\ 8000 < Re < 32000$$

Calculate mass transfer coefficient (k_m) using the following expression

$$Sh = \frac{k_m\left(T/2\right)}{D}$$

For calculations, bulk properties of all protein solutions were assumed similar (as dilute protein solutions were used) with a viscosity of 0.00099 kg/m.s and fluid density of 997 kg/m^3.

For a stirred cell with 25mm diameter (T) and stirring speed of 1500 rpm, the mass transfer coefficients (k_m) for different model solutes were calculated to be:

Solute	**Solute size (nm)**	**D (μm^2/s)**	**k_m (m/s)**
BSA	8	56.9	9.4 x 10^{-6}
TG	22	21.6	6.3 x 10^{-6}
BSA NP	80	5.7	2.2 x 10^{-6}

Table: Particle size and diffusivity values were obtained from DLS analysis.

APPENDIX G

Permeability, process flux, mass transfer coefficient and sieving coefficients values for filtration of various solutes through 20 nm PAA and 300 kDa PES membranes, **Actual sieving coefficient is calculated as** $S_a = \frac{S_{obs}}{S_{obs}+\left[(1-S_{obs})*exp^{(J/k_m)}\right]}$ ***(as described by Mehta and Zydney, (2005))***

Membrane	Solute	Hydraulic permeability, L_p (m/s/Pa x 10^{-9})	Process flux, J (m/s x 10^{-4})	Mass transfer coefficient k_m (m/s x 10^{-6})	Polarisation index, J/k_m	Observed sieving coefficients, S_{obs}	Actual sieving coefficient S_a	Separation factor, $1/S_a$
20 nm PAA membrane (Anodisc)	BSA	6.0	3.5	9.4	37.5	0.927	6.7×10^{-16}	1.5×10^{15}
		5.3	3.1		33.1	0.969	1.4×10^{-13}	7.3×10^{12}
		5.7	3.4		35.7	0.974	1.2×10^{-14}	8.4×10^{13}
	TG	5.5	0.8	6.3	13.8	0.494	1.0×10^{-06}	9.8×10^{05}
		5.7	1.0		16.5	0.569	8.8×10^{-08}	1.1×10^{07}
		5.7	1.0		15.9	0.567	1.6×10^{-07}	6.1×10^{06}
	BSA NP	6.1	0.3	2.2	11.6	0.027	2.6×10^{-07}	3.8×10^{06}
		5.6	0.3		11.7	0.035	2.9×10^{-07}	3.4×10^{06}
		5.4	0.3		12.6	0.012	4.2×10^{-08}	2.4×10^{07}
300 kDa PES membrane (Biomax)	BSA	3.6	1.7	9.4	18.4	0.943	1.7×10^{-07}	5.9×10^{06}
		2.8	1.3		13.2	0.943	2.9×10^{-05}	3.4×10^{04}
		3.6	1.7		17.7	0.981	1.1×10^{-06}	9.0×10^{05}
	TG	5.7	0.5	6.3	7.8	0.257	1.5×10^{-04}	6.7×10^{03}
		2.8	0.4		6.9	0.107	1.3×10^{-04}	8.0×10^{03}
		4.8	0.6		8.9	0.237	4.5×10^{-05}	2.2×10^{04}
	BSA NP	6.6	0.2	2.2	9.0	0.007	9.8×10^{-07}	1.0×10^{06}
		7.0	0.2		9.4	0.006	4.9×10^{-07}	2.0×10^{06}
		7.1	0.2		9.7	0.007	4.3×10^{-07}	2.4×10^{06}

APPENDIX H

Surface charge on protein solutes and membrane surface

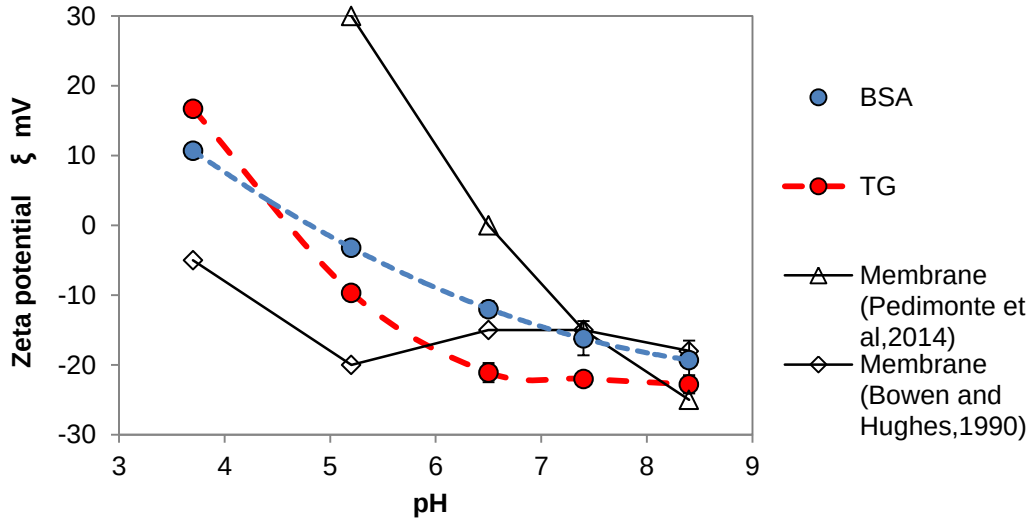

TG and BSA zeta potentials were measured in 10mM phosphate buffers. Zeta potentials for PAA membrane surface (open symbols) are approximations from literature and are measured at a much lower salt concentration (1mM KCl), so the magnitude of values could be lower in buffer conditions similar to those for BSA and TG.

APPENDIX I

Effect of pH on fractionation of binary mixtures of model solutes

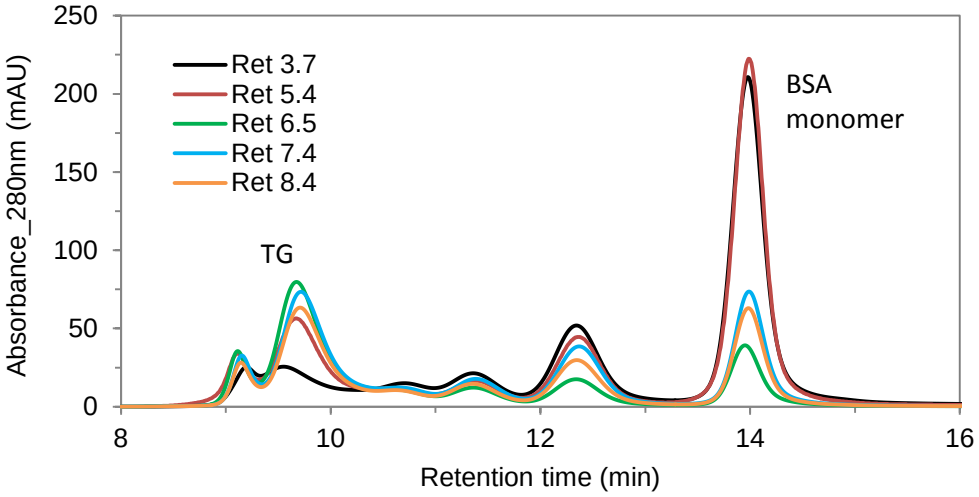

I-1 Size exclusion chromatograms of the retentates collected for fractionation of TG and BSA using PAA membranes: Effect of various solution pH

Overlay of HP-SEC chromatograms of retentates obtained after fractionation of different pH solutions of BSA and TG mixture. 50uL of samples was injected onto TSKgel3000swxl (7.8 x 300 mm, the flow rate of 0.6 mL/min) column equilibrated and eluted with PBS. Abnormal TG peak (9.8 min) observed at pH 3.7 was also observed in the feed solution. Retentate with pH 6.5 shows the smallest BSA peak (~residual BSA).

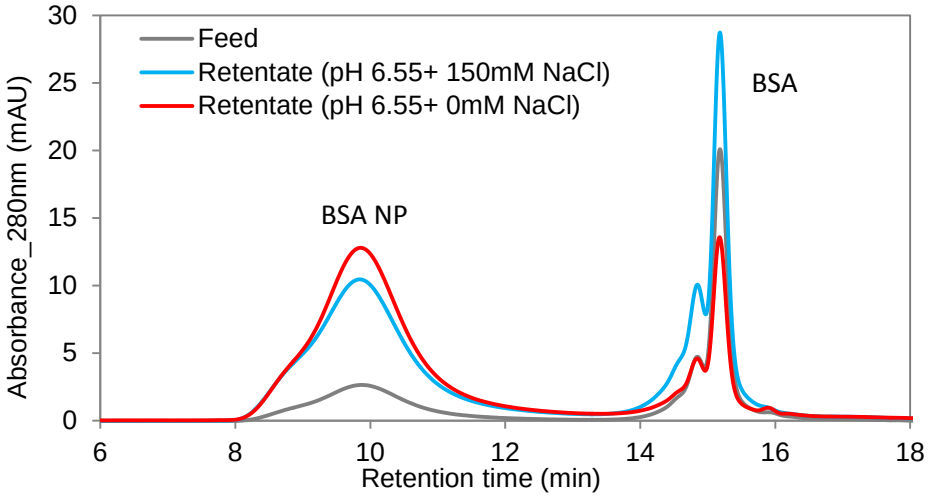

I-2 Size exclusion chromatograms of the retentates collected for fractionation of BSA nanoparticle and BSA using PAA membranes at pH 6.5 (with and without NaCl)

Chromatograms were obtained by injecting 20uL of samples onto BIOSEC 5 (7.8 x300 mm; flow rate 0.8 mL/min) column equilibrated and eluted using PBS. Lowest residual BSA (small BSA peak) and high BSA NP recovery are achieved at pH 6.5 without salt. Retentates are ~4 fold concentrated compared to the feed.

APPENDIX J

Overlay of HP-SEC chromatograms for retentates obtained after extended UF/DF (12 diavolumes) for fractionation of BSA nanoparticles and BSA mixture using PAA and PES membranes.

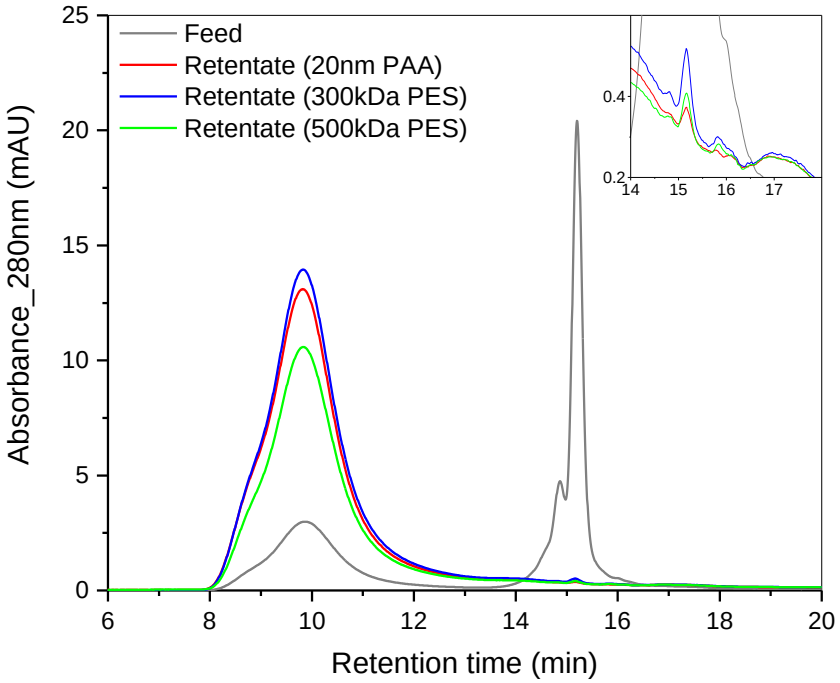

Chromatograms were obtained by injecting 20uL of samples onto BIOSEC 5(7.8 x300 mm; flow rate 0.8 mL/min) column equilibrated and eluted using PBS. Inset (chromatogram magnified at retention time 14-18 minutes) shows peaks of residual BSA in the retentates. 300 kDa PES showed highest residual BSA and highest BSA NP retention. Retentates are ~4 fold concentrated compared to the feed.